

**Effects of macromolecular crowding on protein  
targeting and translocation via SecYEG**

Inaugural Dissertation

zur Erlangung des Doktorgrades  
der Mathematisch-Naturwissenschaftlichen Fakultät  
der Heinrich-Heine-Universität Düsseldorf

vorgelegt von

**Maryna Löwe**

aus Kyiv, Ukraine

Düsseldorf, Januar 2024

aus dem Institut für Biochemie  
der Heinrich-Heine-Universität Düsseldorf

Gedruckt mit der Genehmigung der  
Mathematisch-Naturwissenschaftlichen Fakultät  
der Heinrich-Heine-Universität Düsseldorf

Berichtersteller:

1. Prof. Dr. rer. nat. Alexej Kedrov
2. Prof. Dr. rer. nat. Laura Hartmann

Tag der mündlichen Prüfung: 1.12.2023

*„Das Pergament, ist das der heilige Bronnen,  
Woraus ein Trunk den Durst auf ewig stillt?  
Erquickung hast du nicht gewonnen,  
Wenn sie dir nicht aus eigener Seele quillt.“*

Faust  
Johann Wolfgang von Goethe

# Table of contents

Abbreviations .....	V
Abstract .....	VI
Zusammenfassung .....	VII
1 Introduction .....	9
1.1 Macromolecular crowding .....	9
1.2 Protein transport via Sec machinery .....	16
1.3 Crowding sensors .....	19
2 Aims of the thesis .....	21
3 Results .....	23
3.1 Effects of macromolecular crowding on biological membranes – Review publication .....	23
3.2 Genetically-encoded sensors for measuring macromolecular crowding at the lipid membrane interface – Publication .....	53
3.2.1 Supplemental figures .....	72
3.3 Development of anchoring strategies and other sensor designs .....	86
3.3.1 Transmembrane anchor domains for the crowding sensors .....	86
3.3.1.1 Introduction .....	86
3.3.1.2 Materials and Methods .....	88
3.3.1.3 Results .....	90
A.  Mistic as a potential candidate for the sensor anchoring .....	90
B.  RseC as a potential candidate for the sensor anchoring .....	92
3.3.1.4 Discussion .....	97
3.3.2 Two-component crowding sensor design development .....	100
3.3.2.1 Introduction .....	100
3.3.2.2 Materials and Methods .....	102
3.3.2.3 Results .....	107
A.  Purification and assembly of the sensor components .....	107
B.  Structural analysis of the sensor with and without SpyCatcher .....	110
C.  Sensitivity of the SpyTag-sensors in crowded solutions .....	111
D.  Crowding at the membrane interfaces with synthetic and proteinaceous crowders .....	116
E.  Binding of the SpyTag-sensors to SecE-SpyCatcher in IMVs .....	118
3.3.2.4 Discussion .....	121
3.4 Effects of macromolecular crowding on transport activity and translocation via SecYEG .....	124

---

3.4.1 Introduction.....	124
3.4.2 Materials and methods .....	125
3.4.3 Results .....	131
A.    Effects of the solution crowding on protein targeting and translocation via SecYEG.....	131
B.    Crowding on the membrane interface: Effects on protein targeting and translocation via SecYEG .....	134
C.    Proteinaceous crowding at the membrane interface.....	145
3.4.4 Discussion .....	148
4 Discussion and Outlook .....	152
4.1 Crowding sensors for macromolecular confinement in membranes.....	152
4.2 Effects of macromolecular crowding on protein targeting and translocation via SecYEG.....	155
4.3 Outlook.....	158
4.3.1 The future perspectives for the membrane-associated crowding sensor .....	158
4.3.2 Overcoming obstacles for the characterizations of crowding effects on protein targeting and translocation via SecYEG .....	159
5 References .....	162
6 Appendix.....	177
I.    Curriculum vitae.....	177
II.   List of publications .....	181
III.  Supervised Student Projects.....	182
IV.  Acknowledgements.....	183
V.   Declaration .....	185

---

## Abbreviations

AEBSF	4-(2-Aminoethyl)benzenesulfonyl fluoride hydrochloride
ATP	Adenosine-5-triphosphate
BSA	Bovine serum albumin
CD	Circular dichroism
CMC	Critical micelle concentration
DDM	n-dodecyl- $\beta$ -D-maltoside
DOPC	1,2-dioleoyl-sn-glycero-3-phosphocholine
DOPG	1,2-dioleoyl-sn-glycero-3-phospho-(1'-rac-glycerol)
DTT	Dithiothreitol
EDTA	Ethylenediaminetetraacetic acid
FACS	Fluorescence activated cell sorting
FRAP	Fluorescence recovery after photobleaching
FRET	Förster's resonance energy transfer
GUV	Giant unilamellar vesicles
HPC	Hydroxypropyl cellulose
HPLC	High performance liquid chromatography
IDP	Intrinsically disordered protein
IMAC	Immobilized metal chelate affinity chromatography
IPTG	Isopropyl $\beta$ -d-1-thiogalactopyranoside
LCD	Low-complexity domains
LDAO	Lauryldimethylamine oxide
LLPS	Liquid-liquid phase separation
LPS	Lipopolysaccharide
LSM	Laser scanning microscopy
MALS	Multi-angle light scattering
MBP	Maltose-binding protein
MWCO	Molecular weight cut-off
NTA	Nitrilotriacetic acid
PDB	Protein Data Bank
PE	Phosphatidylethanolamine
PEG	Polyethylene glycol
PG	Phosphatidylglycerol
PMSF	Phenylmethylsulfonyl fluoride
QCM	Quartz crystal microbalance
SAXS	Small-angle X-ray scattering
SDS-PAGE	Sodium dodecyl sulfate-polyacrylamide gel electrophoresis
SEC	Size exclusion chromatography
SPR	Surface plasmon resonance
TCEP	Tris(2-carboxyethyl)phosphine hydrochloride
TMH	Transmembrane helix

## Abstract

Cytoplasm of the living cell is highly crowded by biomacromolecules which occupy around 5-40% of the available volume and have a significant effect on thermodynamic and kinetic properties of vital biological processes, like protein folding and aggregation, enzymatic reactions, etc. Crowding effects are not limited to the cytoplasm, however, less attention has been paid to the crowding of biological membranes, where the integral membrane proteins can occupy from 25 to even 80% of available space thereby affecting lateral protein diffusion, oligomerization equilibria, favor formation of protein clusters and microdomains, whereas the presence of densely packed proteins at the membrane interface can affect membrane-associated processes like protein targeting and translocation, signaling and even lead to spontaneous membrane deformations. A comprehensive understanding of the implications of macromolecular crowding is essential for obtaining valuable insights how cellular organization and essential biological processes are influenced by complex cellular environments.

Simulation and study of crowding effects in artificial systems requires a systematic reconstruction of crowding-induced confinement in the physiologically relevant range. However, so far only a limited number of approaches exist that would allow characterizing the extent of macromolecular confinement on the membrane surface. To work towards overcoming this limitation, a set of the genetically-encoded FRET-based sensors with different designs for probing the macromolecular crowding at the membrane interface were developed and characterized. The sensors allow for measurements of lateral confinement on membranes *in vitro* and are suitable for non-invasive crowding quantification and for study of membrane organization in living cells.

In this thesis the development of model membranes systems with reconstituted SecYEG translocon was aimed to elucidate the effects of macromolecular crowding on post-translational protein targeting and translocation. A set of synthetic polymers as well as protein-based crowder were employed to simulate the complex and native-like conditions in solution or on membrane surfaces. It could be shown, that the synthetic polymers such as Ficoll PM70 and PEG of different sizes were able to inhibit the translocation rates and activity being dependent on the crowder's type, size and concentration. Simulated macromolecular confinement on the surfaces of liposomes with synthetic polymers has also shown a reduction in transport efficiency, whereas protein-based crowder showed both, positive and negative modulating effect of translocation activity of preprotein. In summary, the establishment of these systems provides a starting point for study of macromolecular crowding effects *in vitro* and identifies associated methodological challenges.

---

# Zusammenfassung

Das Zytoplasma der lebenden Zellen ist stark mit diversen Bio-Makromolekülen, wie Proteinen und Nucleinsäuren gefüllt, deren Konzentrationen bis zu 50-400 mg/mL erreichen können. Diese hohen intrinsischen Konzentrationen können bis zu 40% des verfügbaren Volumens einnehmen, während die heterogene Oberflächenbeschaffenheit von komplexen Makromolekülen die unspezifischen Wechselwirkungen zwischen ihnen fördert. Dieser Zustand wird in der wissenschaftlichen Literatur als „*macromolecular crowding*“, oder als makromolekulare Beengung bezeichnet. Vorhandene wissenschaftliche Untersuchungen haben gezeigt, dass die makromolekulare Beengung einen tiefgreifenden Einfluss auf die vitalen biologischen Prozesse in lebenden Zellen hat, darunter Diffusion, Proteinfaltung und -aggregation sowie die Kinetik der enzymatischen Reaktionen. Die gleiche Situation findet auf und in den biologischen Membranen statt, welche in speziellen Fällen sogar bis zu 80% mit integralen Proteinen gefüllt sind. Auch hier sind vielfältige Auswirkungen von makromolekularer Beengung, wie Oligomerisierung und anomale Diffusion von Membranproteinen, sowie die durch die Proteinansammlungen hervorgerufenen morphologischen Veränderungen der Membranoberflächen, beschrieben.

Die biologischen Prozesse, die *in vitro* in verdünnten Lösungen üblicherweise untersucht werden, spiegeln nicht die komplexen Bedingungen im Zytoplasma oder Membranen lebender Organismen wider. Um ein umfassendes Verständnis der komplexen Prozesse zu bekommen, ist es wichtig die makromolekulare Beengung in den Experimenten zu berücksichtigen. Dies erfordert die Nachahmung von Crowding-Bedingungen in physiologisch relevanten Umfang und einen Vergleich mit der tatsächlichen Situation *in vivo*. Bis jetzt existiert nur eine begrenzte Anzahl von Ansätzen, die es ermöglichen das Ausmaß der makromolekularen Beengung auf den Membranoberflächen zu charakterisieren. Daher wurde eine neue Generation genetisch-kodierter und membran-adaptierter Sensoren entwickelt, die eine Quantifizierung des Crowding auf der Membran *in vitro* ermöglichen und für Messungen in einer lebenden Zelle eingesetzt werden können

In dieser Dissertation wurden synthetische sowie protein-basierte Crowders eingesetzt, um die komplexen und nativ-ähnlichen Bedingungen in der Lösung oder auf Membranoberflächen zu simulieren und die Auswirkungen auf die Funktionalität von SecYEG Translocon von *E. coli* zu charakterisieren. So konnte gezeigt werden, dass die synthetischen Polymere wie Ficoll PM70 und PEG in unterschiedlichen Größen eine Inhibierung von Transportprozessen hervorgerufen hat, die wiederum von dem Crowder-Typ, -Größe und -Konzentration abhängig war. Die simulierte makromolekulare Beengung auf den Oberflächen von Liposomen hat ebenfalls eine Verringerung der Transporteffizienz gezeigt.

Die Etablierung und Charakterisierung dieser Systeme ermöglicht es, ein umfassenderes Verständnis zu bekommen, wie biologische Prozesse von komplexer zellulärer Umgebung beeinflusst werden und hilft damit verbundene methodologische Herausforderungen zu identifizieren.

# 1 Introduction

## 1.1 Macromolecular crowding

All vital biological processes, like gene expression, protein translation, cellular respiration, signaling, division and even apoptosis, occur in a unique, highly confined and non-ideal environment that is predestinated to affect the macromolecules and the interactions between them (Ellis, 2001). Cellular interiors exhibit complex media where the constituents vary widely in sizes, from micrometer-sized eukaryotic organelles to comparably smaller macromolecular species, like proteins and ribosomes in cytoplasm, mixtures of proteins and DNA in the nucleus or in the cytoplasm of prokaryotes. Although in general no single macromolecular compound exists in the cellular environment at high concentration, the sum of the all present macromolecular species occupies a considerable portion of the volume (figure 1.1). Such solution is referred as *crowded* and the first obvious consequence of the presence of different macromolecules at high concentrations which occupy certain volume fraction the space, is the decrease of the available free solvent. In the cytoplasm of *E. coli*, the total concentration of proteins and nucleic acids was estimated to reach up to 300-400 g/L (Zimmerman and Trach, 1991). Comparably, the concentration of hemoglobin in erythrocytes was estimated to be more than 300 g/L (Ross and Minton, 1977). Macromolecular concentration inside the nucleus of eukaryotic cells depends on the cell type, but lays in the range of 100 g/L (Hancock, 2007). The corresponding volume occupancy depends also on size distribution of macromolecular compounds and can vary between 5-40% (Ellis and Minton, 2003).

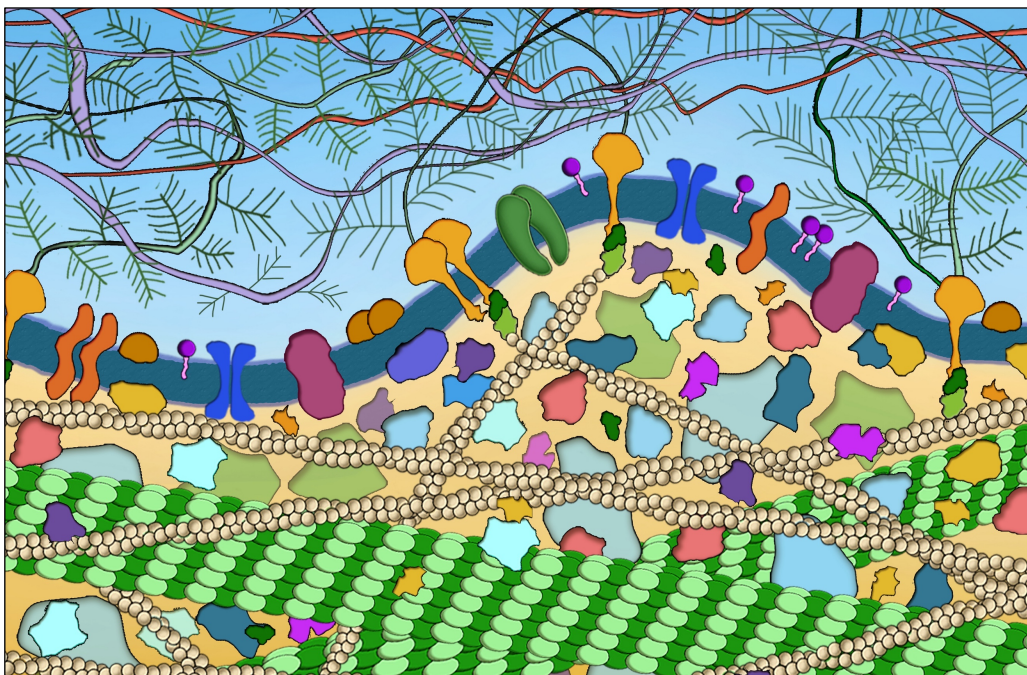


Figure 1.1: Crowded interior of the living cell

A simple model simulation of the volume exclusion suggests that if 30% of a given space is filled by spherical species of defined size, that is a model representation of proteins, there will be no available volume for more species of the same size, since the molecules are mutually impenetrable (Minton, 2001). Smaller particles or solute molecules in this model are less affected by the excluded volume, since with the decreasing particle size the available volume fraction will increase and vice versa, the addition of another large particle would not be possible without displacement of the already existing species. The mobility of the large co-solutes is restricted leading to entropy decrease in confined environment compared to the diluted solutions, which in turn increases the free energy of solute (Ralston, 1990).

The excluded volume effect is only a part of the phenomenon that was termed *macromolecular crowding*. The macromolecules e.g. proteins and nucleic acids present in high concentrations in cellular environment, that act as *crowders*, are commonly simplified in models to the quasi-spherical ideal compounds, but they nevertheless exhibit non-ideal behavior and the wide-ranging heterogeneity of their surfaces, e.g. due to the differences in the primary sequence, spatial configuration and, for proteins, post-translational modifications. Those give rise for so-called soft or *quinary* interactions, including attractive and repulsive forces governed by hydrogen-bonding, electrostatic, polar, and van der Waals interactions providing another degree of complexity for the crowding characterization (McConkey, 1982; Minton, 2013; Sarkar *et al.*, 2013). Additionally, the altered viscosity of the medium in crowded solutions leads to the lowered translational and rotational diffusion of the macromolecules, even if to a smaller extent than protein-protein contacts (Nawrocki *et al.*, 2019; Schavemaker *et al.*, 2018; Wang *et al.*, 2010). The excluded volume effect and the quinary interactions are two primary factors that render the effects of the physiological crowding in the living cell, which potentially affect every biological process. Diffusion of macromolecules, folding, stability, oligomeric state and aggregation of proteins, enzymatic activities, interactions between proteins and nucleic acids were shown to be affected under crowded conditions (Berg *et al.*, 1999; Kuznetsova *et al.*, 2014; Löwe *et al.*, 2020).

The first evidences that the behavior of proteins in volume-excluded environments are different from the studies in the dilute solutions arose more than 60 years ago, upon studying changes in the osmotic pressure of serum albumin and hyaluronic acid mixtures, which exceeded the sum of the osmotic pressures from separate solutions (Laurent and Ogston, 1963). The difference was attributed to the exclusion of the protein from the hyaluronic acid-containing volume fraction (Edmond and Ogston, 1968; Ogston and Preston, 1966). In the year 1971 Laurent reported on the first attempts to characterize the enzymatic activity of hyaluronate lyase, lactate dehydrogenase and trypsin in the presence of PEG and dextran creating the environment that would simulate the intracellular confinement. The addition of the polymers had only moderate influence though causing lower enzymatic activity with a decrease of  $K_m$

values by excluded volume (Laurent, 1971). The pioneer research continued with characterization of hydrolysis of fructose-1,6-bisphosphate by aldolase in the mixtures with different concentrations and sizes of poly(*n*-vinylpyrrolidone) and polyvinyl alcohol. Experiments showed an enhancing effect of low polymer concentrations on reaction rates followed by the inhibition, which was more pronounced for low-molecular weight polymers, suggesting an influence on the enzyme stability (Jancsik and Keleti, 1979; Jancsik *et al.*, 1976). Additionally, specific activity of glyceraldehyde-3-phosphate dehydrogenase showed a complex behavior, including inhibition and activation, depended on the polymer concentration and the enzyme oligomerization (Jancsik and Keleti, 1979). In year 1981, Minton suggested a theory on how the excluded volume effect may alter kinetics of enzymatic reactions and influence the structure of macromolecules, i.e. their shape and the oligomeric state (Minton, 1981). Although the theory is oversimplified and it neglects the naturally occurring quinary interactions between the macromolecules, the predictions of the models show qualitative agreement with experimental data that was not only available to time of publication, but also with research on the crowding effects made nowadays.

A growing attention among researchers worldwide interested in exploring the effects of macromolecular crowding, as well as technical progress and emergence of new advanced measurement techniques and computational simulations have allowed a more comprehensive characterization of the phenomenon. For the role of model crowders that mimic the excluded volume effect, synthetic polymers like polyethylene glycol (PEG), dextran, Ficoll of various sizes or hydroxypropyl cellulose (HPC) are widely used. Proteins as crowders (lysozyme, BSA,  $\beta$ -lactoglobulin, hemoglobin, ovalbumin) modulate a more complex crowding system. Generally, an appropriate candidate should not actively interfere with the probe and the measurement system, be chemically stable and can be concentrated to the levels that would reflect the physiologically relevant crowding conditions (Breydo *et al.*, 2014; Junker *et al.*, 2019; Kuznetsova *et al.*, 2014; Löwe *et al.*, 2020; Uversky *et al.*, 2002; Wang *et al.*, 2010).

Most of crowding-oriented research has focused on mobility of biological macromolecules in complex environments. The ability of bio-macromolecules to undergo translational and rotational motion to enable contacts with their interaction partners is necessary to fulfill their functions within the living cell (Schavemaker *et al.*, 2018). In crowded environments, the macromolecules occupying a certain volume fractions provide steric barriers and alter the diffusion coefficients predicted for the ideal (diluted) solutions by Stokes-Einstein equation (Eq. 1). According to this law, translational ( $D_T$ ) and rotational ( $D_R$ ) diffusion coefficients in Stokes-Einstein-Debye equation (Eq. 2) are inversely proportional to the particle radius and the viscosity of the solvent:

$$D_T = \frac{k_B T}{6\pi\eta R} \quad (\text{Eq. 1})$$

$$D_R = \frac{k_B T}{8\pi\eta R^3} \quad (\text{Eq. 2})$$

This relation can be still applied for small molecules acting as “crowders”, for example sucrose or glycerol, since their size is much smaller than the macromolecules of interest, but with the increasing crowder size the rise of the deviations on diffusion coefficients are observed and show the power law dependence:

$$\frac{D_o^{T,R}}{D_C^{T,R}} = \left(\frac{\eta_C}{\eta_0}\right)^{q_{T,R}} \quad (\text{Eq. 3})$$

where  $D_C$  and  $D_o$  are the diffusion coefficients, and  $\eta_C$  and  $\eta_0$  are the viscosities of the medium with and without crowding, respectively. The exponent  $q$  equals 1 for the diluted solution in the Stokes law, but it changes with emerging crowding, being dependent on both crowder and probe sizes. Several studies with synthetic polymers have shown that in crowded solution with emerging crowder size the diffusion of the particles gets less dependent on the overall solution viscosity, known as *macro-viscosity*. The particles experience the micro-viscosity which depends on the size relation of the crowder and the probe, whereas the translational diffusion is more hampered than the rotational one and the corresponding  $q$ -value decreases for the solutions with synthetic crowders (Junker *et al.*, 2019; Lavalette *et al.*, 2006; Wang *et al.*, 2010). However, in the solutions where crowding is modulated by proteins, an opposite effect on the diffusion coefficients in relation to the predictions have been observed. In the study with chymotrypsin inhibitor 2 in presence of BSA, lysozyme and ovalbumin, the translational diffusion have shown to be only slightly affected, whereas the rotational one was strongly attenuated with corresponding  $q$ -values larger than 1. Here, likely reason is the rise of the soft interactions between the crowders and the probe. Moreover, the experiments in *E. coli* lysate were comparable with the results using protein as crowders: The rotational diffusion coefficients were decreased, whereas the translational diffusion coefficient was not significantly affected compared to the predictions by the laws highlighted above (Wang *et al.*, 2010).

The induced confinement of the crowded medium favors the compaction and stabilization of the proteins in the folded over the denaturated form. The molten globule structure of cytochrome C can be restored by addition of 200 g/L dextran at pH 2, as recorded by circular dichroism (CD) spectra, where in the absence of the crowder the protein is completely unfolded (Sasahara *et al.*, 2003). The melting temperature ( $T_m$ ) of apoflavodoxin increased up to 20°C

in solution containing 40% Ficoll PM70 (w/v) (Stagg *et al.*, 2007). However, this stabilization effect is limited to the hard-core repulsions and is entropically driven. In the crowded solution, where soft interactions take the lead, the enthalpy becomes a determinant of the stabilizing effect, as was shown by destabilization of ubiquitin in BSA- or lysozyme-crowded solutions at different temperatures (Wang *et al.*, 2012).

The structural conformation of intrinsically disordered proteins (IDPs) may be favored in the crowded environments, as was shown for immunoglobulin G binding domain of protein L from *Streptococcus magnus* (Ådén and Wittung-Stafshede, 2014) and for FlgM protein, a flagellar synthesis regulator from *Salmonella typhimurium*, in solutions with synthetic polymers and proteins, respectively (Dedmon *et al.*, 2002). Though, it should be noted that it was not clear whether the secondary structure induced by crowding was comparable to the natural fold upon the binding to  $\sigma^{28}$ , a subunit of the RNA polymerase holoenzyme. However, folding of other several IDPs was shown not to be affected by the macromolecular confinement (Flaugh and Lumb, 2001; Sharma *et al.*, 2022). The conformation of  $\alpha$ -synuclein was only barely affected in presence of high PEG concentrations with various sizes. However, macromolecular crowding was shown to enhance the rates of amyloid formation of  $\alpha$ -synuclein, whereas the lagtime for nucleation and the rate of fibrillation was dependent on the type of crowder in terms of their size and charge as well as the concentration used (Munishkina *et al.*, 2004; Uversky *et al.*, 2002). Accelerated amyloid formation was observed as well on the example of apoC-II protein by the means of volume exclusion with dextran T10 (Hatters *et al.*, 2002).

Modern research developments in the field of cell biology offered new insights on cellular organization and on the physiological state of biological fluids. Instead of being uniformly crowded with macromolecules, the cytoplasm of various cells contains distinct structures, like condensates, cytoplasmic bodies, stress and germ granules, nucleoli etc., that are segregated from liquid environment forming a class of dynamic, membrane-less micro-compartments. Their formation arises through the condensation and clustering of distinct proteins and nucleic acids into droplets with liquid-like characteristics as a response to the environmental changes, oxidative stress or cell cycle phase (André and Spruijt, 2020; Hyman and Brangwynne, 2011). This phenomenon is known as liquid-liquid phase separation (LLPS). Synergy of the excluded volume effect, which increases the effective protein concentration, and the quinary interactions between the biomacromolecules promotes the reversible segregation of condensates in LLPS. The low-complexity domains (LCDs) of intrinsically disordered proteins which show a low diversity of amino acid composition, promote LLPS via multivalent interactions between proteins and other biomacromolecules. The  $\alpha$ -synuclein which carries two LCDs was shown to undergo LLPS either in the presence of PEG or upon reducing pH or upon addition of copper and iron ions. With time the liquid droplets with accumulated  $\alpha$ -synuclein convert into solid-like state, accompanied by accumulation of fibrillar structures (Ray *et al.*, 2020). The LCD of

heterogeneous nuclear ribonucleoprotein A1 (hnRNPA1) is also able to induce LLPS which can be facilitated either by Ficoll and PEG or by changes of the ionic strength or by the presence of RNA. The missense mutations in the class of hnRNPs, typical components of the stress granules, are linked to the development of the stable condensates in pathological disorders (Molliex *et al.*, 2015). LLPS is not only a feature of proteins with intrinsically disordered regions, but can be observed for the globular proteins like human serum albumin in the presence of PEG 8000, Dextran 70 and Ficoll 400 and was shown to be driven by hydrophobic interactions rather than by electrostatic interactions (Patel *et al.*, 2022).

Protein-protein and protein-nucleic acid interactions, protein assembly and changes in oligomeric stoichiometry are favored by macromolecular crowding effects (Minton, 2000). The equilibria of fibrinogen association to dimers was facilitated by BSA concentrations above 40 g/L as well as formation of soluble tubulin oligomers was induced upon addition of dextran in the conditions where the assembly is unfavored (Rivas *et al.*, 1999). The excluded volume effect effectively “concentrates” the interactions partners thus favoring their interactions, as was shown on the example of blunt-end DNA ligation. Under dilute conditions, DNA ligases from *E. coli* or rat liver nuclei were unable to perform the reaction, whereas addition of Ficoll PM70, PEG 6000 or BSA induced effective joining of the DNA fragments (Zimmerman and Pfeiffer, 1983). Alike, the activity of *E. coli* DNA polymerase I was enhanced in the crowded solitons with elevated ionic strength, which otherwise inhibits the reaction and leads to increase of  $K_m$  values. Presence of the 12% of PEG 8000 decreased the estimated  $K_m$  value more than 20-fold in 200 mM KCl in comparison to the non-crowded solution, and the effect was attributed to the increased DNA-protein interaction under crowding conditions (Zimmerman and Harrison, 1987).

As can be seen, the phenomenon of the macromolecular crowding in the cytoplasm plays a significant role in the cellular organization, but it is only a part of the entire story. It is important to recognize that similar situation is observed in biological membranes. The cellular membranes fulfill various functions including transport of molecules, energy metabolism, signal transduction and communication of the cell with the environment and between intrinsic organelles and essentially produce segregated environments for reactions that require specialized conditions. While the lipid bilayer provides a physical boundary and defines the cell and the cellular compartments, the majority of functions of the membrane are ensured by integral proteins spanning the membrane, and peripheral proteins, that are anchored at the interface via lipid contacts or by interactions with the integral proteins. Around a quarter of the whole cellular proteome consists of membrane proteins, and the occupied cellular membrane area ranges from 25% to 80% depending on the cell and membrane type (Dupuy and Engelman, 2008; Kirchoff, 2008; Liu and Scheuring, 2013; Löwe *et al.*, 2020; Sowers and Hackenbrock, 1981). The structural stability and functionality of membrane-anchored proteins

depend strongly on the lipid bilayer, which physico-chemical properties are clearly different from the conditions the cytoplasmic proteins are exposed to. The lipid content of the cellular membranes has also an impact on the membrane organization, as lipids are the primary building blocks and their composition and distribution modulate membrane fluidity, flexibility and function. Biological membranes are highly dynamic and show lateral heterogeneity (Mitchison-Field and Belin, 2023; Mueller *et al.*, 2012; Simons and Sampaio, 2011).

The subject of macromolecular crowding in the membranes is substantially less studied than in cytoplasm, but comparable effects are observed in both systems. In contradiction to the fluid mosaic model proposed by Singer and Nicolson, suggesting unhindered diffusion of proteins within the fluidic membrane (Singer and Nicolson, 1972), the diffusive behavior within the membrane leaflets, which is restricted to the lateral diffusion in 2D dimension, is dependent not only on the protein size and fluidic characteristics of the lipid bilayer, but also on the degree of crowder-protein occupancy and soft interactions with the lipids as the solvent. (Démery and Lacoste, 2018). In eukaryotic cells, specific interactions between lipids within the plasma membrane, primarily cholesterol and glycosphingolipids, with proteins lead to formation of functional units termed as lipid rafts, which commonly contain a distinct set of proteins involved in signal transduction, cell adhesion and membrane trafficking (Harder *et al.*, 1998; Sezgin *et al.*, 2017) and can be seen as example of phase separation in the crowded membranes. Coarse-grained molecular dynamics simulations of Kir potassium channels in membranes at physiologically relevant crowding levels and complex lipid composition reconstructed clustering and reduced protein and lipid diffusion (Duncan *et al.*, 2017). Most affected were the lipids with the tight contact to the protein since, the proteins themselves can modulate their proximate lipid environment and so influence the lipid composition and lead to the changes in membrane structure (Corradi *et al.*, 2018; Marsh, 2008). Conversely, lipids with different acyl chain length can segregate and locally change the membrane thickness thus mediating protein localization and mobility according to the size of the transmembrane domains which avoid the exposure to the aqueous solutions (Sezgin *et al.*, 2017).

The heterogeneous membrane organization is not restricted to the eukaryotic cells, but formation of microdomains similar to lipid rafts were observed in the membranes of prokaryotic organisms and archaea (Bramkamp and Lopez, 2015). High densities of the proteins, for example in the nanodomains or rafts as well as the high protein abundance in the membrane leads to anomalous diffusion that deviates from the predicted behavior outlined in the diffusion laws in non-crowded systems (Démery and Lacoste, 2018; Jeon *et al.*, 2016; Peters and Cherry, 1982). In general, the lateral diffusion rates are reduced with increasing protein density, as was predicted by molecular simulations (Javanainen *et al.*, 2017) and verified by experiments including FRAP measurements of plasma membrane of mammalian cells (Frick *et al.*, 2007) and fluorescence correlation spectroscopy (FCS) studies of selected membrane

proteins in giant unilamellar vesicles (GUVs) (Ramadurai *et al.*, 2009). Complementary, the diffusivity of the peripheral membrane protein was shown to be affected as well and being dependent on the interfacial membrane occupancy (Houser *et al.*, 2016)

High protein crowding on the membranes can induce deformations of lipid bilayers and even lead to the emergence of the structures like buds and tubules. Next to the well-studied scaffold mechanism, which includes clathrin-mediated and Bin-Amphiphysin-Rvs (BAR)-dependent membrane bending, and insertion of amphipathic helices at the membrane interface (Zimmerberg and Kozlov, 2006), it was shown that even globular proteins with various sizes applied via His-tag to the surface of GUVs was sufficient to induce the formation of the tubules due to the increasing lateral pressure on the membrane surface (Stachowiak *et al.*, 2010). The selected examples show that high concentrations of biomacromolecules have significant influence on function and organization of biological membranes. Multifaceted effects of the macromolecular crowding on protein monomer/oligomer equilibria, protein folding and aggregation events, and even on more severe morphological changes like membrane remodeling are described and discussed in detail in the Chapter 3.1 of this thesis based on the systematical review of available research literature (Löwe *et al.*, 2020).

The concentrations of macromolecules in the cytoplasm and in the biological membranes are much higher than the concentrations employed in the vast majority of laboratory experiments nowadays and in the past. It does not necessarily imply that the research conducted in diluted solutions is false, the concepts of molecular biology postulated over decades are still working and moreover primary structural research or some experimental setups like SAXS, mass spectrometry, X-ray crystallography would require highly pure targets and may lead to interferences with added crowder molecules. Moreover, a direct readout from the interior of the living cell is still challenging and is often limited by experimental methodology. The measurements in diluted solutions still account various vital physiological parameters like pH or the ionic strength, but a direct application of the results gained in the diluted solution to describe the physiological state of the system should be approached with caution, as the experimental outcome may not be directly transferable, as not all factors that cause effects in complex systems may be accounted. To get an in-dept understanding on how the biological processes are influenced by the complexity of cellular organization, the consideration of crowding in research should be involved on the routine-based level.

### **1.2 Protein transport via Sec machinery**

Even through the synthesis of membrane proteins is initiated in the cytosol, the subsequent biogenesis is more complex in comparison to their soluble counterparts. From the

thermodynamic point of view, the localization of the membrane proteins in the aqueous phase is unfavorable since the transmembrane segments of membrane proteins are composed of non-polar amino acids that raise the overall hydrophobicity of protein. The insertion into the apolar membrane leaflet is necessary, otherwise the proteins would undergo aggregation in the polar cytoplasmic environment. If spontaneous, the insertion of membrane proteins into the membranes occurs with low efficiency, so targeting to the membrane surface, insertion and correct folding of membrane proteins in the cell is facilitated via a few evolutionarily conserved pathways (Hedin *et al.*, 2011). In all domains of life, the integration and transport of proteins in or through the membrane is facilitated by the Sec translocon, which forms a protein-conducting channel: In the inner membrane of bacteria it is known as SecYEG complex, and in eukaryotes the translocon Sec61 is localized to the membrane of endoplasmic reticulum (Bolhuis, 2004; Oswald *et al.*, 2021; Rapoport *et al.*, 2017).

The transmembrane transport and insertion via SecYEG in bacteria can generally occur in two different ways: Co-translationally via direct interaction of the translocon with the ribosome, and post-translationally i.e. when the protein precursor, or preprotein, has been already completely synthesized in the cytoplasm (figure 1.2). In case of co-translational insertion of membrane proteins, the highly hydrophobic signal sequence on the N-terminus of the nascent chain synthesized by a ribosome is recognized by the signal recognition particle (SRP). The complex is delivered to the membrane surface where it interacts with FtsY receptor and can be transferred to the translocon. Less hydrophobic proteins are not recognized by SRP, but completely translated in the cytoplasm and translocated via a post-translational pathway. In case of the post-translational transport, the nascent precursor protein is stabilized by binding to chaperones to avoid misfolding events and aggregation in the cytoplasm. In gram-negative bacteria the chaperone SecB is involved in the pathway (Steinberg *et al.*, 2018). The active transport of unfolded preproteins through the inner membrane is facilitated by the motor protein SecA, an ATPase which binds to SecYEG on the cytosolic side (Kusters and Driessen, 2011). SecA protein is abundant only in prokaryotic organisms and requires interactions with the anionic lipids like phosphatidylglycerol (PG) or cardiolipin for the high-affinity binding to the SecYEG translocon in order to transport the substrates (Breukink *et al.*, 1992; Kamel *et al.*, 2022; Koch *et al.*, 2016, 2019; Lill *et al.*, 1990)

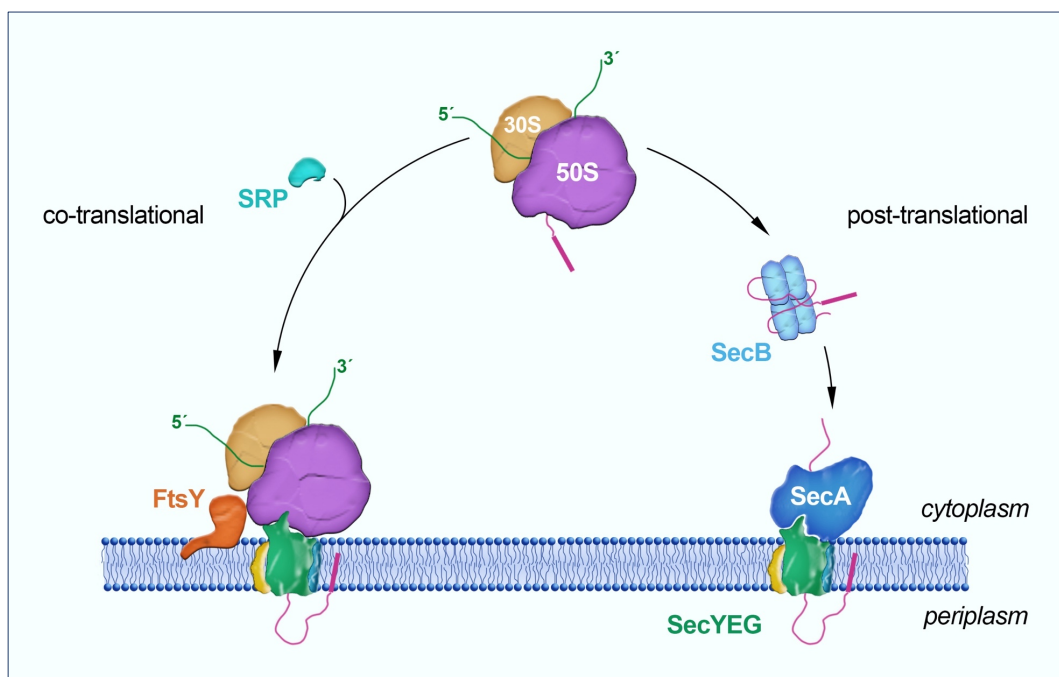


Figure 1.2: Scheme of SecYEG translocon-mediated co-translational and post-translational transport of pre-protein.

In the highly crowded cytoplasm of living cells targeting of newly synthesized proteins and their recognition at the membrane surfaces can become more than challenging. *In vitro* studies of membrane protein insertion and folding are commonly conducted under diluted conditions, with the aim to reduce protein:protein interactions or off-pathway compact intermediates and associated aggregation of highly hydrophobic proteins. As has been reported previously, the aggregation of the proteins increases in the crowded solutions (Breydo *et al.*, 2014; Ellis and Minton, 2003). The role of the chaperones for the stabilization of the unfolded form of newly translated proteins prior to translocation becomes critical. As machineries for targeting, translocation of secretory and insertion outer membrane proteins have been described in great detail (Oswald *et al.*, 2021; Rollauer *et al.*, 2015; Ye *et al.*, 2013) and the primary interactions are well-known, they offer a suitable model system for probing their functioning under crowded conditions. Stability studies performed with the precursor and the mature form of maltose binding protein (MBP) showed that addition of SecB chaperone could completely inhibit protein aggregation even in the crowded environment mediated by Ficoll-70. Addition of SecB led to disaggregation of the mature MBP, but not of the precursor form. However, direct binding of SecB to preMBP prevented a subsequent aggregation, while reducing the fraction of unfolded protein and supporting proper folding (Kulothungan *et al.*, 2009). However, no other study has addressed so far the dynamics of the Sec machinery in crowded environments, where a range of the essential protein:protein and protein:lipid interactions may be modulated by excluded volume and the quinary interactions.

### 1.3 Crowding sensors

Mimicking of the crowding *in vitro* may appear to be straightforward and simple. The estimates of the volume fraction occupancy or measurement of the diffusive behavior of probes in cells allow an application of the crowders in the similar range, which is true to a certain extent. As described above, the influence of macromolecular crowding depends on two factors, the excluded volume effect and quinary interactions between the macromolecules. The overall synergistic influence of the crowding in the living cells is defined by the amount, morphological characteristics of the solutes, like size and shape, as well as their surface properties. As the synthetic polymers can change their hydrodynamic radius as a function of polymer concentration and form aggregates (Junker *et al.*, 2019), the question arises whether the results from *in vitro* experiments can be correlated with the naturally occurring conditions. A complementary, possibly non-invasive method for the direct readout and quantification of the macromolecular confinement in cells and *in vitro* systems would be needed. For that purpose, a range of sensors has been lately developed for studying crowding levels under various conditions (Boersma *et al.*, 2015; Gnutt *et al.*, 2015; Liu *et al.*, 2017; Murade and Shubeita, 2019). The sensors were developed on the basis of Förster's resonance energy transfer (FRET) and exist in different configurations: The FRET-pair can be built up out of synthetic fluorophores or fluorescent proteins and the linker connecting the fluorescent moieties can be of synthetic (PEG polymer) or biomolecular origin, like single-strand nucleotides or sufficiently flexible polypeptide chains. Once placed in the crowded environment, either *in vivo* or *in vitro*, the sensor undergoes a steric compression by the co-solutes thus reducing the distance within the introduced FRET pair, so the crowding may be assessed and compared in various conditions.

However, the understanding of the quantity and the impact of crowding in the membrane and membrane interfaces remains largely uncertain. First attempts to probe the membrane crowding were done by employment of fusion constructs with glycoporphin A and fluorescent proteins forming a FRET pair, and the crowding-dependent dimerization of the glycoporphin was monitored by FRET (Chen *et al.*, 2010). Next to the crowding within the membrane, there is a need for a quick and simple evaluation of the induced confinement on the membrane upon simulation of the interfacial crowding. To this moment several solutions for the problem were proposed: Membrane-grafted PEG polymer with the attached donor fluorophore and the acceptor fluorophore present in the membrane can be applied for sensing of the induced steric confinement of the membrane interface, since the polymer will elongate with increasing crowder abundance leading to the decrease of the FRET signal (Houser *et al.*, 2020). Another approach to characterize the surface occupancy employs antibody binding to the antigen exposed on the crowded surface, as the efficiency of binding will depend on the amount of

crowder and generated the repulsive interaction (Takatori *et al.*, 2023). However, both approaches have specific limitations for application and measurement *in vivo* and on the biological membrane interfaces. Recently, another method was introduced to measure spatial heterogeneities on plasma membranes of living cells. Here the fluorescein isothiocyanate (FITC) fused to cholesterol anchors via PEG linker of various sizes can be inserted or reconstituted into the membrane. The quantification of effective binding avidity of anti-FITC IgG antibody serves as report being dependent on the antigen height and the surface crowding (Arnold *et al.*, 2023). These examples underscore the significant interest to explore novel methods for interfacial crowding characterization. In this thesis the new generation of genetically-encoded and membrane-adapted sensors with different application designs is presented which allows for monitoring of the *in vitro* crowding levels on the membrane and can be employed for the measurements in the living cells.

---

## 2 Aims of the thesis

The excluded volume and quinary interactions between macromolecules in the cytoplasm and at membranes influence thermodynamic and kinetic equilibria in the living cells.

The **first chapter** of this thesis provides a comprehensive overview of the effects of macromolecular crowding on biological membranes based on reviewing the available research literature (to early 2020). The consequences of the crowding with regard to peripheral protein and lateral protein diffusion in the crowded membranes, their oligomerization and clustering behavior as well as aggregation are summarized. Moreover, the significance of macromolecular crowding with regard to membrane deformations like membrane remodeling and fission are discussed. Additionally, Chapter 1 underlines an essential need for qualitative and quantitative characterization of the macromolecular crowding *in vivo*, i.e. the physiologically relevant environment and *in vitro*.

**The second and third chapter** of the thesis aimed to adapt the sensor developed by Boersma and coworkers (Boersma *et al.*, 2015) for the quantification of the crowding in the membrane proximity. For this, several designs of the sensor were developed: Appropriate hydrophobic anchoring domain was introduced and two different linking regions for the connection the transmembrane domain with fluorescent proteins were evaluated. Protocols for the protein isolation and anchoring for a stable incorporation of the sensor in the membrane were established. Finally, the sensor performance was characterized by employing diverse crowding agents of synthetic and proteinaceous origin and the first implementation of the sensor in the physiologically relevant environment was shown. In addition to the developed sensor constructs, different anchoring strategies and alternative sensor designs were proposed and characterized. In the third chapter of the thesis two different proteins, Mistic and transmembrane domains of RseC protein, were characterized as potential candidates for the membrane anchoring.

The biochemical research is most commonly conducted in diluted environments which do not represent the natural confinement of the biological systems. Based on the research data available on the effects of the crowding in the solution and in the biological membranes, it is assumed that the targeting and transport of proteins through SecYEG translocon from *E. coli* are also affected. The **fourth chapter** of this thesis aimed to elucidate the effects of macromolecular crowding on targeting and translocation of preprotein pOmpA via SecYEG channel under crowded conditions in terms of protein translocation activity and kinetics. Solution crowding was induced by synthetic polymers, e.g. Ficoll PM70 and PEG of different sizes, whereas the crowding on the membrane interface was mimicked by both synthetic and proteinaceous crowding agents. Furthermore, the interaction of the motor ATPase SecA with

## 2 Aims of the thesis

---

crowded and non-crowded membranes was evaluated by biochemical and biophysical methods.

## 3 Results

### 3.1 Effects of macromolecular crowding on biological membranes – Review publication

Title:	<b>The more the merrier: effects of macromolecular crowding on the structure and dynamics of biological membranes</b>
Authors:	Maryna Löwe, Milara Kalacheva, Arnold J. Boersma and Alexej Kedrov
Published in:	FEBS Journal (The FEBS Journal)
Impact factor:	5.62
Proportionate work:	70 %
Own contribution to this manuscript:	Literature research, writing and editing of the manuscript, preparing of figures 1-4.

# The more the merrier: effects of macromolecular crowding on the structure and dynamics of biological membranes

Maryna Löwe<sup>1</sup>, Milara Kalacheva<sup>2</sup>, Arnold J. Boersma<sup>2</sup> and Alexej Kedrov<sup>1</sup> 

<sup>1</sup> Synthetic Membrane Systems, Institute of Biochemistry, Heinrich Heine University Düsseldorf, Germany

<sup>2</sup> DWI Leibniz Institute for Interactive Materials, Aachen, Germany

## Keywords

anomalous diffusion; clustering; glycocalyx; intrinsically disordered proteins; membrane dynamics; membrane morphology; phase separation; protein:protein interactions; rafts; sensors

## Correspondence

A. Kedrov, Heinrich Heine University Düsseldorf, Düsseldorf, Germany  
 Tel: 0049 211 81 13731  
 E-mail: Kedrov@hhu.de  
 and

A. J. Boersma, DWI Leibniz Institute for Interactive Materials, Aachen, Germany  
 Tel: 0049 241 80 23335  
 E-mail: Boersma@dwil.rwth-aachen.de

(Received 21 February 2020, revised 18 May 2020, accepted 19 May 2020)

doi:10.1111/febs.15429

Proteins are essential and abundant components of cellular membranes. Being densely packed within the limited surface area, proteins fulfil essential tasks for life, which include transport, signalling and maintenance of cellular homeostasis. The high protein density promotes nonspecific interactions, which affect the dynamics of the membrane-associated processes, but also contribute to higher levels of membrane organization. Here, we provide a comprehensive summary of the most recent findings of diverse effects resulting from high protein densities in both living membranes and reconstituted systems and display why the crowding phenomenon should be considered and assessed when studying cellular pathways. Biochemical, biophysical and computational studies reveal effects of crowding on the translational mobility of proteins and lipids, oligomerization and clustering of integral membrane proteins, and also folding and aggregation of proteins at the lipid membrane interface. The effects of crowding pervade to larger length scales, where interfacial and transmembrane crowding shapes the lipid membrane. Finally, we discuss the design and development of fluorescence-based sensors for macromolecular crowding and the perspectives to use those in application to cellular membranes and suggest some emerging topics in studying crowding at biological interfaces.

## Introduction

Biological membranes are essential and intrinsically complex boundaries for individual cells and intracellular organelles. Amphipathic lipid molecules arranged into an anisotropic bilayer form the elementary membrane that is capable to prevent the passage of ions, polar solutes, and macromolecules, and to maintain the unique and specific luminal contents (Fig. 1A). Next to this barrier function, cellular membranes serve

as interfaces for biochemical reactions within vital cellular pathways, such as energy metabolism, signal transduction and transport processes, and the membrane organization largely determines the identity and functionality of the cells and their compartments [1,2]. The vast majority of functions are carried out by integral proteins, whose hydrophobic domains are stabilized by interactions with apolar acyl chains of lipids,

## Abbreviations

AFM, atomic force microscopy; AMPA,  $\alpha$ -amino-3-hydroxy-5-methyl-4-isoxazolepropionic acid; BAM,  $\beta$ -barrel assembly machinery; BSA, bovine serum albumin; CCT, CTP-phosphocholine cytidyltransferase; cryo-ET, cryo-electron tomography; ENTH, Epsin N-terminal homology domain; ER, endoplasmic reticulum; ESCRT, endosomal sorting complexes required for transport; FCS, fluorescence correlation spectroscopy; FP, fluorescent protein; FRET, Förster's resonance energy transfer; GFP, green fluorescent protein; GPCR, G protein-coupled receptor; GPMV, giant plasma membrane vesicle; GUV, giant unilamellar vesicle; IDR, intrinsically disordered region; IDP, intrinsically disordered protein; LD, lipid droplet; LHC, light-harvesting complex; LUV, large unilamellar vesicle; NMDA, N-Methyl-D-aspartate; OMP, outer membrane protein; PEG, polyethylene glycol; PSD, postsynaptic density; RBC, red blood cell; SPT, single-particle tracking; TMH, transmembrane helix; UPR, unfolded protein response.

but also peripheral proteins that are adsorbed on the membrane via interactions with lipids or membrane-embedded proteins [3].

While the research on cytoplasmic proteins and their functional networks continuously flourished over the last half a century, the understanding of the membrane spatial organization lagged far behind. The early ‘fluid mosaic model’ of the membrane, which implied that proteins freely diffuse in the lateral directions within the fluid-like membrane, was based on the sparse data available on the membrane structure and dynamics (Fig. 1A) [4,5]. The model dominated the following decades, until technical developments in biophysical techniques, such as fluorescence, electron and atomic force microscopy, but also high-resolution proteomics and lipidomics, made it possible to visualize the actual complexity of the cellular membranes [6–12]. Today, cellular membranes are seen as heterogeneous mosaic environments, where structurally distinct domains with sizes ranging from tens of nanometers to micrometers serve as platforms for specific reactions, such as cell adhesion [13], chemoreception [14] or signalling [15].

### The intrinsic complexity of cellular membranes

Both the phospholipid and the protein contents of cellular membranes are highly diverse and dynamic: in a single eukaryotic cell, hundreds of different lipid structures are unevenly distributed between organelles, and up to 25% of proteins synthesized in cells are inserted into membranes in a broad range of topologies [1,16]. The lipid composition greatly determines physico-chemical properties of the membrane, such as fluidity, curvature and the asymmetric charge distribution. In the most general view, the endoplasmic reticulum (ER) membrane is relatively thin and loosely packed, while the plasma membrane is a rigid interface of a higher thickness, as determined by abundant sphingolipids and sterol molecules. Notably, the difference in the membrane composition between organelles is maintained despite the extensive vesicle trafficking, and the decisive sorting takes place within Golgi complex [2]. Fundamental roles of the lipids in the spatial organization of the membrane proteome have been revealed over the last two decades. Sphingolipids and sterol molecules abundant in the plasma membrane facilitate the separation of ordered and disordered phases at the

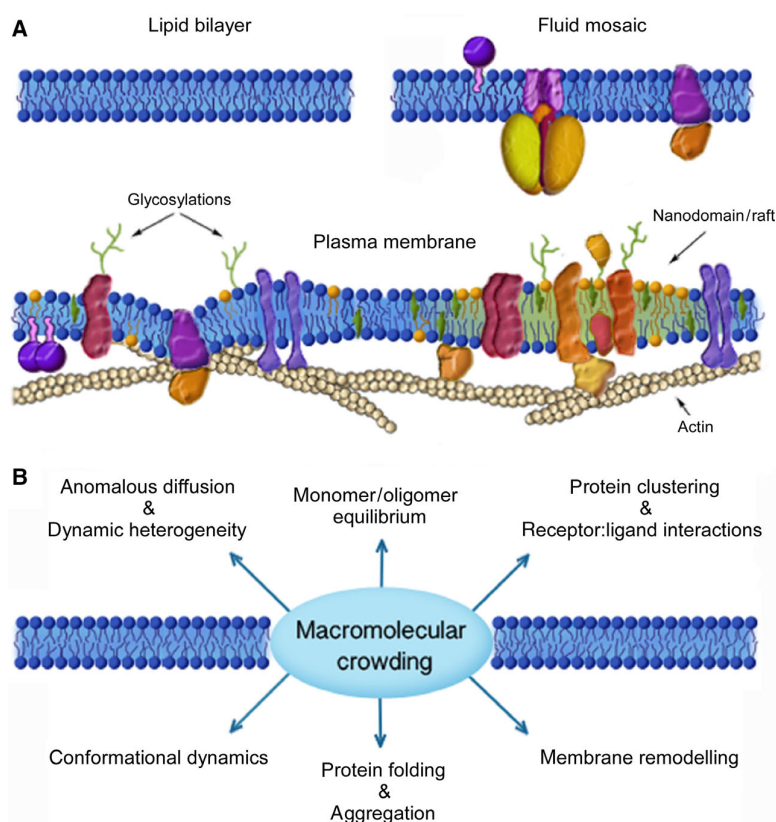


**Fig. 1.** Complexity of biological membranes. (A) Lipid bilayer (left) is an essential basis of a biological membrane. The membrane identity and functioning are determined by the composition of lipid molecules and proteins incorporated and anchored at the lipid bilayer. Low protein density is approximated by the ‘fluid mosaic’ model (right), while dense and specifically organized mosaic packing is commonly observed in membranes of living cells (bottom). Extensive interactions with the actin cytoskeleton affect the plasma membrane dynamics, and specific lipid: protein interactions build the ground for the assembly of densely packed membrane nanodomains, or rafts. (B) Macromolecular crowding affects a broad range of processes in biological membranes and contributes to the membrane morphology.

submicron scale and ensure the assembly of the functional raft domains with specific composition of densely packed proteins [6]. These domains are stabilized via protein:protein and protein:lipid interactions, as well as contacts with the cytoskeleton at the cytoplasmic side of the membrane (Fig. 1A), and their organization, dynamics and regulation have been recently reviewed elsewhere [15,17]. Furthermore, organelle-specific membrane thickness appears to determine the localization of integral membrane proteins along the trafficking pathway, so the optimal matching is achieved between the acyl chains and the hydrophobic transmembrane domains [18].

Membrane proteins constitute large part of cellular membranes and include not only integral proteins with transmembrane domains, but also soluble proteins peripherally bound to lipid leaflets via lipid anchors, hydrophobic interfaces or amphipathic helices, or docked on transmembrane proteins to form functional complexes [19,20]. The membrane proteome is highly dynamic, and substantial changes upon the development of pathologies, viral infections and between primary and immortalized cell cultures have been described [21–23]. Being abundant, membrane proteins may dominate the total membrane mass. Differences in membrane proteomes and protein abundance build a basis for the fractionation analysis of cellular organelles [24]. Literature provides several estimates for the area occupied by proteins in cellular membranes. In red blood cells (RBCs), one of the simplest mammalian cell types, transmembrane proteins such as the band 3 anion transporters and glycophorins occupy approximately 25% of the cellular membrane area, as suggested by the buoyant density and the dry mass measurements [25]. In a comprehensive analysis, the composition and the architecture of a synaptic vesicle from rat brain were described, offering an average protein:lipid mass ratio of 2 : 1 [26]. Data available on immortalized cell lines show a membrane protein occupancy around 40 000 to 50 000 per  $\mu\text{m}^2$  in HeLa cells [21]. Alike, analysis of the protein synthesis rate and the density of the Golgi apparatus and ER membranes in hamster kidney cells provided estimates of around 30 000 to 40 000 individual membrane proteins per  $\mu\text{m}^2$  [27].

It is important to emphasize the diversity of protein densities naturally occurring in different cell types and even on individual membranes within the single cell [22]. Specialized membranes or mesoscopic membrane domains commonly demonstrate higher protein densities, as those may be beneficial for assembly of functional complexes within the membrane and at the membrane interface. High protein density, 40 to 50%

of the surface area, was reported for the inner mitochondrial membranes based on electrophoretic displacement experiments [28]. The density roughly corresponds to an average protein:lipid mass ratio of 4 : 1, with a substantial contribution of protein extramembrane domains, such as  $F_1$  component of the ATP synthase. The density of rhodopsin packed in the specialized rod outer segment disc membranes is estimated to be 30 000 to 55 000 monomers per  $\mu\text{m}^2$ . This density corresponds to 50% of the surface area, using a monomer surface area of approximately  $10 \text{ nm}^2$ , in agreement with atomic force microscopy (AFM) imaging [29]. Probably, the highest degree of protein packing of  $\sim 80\%$  is reached in plant thylakoid membranes and phototrophic microorganisms, where the high density of the light-harvesting complexes (LHCs) and reaction centres is vital for the efficient electron transfer within photosynthetic units [30,31].

### Macromolecular crowding in solution and in the membranes

Macromolecular crowding has been commonly associated with the cytoplasm that contains a dense and highly diverse pool of macromolecules, the largest share of which are proteins and nucleic acids. The total concentration of macromolecules seen as crowding agents, or *crowders*, varies between 50 and  $400 \text{ g}\cdot\text{L}^{-1}$ , depending on cell type [32,33]. Both in solution and in the membrane, the crowders nonspecifically exclude volume from other cosolutes, providing an entropic penalty for larger cosolutes and reducing their configurational entropy [34]. The system attempts to reach a thermodynamic state of maximum entropy by providing more space to the crowders, which is commonly achieved by reducing the volume of another process. In addition to these steric excluded volume effect, crowders present ample surface to interact promiscuously by noncovalent interactions. Hydrogen-bonding, hydrophobic, electrostatic and van der Waals interactions with other macromolecules, often referred as *soft* or *quinary interactions*, provide additional attractive and repulsive forces [35]. Different nature and shapes of crowders modulate the intermolecular interactions, but may also contribute to the change of the solvent properties, enhancing the effective intracellular viscosity and perturbed, or *anomalous*, diffusion [36,37]. Together, these contributions modulate translational mobility, conformational dynamics, assembly and functionality of macromolecules, determining the cellular organization and homeostasis. A multitude of effects of crowding on protein aggregation, folding, stability and oligomerization as well as catalytic

activity of enzymes and protein:protein interactions in solution has been documented and extensively reviewed elsewhere [34–36,38–40]. However, these effects, in particular the contribution of the quinary interactions, remain hard to predict because they depend on the size, shape, concentration of both the crowder and the biochemical reaction under investigation [36,41–43].

When the complexity and the patchwork-like organization of cellular membranes became evident, the significance of macromolecular crowding for the membrane-associated processes was rapidly anticipated, and the steadily accumulated data from multidisciplinary studies since reveal the diverse manifestations of crowding [44,45]. The consequences of macromolecular crowding in membranes and their interfaces may be more complex than observed in the solution due to the lipid membrane anisotropy and asymmetry observed in living cells [46]. Although smaller than proteins, lipids cannot be compared to water as a solvent and should also be seen as crowders, which extensively interact with embedded proteins via hydrophobic and electrostatic interactions. *Vice versa*, abundant proteins are changing the membrane structure within the hydrophobic core and at the polar interface, with a putative effect on the proximate aqueous solvent. Even at low protein:lipid ratios, the mobility of proteins within the lipid bilayer is limited to two-dimensional diffusion and it is largely determined by the bilayer viscosity [47]. Furthermore, lipid dimensions and physico-chemical properties may lead to sorting and clustering of membrane proteins in a concentration-dependent manner [18,48]. On the other hand, membrane proteins interfere with and restructure their proximal lipid environment, and protein crowding in lipid membranes may cause immense changes in the lipid packing and the membrane morphology. Finally, macromolecular crowding in the aqueous phase affects interactions at the membrane as well. It enhances protein adsorption to the membrane, affects their assembly and dynamics, and ultimately modulates biochemical pathways, as it is described throughout this Review.

#### Mimetics of macromolecular crowding for *in vitro* studies

Simplified and well-defined model systems allow scrutinizing complex effects of macromolecular crowding. Diverse crowders can be included in biochemical reactions *in vitro* with physiological relevant volume fractions [36]. A good rule of thumb is that the crowder should be smaller than the protein under investigation

but much larger than the solvent molecule to obtain the most substantial effects. A common crowder is the synthetic polyethylene glycol (PEG), which is a water-soluble linear polymer available in different sizes. Another common crowder is Ficoll, a chemically cross-linked sucrose-based polymer. Ficoll is well hydrated and usually assumed to be roughly spherical with fewer interactions with biomolecules than PEG. Dextran is a sugar-based polymer with varying degrees of branching, depending on the origin species. Protein-based crowders should be somewhat more relevant to understand *in vivo* crowding as they are able to mimic the surface heterogeneity of biological macromolecules. Inert proteins, like bovine serum albumin (BSA) or lysozyme, can be considered for crowding studies since they are available in the sufficient amounts and can be concentrated to naturally abundant crowding levels [43,49]. However, crowding studies *in vitro* should be interpreted with care. Concentrating crowders may lead to decrease in effective crowder radius [50], or self-association and phase separations [51,52], which are not always easily detectable but can deviate crowding effects. Furthermore, induced effects are often specific for a crowder and may arise from quinary interactions with the molecule under investigation [41], and the complexity in these interactions as well as the challenges to scrutinize those experimentally have been recently reviewed elsewhere [35,36,53]. Hence, to draw a general conclusion on the effect of crowding, different crowders need to be compared to determine the contributions of the excluded volume and soft interactions.

Synthetic lipid membranes offer a competitive tool to study dynamics of proteins and lipids in a well-defined, although their simplified environment lacks the physiological complexity of protein and lipid composition. Synthetic membranes have been extensively employed to study effects of macromolecular crowding in biochemical and biophysical experiments, and several approaches to mimic abundance of macromolecules have been implemented up to date. As described below, a broad range of studies has been focused on effects of crowding at the membrane interfaces, when anchoring solvent-exposed macromolecules to the membrane surface at varying densities. Different soluble proteins could be docked via specific bonds with functional head groups of synthetic lipids, for example streptavidin:biotin or polyhistidine: $\text{Ni}^{2+}$ -NTA interactions [54,55]. Alternatively, commercially available conjugates of PEGs with lipid molecules are reconstituted into lipid bilayers at defined ratios to mimic crowding at the interface [56], while considering that loosely coiled PEG molecules may block protein:

lipid interactions [57] or build up interactions with hydrophobic and nonpolar side chains of solvated proteins [38]. Aiming to study crowding effects within the lipid membrane core, purified integral membrane proteins or detergent-stabilized extracts from cellular membranes are reconstituted into synthetic lipid bilayers at varying densities [58–60], though careful controlling for potential protein aggregation is required. On the other hand, native biological membranes, such as giant plasma membrane vesicles (GPMVs), or isolated organelle membranes can be used to monitor the dynamics of proteins and lipids down to single-molecule level, for example by means of fluorescent microscopy [46,61], but also intact cells with overexpressed membrane proteins have been successfully employed to probe the physiological effects of crowding [62].

In this review, we summarize findings from biochemical, biophysical and computational studies, which show the multifaceted effects of macromolecular crowding on membrane-associated processes. We describe the translational mobility of proteins and lipids within crowded membranes and sum up observations on how the crowding modulates the oligomeric state and clustering of integral membrane proteins. Further, we focus on dynamics of membrane-associated proteins under crowded conditions and specifically address the effects of crowding on membrane transport processes. We also present the most recent findings on the role of crowding-induced entropic forces in shaping the lipid membrane. Finally, we discuss the design and development of fluorescence-based sensors for macromolecular crowding and the perspectives to use those in application to cellular membranes.

## Diffusion in crowded membranes and at the interfaces

### Two-dimensional diffusion in lipid membranes

Translational mobility of macromolecules determines the kinetics and equilibria of larger complex assembly and interactions of proteins with substrates. The translational mobility of lipids and proteins within the cellular membrane is limited to two-dimensional diffusion, with an exception for relatively rare events of topology inversion. Upon Brownian motion of molecules, their mean square displacement  $\langle r^2 \rangle$  is proportional to time  $t$  and the diffusion coefficient  $D$  (Fig. 2A). According to Saffman–Delbrück model [47],  $D$  of a particle, protein or lipid, within the idealized fluid membrane is largely determined by the viscosity of the membrane ( $\mu_m \sim 0.05\text{--}0.1 \text{ Pa}\cdot\text{s}$ , [63,64]) and weakly influenced by the low viscosity of the

surrounding medium.  $D$  shows a linear dependence on the depth of embedding into the membrane ( $h$ ) and a logarithmic dependence on the particle radius ( $R$ ) (Fig. 2A). The particle radius for the transmembrane protein is determined not only by its own structure, but also by the tightly associated annular lipid shell [65,66]. Validity of Saffman–Delbrück model was experimentally confirmed, for example, by measuring diffusion coefficients of membrane proteins of different sizes of diffusion in homogeneous lipid bilayers at low protein:lipid ratios [58,64].

However, Saffman–Delbrück model does not account for the heterogeneous composition of native cellular membranes and specific protein:lipid contacts, which may occur even in model membranes. For instance, individual membrane proteins change their mobility when forming clusters together with the proximal solvating lipids [66,67]. Changes in the membrane thickness and the associated hydrophobic mismatch between lipids and incorporated proteins can modulate the diffusion behaviour in a complicated manner, up to the transition from a weak dependence  $D \sim \ln(1/R)$  to the more pronounced size-dependent Stokes-like diffusion, where  $D \sim 1/R$  [45,67–69]. Interactions of the membrane-embedded proteins with the cytoskeleton and confinement induced by protein crowding in cellular membranes further lead to subdiffusion (Fig. 2B). To characterize those deviations from the Brownian diffusion, an anomalous diffusion parameter  $\alpha$  is introduced when analysing the molecule displacement (Fig. 2B). For the Brownian diffusion,  $\alpha$  equals 1, but it is lower for the confined motion, which is a common case in cellular, but also model membranes. As elaborate descriptions and analyses of diffusion processes in the membrane have been broadly reviewed [45,70–72], we will briefly outline here how macromolecular crowding modulates translational dynamics within the membrane plane.

### Macromolecular crowding hinders the lateral mobility in membranes

The effect of a densely packed environment on protein mobility was illustrated by an early study of bacteriorhodopsin in reconstituted liposomes via fluorescence microphotolysis [73]. The diffusion coefficient of the protein was reduced by 20-fold upon increasing the protein:lipid ratio from 1 : 210 up to 1 : 30. The effect could not be assigned solely to changes in the membrane viscosity but implied steric hindrance within the crowded membrane. The conclusion was corroborated by studies *in vivo*. As one example, diffusion of transmembrane and peripherally bound proteins was

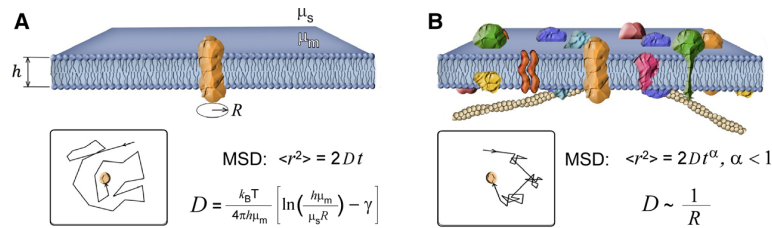


**Fig. 2.** Non-Brownian diffusion in crowded membranes. (A) A particle (brown) demonstrates Brownian diffusion within an idealized homogeneous membrane, as illustrated by its trajectory (below). The mean square displacement (MSD) of the particle linearly depends on the diffusion coefficient  $D$  and time  $t$ . Diffusion coefficient  $D$  is approximated by the Saffman-Debrueck model and shows a weak logarithmic dependence of the particle size  $R$ , but also depends on the viscosity of the membrane ( $\mu_m$ ) and solvent ( $\mu_s$ ) and the depth of the membrane anchoring  $h$ .  $\gamma$  is Euler constant. (B) Within the nonhomogeneous and/or crowded membrane, a particle may experience transient confinement events and deviate from Brownian diffusion, so the anomalous diffusion parameter  $\alpha$  is below 1. The diffusion coefficient  $D$  in the crowded membrane may strongly depend on the particle size.

strongly affected upon changing the membrane protein density in COS-7 cells [74]. More recently, high-sensitivity approaches have made it possible to characterize diffusion in more detail. In particular, diffusion of proteins and lipids in membranes of giant unilamellar vesicles (GUVs) was systematically analysed by fluorescence correlation spectroscopy (FCS) upon varying the protein:lipid ratio [58]. The experiment showed a linear decrease in the diffusion coefficients of several  $\alpha$ -helical membrane proteins, but also lipids, upon increasing the protein content. The study suggested a modest contribution of the anomalous diffusion ( $\alpha \sim 0.9$ ) for the highest protein density examined (molar protein:lipid ratio of 1 : 1500) but anticipated further reduction in the mobility upon increasing the protein content towards the naturally occurring levels. GPMVs detached from the cell surface upon a chemical treatment offer a competitive, physiologically relevant mimetic of a cellular membrane [75]. GPMVs are characterized by a high protein content, but lack the membrane-associated cytoskeleton. Diffusion of proteins and lipids within the GPMV membrane is reduced 3- to 5-fold in comparison with GUVs, likely due to the higher protein density [76,77]. However, limited protein:protein and protein:lipid cross-linking upon the GPMV formation may also have an influence on the dynamics and mobility within the membrane [75].

### Origins of anomalous diffusion in crowded membranes

Single-molecule imaging techniques, in particular, single-particle tracking (SPT) and high-speed AFM [78–80], reveal further details of lipid and protein diffusion in native and model membranes. Surprisingly, even

simple systems, such as a homogeneous lipid membrane, may manifest a substantial dynamic heterogeneity at the single-molecule level: individual lipid molecules were observed in two mobility modes with characteristic diffusion coefficients of 0.07 and 4.4  $\mu\text{m}^2/\text{s}$ , suggesting a nonuniform structure of the membrane, where local ‘corrals’ areas with a diameter of 100–200 nm exist [78]. Cellular membranes provide a more complex matrix for protein diffusion, where the heterogeneity of the protein and lipid content is accompanied by interactions with the tethered actin cytoskeleton, forming a so-called picket fence structure [17,81,82], and the actin:membrane tether points are commonly associated with densely packed raft nanodomains [83,84]. Protein diffusion in the cellular plasma membrane occurs at lower rates than in corresponding GPMVs, which lack the cytoskeleton [77], and the effect of minimal actin cortex on the lateral diffusion and lipid organization can be reconstituted *in vitro* [85,86]. SPT in native plasma membranes revealed a ‘hop diffusion’ for proteins trapped within 200–500 nm-sized membrane areas defined by the actin mesh. Proteins were able to cross, or ‘hop over’ the actin barrier and get into a neighbouring ‘cage’, and their diffusion was sensitive to the dynamic actin remodelling [81,87,88]. Complementary to fluorescence-based detection, high-speed AFM visualizes single proteins in the native environment down to subnanometer resolution based on variations in their height in time frames below 100 ms [80]. High-speed AFM was employed to characterize lateral movements of label-free outer membrane protein (OMP) OmpF reconstituted in model membranes at a high density, where the proteins occupied  $\sim 50\%$  of the membrane surface [89]. Distinct diffusion modes were observed for OmpF trimers: a substantial fraction of protein

was found to be nearly immobile and preferentially assembled into large clusters. At the same time, individual porins showed increased displacement velocity up to  $15 \text{ nm}\cdot\text{s}^{-1}$  and could switch between a freely diffusing state and being associated with OmpF clusters. Collisional interactions of individual porins with clusters led to rearrangements within the membrane, and the dynamic heterogeneity in diffusion of single molecules determined a static heterogeneity at the mesoscopic level. Later studies performed with lysenin, a pore-forming protein, revealed up to four distinct diffusion regimes within the densely packed protein arrays at the membrane interface [60]. Lysenins captured by their neighbouring molecules formed a solid and sliding glass-like phase, where proteins can be trapped over several minutes, while the average residence time in the nonhampered state was shorter than 10 s.

Multiple simulation studies on the atomic and coarse-grained levels corroborate the drastic decrease in the lipid and protein mobility upon increasing the protein concentration [90–93]. These studies predict anomalous diffusion and pronounced deviations from Saffman–Delbrück model towards Stokes-like dependence of the diffusion coefficient on the molecular size. Large protein:lipid clusters observed in simulations substantially affect the diffusion: when individual molecules transiently interact with clusters, their mobility is temporarily hindered. The resulting dynamic heterogeneity determines the pronounced Stokes-like diffusion of proteins at the native-like protein:lipid ratios from 1 : 300 and higher [93]. Thus, the mobility of membrane-embedded proteins has a stronger size dependence at the physiological levels of crowding: proteins with smaller radii can neglect the effect of lateral confinement more efficiently in comparison with the larger species, and diffusion of proteins clusters  $> 10 \text{ nm}$  in diameter will be significantly hindered [94]. Reduction in net mobility and an increased contribution of the anomalous diffusion in crowded lipid membranes are also observed for transmembrane  $\beta$ -barrel proteins. Coarse-grained simulations suggested that the diffusion rates of lipids reduced by approximately twofold, from 8 to  $4\cdot 10^{-7} \text{ cm}^2\cdot\text{s}^{-1}$ , and the parameter  $\alpha$  dropped to 0.8 when the sizable  $\beta$ -barrel OMPs OmpF or FhuA of *E. coli* occupied 40% of the membrane surface area [91]. The lateral mobility of the proteins themselves decreased linearly with the increasing packing density, which could be attributed to transient collisional protein:protein interactions in agreement with experimental observations [89]. Increasing the protein density led to the

almost complete immobilization of FhuA because the protein readily formed large clusters, as described in the following chapters.

Formation of densely packed membrane protein clusters raises a challenge for the quality control and repair/degradation of damaged or misfolded proteins, as in the case of the large LHCs in photosynthetic membranes [30,31]. One described recycling mechanism is based on the phosphorylation and disassembly of the damaged complexes within the densely packed regions of grana membranes [95]. Higher mobility of individual subunits allows them to diffuse out of the crowded environment and accumulate at the peripheral grana margins. These highly curved membrane areas are enriched with the quality control components such as Deg and FtsH proteases, which serve for degradation or recycling of the LHC subunits. The nascent LHCs are assembled in the less crowded stroma membrane and localize to the grana upon the lateral diffusion, where they are stably embedded via protein:protein and protein:lipid interactions.

#### Diffusion of peripheral membrane proteins

Although much less studied, the lateral diffusion of peripheral proteins is also sensitive to the crowding level. According to Saffman–Delbrück model (Fig. 2A), the mobility of peripheral proteins should be higher than for integral membrane proteins, due to limited interactions with the viscous lipid bilayer. Indeed, the diffusion coefficient  $D \approx 2 \mu\text{m}^2/\text{s}$  determined by FCS for the membrane-anchored avidin, a protein of 60 kDa, in a planar lipid bilayer could be compared to that of highly mobile lipid molecules, despite  $\sim 100$ -fold difference in their molecular masses [55]. Increasing the avidin density led to anomalous diffusion, once the protein occupied as little as 5% of the membrane surface – a threshold remarkably close to the one observed for integral membrane proteins [58]. The anomalous diffusion parameter approached 0.7 at higher concentrations of avidin, though the enhanced crowding was accompanied with the phase separation at the membrane interface [55]. Diffusion at the crowded membrane interface was further studied by Stachowiak and coworkers [96]. Soluble polyhistidine-tagged proteins of sizes ranging from 5 to 150 kDa were anchored to synthetic  $\text{Ni}^{2+}$ -NTA chelating lipid groups within the supported lipid bilayer. The protein density could be tuned by changing the abundance of the chelating lipids. Upon switching from the diluted to the densely packed state, an approx. 7-fold decrease in diffusion coefficients was measured by FCS for all

studied proteins. The diffusion coefficients were inversely proportional to the peripheral protein density at the membrane interface rather than the size of the diffusing particle. It must be noted here that increasing the density of macromolecules, such as peripheral proteins or coiled polymers, at one of the membrane leaflets may cause the membrane deformation, either due to changes in the leaflet area upon binding or due to steric repulsion between bulky moieties at the interface. The effects of the peripheral crowding on the membrane morphology *in vitro* and *in vivo* are discussed in details below.

Experimental observations made in diverse model systems confirm that the high density of protein packing within the lipid membrane and at the interface has a prominent effect on the lateral diffusion of proteins, but also lipids. The non-Brownian mobility and decreased diffusion coefficients reflect hindrances for the lateral diffusion due to extensive interactions within the nonhomogeneous crowded membrane or with the proximate cytoskeleton cortex. The membrane complexity causes dynamic heterogeneity of diffusion as individual molecules switch between confined to freely diffusing states. Enhanced transient interactions within the crowded membrane may be important for the assembly of functionally important protein clusters and oligomers, as discussed below.

### Quaternary structure of proteins in crowded membranes

The functionality of soluble and membrane proteins often depends on their association into homo- or heterooligomeric complexes. The apparent affinity of the interaction is modulated by naturally occurring crowding via the excluded volume effect and either attractive or repulsive quinary interactions [43]. However, crowding changes the lateral diffusion with an effect on the kinetics of protein complex assembly [97]. The concentration-dependent oligomerization of membrane proteins has been reported in several *in silico* studies for systems composed of lipids and proteins at varying densities, so that the effect of the excluded volume on protein:protein interactions could be examined [91,98,99]. It should be noted though, that similar to ‘wet-lab’ studies on macromolecular crowding, the developments of computational modelling of those processes are still in their early phase. Thus, suboptimally tuned force fields may result in non-native oligomeric structures and excessive irreversible aggregation of protein in simulated membranes [100,101].

### Oligomerization of $\beta$ -barrel membrane proteins

The simulations of  $\beta$ -barrel proteins from the outer membrane of *E. coli* suggested that their propensity to form clusters within the lipid bilayer varied substantially, being the highest for the iron transporter FhuA [91]. In contrast, the intrinsically trimeric porin OmpF was not able to assemble into higher oligomers in small-scale simulations. However, elongated clusters were reported for the more extensive micrometer-sized membranes [91,102]. The clustering of OMPs was mediated by aromatic and hydrophobic amino acid residues and lacked the specificity in geometry. Therefore, formed oligomers were heterogeneous in protomer orientation, and also clusters of different OMPs could be observed, while transmembrane  $\alpha$ -helices (TMHs) were excluded from the interaction [102,103]. Notably, high-resolution imaging of the outer membrane of *E. coli* revealed large proteinaceous ‘islands’ of 500 nm in diameter. These islands were centred around BAM complexes involved in the insertion of nascent proteins, and they also induced clustering of proteins in the inner membrane *via* proteinaceous bridges [103,104]. The OMP ‘islands’ diffused passively to the cell poles before the division; hence, these ageing proteins were distributed unequally between daughter cells. Thus, the propensity of OMPs to form large clusters in the crowded membrane could be crucial for the protein turnover in the bacterial outer membranes.

### Oligomerization of $\alpha$ -helical membrane proteins

The effects of the crowded environment on protein:protein interactions were experimentally probed for glycophorin A (GpA, single TMH), the abundant membrane protein in RBCs and G protein-coupled receptors (GPCRs, 7 TMHs). GpA oligomerization was studied in RBC-extracted vesicles as a reliable mimic of the cellular membrane [105]. Measuring Förster’s resonance energy transfer (FRET) efficiency between fluorescent proteins (FPs) genetically fused to GpA revealed an equilibrium between GpA monomers and dimers. The monomer fraction ranged between 20 and 70%, which depended on GpA expression levels. GpA exists solely as a dimer in detergent micelles and reconstituted proteoliposomes, and hence, the heterologous crowding in cellular membranes reduced the apparent affinity of GpA assembly, and could be a vital factor tuning protein:protein interactions in the lipid environment. This hypothesis was further supported by direct measurements of the GpA dimer stability in membranes [59]. To this end, biotinylated

GpAs were coupled to bulky monovalent streptavidin molecules at the membrane interface, so that only one protomer within a GpA dimer could bind streptavidin. At the same time, the other site on the GpA dimer was not accessible due to the steric overlap. The shielded site occasionally opened by dimer dissociation, so that the dimer kinetic stability determined the efficiency of GpA-biotin:streptavidin assembly. The elegant assay was employed to study whether the GpA dimer was affected by a native-like crowding mimicked by co-reconstituted membrane protein extract from *E. coli*. The experiments revealed a substantial destabilization of GpA dimers by  $5 \text{ kcal}\cdot\text{mol}^{-1}$  when the crowders were present at relatively low protein:lipid mass ratio of 1 : 7. The effect was attributed to competition for the binding surface of GpA with other potential protein partners in the crowded membrane. Those quinary interactions could involve common dimerization motifs, such as GxxxG glycine zippers within TMHs [106]. On the other hand, elevated crowding and large excluded volume within the ER membrane may trigger the oligomerization of Ire1 sensor kinases and promote the unfolded protein response (UPR) [107]. Contacts between the luminal domains of Ire1 protomers mediate the oligomerization of this single-pass membrane protein. Oligomerization is triggered by interactions of Ire1 with unfolded proteins in the ER lumen, but also by the stress within the lipid membrane that attenuates the topology of the amphipathic helix within the kinase [107,108]. A similar effect on the amphipathic helix can be achieved by increasing the apparent protein density in ER, for example, upon the accumulation of saturated lipids and the formation of protein-depleted islands: the islands and the expelled membrane proteins contribute to the excluded volume within the ER membrane and correlate with Ire1 clustering and UPR activation [109].

GPCRs are the most abundant class of eukaryotic membrane receptors with utmost biomedical importance. Their oligomerization has been considered as a general mechanism to tune the signal transduction [110]. In contrast to structural studies, where only monomers of GPCRs have been visualized despite being trapped in different functional states, homo- and heterodimers and higher oligomers have been observed in cellular membranes. GPCRs are often found in segregated clusters within cellular membranes, where their density may influence their quaternary dynamics and function. The abundance levels of GPCRs of different classes may define the balance between homo- and heterooligomers. Coarse-grained simulations of the sphingosine-1-phosphate receptor 1 (S1P1) in a native-like

asymmetric lipid membrane revealed rapid dimer formation, which involved approximately 20% of GPCRs [90]. The dimer fraction remained in a dynamic equilibrium with S1P1 monomers along the simulation time, while both symmetric and asymmetric orientation of protomers were observed. FRET-based analysis in simplified liposomal membranes confirmed that formation and dissociation of dimers and higher oligomers is a highly dynamic process, and the association energy is a GPCR-specific parameter that varied between  $3.9 \text{ kcal}\cdot\text{mol}^{-1}$  for  $\beta_2$ -AR adrenergic receptor and  $-15 \text{ kcal}\cdot\text{mol}^{-1}$  for cannabinoid receptor type 1 [111]. Importantly, the fraction of homooligomers depended on the density of receptors in the membrane, with an exception for rhodopsin, which could be detected only as a homodimer, which has the lowest association energy. It should be noted that reducing the density of rhodopsin molecules in native rod disk membranes by 50% accelerated the flash response of the receptor by 1.7-fold. Thus, the high-density packing within the specialized membrane suppresses the conformational dynamics, but likely enhances the photon capture efficiency [112].

In brief, the excluded volume generated by transmembrane crowders thus promotes clustering of membrane proteins. Sterically confined proteins may then assemble into functional oligomers of a specific geometry or function within large phase separated clusters [113]. Differently, quinary interactions with crowders are capable to compete with specific protein contacts and greatly reduce their stability. To ensure the efficient protein:protein assembly under natively crowded conditions, specific lipid molecules, such as cardiolipin, cofactors or axillary protein subunits and the cytoskeleton may contribute to the binding interfaces and stabilize functional oligomers in cellular membranes.

### Cluster assembly and recognition reactions at the membrane interface

Clustering of dedicated proteins, cadherins and integrins, at focal adhesions within the plasma membrane, is crucial to mediate cell:cell and cell:surface interactions [114]. While the cytoskeleton contributes to the assembly and the stability of these clusters, membrane proteins not involved in the adhesion should be expelled from the contact areas. Similarly, protein segregation takes place within membranes of the immunological synapse. When a contact focus between a T cell and major histocompatibility complexes of an infected cell is built, clustered T-cell receptors cause the local exclusion of other membrane proteins, such as CD45

phosphatase [115,116]. The formed membrane domains enriched with the receptors cannot be categorized as rafts due to the absence of conventional markers, and their assembly principles are not fully understood. A simple mechanism based on crowding and size-dependent protein segregation has been recently derived from a model system, where modular binding and nonbinding proteins were reconstituted into opposing GUVs to study membrane:membrane interactions and protein localization at the interface [117]. The length and the density of reconstituted proteins were altered systematically, and the protein enrichment at the intermembrane contact interface was subsequently quantified. Coupled binding proteins from opposing membranes accumulated at the adhesion interface. Their length, and therefore the intermembrane distance within the adhesion area, set a threshold on the dimensions of nonbinding proteins allowed to partition. Nonbinding proteins, which long extramembrane domains exceeded the intermembrane distance, were largely expelled from the adhesion interface or might be engulfed into the membrane invaginations, once the membrane deformation was possible. This model-based mechanism translates to cellular systems in the example of clustered T-cell receptors and isoforms of CD45 reconstituted into GUVs [118]. Potential lateral *cis*-interactions between the enriched binding proteins [119] and recruitment of specific accessory proteins to the adhesion interfaces further contribute to the excluded volume effect and reduce the accessible area within the adhesion. Therefore, nonbinding proteins are preferentially distributed over the free-standing membrane in a size-dependent manner.

### Receptor clustering is mediated by crowding in solution

The postsynaptic density (PSD) within a synapse is another example of a crowded membrane interface, where the ubiquitous receptors of neurotransmitters, such as glutamate, NMDA and AMPA, ensure the transduction of the signal across the membrane to initiate the response cascade (Fig. 3) [120]. Early electron microscopy images visualized PSD as a layer of ~ 25 nm at the cytoplasmic side of the membrane. This layer shows a remarkable contrast due to an anomalously high density of soluble scaffold proteins, such as PSD-95 that interacts with the membrane-embedded receptors. Astonishingly, the density of AMPA receptors within the PSD, which is ~ 1000 molecules· $\mu\text{m}^{-2}$ , exceeds its density in the extrasynaptic membrane by 100-fold [121]. While the receptors demonstrate normal diffusion in the extrasynaptic membrane, their lateral diffusion within

the PSD is anomalous, and a significant fraction of receptors are nearly immobile. Potential involvement of macromolecular crowding in retaining the receptors within the functional spot was probed in Monte Carlo simulations [122]. These simulations suggested that increasing the density of unspecific crowders within the PSD leads to the accumulation of AMPA receptors, and their residence time within the PSD may go beyond several hours. Surprisingly, super-resolution fluorescence revealed that, under highly crowded conditions within PSD, scaffold proteins PSD-95 undergo phase separation and form clusters near the synaptic membrane surface [123]. These clusters are ~ 80 nm in diameter and colocalize with membrane domains enriched with AMPA receptors, so PSD-95 may contribute to either the assembly of the membrane domains or their retention within the PSD [124]. Such stabilization of membrane clusters by their soluble counterparts was recently also implied for phase-separated proteasomes at the surface of the ER [125]. In this case, the proteasomes clustered in the ribosome-rich environment and engaged in the processing of membrane-bound substrates. In this manner, the requirements for Cdc48/p97 ATPase were bypassed, but it also suggests that components of ER-associated degradation machinery are colocalized and clustered within the membrane [126]. It also seems plausible that the ubiquitous intrinsically disordered regions (IDRs) within membrane proteins, such as NMDA receptors and various kinases, have a particular contribution to protein oligomerization and clustering under crowded conditions [127,128]. These largely unstructured polypeptides regulate recognition events, receptor-mediated signalling and protein oligomerization. The conformational dynamics of IDRs in a crowded environment have been recently evaluated [36,129]. The conformational flexibility of loosely packed IDRs can be affected by the crowded environment, and their compacted states commonly associated with protein:protein binding may be favoured. However, more complex scenarios cannot be ruled out, as certain intrinsic disordered proteins (IDPs) are insensitive to the elevated crowding or may even undergo further crowding-induced destabilization/unfolding [129]. Preservation of their disordered state in crowded environment may be one of the key features for the appropriate functionality maintenance.

### Lipid droplet proteome is sensitive to the surface crowding

Binding of peripheral proteins to the membrane is facilitated by weak interactions and may be particularly sensitive to the steric exclusion at the interface

[19]. The case was recently illustrated by studying the proteome dynamics of lipid droplets (LDs). LDs are micrometer-sized intracellular organelles which store neutral lipids, and their solid core is enveloped by a lipid monolayer [130]. The lipid monolayer does not allow the integration of transmembrane proteins but forms an interface for peripheral binding of proteins containing amphipathic helices or apolar anchors. These proteins are often involved in fatty acid and lipid metabolism and mediate LD transformations according to the cellular needs. Among those, CTP-phosphocholine cytidyltransferase (CCT) mediates PC synthesis during the growth phase of LD. CCT is anchored to the lipid monolayer with an unusually long amphipathic helix (54 amino acid). This contact is lost upon the lipid starvation and LD shrinking, so CCT is released into the cytoplasm and nucleus when its activity is not required. Cellular and reconstituted systems were used to demonstrate that the association of CCT with the LD interface strongly depends on the crowding level at the surface [131]. Shrinking of the available surface area led to higher collision rates with tightly bound proteins, such as lipases and acyltransferases, but also a synthetic mimetic (PEG), resulting in a loss of CCT:monolayer contacts. The crowding at the LD surface could be also tuned by overexpressing enzymes, allowing determination of the competitive protein interactions with the lipid monolayer. The analysis of known structures of LD-associated proteins revealed that hydrophobic helical hairpins ensure tight binding of competing enzymes. At the same time, the affinity of CCT could be enhanced by increasing the

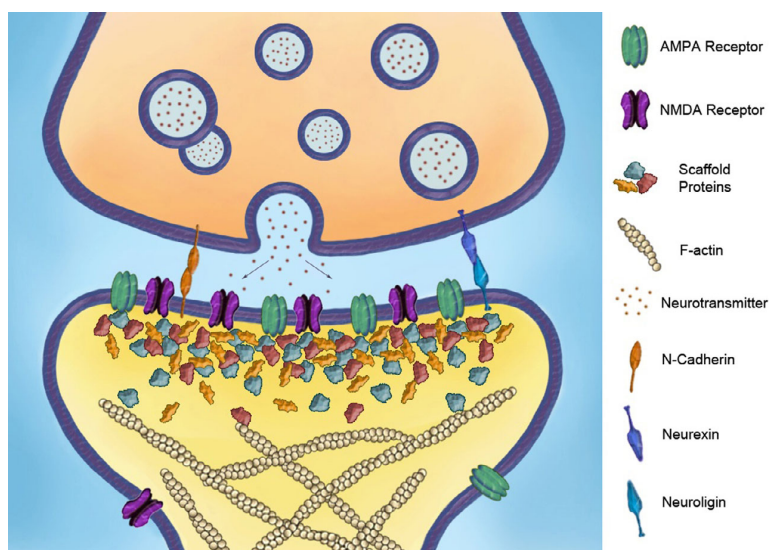
length of its amphipathic helix. Therefore, the propensity to anchor at the crowded interfaces may be a LD-specific targeting factor [132].

Hence, steric exclusion and protein clustering at the membrane interface provide simple but efficient tools to orchestrate cellular pathways, from adhesion to signal transduction and metabolism. These physical interactions contribute to the mosaic organization of the biological membranes, together with specific protein:protein and protein:lipid contacts. The described interplay between the membrane organization and the crowding within the proximate aqueous phase also indicates that membrane-associated processes are sensitive to the cellular homeostasis and crowding levels in the cytoplasm, as reviewed in the following sections.

### Crowding in solution modulates membrane:protein interactions

Exclusion of molecules from the solvent and their accumulation at the membrane interface may play a key role in their activity and interactions with lipids and membrane-anchored receptors. Several studies demonstrated that localization and condensation of soluble proteins at the lipid membrane interface is sensitive to the macromolecular crowding and, occasionally, phase separation in solution. In a simplified interpretation, the excluded volume in the aqueous phase favours the accumulation of membrane-binding proteins at the membrane interface [133,134]. Their enhanced local concentration promotes protein:lipid and protein:protein interactions, oligomerization and/

**Fig. 3.** Crowded environment of the postsynaptic density (PSD). PSD is a dynamic assembly of receptors, scaffold proteins and actin cortex within and proximate to the neuronal postsynaptic membrane. The high density of neurotransmitter (AMPA, NMDA) receptors is a prerequisite for the efficient signal transduction. The receptor density within the PSD is 1000-fold higher than within the plasma membrane. The enrichment and low mobility of receptors within the synaptic membrane is maintained via their interactions with abundant scaffold proteins, such as PSD-95 in the cytoplasm. Thus, macromolecular crowding at the membrane interface induces restructuring within the lipid bilayer.



or aggregation, while soluble proteins and crowders that do not associate with the membrane are largely excluded from the interface [135]. Thus, a twofold higher affinity to lipid vesicles was reported for the phospholipase A1, when as little as 2 % (w/v) of the inert polysaccharide Ficoll 400 was added to the solution [136]. A comparable crowding level imposed by Ficoll PM70 strongly enhanced the virus:receptor recognition on the surface of living cells. In this case, sterically excluded large viral particles accumulated in the proximity to the membrane, while small inhibitor peptides remained distributed in the aqueous phase [137]. Notably, the excluded volume effect recently allowed optimization of the production of universal donor RBCs via enzymatic cleavage of antigen oligosaccharides [138]. The biotechnological process commonly requires substantial amounts of RBC-modifying enzymes, which raises the cost significantly. To increase the concentration of enzymes proximate to the membrane, inert soluble crowders such as Ficoll PM70, dextran and hyperbranched polyglycerol were introduced. Fluorescence imaging confirmed the crowder-dependent accumulation of enzymes on the cell surface, in agreement with the excluded volume effect. As a result, the efficiency of the RBC-modifying enzymes could be increased up to 440-fold [138].

### Crowding-dependent assembly of cell division proteins

Protein:lipid interactions and associated membrane remodelling form a basis of cell division. The process has been extensively studied in bacterial systems and shows a remarkable sensitivity to the macromolecular crowding. Bacterial protein FtsZ, a homolog of tubulin essential for the cell division, forms ribbon-like filaments in the presence of polysaccharide crowders, such as dextran and Ficoll. These filaments undergo further phase separation in PEG:dextran and PEG:DNA mixtures [139,140]. A cofactor, DNA-binding protein SlmA mediates the phase separation of FtsZ. Notably, once encapsulated inside lipid vesicles, FtsZ:SlmA condensation occurs mostly at the membrane surface in a GTP-sensitive manner. This localization may be important for the downstream interactions of FtsZ with membrane-associated proteins FtsA and ZapA, as well as the subsequent formation of an active division site in a living cell. Crowding effects may further facilitate the cell division process, as the accumulation of FtsA, a bacterial homolog of actin, at the lipid membrane interface induces membrane instability of liposomes, that is, tubulation and formation of smaller vesicles, in the presence of ATP [141]. Anchoring FtsA

to the membrane is mediated by its amphipathic helix, but neither binding alone nor FtsA oligomerization in the absence of ATP causes changes in the lipid membrane morphology. It seems plausible that ATP binding triggers a conformational change within preassembled FtsA clusters, which repositions the amphipathic helices within the scaffolding membrane and provides the deformation force. Whether this membrane remodelling constitutes a natural part of the divisome formation remains to be tested. Complementary insights on membrane-associated crowding have recently been gained by studying oligomerization of another actin homolog, MreB. MreB maintains the elongated shape of bacteria and assembles into aligned filaments in the lumen of liposomes, thus stretching vesicles on the micrometer scale [56]. Similar to FtsA, spontaneous binding of MreB to the lipid leaflet is not sufficient to initiate protein oligomerization. The filament growth is triggered instead by crowding at the membrane interface, as shown by lipid-conjugated PEG polymers as crowders. Oligomerization of membrane-bound MreB was dependent on the size of PEG, ranging between 350 Da and 5 kDa, as well as the density of the polymer on the surface. Once PEG covered the entire surface, filament formation was rapidly abolished because the prerequisite membrane partitioning of MreB cannot occur [142]. It was concluded that the reduction in the accessible surface area stimulates the self-association of the membrane-bound MreB protomers, in agreement with the excluded volume effect. However, more complicated scenarios involving phase separation on the surface before the filament formation cannot be ruled out.

### Membrane-associated protein aggregation under crowded conditions

Protein folding and aggregation under native-like crowded conditions have been extensively studied in solution. Under the steric pressure, unfolded polypeptide chains tend to interact with cellular chaperones [143,144], but also aggregate and assemble into fibrils due to compaction into non-native states and enhanced protein:protein interactions [145,146]. Fibrillogenesis is associated with several neurodegenerative diseases mediated by IDPs, such as A $\beta$ , synuclein and prion protein [147]. Interactions of IDPs with membranes containing anionic lipids promote the formation of the secondary structure and contribute to aggregation [148,149]. The theoretical considerations predict that a large exclusion volume in the aqueous phase enhances the IDP association with the lipid

surface. The increased surface density of the proteins would trigger the oligomerization and conversion into  $\beta$ -helical fibres. Indeed, aggregation of A $\beta$  on the surface was enhanced when Ficoll PM 70 was present in solution in concentrations of up to 200 g/L [150]. The aggregation was much reduced at 350 g/L of Ficoll, however, where the elevated viscosity hindered A $\beta$  diffusion and thus shielded the excluded volume effect. A more sophisticated system composed of the synuclein, lipid vesicles and the membrane-associated chaperone Hsp27 was studied by fluorescence anisotropy and single-molecule FRET [151]. As Hsp27 sterically blocked the binding sites on the membrane, it nonspecifically reduced the synuclein accumulation and promoted the soluble form of the IDP. The assay led to a discovery of a bimodal binding of the synuclein to the lipid membrane via its N-terminal and central domains. While Hsp27-induced crowding mainly affected the N-terminal binding, the central part of the synuclein molecule could interact with the lipid leaflet even in the presence of the crowder. The resulting partially folded conformation of the synuclein was resistant to aggregation, suggesting that the abundance of membrane-bound proteins in living cells likely affects the conformational equilibrium of IDPs [151]. Somewhat differently to IDPs, folding of a small, 31 amino acid long zinc finger protein covalently anchored to a lipid monolayer at a high density could not be accomplished, likely due to steric repulsion between otherwise structured domains [152]. Under these crowded conditions and reduced degrees of freedom, the protein acquired partial  $\alpha$ -helical fold. The remaining polypeptide chain remained unstructured, possibly in an extended, polymer brush-like conformation. The complete folding of the zinc finger could be restored once a 5-fold excess of lipids was supplied to the monolayer, releasing the steric constraints.

*In vitro* studies on membrane protein folding are commonly conducted under diluted conditions, to reduce unwanted protein:protein interactions and off-pathway compact intermediates that result in aggregation of the highly hydrophobic proteins. However,  $\beta$ -barrel membrane proteins are usually less hydrophobic, as their transmembrane domains are composed of alternating polar and apolar residues. Therefore, insertion of two OMPs of *E. coli*, OmpA and OmpT, into liposomes was studied to probe the effect of macromolecular crowding [153]. The highly crowded interior of the periplasm that is built from a layer of peptidoglycan, substrate-binding domains of transporters and secretion factors, was mimicked by Ficoll PM70 [154,155]. The presence of 20% Ficoll had no significant effect on the membrane insertion rate of OmpT

but reduced the overall efficiency, likely causing some aggregation of the protein. In contrast, the insertion of OmpA approached 100% both in the absence and presence of the crowder. The higher solubility of OmpA was attributed to the chaperoning function of its sizeable periplasmic domain. Notably, the insertion kinetics of OmpA decreased 8-fold in the presence of Ficoll. This decrease was attributed to the excluded volume effect, albeit that the mechanism deserves further investigation. One possible scenario is that the sterically hindered OmpA adopts a compact or an oligomeric form, which undergoes slow conversion and insertion at the membrane interface. As the BAM and chaperoning machinery for OMP targeting and insertion has been described in great detail, probing its functioning and requirements under crowded conditions would be of major interest [104].

Described examples illustrate how dynamics of peripheral proteins at the membrane interface may be affected by macromolecular crowding. The steric exclusion from the solvent causes protein accumulation at the interface and modulates the avidity for the complex assembly or aggregation/phase separation at the interface. Thus, protein localization to the membrane interface depends not only on the intrinsic protein:lipid affinity, but also on the crowding status in the surrounding solvent and at the available membrane surface.

### Crowding-mediated transport through biological membranes

The influence of soluble crowders on membrane-associated processes via the steric exclusion plays a fundamental role in the cellular homeostasis. Swelling and shrinking of cells by differences in the osmotic pressure across the membrane alters the concentration of solutes and macromolecules in the cytoplasm. Dedicated cellular systems sense these changes and activate solute transporters and ion channels in the cytoplasmic membrane to restore the osmotic equilibrium. Early experimental data on the volume recovery of RBCs after osmotic stress showed that the albumin content determined the final RBC volume [156]. This implies that the RBC senses the intracellular protein concentration. These data were explained by the function of an ion transporter that set the osmotic strength accordingly. Minton *et al.* provided a theoretical explanation in which the effect of the cytosolic crowding on kinases and their interactions with the membrane proteins within the two-component system was considered based on scaled particle theory [133]. The developed framework suggests that the

kinase:transporter association and the phosphorylation efficiency depend on the concentration of macromolecules in the cytoplasm and the volume they take up. This earlier work provides a tentative two-component pathway for crowding homeostasis.

### Conformational dynamics of transporters and channels is mediated by crowding

Direct modulation of the transport activity by crowding has been lately shown for bacterial transporters and channels. Functioning of ATP-binding cassette (ABC) transporters is determined by conformational changes within their bulky ATPase domains exposed to the cytoplasm, where they may be affected by the crowder molecules. Indeed, *in vitro* analysis of a bacterial ABC transporter that couples betaine uptake to ATP hydrolysis revealed its sensitivity to high molecular weight PEGs [157]. The activation profile of the transporter reconstituted into lipid-based nanodiscs shifted to lower ionic strength, and maximum activity was reached at 75 mM KCl when the reaction was supplemented with 8 % PEG 6000. The activation of the transporter is linked to electrostatic interactions within its ATPase domains, so the crowder-induced excluded volume effect counters the electrostatic repulsion between the two lobes of the domain at low ionic strength. The crowding sensitivity was also reported for the secondary transporter ProP, where the proline uptake was significantly stimulated in the presence of either PEG or BSA [158]. The modulation mechanism has not yet been completely understood, but it may involve long C-terminal domains, which activate or regulate osmotically sensitive transporters [158,159]. The C-terminal domain of ProP either forms a coiled-coil with neighbouring protomers or interacts with the lipid bilayer. Macromolecular crowding near the membrane interface may shift this conformational equilibrium, affecting the protein functional response.

Members of a broad class of mechanosensitive channels found in bacteria and eukaryotes switch between closed and open conformations to allow flux of water and ions in response to changes in the membrane tension. The macromolecular crowding near the membrane interface tunes the activity of MscS channel, as crowders interact with the large extramembrane domain of the channel [160]. Another well-studied example, the mechanosensitive channel of large conductance, MscL of *E. coli*, allows rapid efflux of water and aqueous solutes under hypotonic conditions. The channel lacks extramembrane domains, and its gating is achieved by forces within the lipid bilayer. Increasing turgor pressure and the associated tension within

the lipid membrane cause tilting of TMHs within the channel in a diaphragm-like fashion, thus opening a sizeable central pore of  $\sim 25$  Å [161]. A theoretical study by Linden and coworkers suggested that the gating-associated expansion of MscL reduces the membrane area available for other proteins and thus contributes to the excluded volume [162]. The associated entropic cost was estimated to be  $\sim 2 k_{\text{B}}T$ , which is a remarkably high value in comparison with the gating energy of MscL, which can be as low as  $4 k_{\text{B}}T$  in the lipid bilayer [161]. Although the experimental validation of the crowding-dependent ion currents has yet to be provided, and the net effects involved may be somewhat lower than predicted, it likely remains a factor in the functioning of mechanosensitive channels, both in prokaryotic and eukaryotic cells.

### Polymer translocation under crowded conditions

Translocation of unfolded polypeptide chains through cellular membranes is an essential reaction taking place in the cytoplasmic membrane of bacteria and at the surfaces of eukaryotic organelles [163]. Statistical physics analysis suggests that the macromolecular crowding itself may be a driving force for the translocation because extensive steric pressure and repulsive interactions on the *cis*-side of the membrane will target polymer transport through the membrane-embedded pore [164,165]. Once crowders are present on both sides of the membrane, the substrate will predominantly localize in the compartment with larger crowders, as those result in a lower osmotic pressure [166]. However, specific attractive interactions with crowders may have a dominant effect on the direction of the transport [165]. Most recently, protein transport through a membrane-embedded  $\alpha$ -haemolysin nanopore with a crowded solution phase was studied experimentally [167]. Haemolysin, a pore-forming bacterial toxin, has extensive use in nanotechnology applications where its wide transmembrane channel allows translocation of synthetic and biopolymers, such as DNA strands and polypeptide chains [168]. Single-channel conductivity of the membrane-embedded haemolysin pores was recorded in the presence of Syn B2, a 23 amino acid long polypeptide, with PEG crowders at both sides of the membrane. Small PEG molecules of 1000 and 2000 Da could partition into the pore and inhibit the protein translocation. Instead, both PEGs 4000 or 8000 kinetically favoured interactions between the haemolysin and the polypeptide. This effect is likely due to the entropic crowding-out of Syn B2 from the solution phase, resulting in trapping the polypeptide within the pore. Notably, PEG 8000 had a weaker effect on

Syn B2:haemolysin association than PEG 6000, which could not solely be explained by the excluded volume. Instead, the observed size dependence was related to the osmotic pressure arising from the small and large crowders, in agreement with the theoretical predictions [166,167], although also different effects of PEGs on diffusion and compaction state of Syn B2 peptide could play a role.

As illustrated above for membrane transport reactions, individual cellular pathways may be sensitive to different and, potentially, additive factors of macromolecular crowding. Membrane and cytosolic crowding may affect conformational dynamics of the transport machinery, but also its macromolecular substrates. Importantly, crowding may be a triggering factor for cellular pathways, for example via two-component system activation at the lipid membrane interface.

## Membrane remodelling and fission

### Steric repulsion at the interface induces the membrane deformations

Dynamic morphology of cellular membranes, as well as their ability to undergo fusion and fission, is prerequisites for a variety of cellular processes including motility, cytokinesis, vesicle budding and cell signalling [3,169,170]. Changing the membrane shape involves local distortions of the lipid packing, and the arising lateral tension forces should be attenuated to stabilize the new architecture. Because the lipid bilayer packing is determined by structures of lipid head groups and acyl chains, its mechanical properties depend on the lipid composition [171]. These mechanical properties are highly dynamic, as cells tune their lipid composition in response to a changing environment or upon switching between growth phases. Moreover, biological membranes commonly show an asymmetry in the lipid composition between the leaflets, which is built and maintained by lipoactive enzymes and transmembrane flippase proteins and may contribute to the membrane curvature [170]. However, tuning the membrane shape with a high temporal and spatial precision can barely be achieved via restructuring of the cellular lipidome, but instead relies on several protein-based machineries [170,172]. These dedicated soluble proteins insert into the membrane with their amphipathic domains to increase the leaflet area on one side of the membrane. For example, Epsin and Arf proteins bind to the membrane in a crescent-shaped conformation characteristic for Bin/Amphiphysin/Rvs (BAR)-domain containing proteins, and sufficiently strong electrostatic

interactions with lipid head groups serve to remodel the bilayer. Oligomerization of the membrane-associated proteins commonly enhances membrane deformation. It stabilizes the altered structure, which is the case for COPI-, COPII- and clathrin-coated vesicles, or bacterial FtsA/FtsZ proteins, as described above [141]. Membrane remodelling by these mechanisms has been extensively studied and could be reproduced *in vitro*, inspiring the engineering of synthetic membrane scaffolds based on DNA origami of varying structures [173].

Complementary to these specialized systems, accumulated experimental evidence indicates that macromolecular crowding shapes lipid membranes *in vitro* and *in vivo*. The membrane-deforming proteins Epsin, with its N-terminal homology domain (ENTH), and Sar1p, did not require amphipathic helices to induce the membrane tubulation and fission once the proteins were anchored at a sufficiently high density at the GUV surface via polyhistidine tags (Fig. 4A,B) [54,174]. Moreover, even the histidine-tagged green fluorescent protein (GFP) and, to a lower extent, mOrange, but not the maltose-binding protein, could induce the formation of thin membrane tubules with a diameter of approximately 28 nm [175,176]. The tubulation effect was assigned to the entropy-based steric repulsion between proteins bound to the lipid bilayer at high density, though protein oligomerization may be also required, as shown for the matrix protein M1 of the influenza A virus [177]. A surface coverage of 20% could be estimated as a minimal threshold for tubulation if proteins were to be considered as hard spheres bound to the elastic membrane. Increasing the crowder size causes a rapid nonlinear stimulation of the tubule growth [54]. In agreement with this, larger crowders, for example, full-length Epsin, are able to induce membrane curvature at a lower coverage density. Comparing two proteins of similar molecular weights, GFP and the N-BAR domain of endophilin, showed that the BAR-induced tubulation required substantially lower protein density, though enhanced membrane remodelling via GFP has been recently reported [178]. However, the moderate effect of the steric pressure between compactly folded proteins on the membrane morphology may vanish when peripherally bound proteins are present at both sides of the cellular membrane [170,176].

### Membrane remodelling by disordered biopolymers

More than 40% of human proteins contain IDRs, which include domains in cytoplasmic loops of integral

membrane proteins or membrane-remodelling proteins [128,179]. Experiments on the crowding-induced tubulation revealed that IDRs within Epsin and the adaptor protein AP180 strongly enhanced the membrane remodelling, as it would be expected from the contribution of IDRs to the steric repulsion [54,174,180]. The role of IDRs in membrane tubulation and fission was further investigated using membrane-remodelling proteins amphiphysin and FCHo1/2, in which BAR domains are extended with disordered regions [181]. BAR domains alone caused extensive growth of stable tubules on the surface of large unilamellar vesicles (LUVs). On the other hand, full-length amphiphysin and FCHo1 disintegrated LUVs into highly curved vesicles of 10-fold smaller diameter (20 vs. 200 nm of the intact vesicle). A similar effect was achieved when isolated IDRs were bound to the vesicle surface. Thus, BAR domains stabilize the curved tubular structure of the membrane, while IDR extensions enhance the steric pressure, therefore allowing membrane fission (Fig. 4C). Similar to IDRs, unfolding of lipid-anchored proteins could induce membrane deformations [182]. Anchoring of the folded human serum albumin to the surface of GUVs or liposomes resulted in minor

membrane deformations, but enhanced tubulation was induced when the protein was chemically unfolded. Although the experimental evidence does not entirely explain the physiological role of IDPs/IDRs on membrane tubulation and fission in living organisms, it highlights a potential contribution of protein crowding to these processes.

While proteins are highly abundant at the membrane interfaces, other macromolecules may also contribute to crowding. Most recently, a direct connection between the density of the cell surface glycocalyx and the morphology of the plasma membrane was identified [62]. Glycocalyx is built of extensively glycosylated mucin proteins forming ‘bottlebrush’ structures of up to 20 MDa at the extracellular side of the plasma membrane. Increasing the expression levels of different types of mucin led to the membrane tubulation and shedding of small vesicles, similar to the effect of IDRs described above [181]. These morphological changes were dependent on the glycosylation status of mucins, as enzymatic ‘shaving’ of polysaccharides caused smoothing of the cell surface. The elevated surface density of glycosylated mucin molecules was recognized as a primary factor

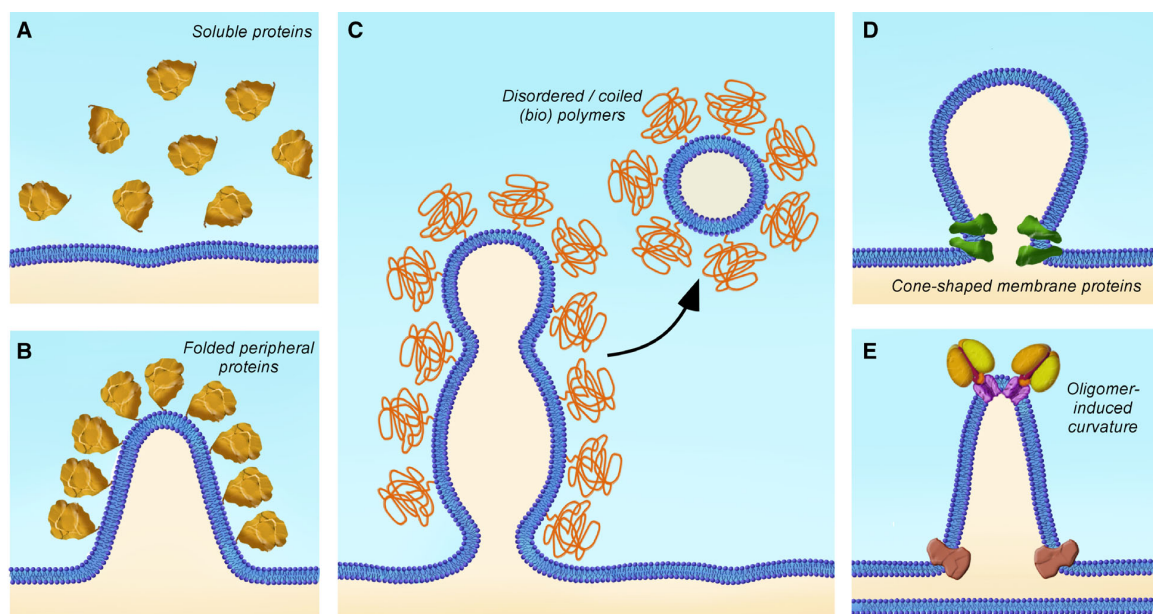


**Fig. 4.** Membrane remodelling via macromolecular crowding. (A) In the absence of membrane-anchoring domains, soluble proteins are largely excluded from the lipid bilayer interface. (B) Abundant membrane-bound globular proteins cause deformation and tubulation of the lipid bilayer due to entropic forces. (C) Entropy-based tubulation and membrane fission are strongly induced by unstructured synthetic polymers, intrinsically disordered protein domains, and polysaccharides. (D) Cone-shaped membrane proteins cause local membrane deformations and induce vesicle budding. (E) Angular-shaped dimers of the ATP synthase stabilize highly curved structure at the edge of the mitochondrial cristae.

to trigger membrane remodelling, where mucins switched from the ‘mushroom’ to the ‘brush’ packing-mode at a concentration 700-1,000 molecules/ $\mu\text{m}^2$ . The mucin-covered tubules were stabilized by the actin cytoskeleton, and once the actin was depolymerized, the tubules manifested high elasticity and a propensity to form small vesicles. Because vesicle spreading and extensive tubulations are hallmarks of many cancer cell types, a key role of the enriched glycocalyx and associated membrane morphologies in tumorigenesis was proposed [62].

#### Densely packed membrane proteins may stabilize membrane curvature

The shape of the membrane is affected by the incorporated proteins [3]. Advances in structural analysis revealed the universe of three-dimensional folds acquired by integral membrane proteins and their complexes, which may strongly deviate from a simplified cylindrical perspective [183]. Because the structure of the proximal lipid bilayer is affected by the protein shape, the intrinsically high and diverse protein content in cellular membranes will considerably contribute to the distribution of the lateral forces [99,184]. Functionally important membrane remodelling has been shown for the matrix protein M2 of influenza A virus [185,186]. The protein is assembled from four individual transmembrane  $\alpha$ -helices and is involved in the budding of nascent viral particles without the recruitment of the host ESCRT machinery. Electron paramagnetic resonance-based analysis and simulations suggested that the conical shape of a single M2 protein is sufficient to deform the fluid lipid bilayer locally. The entropy-driven accumulation and clustering of multiple M2 proteins cause mesoscopic membrane deformations towards the scission event (Fig. 4D). Another remarkable example of membrane remodelling by clustered proteins is mitochondrial  $F_1F_0$  ATP synthase: its transmembrane domain consists of a highly symmetric ring of  $F_0c$  subunits and the  $F_0a$  subunit, which forms the passage for protons. This complex can be seen as a cylinder in the membrane [187]. However, within the physiological dimer, ATP synthases are strongly tilted, with an angle ranging between 55 and 90°, thus preventing the steric clash between the sizeable ATPase domains. Notably, the tilt between protomers causes a marked bending of the lipid bilayer, and, once clustered in rows, dimers of the ATP determine the architecture of mitochondrial cristae, stabilizing their sharp edges (Fig. 4E) [188,189].

#### Steric repulsion at the interface modulates the phase separation within the lipid bilayer

A different feature of crowding-mediated membrane remodelling was reported for phase-separated lipid bilayers [190]. Once peripheral proteins were densely bound within patches of gel-phase lipids in GUVs, they exerted a steric hindrance-induced pressure and caused partial or complete mixing of the initially separated lipid phases. The effect had a clear dependence on the protein size, as transferrin receptors (150 kDa) required 10%, and GFP (26 kDa) 25% of receptor lipids to trigger phase mixing. In contrast, only partial mixing was observed for ubiquitin (5 kDa) even in the presence of 50% receptors. Also, both nanodiscs, which are large discoidal protein:lipid particles, and bulky synthetic polymers bound to phase-separated membranes caused substantial mixing [191,192]. Notably, once the crowders were displaced from the membrane surface by EDTA treatment, the macroscopic phase separation restored within several minutes.

The entropy-driven propensity to remodel the lipid membrane is a unique manifestation of the macromolecular crowding which is only possible within the two-dimensional setting. Bulky and unstructured molecules, either proteins or polysaccharides, accumulated at the lipid bilayer interface cause membrane deformations, such as tubulation and fission. It remains to be shown how the membrane deformation in the presence of crowders correlates with the mechanical properties of the lipid bilayer and also specific crowder:lipid interactions. Nevertheless, results from *in vitro* and *in vivo* studies suggest that the interfacial crowding may sculpture cellular membranes on the macroscopic scale and, together with the cytoskeleton, determine the morphology of living cells.

#### Quantification of macromolecular crowding

To mimic the physiological macromolecular crowding *in vitro*, quantitative analysis of crowding *in vivo* is required. In principle, cell volume changes [156,193], dry cell mass [33,194], cell buoyant density [195], water content by Raman scattering [196] and other methods provide the solute content of the cytoplasm or the periplasmic space of bacteria. The solute content is less predictive though for the actual magnitude of crowding effects: the cumulative effect depends on the size, shape and surface properties of all molecules involved. Moreover, the magnitude of crowding effects close to the intracellular side of the membrane is mostly unknown, despite its importance for membrane function.

Molecular probes offer complementary insights into the magnitude of macromolecular crowding. For example, diffusion of a fluorescent tracer protein in solution or within the lipid membrane provides information on the macromolecular crowding because the lateral and rotational diffusion decrease upon collisions [197–199]. However, the intrinsic dependence of diffusion on multiple factors, such as confinement or transient interactions with lipids, may hamper the determination of macromolecular crowding. [81,200–202]. Instead, monitoring protein conformation or folding would give insight into the magnitude of the steric exclusion that generally favours polymer compaction, albeit that attractive quinary interactions with the target proteins may diminish the effect of excluded volume [35,41,203–205].

Currently, three probes have been presented that sense the excluded volume from crowding in aqueous solutions. These probes are based on PEG polymers [206], DNA [207] or a disordered polypeptide chain [208]. These are all flexible constructs that compress with increasing macromolecular crowding. The resulting end-to-end distance within the probe is easily measured by FRET, either by conjugation with small-molecule fluorescent dyes or FPs. Thus, the protein probe contains two FPs with a flexible polypeptide linker in between extended with two  $\alpha$ -helices (Fig. 5A, B). FPs have little interaction with the cytoplasm, and the  $\alpha$ -helices are rigid and well-hydrated to prevent additional interactions. The protein probe has the crucial advantage that it is entirely genetically encoded, allowing expression in many different hosts, genetic fusions with localization tags or other proteins, and manipulation of its structure through genetic engineering. The majority of applications involve this protein-based class of probes, which function in bacteria [208–211], yeast [210,212] and mammalian cell lines [208,213,214], as well as their compartments [210,215]. It allowed crowding determination under stress conditions, such as osmotic stress [211,213] and ageing [212].

What do such probes measure? Various theoretical models and simulations attempt to predict polymer compression induced by macromolecular crowders. No theory captures the experimental observations completely, which is in part a consequence of the conformational complexity of polymers. However, the depletion force is a useful theoretical framework and explains observations at least qualitatively [216–218]. In these terms, the macromolecular crowders do not fit cavities of given protein conformations, leading to spaces depleted of crowder. The difference in osmotic pressure with the crowded medium outside the protein

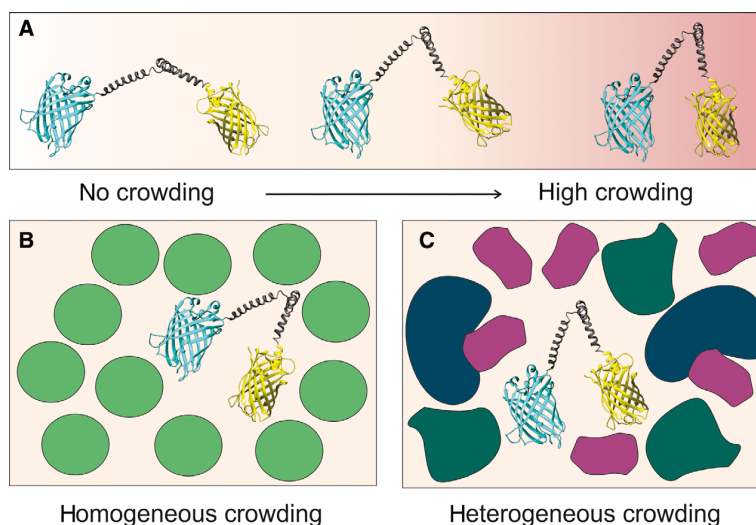
is relieved by compression of the protein, which in turn provides more configurational entropy for the crowders. In another model, scaled particle theory adapted for polymers, the polymer would be placed in a crowded solution, which leads to a decrease in configurational entropy of all the crowders, which also is relieved by polymer compression [219].

### Development of the genetically encoded sensors for crowding

To systematically characterize the probe dynamics, a set of nine probes with varied linker composition was recently designed, so the effects of unstructured and  $\alpha$ -helical domains were systematically investigated [209]. Inducing crowding with a range of different synthetic polymers and proteins showed that compression of probes is higher with higher crowder concentration and with the size of the crowder until it reaches a plateau at  $\sim 4$  nm radius (the diameters of the probes are in the range of 6–8 nm). Further, the larger the probe, the more it is compressed by crowding. These observations follow partially a scaling law derived from depletion force arguments, where the compression scales with the size of the probe and concentration of the crowders. This theory is not yet complete because the size of the crowder is not yet incorporated correctly. Nonetheless, these probes measure the crowder concentration when the crowders are  $> 2$  nm, freely diffusing, and do not have attractive interactions with the probes.

The expression of the FP-containing probes in cells allows measuring the FRET efficiency and thus the macromolecular crowding *in vivo*. In the absence of an accurate description of the probe conformational dynamics, we content with the comparison of FRET ratios with those obtained in solutions crowded with Ficoll PM70 to indicate the crowding (Fig. 5B,C) [208]. In *E. coli* cells, the cytoplasm crowding is equivalent to  $\sim 18\%$  w/w Ficoll PM70 and can increase up to 30 % w/w with osmotic upshift of 1 OsM. These values are similar, albeit somewhat lower than biopolymer volume fractions previously determined by cell dry weight. FRET efficiency recorded in HEK293 cells, on the other hand, corresponds to 5 % w/w Ficoll equivalents, so the eukaryotic cytoplasm is less crowded, while a 450 mOsM upshift results in  $\sim 20\%$  w/w Ficoll equivalents. Interestingly, the compression of the probes scales with the solute concentration in *E. coli* cells as they do in a crowded buffer, with the caveat that this requires  $\alpha$ -helices in the linker of the probes [209]. We hypothesize that the  $\alpha$ -helices reduce associative interactions of the linker with the

**Fig. 5.** Compression of a FRET-based macromolecular crowding probe. Genetically encoded probes/sensors of macromolecular crowding rely on measuring Förster's resonance energy transfer between two fluorescent proteins coupled by a semiflexible linker domain. (A) The probe occupies a continuum of conformations that become more condensed on average with increasing macromolecular crowding. Changes in the spatial dimensions and the distance between the fluorescent proteins result in changes in FRET efficiency. Schematic of homogeneously (B) and heterogeneously (C) shaped and sized macromolecular crowders. Both the crowder size and shape affect crowding-sensitive proteins.



proteome. Next to the cytoplasm of the different species, these FP-based probes can be specifically targeted to subcellular compartments, that is, the ER lumen and the nucleus [210,215]. Also, the changes in FRET can be determined by fluorescence lifetime imaging, which provides high resolution and allows untangling putative sensor populations [215,220].

New generations of macromolecular crowding probes with increased robustness allowed better assessment of crowding under challenging conditions, to address questions on how crowding and the biomacromolecular organization changes with environmental stresses, and how the cell responds. To this end, constitutive instead of inducible promoters, as well as faster maturing FPs, overcame artefacts resulting from slow FP maturation [210]. The measurement under these conditions showed that the crowding levels after adaptation of *E. coli* to osmotic stress provided similar, or even slightly lower levels than in unstressed cells [211]. The biopolymer volume fraction was previously determined to be higher in adapted cells, which means that a change in biomacromolecular organization, such as phase separation, must have taken place [221]. A similar conclusion could be drawn by depleting the cells of ATP, suggesting the importance of the organization compared to the total protein content [211].

Substituting the cyan/yellow (mCerulean3 or mTurquoise2/mCitrine or mVenus) FPs for green/red (Clover/Ruby, GFP/mCherry or EGFP/mScarlet-I) provides probes that can be used under less autofluorescence, with less pH sensitivity and allows for more straightforward normalization ( $N_{\text{FRET}}$ ) due to a lower bleed through [212–214]. The probes were applied to

study adaptation of mammalian cells to osmotic stress and under the very challenging conditions of yeast replicative ageing [212,213]. The latter experiments tracked the ageing of an individual cell over ~ 2 days, with drifting cell physiology and pH. Here, somewhat surprisingly, the macromolecular crowding is maintained and is even more stable than the difference between individual cells despite an increasing organellar crowding and pH [212]. This observation suggests tight regulation of macromolecular crowding. Altogether, probes for macromolecular crowding under stress conditions strongly suggest that macromolecular crowding is maintained in a window, that is, crowding homeostasis [39].

The advances in the development of the genetically encoded FRET-based probes may be further employed to design probes for measuring crowding at lipid membrane interfaces. Two major challenges here are to target and anchor the probe to the membrane interface in a suitable geometry, and to tune the structure of the probe, so a sufficient sensitivity to the interfacial crowding is achieved. In the simplest scenario, the probe can be docked to NTA-containing liposomes via a polyhistidine tag. However, such design allows only *in vitro* analysis, thus limiting the spectra of applications. One potent strategy would be to express FPs as a fusion with a 'carrier' membrane protein of a known structure, so inter-FP distances can be determined. Here, targeting mechanisms of membrane proteins should be taken into account, as large extramembrane domains within the membrane protein may distort the membrane partitioning and result in aberrant and degradation-prone conformations. Alternatively,

anchoring of the probe can be achieved post-translationally, via moderately hydrophobic domain, such as helical hairpin or Mistic protein [222], fused between FPs. Tuning the composition of the linkers within the probe may minimize their interactions with the lipid head groups. Furthermore, introducing linkers of different lengths may pave the way to measure crowding levels at various distances from the membrane interface deeper in the cytoplasm.

### Conclusion and perspectives

Advances in structural and cellular biology witnessed over the last decades have offered insights in molecular mechanisms of membrane proteins and their complexes, but also the overall architecture of cellular membranes [46]. The highly mosaic, asymmetric and heterogeneous compositions of these membranes have indicated that their functionality cannot be described solely by composition deduced from ‘-omics’ approaches, but detailed insights on the spatial and temporal dynamics is essential. Furthermore, the observed high and nonuniform density of proteins within the heterogeneous lipid bilayer and at the interface evidences that macromolecular crowding is an intrinsic feature of the cellular membrane. Two effective mechanisms of crowding are steric exclusion and quinary interactions. The entropy-based steric exclusion favours compaction of individual structures and leads to protein clustering within the lipid bilayer and at the membrane interface. The less predictive quinary interactions can counterbalance these effects. As summarized here, macromolecular crowding affects a broad range of membrane-associated cellular pathways and, next to specific protein:protein and protein:lipid contacts, determines the membrane organization at various scales. Importantly, membrane-associated processes demonstrate a strong dependence on the crowding in the aqueous phase both *in vitro* and in the cytosol of a living cell, as steric exclusion by solute crowders causes protein accumulation at the surface. *Vice versa*, crowding at membrane interface modulates the competitive binding of proteins and may result in protein release back into the aqueous phase. Furthermore, the macroscopic effect of the steric exclusion at the membrane interface is illustrated by extensive membrane remodelling and fission.

Despite the general appreciation of the macromolecular crowding effects, their role in most cellular processes remains to be elucidated. On the one hand, well-characterized cellular pathways should be employed as model systems to evaluate the effects of crowding. One prominent example is the universally

conserved Sec pathway for protein translocation and membrane insertion [223]. Here, crowding may affect the initial targeting of polypeptide chains to the membrane by altering their folding state and/or interactions with chaperones, may modulate its interactions with the membrane-embedded protein channel Sec61/SecYEG and may interfere with the assembly of larger complexes between the channel and the accessory chaperones or, occasionally, the degradation machinery. Also interactions of lipoproteins, such as small Ras GTPases, with the membrane may be sensitive to the interfacial crowding [224], and their medically relevant dynamics should be investigated under physiologically relevant conditions. On the other hand, the effects of macromolecular crowding obviously go beyond individual pathways and likely contribute to the global organization of cellular membranes. For instance, formation of phase separated raft nanodomains in the plasma membrane has been largely attributed to protein:lipid interactions, but also the involvement of the actin skeleton has been acknowledged [86,225]. Recent evidences for the effects of interfacial crowding on the lipid phase separation reviewed here point to the potential role of crowding to serve as a regulator for the raft dynamics and their spatial dimensions. Moreover, the crowding effects induced by ubiquitous IDRs within membrane proteins have been barely addressed, although an extensive knowledge on IDR dynamics has been accumulated from studying disordered proteins. The ability of IDPs/IDRs to undergo phase separation in solution further strengthens the potential of membrane crowding to contribute to raft assemblies, although the roles of the steric repulsion and attractive quinary interactions should be examined.

Understanding the dynamics of such multicomponent systems will essentially require a combination of *in vitro*, *in silico* and *in vivo* studies, where different aspects of crowded environment can be assessed in future. Molecular dynamics simulations performed either at the atomic or the coarse-grained level are a powerful tool to study protein interactions, as exemplified by the analysis of densely packed membrane proteins. To get insights on cellular membrane dynamics, dynamics of multiple species of proteins within simulated membranes have to be studied in future, so both steric exclusion and quinary interaction effects are probed. Protein:lipid interactions and the conformational dynamics of proteins at the membrane interface under crowded conditions are among other prominent aims for computational analysis. Real-life experiments need to provide input for *in silico* studies and *vice versa*. Visualization of the native cellular milieu is,

probably, the most direct approach to study the membrane organization. Next to the super-resolution microscopy, cryo-electron tomography (cryo-ET) is rapidly developing into a ‘magic bullet’ to tackle processes in crowded cellular environments, including those within the cellular membranes [8,226]. With ongoing improvements in its spatial resolution, cryo-ET will help to identify not only the localization and association of macromolecules within a cell, but also their distribution in terms of density and effects of those on the membrane morphology. Quantification of crowding effects, either by diffusion or dedicated sensors, will offer another piece of the puzzle of the crowding effects.

### Acknowledgements

We would like to thank Cornelia Monzel, Sander Smits and Stephan Schott for careful reading and commenting on the manuscript. A.K. acknowledges the financial support from the German Research Foundation (Deutsche Forschungsgemeinschaft, DFG) via grants KE1879/3-1 and CRC 1208 ‘Identity and dynamics of biological membranes’ (project number 267205415). A.J.B acknowledges the financial support from The Netherlands Organization for Scientific Research (NWO) VIDI grant 723.015.002.

### Conflict of interest

The authors declare no conflict of interest.

### Author contribution

All authors contributed to writing and editing the paper.

### References

- 1 Van Meer G, Voelker DR & Feigenson GW (2008) Membrane lipids: Where they are and how they behave. *Nat Rev Mol Cell Biol* **9**, 112–124.
- 2 Holthuis JCM & Menon AK (2014) Lipid landscapes and pipelines in membrane homeostasis. *Nature* **510**, 48–57.
- 3 de la Serna JB, Schütz GJ, Eggeling C & Cebecauer M (2016) There is no simple model of the plasma membrane organization. *Front Cell Dev Biol* **4**, 106.
- 4 Frye LD & Edidin M (1970) The rapid intermixing of cell surface antigens after formation of mouse-human heterokaryons. *J Cell Sci* **7**, 319–335.
- 5 Singer SJ & Nicolson GL (1972) The fluid mosaic model of the structure of cell membranes. *Science* **175**, 720–731.
- 6 Harder T, Scheffele P, Verkade P & Simons K (1998) Lipid domain structure of the plasma membrane revealed by patching of membrane components. *J Cell Biol* **141**, 929–942.
- 7 Saka SK, Honigsmann A, Eggeling C, Hell SW, Lang T & Rizzoli SO (2014) Multi-protein assemblies underlie the mesoscale organization of the plasma membrane. *Nat Commun* **5**, 4509.
- 8 Beck M & Baumeister W (2016) Cryo-electron tomography: Can it reveal the molecular sociology of cells in atomic detail? *Trends Cell Biol* **26**, 825–837.
- 9 Fotiadis D (2012) Atomic force microscopy for the study of membrane proteins. *Curr Opin Biotechnol* **23**, 510–515.
- 10 Engelman DM (2005) Membranes are more mosaic than fluid. *Nature* **438**, 578–580.
- 11 Laganowsky A, Reading E, Allison TM, Ulmschneider MB, Degiacomi MT, Baldwin AJ & Robinson CV (2014) Membrane proteins bind lipids selectively to modulate their structure and function. *Nature* **510**, 172–175.
- 12 Shevchenko A & Simons K (2010) Lipidomics: Coming to grips with lipid diversity. *Nat Rev Mol Cell Biol* **11**, 593–598.
- 13 Goyette J & Gaus K (2017) Mechanisms of protein nanoscale clustering. *Curr Opin Cell Biol* **44**, 86–92.
- 14 Koler M, Peretz E, Aditya C, Shimizu TS & Vaknin A (2018) Long-term positioning and polar preference of chemoreceptor clusters in *E. coli*. *Nat Commun* **9**, 4444.
- 15 Sezgin E, Levental I, Mayor S & Eggeling C (2017) The mystery of membrane organization: Composition, regulation and roles of lipid rafts. *Nat Rev Mol Cell Biol* **18**, 361–374.
- 16 Von Heijne G (2006) Membrane-protein topology. *Nat Rev Mol Cell Biol* **7**, 909–918.
- 17 Jacobson K, Liu P & Lagerholm BC (2019) The lateral organization and mobility of plasma membrane components. *Cell* **177**, 806–819.
- 18 Sharpe HJ, Stevens TJ & Munro S (2010) A comprehensive comparison of transmembrane domains reveals organelle-specific properties. *Cell* **142**, 158–169.
- 19 Johnson JE & Cornell RB (1999) Amphitropic proteins: Regulation by reversible membrane interactions. *Mol Membr Biol* **16**, 217–235.
- 20 Sahin C, Reid DJ, Marty MT & Landreh M (2020) Scratching the surface: native mass spectrometry of peripheral membrane protein complexes. *Biochem Soc Trans* **48**, 547–558.
- 21 Itzhak DN, Tyanova S, Cox J & Borner GHH (2016) Global, quantitative and dynamic mapping of protein subcellular localization. *Elife* **5**, e16950.
- 22 Itzhak DN, Davies C, Tyanova S, Mishra A, Williamson J, Antrobus R, Cox J, Weekes MP & Borner GHH (2017) A mass spectrometry-based

- approach for mapping protein subcellular localization reveals the spatial proteome of mouse primary neurons. *Cell Rep* **20**, 2706–2718.
- 23 Jean Beltran PM, Mathias RA & Cristea IM (2016) A portrait of the human organelle proteome in space and time during cytomegalovirus infection. *Cell Syst* **3**, 361–373.
  - 24 Graham JM (2015) Fractionation of subcellular organelles. *Curr Protoc Cell Biol* **69**, 3.1.1–3.1.22.
  - 25 Dupuy AD & Engelman DM (2008) Protein area occupancy at the center of the red blood cell membrane. *Proc Natl Acad Sci U S A* **105**, 2848–2852.
  - 26 Takamori S, Holt M, Stenius K, Lemke EA, Grønborg M, Riedel D, Urlaub H, Schenck S, Brügger B, Ringler P *et al.* (2006) Molecular anatomy of a trafficking organelle. *Cell* **127**, 831–846.
  - 27 Quinn P, Griffiths G & Warren G (1984) Density of newly synthesized plasma membrane proteins in intracellular membranes II. *Biochemical Studies J Cell Biol* **98**, 2142–2147.
  - 28 Sowers AE & Hackenbrock CR (1981) Rate of lateral diffusion of intramembrane particles: Measurement by electrophoretic displacement and rerandomization. *Proc Natl Acad Sci U S A* **78**, 6246–6250.
  - 29 Fotiadis D, Liang Y, Filipek S, Saperstein DA, Engel A & Palczewski K (2003) Rhodopsin dimers in native disc membranes. *Nature* **421**, 127–128.
  - 30 Kirchhoff H (2008) Molecular crowding and order in photosynthetic membranes. *Trends Plant Sci* **13**, 201–207.
  - 31 Liu LN & Scheuring S (2013) Investigation of photosynthetic membrane structure using atomic force microscopy. *Trends Plant Sci* **18**, 277–286.
  - 32 Fulton AB (1982) How crowded is the cytoplasm? *Cell* **30**, 345–347.
  - 33 Zimmerman SB & Trach SO (1991) Estimation of macromolecule concentrations and excluded volume effects for the cytoplasm of *Escherichia coli*. *J Mol Biol* **222**, 599–620.
  - 34 Ellis RJ (2001) Macromolecular crowding: Obvious but underappreciated. *Trends Biochem Sci* **26**, 597–604.
  - 35 Sarkar M, Li C & Pielak GJ (2013) Soft interactions and crowding. *Biophys Rev* **5**, 187–194.
  - 36 Kuznetsova IM, Turoverov KK & Uversky VN (2014) What macromolecular crowding can do to a protein. *Int J Mol Sci* **15**, 23090–23140.
  - 37 Wang Y, Li C & Pielak GJ (2010) Effects of proteins on protein diffusion. *J Am Chem Soc* **132**, 9392–9397.
  - 38 Zhou H-X, Rivas G & Minton AP (2008) Macromolecular crowding and confinement: biochemical, biophysical, and potential physiological consequences. *Annu Rev Biophys* **37**, 375–397.
  - 39 Van Den Berg J, Boersma AJ & Poolman B (2017) Microorganisms maintain crowding homeostasis. *Nat Rev Microbiol* **15**, 309–318.
  - 40 Wang Y, Sarkar M, Smith AE, Krois AS & Pielak GJ (2012) Macromolecular crowding and protein stability. *J Am Chem Soc* **134**, 16614–16618.
  - 41 Monteith WB, Cohen RD, Smith AE, Guzman-Cisneros E & Pielak GJ (2015) Quinary structure modulates protein stability in cells. *Proc Natl Acad Sci U S A* **112**, 1739–1742.
  - 42 Sarkar M, Lu J & Pielak GJ (2014) Protein-crowder charge and protein stability. *Biochemistry* **53**, 1601–1606.
  - 43 Guseman AJ, Perez Goncalves GM, Speer SL, Young GB & Pielak GJ (2018) Protein shape modulates crowding effects. *Proc Natl Acad Sci U S A* **115**, 10965–10970.
  - 44 Grasberger B, Minton AP, DeLisi C & Metzger H (1986) Interaction between proteins localized in membranes. *Proc Natl Acad Sci U S A* **83**, 6258–6262.
  - 45 Guigas G & Weiss M (2016) Effects of protein crowding on membrane systems. *Biochim Biophys Acta – Biomembr* **1858**, 2441–2450.
  - 46 Lorent JH, Levental KR, Ganesan L, Rivera-Longsworth G, Sezgin E, Doktorova M, Lyman E, Levental I (2020) Plasma membranes are asymmetric in lipid unsaturation, packing and protein shape. *Nat Chem Biol* **16**, 644–652. <http://doi.org/10.1038/s41589-020-0529-6>
  - 47 Saffman PG & Delbrück M (1975) Brownian motion in biological membranes. *Proc Natl Acad Sci U S A* **72**, 3111–3113.
  - 48 Surma MA, Klose C & Simons K (2012) Lipid-dependent protein sorting at the trans-Golgi network. *Biochim Biophys Acta – Mol Cell Biol Lipids* **1821**, 1059–1067.
  - 49 Li C, Wang Y & Pielak GJ (2009) Translational and rotational diffusion of a small globular protein under crowded conditions. *J Phys Chem B* **113**, 13390–13392.
  - 50 Wenner JR & Bloomfield VA (1999) Crowding effects on EcoRV kinetics and binding. *Biophys J* **77**, 3234–3241.
  - 51 Levi V & González Flecha FL (2002) Reversible fast-dimerization of bovine serum albumin detected by fluorescence resonance energy transfer. *Biochim Biophys Acta – Proteins Proteomics* **1599**, 141–148.
  - 52 Alberti S, Saha S, Woodruff JB, Franzmann TM, Wang J & Hyman AA (2018) A user's guide for phase separation assays with purified proteins. *J Mol Biol* **430**, 4806–4820.
  - 53 Kuznetsova IM, Zaslavsky BY, Breydo L, Turoverov KK & Uversky VN (2015) Beyond the excluded volume effects: mechanistic complexity of the crowded milieu. *Molecules* **20**, 1377–1409.
  - 54 Stachowiak JC, Schmid EM, Ryan CJ, Ann HS, Sasaki DY, Sherman MB, Geissler PL, Fletcher DA & Hayden CC (2012) Membrane bending by protein-protein crowding. *Nat Cell Biol* **14**, 944–949.

- 55 Horton MR, Höfling F, Rädler JO & Franosch T (2010) Development of anomalous diffusion among crowding proteins. *Soft Matter* **6**, 2648–2656.
- 56 Garenne D, Libchaber A & Noireaux V (2020) Membrane molecular crowding enhances MreB polymerization to shape synthetic cells from spheres to rods. *Proc Natl Acad Sci U S A* **117**, 1902–1909.
- 57 Immordino ML, Dosio F & Cattel L (2006) Stealth liposomes : review of the basic science, rationale, and clinical applications, existing and potential. *Int J Nanomedicine* **1**, 297–315.
- 58 Ramadurai S, Holt A, Krasnikov V, Van Den Bogaart G, Killian JA & Poolman B (2009) Lateral diffusion of membrane proteins. *J Am Chem Soc* **131**, 12650–12656.
- 59 Hong H & Bowie JU (2011) Dramatic destabilization of transmembrane helix interactions by features of natural membrane environments. *J Am Chem Soc* **133**, 11389–11398.
- 60 Munguira I, Casuso I, Takahashi H, Rico F, Miyagi A, Chami M & Scheuring S (2016) Glasslike membrane protein diffusion in a crowded membrane. *ACS Nano* **10**, 2584–2590.
- 61 Schneider F, Waithe D, Clausen MP, Galiani S, Koller T, Ozhan G, Eggeling C & Sezgin E (2017) Diffusion of lipids and GPI-anchored proteins in actin-free plasma membrane vesicles measured by STED-FCS. *Mol Biol Cell* **28**, 1507–1518.
- 62 Shurer CR, Kuo JC, Feigenson GW, Reesink HL, Paszek MJ, Gandhi JG & Colville MJ (2019) Physical principles of membrane shape regulation by the glycocalyx. *Cell* **177**, 1757–1770.
- 63 Vaz WLC, Goodsaid-Zalduondo F & Jacobson K (1984) Lateral diffusion of lipids and proteins in bilayer membranes. *FEBS Lett* **174**, 199–207.
- 64 Weiß K, Neef A, Van Q, Kramer S, Gregor I & Enderlein J (2013) Quantifying the diffusion of membrane proteins and peptides in black lipid membranes with 2-focus fluorescence correlation spectroscopy. *Biophys J* **105**, 455–462.
- 65 Lee AG (2004) How lipids affect the activities of integral membrane proteins. *Biochim Biophys Acta – Biomembr* **1666**, 62–87.
- 66 Niemela PS, Miettinen MS, Monticelli L, Hammaren H, Bjelkmar P, Murtola T, Lindahl E & Vattulainen I (2010) Membrane proteins diffuse as dynamic complexes with lipids. *J Am Chem Soc* **132**, 7574–7575.
- 67 Camley BA & Brown FLH (2012) Contributions to membrane-embedded-protein diffusion beyond hydrodynamic theories. *Phys Rev E – Stat Nonlinear Soft Matter Phys* **85**, 23–25.
- 68 Naji A, Levine AJ & Pincus PA (2007) Corrections to the Saffman-Delbrück mobility for membrane bound proteins. *Biophys J* **93**, L49–L51.
- 69 Gambin Y, Lopez-Esparza R, Reffay M, Sieracki E, Gov NS, Genest M, Hodges RS & Urbach W (2006) Lateral mobility of proteins in liquid membranes revisited. *Proc Natl Acad Sci U S A* **103**, 2098–2102.
- 70 Chiantia S, Ries J & Schwille P (2009) Fluorescence correlation spectroscopy in membrane structure elucidation. *Biochim Biophys Acta – Biomembr* **1788**, 225–233.
- 71 Höfling F & Franosch T (2013) Anomalous transport in the crowded world of biological cells. *Reports Prog Phys* **76**, 1–55.
- 72 Marrink SJ, Corradi V, Souza PCT, Ingólfsson HI, Tieleman DP & Sansom MSP (2019) Computational modeling of realistic cell membranes. *Chem Rev* **119**, 6184–6226.
- 73 Peters R & Cherry RJ (1982) Lateral and rotational diffusion of bacteriorhodopsin in lipid bilayers: experimental test of the Saffman-Delbrück equations. *Proc Natl Acad Sci U S A* **79**, 4317–4321.
- 74 Frick M, Schmidt K & Nichols BJ (2007) Modulation of lateral diffusion in the plasma membrane by protein density. *Curr Biol* **17**, 462–467.
- 75 Levental KR & Levental I (2015) Giant plasma membrane vesicles: models for understanding membrane organization. *Curr Top Membr* **75**, 25–57.
- 76 Sezgin E, Levental I, Grzybek M, Schwarzmann G, Mueller V, Honigsmann A, Belov VN, Eggeling C, Coskun Ü, Simons K *et al.* (2012) Partitioning, diffusion, and ligand binding of raft lipid analogs in model and cellular plasma membranes. *BBA – Biomembr* **1818**, 1777–1784.
- 77 Worch R, Petrasek Z, Schwille P & Weidemann T (2017) Diffusion of single-pass transmembrane receptors: from the plasma membrane into giant liposomes. *J Membr Biol* **250**, 393–406.
- 78 Saxton MJ & Jacobson K (1997) Single-particle tracking: applications to membrane dynamics. *Annu Rev Biophys Biomol Struct* **26**, 373–399.
- 79 Ritchie K, Shan XY, Kondo J, Iwasawa K, Fujiwara T & Kusumi A (2005) Detection of non-Brownian diffusion in the cell membrane in single molecule tracking. *Biophys J* **88**, 2266–2277.
- 80 Heath GR & Scheuring S (2019) Advances in high-speed atomic force microscopy (HS-AFM) reveal dynamics of transmembrane channels and transporters. *Curr Opin Struct Biol* **57**, 93–102.
- 81 Ritchie K, Iino R, Fujiwara T, Murase K, Kusumi A, Ritchie K, Iino R, Fujiwara T & Murase K (2003) The fence and picket structure of the plasma membrane of live cells as revealed by single molecule techniques. *Mol Membr Biol* **20**, 13–18.
- 82 Vogel SK, Greiss F, Khmelinskaia A & Schwille P (2017) Control of lipid domain organization by a biomimetic contractile actomyosin cortex. *Elife* **6**, e24350.

- 83 Chichili GR & Rodgers W (2009) Cytoskeleton – membrane interactions in membrane raft structure. *Cell Mol Life Sci* **66**, 2319–2328.
- 84 Lillemeier BF, Pfeiffer JR, Surviladze Z, Wilson BS & Davis MM (2006) Plasma membrane-associated proteins are clustered into islands attached to the cytoskeleton. *Proc Natl Acad Sci U S A* **103**, 18992–18997.
- 85 Heinemann F, Vogel SK & Schwille P (2013) Lateral membrane diffusion modulated by a minimal actin cortex. *Biophys J* **104**, 1465–1475.
- 86 Honigsmann A, Sadeghi S, Keller J, Hell SW, Eggeling C & Vink R (2014) A lipid bound actin meshwork organizes liquid phase separation in model membranes. *Elife* **2014**, e01671.
- 87 He W, Song H, Su Y, Geng L, Ackerson BJ, Peng HB & Tong P (2016) Dynamic heterogeneity and non-Gaussian statistics for acetylcholine receptors on live cell membrane. *Nat Commun* **7**, 11701.
- 88 Andrews NL, Lidke KA, Pfeiffer JR, Burns AR, Wilson BS, Oliver JM & Lidke DS (2008) Actin restricts FceRI diffusion and facilitates antigen-induced receptor immobilization. *Nat Cell Biol* **10**, 955–963.
- 89 Casuso I, Khao J, Chami M, Paul-Gilloteaux P, Husain M, Duneau JP, Stahlberg H, Sturgis JN & Scheuring S (2012) Characterization of the motion of membrane proteins using high-speed atomic force microscopy. *Nat Nanotechnol* **7**, 525–529.
- 90 Koldsø H & Sansom MSP (2015) Organization and dynamics of receptor proteins in a plasma membrane. *J Am Chem Soc* **137**, 14694–14704.
- 91 Goose JE & Sansom MSP (2013) Reduced lateral mobility of lipids and proteins in crowded membranes. *PLoS Comput Biol* **9**, e1003033.
- 92 Jeon J-H, Javanainen M, Martinez-Seara H, Metzler R & Vattulainen I (2016) Protein crowding in lipid bilayers gives rise to Non-Gaussian anomalous lateral diffusion of phospholipids and proteins. *Phys Rev X* **6**, 021006.
- 93 Javanainen M, Martinez-Seara H, Metzler R & Vattulainen I (2017) Diffusion of integral membrane proteins in protein-rich membranes. *J. Phys Chem Lett* **8**, 4308–4313.
- 94 Guigas G & Weiss M (2008) Influence of hydrophobic mismatching on membrane protein diffusion. *Biophys J* **95**, 25–27.
- 95 Puthiyaveetil S, Tsabari O, Lowry T, Lenhart S, Lewis RR, Reich Z & Kirchhoff H (2014) Compartmentalization of the protein repair machinery in photosynthetic membranes. *Proc Natl Acad Sci U S A* **111**, 15839–15844.
- 96 Houser JR, Busch DJ, Bell DR, Li B, Ren P & Stachowiak JC (2016) The impact of physiological crowding on the diffusivity of membrane bound proteins. *Soft Matter* **12**, 2127–2134.
- 97 Zhou H-X (2009) Crowding effects of membrane proteins. *J Phys Chem B* **113**, 7995–8005.
- 98 Domański J, Marrink SJ & Schäfer LV (2012) Transmembrane helices can induce domain formation in crowded model membranes. *Biochim Biophys Acta – Biomembr* **1818**, 984–994.
- 99 Duncan AL, Reddy T, Koldsø H, Hélie J, Fowler PW, Chavent M & Sansom MSP (2017) Protein crowding and lipid complexity influence the nanoscale dynamic organization of ion channels in cell membranes. *Sci Rep* **7**, 16647.
- 100 Javanainen M, Martinez-Seara H & Vattulainen I (2017) Excessive aggregation of membrane proteins in the Martini model. *PLoS One* **12**, e0187936.
- 101 Alessandri R, Souza PCT, Thallmair S, Melo MN, De Vries AH & Marrink SJ (2019) Pitfalls of the Martini model. *J Chem Theory Comput* **15**, 5448–5460.
- 102 Chavent M, Duncan AL, Rassam P, Birkholz O, Hélie J, Reddy T, Beliaev D, Hambly B, Piehler J, Kleanthous C *et al.* (2018) How nanoscale protein interactions determine the mesoscale dynamic organisation of bacterial outer membrane proteins. *Nat Commun* **9**, 2846.
- 103 Rassam P, Copeland NA, Birkholz O, Tóth C, Chavent M, Duncan AL, Cross SJ, Housden NG, Kaminska R, Seger U *et al.* (2015) Supramolecular assemblies underpin turnover of outer membrane proteins in bacteria. *Nature* **523**, 333–336.
- 104 Rollauer SE, Soorshjani MA, Noinaj N & Buchanan SK (2015) Outer membrane protein biogenesis in Gram-negative bacteria. *Philos Trans B* **370**, 1–10.
- 105 Chen L, Novicky L, Merzlyakov M, Hristov T & Hristova K (2010) Measuring the energetics of membrane protein dimerization in mammalian membranes. *J Am Chem Soc* **132**, 3628–3635.
- 106 Moore DT, Berger BW & DeGrado WF (2008) Protein-protein interactions in the membrane: sequence, structural, and biological motifs. *Structure* **16**, 991–1001.
- 107 Covino R, Hummer G & Ernst R (2018) Review integrated functions of membrane property sensors and a hidden side of the unfolded protein response. *Mol Cell* **71**, 458–467.
- 108 Volmer R, Van Der Ploeg K & Ron D (2013) Membrane lipid saturation activates endoplasmic reticulum unfolded protein response transducers through their transmembrane domains. *Proc Natl Acad Sci U S A* **110**, 4628–4633.
- 109 Shen Y, Zhao Z, Zhang L, Shi L, Shahriar S, Chan RB, DI Paolo G & Min W (2017) Metabolic activity induces membrane phase separation in endoplasmic reticulum. *Proc Natl Acad Sci U S A* **114**, 13394–13399.
- 110 Milligan G, Ward RJ & Marsango S (2019) GPCR homo-oligomerization. *Curr Opin Cell Biol* **57**, 40–47.

- 111 Walsh SM, Mathiasen S, Christensen SM, Fay JF, King C, Provasi D, Borrero E, Rasmussen SGF, Fung JJ, Filizola M *et al.* (2018) Single proteoliposome high-content analysis reveals differences in the homo-oligomerization of GPCRs. *Biophys J* **115**, 300–312.
- 112 Calvert PD, Govardovskii VI, Krasnoperova N & Anderson RE (2001) Membrane protein diffusion sets the speed of rod phototransduction. *Nature* **411**, 90–94.
- 113 Heinkel F, Abraham L, Ko M, Chao J, Bach H, Hui LT, Li H, Zhu M, Ling YM, Rogalski JC *et al.* (2019) Phase separation and clustering of an ABC transporter in *Mycobacterium tuberculosis*. *Proc Natl Acad Sci U S A* **116**, 16326–16331.
- 114 Kechagia JZ, Ivaska J & Roca-Cusachs P (2019) Integrins as biomechanical sensors of the microenvironment. *Nat Rev Mol Cell Biol* **20**, 457–473.
- 115 Douglass AD & Vale RD (2005) Single-molecule microscopy reveals plasma membrane microdomains created by protein-protein networks that exclude or trap signaling molecules in T cells. *Cell* **121**, 937–950.
- 116 James JR & Vale RD (2012) Biophysical mechanism of T-cell receptor triggering in a reconstituted system. *Nature* **487**, 64–69.
- 117 Schmid EM, Bakalar MH, Choudhuri K, Weichsel J, Ann HS, Geissler PL, Dustin ML & Fletcher DA (2016) Size-dependent protein segregation at membrane interfaces. *Nat Phys* **12**, 704–711.
- 118 Carbone CB, Kern N, Fernandes RA, Hui E & Su X (2017) In vitro reconstitution of T cell receptor-mediated segregation of the CD45 phosphatase. *Proc Natl Acad Sci U S A* **E9338–E9345**.
- 119 Fenz SF, Bihl T, Schmidt D, Merkel R, Seifert U, Sengupta K & Smith AS (2017) Membrane fluctuations mediate lateral interaction between cadherin bonds. *Nat Phys* **13**, 906–913.
- 120 Chen X, Winters C, Azzam R, Li X, Galbraith JA, Leapman RD & Reese TS (2008) Organization of the core structure of the postsynaptic density. *Proc Natl Acad Sci U S A* **105**, 4453–4458.
- 121 Tanaka JI, Matsuzaki M, Tarusawa E, Momiyama A, Molnar E, Kasai H & Shigemoto R (2005) Number and density of AMPA receptors in single synapses in immature cerebellum. *J Neurosci* **25**, 799–807.
- 122 Santamaria F, Gonzalez J, Augustine GJ & Raghavachari S (2010) Quantifying the effects of elastic collisions and non-covalent binding on glutamate receptor trafficking in the post-synaptic density. *PLoS Comput Biol* **6**, e1000780.
- 123 MacGillivray HD, Song Y, Raghavachari S & Blanpied TA (2013) Nanoscale scaffolding domains within the postsynaptic density concentrate synaptic ampa receptors. *Neuron* **78**, 615–622.
- 124 Li TP, Song Y, Macgillivray HD, Blanpied TA & Raghavachari S (2016) Protein crowding within the postsynaptic density can impede the escape of membrane proteins. *Journal Neurosci* **36**, 4276–4295.
- 125 Albert S, Wietrzynski W, Lee C, Schaffer M, Beck F, Schuller JM, Salome PA, Plitzko JM, Baumeister W & Engel BD (2020) Direct visualization of degradation microcompartments at the ER membrane. *Proc Natl Acad Sci U S A* **117**, 1069–1080.
- 126 Ruggiano A, Foresti O & Carvalho P (2014) ER-associated degradation: protein quality control and beyond. *J Cell Biol* **204**, 869–879.
- 127 Uversky VN (2011) Multitude of binding modes attainable by intrinsically disordered proteins: a portrait gallery of disorder-based complexes. *Chem Soc Rev* **40**, 1623–1634.
- 128 Kjaergaard M & Kragelund BB (2017) Functions of intrinsic disorder in transmembrane proteins. *Cell Mol Life Sci* **74**, 3205–3224.
- 129 Fonin AV, Darling AL, Kuznetsova IM, Turoverov KK & Uversky VN (2018) Intrinsically disordered proteins in crowded milieu: when chaos prevails within the cellular gumbo. *Cell Mol Life Sci* **75**, 3907–3929.
- 130 Olzmann JA & Carvalho P (2019) Dynamics and functions of lipid droplets. *Nat Rev Mol Cell Biol* **20**, 137–155.
- 131 Kory N, Thiam A, Farese RV & Walther TC (2015) Protein crowding is a determinant of lipid droplet protein composition. *Dev Cell* **34**, 351–363.
- 132 Prévost C, Sharp ME, Kory N, Lin Q, Voth GA, Farese RVJ & Walther TC (2018) Mechanism and determinants of amphipathic helix-containing protein targeting to lipid droplets. *Dev Cell* **44**, 73–86.
- 133 Minton AP, Colclasure GC & Parkert JC (1992) Model for the role of macromolecular crowding in regulation of cellular volume. *Proc Natl Acad Sci U S A* **89**, 10504–10506.
- 134 Kim JS & Yethiraj A (2010) Crowding effects on association reactions at membranes. *Biophys J* **98**, 951–958.
- 135 Nawrocki G, Im W, Sugita Y & Feig M (2019) Clustering and dynamics of crowded proteins near membranes and their influence on membrane bending. *Proc Natl Acad Sci U S A* **116**, 24562–24567.
- 136 Wei Y, Mayoral-Delgado I, Stewart NA & Dymond MK (2019) Macromolecular crowding and membrane binding proteins: the case of phospholipase A1. *Chem Phys Lipids* **218**, 91–102.
- 137 Rincon V, Bocanegra R, Rodriguez-Huete A, Rivas G & Mateu MG (2011) Effects of macromolecular crowding on the inhibition of virus assembly and virus-cell receptor recognition. *Biophys J* **100**, 738–746.
- 138 Chapanian R, Kwan DH, Constantinescu I, Shaikh FA, Rossi NAA, Withers SG & Kizhakkedathu JN (2014) Enhancement of biological reactions on cell

- surfaces via macromolecular crowding. *Nat Commun* **5**, 4683.
- 139 González JM, Jiménez M, Vélez M, Mingorance J, Andreu JM, Vicente M & Rivas G (2003) Essential cell division protein FtsZ assembles into one monomer-thick ribbons under conditions resembling the crowded intracellular environment. *J Biol Chem* **278**, 37664–37671.
- 140 Monterroso B, Zorrilla S, Sobrinos-Sanguino M, Robles-Ramos MA, López-Álvarez M, Margolin W, Keating CD & Rivas G (2019) Bacterial FtsZ protein forms phase-separated condensates with its nucleoid-associated inhibitor SlmA. *EMBO Rep* **20**, e45946.
- 141 Conti J, Viola MG & Camberg JL (2018) FtsA reshapes membrane architecture and remodels the Z-ring in *Escherichia coli*. *Mol Microbiol* **107**, 558–576.
- 142 Pozzi D, Colapicchioni V, Caracciolo G, Piovesana S, Capriotti AL, Palchetti S, De Grossi S, Riccioli A, Amenitsch H & Laganà A (2014) Effect of polyethyleneglycol (PEG) chain length on the bio-nano- interactions between PEGylated lipid nanoparticles and biological fluids: From nanostructure to uptake in cancer cells. *Nanoscale* **6**, 2782–2792.
- 143 Martin J & Hartl FU (1997) The effect of macromolecular crowding on chaperonin-mediated protein folding. *Proc Natl Acad Sci U S A* **94**, 1107–1112.
- 144 Kulothungan SR, Das M, Johnson M, Ganesh C & Varadarajan R (2009) Effect of crowding agents, signal peptide, and chaperone secb on the folding and aggregation of *e. coli* maltose binding protein. *Langmuir* **25**, 6637–6648.
- 145 Munishkina LA, Ahmad A, Fink AL & Uversky VN (2008) Guiding protein aggregation with macromolecular crowding. *Biochemistry* **47**, 8993–9006.
- 146 White DA, Buell AK, Knowles TPJ, Welland ME & Dobson CM (2010) Protein aggregation in crowded environments. *J Am Chem Soc* **132**, 5170–5175.
- 147 Uversky VN, Oldfield CJ & Dunker AK (2008) Intrinsically disordered proteins in human diseases: introducing the D 2 concept. *Annu Rev Biophys* **37**, 215–246.
- 148 Bokvist M, Lindström F, Watts A & Gröbner G (2004) Two types of Alzheimer's  $\beta$ -Amyloid (1–40) peptide membrane interactions: aggregation preventing transmembrane anchoring versus accelerated surface fibril formation. *J Mol Biol* **335**, 1039–1049.
- 149 Dikiy I & Eliezer D (2012) Folding and misfolding of alpha-synuclein on membranes. *Biochim Biophys Acta – Biomembr* **1818**, 1013–1018.
- 150 Bokvist M & Grobner G (2007) Misfolding of amyloidogenic protein at membrane surfaces: impact of macromolecular crowding. *J Am Chem. Soc* **129**, 14848–14849.
- 151 Banerjee PR, Moosa MM & Deniz AA (2016) Two-dimensional crowding uncovers a hidden conformation of  $\alpha$ -synuclein. *Angew Chemie – Int Ed* **55**, 12789–12792.
- 152 Liu W, Fu L, Wang Z, Sohrabpour Z, Li X, Liu Y, Wang H & Yan ECY (2018) Two dimensional crowding effects on protein folding at interfaces observed by chiral vibrational sum frequency generation spectroscopy. *Phys Chem Chem Phys* **20**, 22421–22426.
- 153 Ye C, Chai Q, Zhong M & Wei Y (2013) Effect of crowding by Ficolls on OmpA and OmpT refolding and membrane insertion. *Protein Sci* **22**, 239–245.
- 154 De Geyter J, Tsigotaki A, Orfanoudaki G, Zorzini V, Economou A & Karamanous S (2016) Protein folding in the cell envelope of *Escherichia coli*. *Nat Microbiol* **1**, 16107.
- 155 McNulty BC, Young GB & Pielak GJ (2006) Macromolecular crowding in the *Escherichia coli* periplasm maintains  $\alpha$ -synuclein disorder. *J Mol Biol* **355**, 893–897.
- 156 Colclasure GC & Parker JC (1991) Cytosolic protein concentration is the primary volume signal dog red cells. *J Gen Physiol* **98**, 881–892.
- 157 Karasawa A, Swier LJYM, Stuart MCA, Brouwers J, Helms B & Poolman B (2013) Physicochemical factors controlling the activity and energy coupling of an ionic strength-gated ATP-binding cassette (ABC) transporter. *J Biol Chem* **288**, 29862–29871.
- 158 Culham DE, Meinecke M & Wood JM (2012) Impacts of the osmolality and the lumenal ionic strength on osmosensory transporter ProP in proteoliposomes. *J Biol Chem* **287**, 27813–27822.
- 159 Ressler S, Terwisscha Van Scheltinga AC, Vorrhein C, Ott V & Ziegler C (2009) Molecular basis of transport and regulation in the Na<sup>+</sup>/betaine symporter BetP. *Nature* **458**, 47–52.
- 160 Rowe I, Anishkin A, Kamaraju K, Yoshimura K & Sukharev S (2014) The cytoplasmic cage domain of the mechanosensitive channel MscS is a sensor of macromolecular crowding. *J Gen Physiol* **143**, 543–557.
- 161 Perozo E, Kloda A, Cortes DM & Martinac B (2002) Physical principles underlying the transduction of bilayer deformation forces during mechanosensitive channel gating. *Nat Struct Biol* **9**, 696–703.
- 162 Lindén M, Sens P & Phillips R (2012) Entropic tension in crowded membranes. *PLoS Comput Biol* **8**, e1002431.
- 163 Agarraberes FA & Dice JF (2001) Protein translocation across membranes. *Biochim Biophys Acta – Biomembr* **1513**, 1–24.

- 164 Gopinathan A & Kim YW (2007) Polymer translocation in crowded environments. *Phys Rev Lett* **99**, 228106.
- 165 Cao WP, Sun LZ, Wang C & Luo MB (2011) Monte Carlo simulation on polymer translocation in crowded environment. *J Chem Phys* **135**, 174901.
- 166 Chen Y & Luo K (2013) Dynamics of polymer translocation through a nanopore induced by different sizes of crowding agents. *J Chem Phys* **138**, 204903.
- 167 Larimi MG, Mayse LA & Movileanu L (2019) Interactions of a polypeptide with a protein nanopore under crowding conditions. *ACS Nano* **13**, 4469–4477.
- 168 Ayub M & Bayley H (2016) Engineered transmembrane pores. *Curr Opin Chem Biol* **34**, 117–126.
- 169 Lipowsky R, Risselada HJ, Jahn R, Sykes C, Baumgart T, Frolov VA, Dimova R, Lauritsen L, Voth GA, Deserno M *et al.* (2018) The 2018 biomembrane curvature and remodeling roadmap. *J Phys D Appl Phys* **51**, 343001.
- 170 Kozlov MM, Campelo F, Liska N, Chernomordik LV, Marrink SJ & McMahon HT (2014) Mechanisms shaping cell membranes. *Curr Opin Cell Biol* **29**, 53–60.
- 171 Zimmerberg J & Gawrisch K (2006) The physical chemistry of biological membranes. *Nat Chem Biol* **2**, 564–567.
- 172 Shi Z & Baumgart T (2015) Membrane tension and peripheral protein density mediate membrane shape transitions. *Nat Commun* **6**, 5974.
- 173 Franquelim HG, Khmelinskaia A, Sobczak JP, Dietz H & Schwille P (2018) Membrane sculpting by curved DNA origami scaffolds. *Nat Commun* **9**, 811.
- 174 Snead WT, Hayden CC, Gadok AK, Zhao C, Lafer EM, Rangamani P & Stachowiak JC (2017) Membrane fission by protein crowding. *Proc Natl Acad Sci U S A* **114**, E3258–E3267.
- 175 Stachowiak JC, Hayden CC & Sasaki DY (2010) Steric confinement of proteins on lipid membranes can drive curvature and tubulation. *Proc Natl Acad Sci U S A* **107**, 7781–7786.
- 176 Chen Z, Atefi E & Baumgart T (2016) Membrane shape instability induced by protein crowding. *Biophys J* **111**, 1823–1826.
- 177 Dahmani I, Ludwig K & Chiantia S (2019) Influenza A matrix protein M1 induces lipid membrane deformation via protein multimerization. *Biosci Rep* **39**, BSR20191024.
- 178 Steinkühler J, Knorr RL, Zhao Z, Bhatia T, Bartelt SM, Wegner S, Dimova R & Lipowsky R (2020) Controlled division of cell-sized vesicles by low densities of membrane-bound proteins. *Nat Commun* **11**, 905.
- 179 Van Der Lee R, Buljan M, Lang B, Weatheritt RJ, Daughdrill GW, Dunker AK, Fuxreiter M, Gough J, Gsponer J, Jones DT *et al.* (2014) Classification of intrinsically disordered regions and proteins. *Chem Rev* **114**, 6589–6631.
- 180 Busch DJ, Houser JR, Hayden CC, Sherman MB, Lafer EM & Stachowiak JC (2015) Intrinsically disordered proteins drive membrane curvature. *Nat Commun* **6**, 7875.
- 181 Snead WT, Zeno WF, Kago G, Perkins RW, Blair Richter J, Zhao C, Lafer EM & Stachowiak JC (2019) BAR scaffolds drive membrane fission by crowding disordered domains. *J Cell Biol* **218**, 664–682.
- 182 Siaw HMH, Raghunath G & Dyer RB (2018) Peripheral protein unfolding drives membrane bending. *Langmuir* **34**, 8400–8407.
- 183 Doyle DA, Cabral JM, Pfuetzner RA, Kuo A, Gulbis JM, Cohen SL, Chait BT & MacKinnon R (1998) The structure of the potassium channel: molecular basis of K<sup>+</sup> conduction and selectivity. *Science* **280**, 69–77.
- 184 Fowler PW, Hélie J, Duncan A, Chavent M, Koldso H & Sansom MSP (2016) Membrane stiffness is modified by integral membrane proteins. *Soft Matter* **12**, 7792–7803.
- 185 Madsen JJ, Grime JMA, Rossman JS & Voth GA (2018) Entropic forces drive clustering and spatial localization of influenza A M2 during viral budding. *Proc Natl Acad Sci U S A* **115**, E8595–E8603.
- 186 Paulino J, Pang X, Hung I, Zhou HX & Cross TA (2019) Influenza A M2 channel clustering at high protein/lipid ratios: viral budding implications. *Biophys J* **116**, 1075–1084.
- 187 Klusch N, Murphy BJ, Mills DJ, Yildiz Ö & Kühlbrandt W (2017) Structural basis of proton translocation and force generation in mitochondrial ATP synthase. *Elife* **6**, e33274.
- 188 Dudkina NV, Heinemeyer J, Keegstra W, Boekema EJ & Braun HP (2005) Structure of dimeric ATP synthase from mitochondria: An angular association of monomers induces the strong curvature of the inner membrane. *FEBS Lett* **579**, 5769–5772.
- 189 Blum TB, Hahn A, Meier T, Davies KM & Kühlbrandt W (2019) Dimers of mitochondrial ATP synthase induce membrane curvature and self-assemble into rows. *Proc Natl Acad Sci U S A* **116**, 4250–4255.
- 190 Scheve CS, Gonzales PA, Momin N & Stachowiak JC (2013) Steric pressure between membrane-bound proteins opposes lipid phase separation. *J Am Chem Soc* **135**, 1185–1188.
- 191 Zeno WF, Johnson KE, Sasaki DY, Risbud SH & Longo ML (2016) Dynamics of crowding-induced mixing in phase separated lipid bilayers. *J Phys Chem B* **120**, 11180–11190.
- 192 Imam ZI, Kenyon LE, Carrillo A, Espinoza I, Nagib F & Stachowiak JC (2016) Steric pressure among membrane-bound polymers opposes lipid phase separation. *Langmuir* **32**, 3774–3784.

- 193 Al-Habori M (2001) Macromolecular crowding and its role as intracellular signalling of cell volume regulation. *Int J Biochem Cell Biol* **33**, 844–864.
- 194 Aknoun S, Savatier J, Bon P, Galland F, Abdeladim L, Wattellier B & Monneret S (2015) Living cell dry mass measurement using quantitative phase imaging with quadriwave lateral shearing interferometry : an accuracy and sensitivity discussion quantitative phase imaging with quadriwave. *J Biomed Opt* **20**, 126009.
- 195 Kubitschek HE, Baldwin WW, Schroeter SJ & Graetzer R (1984) Independence of buoyant cell density and growth Rate in *Escherichia coli*. *J Bacteriol* **158**, 296–299.
- 196 Movasaghi Z, Rehman S & Rehman IU (2007) Raman spectroscopy of biological tissues. *Appl Spectrosc Rev* **42**, 493–541.
- 197 Luby-Phelps K, Castle PE, Taylor DL & Lanni F (1987) Hindered diffusion of inert tracer particles in the cytoplasm of mouse 3T3 cells. *Proc Natl Acad Sci U S A* **84**, 4910–4913.
- 198 Delarue M, Brittingham GP, Pfeffer S, Surovtsev IV, Pinglay S, Kennedy KJ, Schaffer M, Gutierrez JI, Sang D, Poterewicz G *et al.* (2018) mTORC1 controls phase separation and the biophysical properties of the cytoplasm by tuning crowding. *Cell* **174**, 338–349.
- 199 Mika JT, Thompson AJ, Dent MR, Brooks NJ, Michiels J, Hofkens J & Kuimova MK (2016) Measuring the viscosity of the *Escherichia coli* plasma membrane using molecular rotors. *Biophys J* **111**, 1528–1540.
- 200 Konopka MC, Shkel IA, Cayley S, Record MT & Weisshaar JC (2006) Crowding and confinement effects on protein diffusion in vivo. *J Bacteriol* **188**, 6115–6123.
- 201 Nawrocki G, Wang PH, Yu I, Sugita Y & Feig M (2017) Slow-down in diffusion in crowded protein solutions correlates with transient cluster formation. *J Phys Chem B* **121**, 11072–11084.
- 202 Schavemaker PE, Śmigiel WM & Poolman B (2017) Ribosome surface properties may impose limits on the nature of the cytoplasmic proteome. *Elife* **6**, e30084.
- 203 Guzman I, Gelman H, Tai J & Gruebele M (2014) The extracellular protein VlsE is destabilized inside cells. *J Mol Biol* **426**, 11–20.
- 204 Groen J, Foschepoth D, Te Brinke E, Boersma AJ, Imamura H, Rivas G, Heus HA & Huck WTS (2015) Associative interactions in crowded solutions of biopolymers counteract depletion effects. *J Am Chem Soc* **137**, 13041–13048.
- 205 Mu X, Choi S, Lang L, Mowray D, Dokholyan NV, Danielsson J & Oliveberg M (2017) Physicochemical code for quinary protein interactions in *Escherichia coli*. *Proc Natl Acad Sci U S A* **114**, E4556–E4563.
- 206 Gnutt D, Gao M, Brylski O, Heyden M & Ebbinghaus S (2015) Excluded-volume effects in living cells. *Angew Chemie – Int Ed* **54**, 2548–2551.
- 207 Murade CU & Shubeita GT (2019) A molecular sensor reveals differences in macromolecular crowding between the cytoplasm and nucleoplasm. *ACS Sensors* **4**, 1835–1843.
- 208 Boersma AJ, Zuhorn IS & Poolman B (2015) A sensor for quantification of macromolecular crowding in living cells. *Nat Methods* **12**, 227–229.
- 209 Liu B, Åberg C, van Eerden FJ, Marrink SJ, Poolman B & Boersma AJ (2017) Design and properties of genetically encoded probes for sensing macromolecular crowding. *Biophys J* **112**, 1929–1939.
- 210 Liu B, Mavrova SN, Van Den Berg J, Kristensen SK, Mantovanelli L, Veenhoff LM, Poolman B & Boersma AJ (2018) Influence of fluorescent protein maturation on FRET measurements in living cells. *ACS Sensors* **3**, 1735–1742.
- 211 Liu B, Hasrat Z, Poolman B & Boersma AJ (2019) Decreased effective macromolecular crowding in *Escherichia coli* adapted to hyperosmotic stress. *J Bacteriol* **209**, 1–11.
- 212 Mouton SN, Thaller DJ, Crane MM, Rempel IL, Kaeberlein M, Lusk CP, Boersma AJ & Veenhoff LM. A physicochemical roadmap of yeast replicative aging. submitted.
- 213 Gnutt D, Brylski O, Edengeiser E, Havenith M & Ebbinghaus S (2017) Imperfect crowding adaptation of mammalian cells towards osmotic stress and its modulation by osmolytes. *Mol Biosyst* **13**, 2218–2221.
- 214 Sukenik S, Ren P & Gruebele M (2017) Weak protein-protein interactions in live cells are quantified by cell-volume modulation. *Proc Natl Acad Sci U S A* **114**, 6776–6781.
- 215 Holman D, Parutto P, Chambers JE, Fantham M, Young LJ, Marciniak SJ, Kaminski CF, Ron D & Avezov E (2018) Single particle trajectories reveal active endoplasmic reticulum luminal flow. *Nat Cell Biol* **20**, 1118–1125.
- 216 Asakura S & Oosawa F (1958) Interaction between particles suspended in solutions. *J Polym Sci* **XXXIII**, 183–192.
- 217 Marenduzzo D, Finan K & Cook PR (2006) The depletion attraction: An underappreciated force driving cellular organization. *J Cell Biol* **175**, 681–686.
- 218 Kang H, Pincus PA, Hyeon C & Thirumalai D (2015) Effects of macromolecular crowding on the collapse of biopolymers. *Phys Rev Lett* **114**, 068303.
- 219 Minton AP (2005) Models for excluded volume interaction between an unfolded protein and rigid macromolecular cosolutes: Macromolecular crowding and protein stability revisited. *Biophys J* **88**, 971–985.
- 220 Schwarz J, J Leopold H, Leighton R, Miller RC, Aplin CP, Boersma AJ, Heikal AA & Sheets ED

- (2019) Macromolecular crowding effects on energy transfer efficiency and donor-acceptor distance of hetero-FRET sensors using time-resolved fluorescence. *Methods Appl Fluoresc* **7**, 025002.
- 221 Konopka MC, Sochacki KA, Bratton BP, Shkel IA, Record MT & Weisshaar JC (2009) Cytoplasmic protein mobility in osmotically stressed *Escherichia coli*. *J Bacteriol* **91**, 231–237.
- 222 Broecker J, Fiedler S, Gimpl K & Keller S (2014) Polar interactions trump hydrophobicity in stabilizing the self-inserting membrane protein mistic. *J Am Chem Soc* **136**, 13761–13768.
- 223 Park E & Rapoport TA (2012) Mechanisms of Sec61/SecY-mediated protein translocation across membranes. *Annu Rev Biophys* **41**, 21–40.
- 224 Nussinov R, Tsai CJ & Jang H (2018) Oncogenic ras isoforms signaling specificity at the membrane. *Cancer Res* **78**, 593–602.
- 225 Simons K & Gerl MJ (2010) Revitalizing membrane rafts: new tools and insights. *Nat Rev Mol Cell Biol* **11**, 688–699.
- 226 Dunstone MA & de Marco A (2017) Cryo-electron tomography: An ideal method to study membrane-associated proteins. *Philos Trans R Soc. B Biol Sci* **372**, 20160210.

---

### 3.2 Genetically-encoded sensors for measuring macromolecular crowding at the lipid membrane interface – Publication

Title:	<b>Probing macromolecular crowding at the lipid membrane interface with genetically-encoded sensors</b>
Authors:	Maryna Löwe, Sebastian Hänsch, Eymen Hachani, Lutz Schmitt, Stefanie Weidtkamp-Peters and Alexej Kedrov
Published in:	Protein Science
Impact factor:	8.0
Proportionate work:	80 %
Own contribution to this manuscript:	Design of experiments, expression and purification of (membrane) proteins, spectroscopy of the crowding sensor constructs, data analysis (except for MALS and SR-SIM), preparing of figures, writing and editing of the manuscript

Received: 1 May 2023 | Revised: 25 August 2023 | Accepted: 28 September 2023

DOI: 10.1002/pro.4797

## RESEARCH ARTICLE



# Probing macromolecular crowding at the lipid membrane interface with genetically-encoded sensors

Maryna Löwe<sup>1</sup> | Sebastian Hänsch<sup>2</sup> | Eymen Hachani<sup>3</sup> |  
Lutz Schmitt<sup>3</sup> | Stefanie Weidtkamp-Peters<sup>2</sup> | Alexej Kedrov<sup>1</sup>

<sup>1</sup>Synthetic Membrane Systems, Institute of Biochemistry, Heinrich Heine University Düsseldorf, Düsseldorf, Germany

<sup>2</sup>Center for Advanced imaging, Heinrich Heine University Düsseldorf, Düsseldorf, Germany

<sup>3</sup>Institute of Biochemistry, Heinrich Heine University Düsseldorf, Düsseldorf, Germany

**Correspondence**

Alexej Kedrov, Synthetic Membrane Systems, Institute of Biochemistry, Heinrich Heine University Düsseldorf, Universitätsstraße 1, Düsseldorf 40225, Germany.  
Email: [kedrov@hhu.de](mailto:kedrov@hhu.de)

**Funding information**

Deutsche Forschungsgemeinschaft, Grant/Award Number: Ke1879/3; Collaborative Research Center 1208

**Review Editor:** Aitziber L. Cortajarena

**Abstract**

Biochemical processes within the living cell occur in a highly crowded environment, where macromolecules, first of all proteins and nucleic acids, occupy up to 30% of the volume. The phenomenon of macromolecular crowding is not an exclusive feature of the cytoplasm and can be observed in the densely protein-packed, nonhomogeneous cellular membranes and at the membrane interfaces. Crowding affects diffusional and conformational dynamics of proteins within the lipid bilayer, alters kinetic and thermodynamic properties of biochemical reactions, and modulates the membrane organization. Despite its importance, the non-invasive quantification of the membrane crowding is not trivial. Here, we developed a genetically-encoded fluorescence-based sensor for probing the macromolecular crowding at the membrane interfaces. Two sensor variants, both composed of fluorescent proteins and a membrane anchor, but differing by flexible linker domains were characterized in vitro, and the procedures for the membrane reconstitution were established. Steric pressure induced by membrane-tethered synthetic and protein crowders altered the sensors' conformation, causing increase in the intramolecular Förster's resonance energy transfer. Notably, the effect of protein crowders only weakly correlated with their molecular weight, suggesting that other factors, such as shape and charge contribute to the crowding via the quinary interactions. Finally, measurements performed in inner membrane vesicles of *Escherichia coli* validated the crowding-dependent dynamics of the sensors in the physiologically relevant environment. The sensors offer broad opportunities to study interfacial crowding in a complex environment of native membranes, and thus add to the toolbox of methods for studying membrane dynamics and proteostasis.

**KEYWORDS**

biological interfaces, biosensors, excluded volume, fluorescence spectroscopy, FRET, membrane dynamics, quinary interactions, steric repulsion

This is an open access article under the terms of the [Creative Commons Attribution-NonCommercial](https://creativecommons.org/licenses/by-nc/4.0/) License, which permits use, distribution and reproduction in any medium, provided the original work is properly cited and is not used for commercial purposes.

© 2023 The Authors. *Protein Science* published by Wiley Periodicals LLC on behalf of The Protein Society.

*Protein Science*. 2023;32:e4797.  
<https://doi.org/10.1002/pro.4797>

[wileyonlinelibrary.com/journal/pro](https://wileyonlinelibrary.com/journal/pro)

1 of 18

## 1 | INTRODUCTION

The interiors of a living cell are recognized as crowded environments, where the concentration of biological macromolecules, predominantly proteins, polynucleotides and their complexes lays in the range of 150–200 mg/mL for eukaryotic cells, and it may reach 400 mg/mL for the bacterial cytoplasm (Speer et al., 2022; Srere, 1980; Zimmerman & Trach, 1991). In the most generalized view, those macromolecules are seen as hard-core spheres due to their compact folded state. Repulsive entropic interactions during their random collisions render the “excluded volume”, that is, the space not accessible for biological molecules, which may account for 10%–30% of the cytoplasm volume (Rivas & Minton, 2018). More recently, intrinsic surface properties of the macromolecules gained attention, as it has become evident that the charge and shape of interacting molecules determine the patterns of more complex crowding effects (Guseman et al., 2018; Kuznetsova et al., 2015; Speer et al., 2022). Those properties define the so-called “quinary” interactions, and together with the excluded volume they typically decrease diffusion rates of molecules (Nawrocki et al., 2017), affect their conformation and folding (Bai et al., 2017; Guseman et al., 2018; Kuznetsova et al., 2014; van den Berg et al., 1999), and modulate thermodynamic and kinetic properties of biochemical reaction involving one or a few molecules (Minton & Wilf, 1981; Rohwer et al., 1998; Zimmerman & Pfeiffer, 1983). For the more detailed overview of the theory and implications of the macromolecular crowding, first of all in solution, we refer the reader to the recent reviews on the topic (Rivas & Minton, 2022; Speer et al., 2022).

Although less investigated so far, macromolecular crowding has been also described for the cellular membranes, where the heterogeneous lipid bilayer and ubiquitous integral and peripheral proteins build a complex fluid mosaic structure (Engelman, 2005; Robertson, 2018; Sezgin et al., 2017). The crowding levels mediated by the membrane proteins, anchored cytoskeleton and eventually polysaccharides are highly specific for cell types and intracellular localization. In red blood cells, proteins occupy 25%–30% of the total plasma membrane area (Dupuy & Engelman, 2008), but the protein content may reach 50% within the light-sensitive membrane of the eye rod (Fotiadis et al., 2003), and further up to 80% in the densely packed thylakoid membranes (Kirchhoff, 2008; Liu & Scheuring, 2013). This high spatial density of proteins within the lipid bilayer or associated with the membrane interface affects essential cellular processes,

including transport across the membrane, cell signaling and energy metabolism, but may also mediate protein distribution within the membrane and affect the membrane morphology on the meso-scale (Guigas & Weiss, 2016; Löwe et al., 2020). Despite being an intrinsic property of the cellular membranes, the macromolecular crowding is rarely addressed in molecular studies performed either in native or reconstituted membrane systems. One bottleneck here is quantification of the crowding level and mimicking it appropriately with either proteinaceous or synthetic crowding agent. Previously, a few attempts have been taken to assess the crowding in lipid membranes using non-invasive fluorescence-based approaches. In an early example, crowding-dependent dimerization of the fluorescently-labeled glycophorin A was studied when monitoring changes in Förster’s resonance energy transfer (FRET) (Chen et al., 2010). Another approach for the measurement of the interfacial membrane coverage was proposed by the group of Stachowiak and co-workers (Houser et al., 2020). The developed synthetic system comprised a polyethylene glycol (PEG) chain anchored at the liposome interface and bearing a donor fluorophore on its free end, and acceptor fluorophores incorporated into the membrane plane. Upon binding of protein crowders to the lipid membrane, the steric pressure forced the PEG molecules to elongate and extend over the surface, thus causing decrease in the FRET efficiency. Most recently, functionalized PEG molecules could be also anchored into the plasma membrane and their crowding-dependent accessibility was tested by antibodies, offering a tool for measuring crowding at the outer border of a living cell (Arnold et al., 2023; Takatori et al., 2023).

Here, we describe a genetically-encoded sensory protein that is suitable for probing the interfacial crowding in synthetic and native membranes. The sensor consists of two fluorescent proteins forming a FRET pair (Boersma et al., 2015), which are connected via a flexible linker and a hydrophobic domain. The hydrophobic domain serves as an anchor, so the sensor is stably incorporated into synthetic liposomes or the cytosolic interface of the cellular membrane. The sensor is sterically compressed by the soluble and membrane-coupled crowders, so the associated changes in FRET efficiency report on the lateral confinement at the membrane surface. We demonstrate that the crowding induced by either proteins or polymers of varying sizes may be assessed using the sensor, and the measurements may be carried out also in native cellular membranes, thus offering a robust approach for crowding analysis in complex environments.

## 2 | RESULTS

### 2.1 | Design and expression of the crowding sensors

The primary elements of the FRET-based protein sensor are two fluorescent moieties, such as mCerulean and mCitrine fluorescent proteins, which emission and excitation spectra partially overlap, and a flexible linker, whose structural properties may be altered (Boersma et al., 2015; Liu et al., 2017). Designing a membrane-associated sensor further required: (i) stable anchoring of the sensor within the lipid bilayer or at the interface of the native and reconstituted membranes; (ii) *cis*-configuration of two fluorescent proteins relative to the membrane plane; and (iii) sufficient flexibility of the intramolecular linkers to allow the crowding-dependent conformational dynamics. A transmembrane helical pair, or *hairpin*, was considered as a suitable membrane anchor, where the fluorescent proteins could be positioned at its N- and C-terminal ends. First, membrane-embedded helical pairs play an important role in membrane protein folding and manifest high stability within the lipid bilayer (Engelman & Steitz, 1981; Kedrov et al., 2007). Second, a helical hairpin would ensure the appropriate topology of the sensor, so the fluorescent

proteins would be positioned in proximity to each other at the same side of the membrane.

The recent structure of the membrane-embedded SecYEG translocon of *Escherichia coli* visualized a helical hairpin built of TMHs 1–2 of SecE (Kater et al., 2019) (Suppl. Figure 1A). Although being a part of the quaternary complex, the hairpin has minimal contacts with other TMHs of the translocon or within the translocon dimer, and so it forms a stably folded structural unit (Breyton et al., 2002). Indeed, the SecE TMH 1–2 hairpin, optionally extended with either a N- or C-terminal soluble domain, was efficiently expressed in *E. coli* as a membrane protein, validating the choice of the potential anchor (Suppl. Figure 1B). Next, the SecE hairpin was cloned into the middle of the soluble crowding sensor (Boersma et al., 2015) resulting in two constructs, where the intramolecular linkers either consisted of flexible Gly-Ser-Gly repeats (further referred as (GSG)<sub>6</sub>-SecE) or also contained Glu-Ala-Ala-Ala-Lys repeats forming soluble  $\alpha$ -helices ( $\alpha$ H-SecE; Figure 1a). Both sensors were overexpressed in *E. coli* and incorporated into membranes as the full-length proteins, while the degradation products were largely localized to the cytoplasmic fraction (Suppl. Figure 2). Repetitive washes of the membrane fraction, also with either sodium carbonate or urea, which remove loosely attached peripheral proteins,

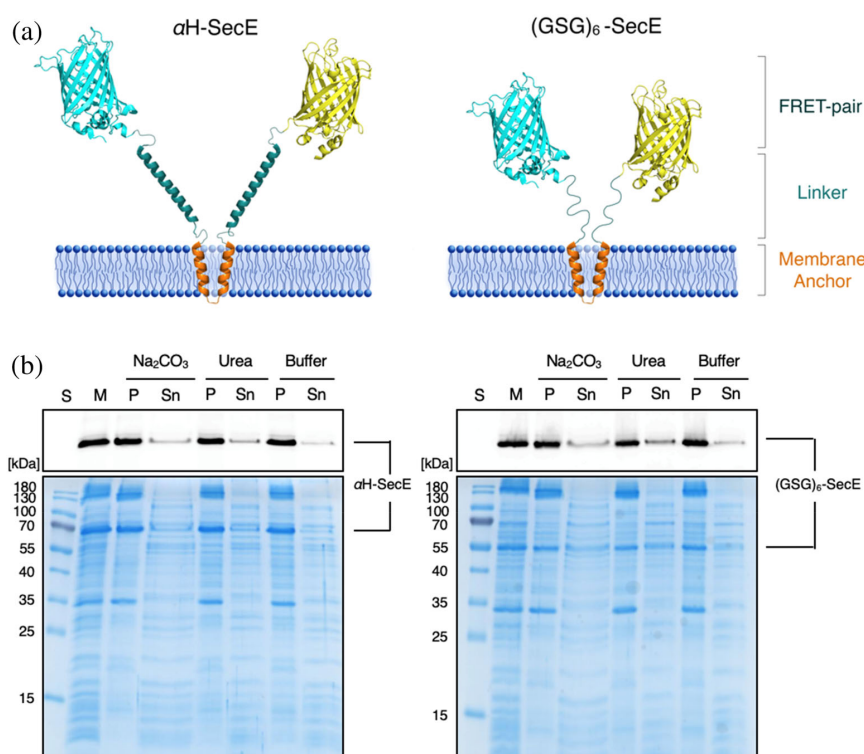


**FIGURE 1** Design and expression of membrane crowding sensors. (a) Schematic representation of the designed sensors. (b) SDS-PAGE of crude membrane extract containing the indicated sensor prior (“M”) and after incubation/washing with either Na<sub>2</sub>CO<sub>3</sub>, urea or the storage buffer. “P” and “Sn”, pellet and supernatant fractions after the incubation, respectively. “S”: PageRuler Prestained Protein ladder (Thermo Fisher Scientific). Top: In-gel fluorescence; bottom: Coomassie-stained gels.

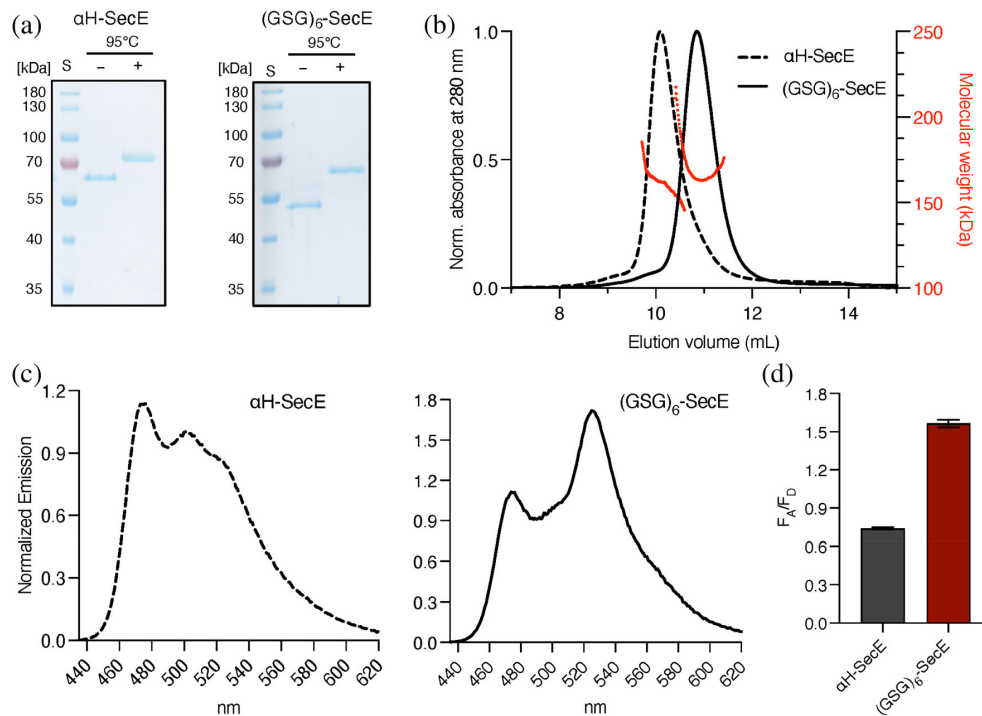


**FIGURE 2** Isolation and characterization of the membrane crowding sensors. (a) SDS-PAGE of purified  $\alpha$ H-SecE and  $(\text{GSG})_6$ -SecE sensors, with and without thermal denaturation. (b) SEC-MALS profiles of the purified sensors constructs and determination of the molar masses. (c) Fluorescence emission spectra of purified and detergent-solubilized sensors (normalized at 500 nm). (d) Calculated Förster's resonance energy transfer (FRET) efficiency for the detergent-solubilized sensors.

did not affect the localization of the sensor molecules (Figure 1b). Thus, the hydrophobic helical hairpin ensured stable anchoring of both constructs within the membrane.

To isolate the sensors for further characterization, the membranes were solubilized with 1% n-dodecyl  $\beta$ -D-maltoside (DDM) and the tagged sensors were purified via the metal affinity and size exclusion chromatography (SEC; Figure 2a, b). The migration of the sensors on SEC was unexpectedly fast for the proteins of  $\sim 70$  kDa, but could be potentially explained by the presence of DDM micelle of 76 kDa (Strop & Brunger, 2005), extended protein conformations and/or protein oligomerization. The molecular weights and the oligomeric state of both sensors were analyzed then by SEC coupled to multi-angle light scattering (SEC-MALS; Figure 2b). After subtracting the predicted mass of the DDM micelle, the average molecular weights were  $84 \pm 3$  kDa for  $\alpha$ H-SecE and  $92 \pm 1$  kDa for  $(\text{GSG})_6$ -SecE sensors. These values exceeded the weights of the monomeric sensors and suggested partial dimerization, which could be induced at the elevated protein concentration of 0.55 mg/mL in the SEC-MALS experiment. To tackle whether

the dimerization is dependent on the hydrophobic anchor, we examined a mutant sensor where the anchor domain was substituted with a polar polypeptide. While the calculated molecular mass of the protein is 59 kDa, the apparent mass determined in SEC-MALS experiments ranged from 72 kDa at 0.5 mg/mL to 80 kDa at 3.4 mg/mL (Suppl. Figure 3), and even larger species with the mass to 130 kDa could be resolved. Thus, the oligomerization propensity of the sensors at high concentrations could be related to the constituting fluorescent proteins, but unlikely to have substantial influence at the low levels of the sensor required for the spectroscopy applications.

## 2.2 | Spectroscopic characterization of the crowding sensors

The absorbance spectra of purified and detergent-solubilized  $\alpha$ H-SecE and  $(\text{GSG})_6$ -SecE sensors manifested the specific peaks for mCerulean and mCitrine at 433 and 515 nm, respectively (Suppl. Figure 4), and the difference in the peak intensities correlated with the extinction coefficients of the

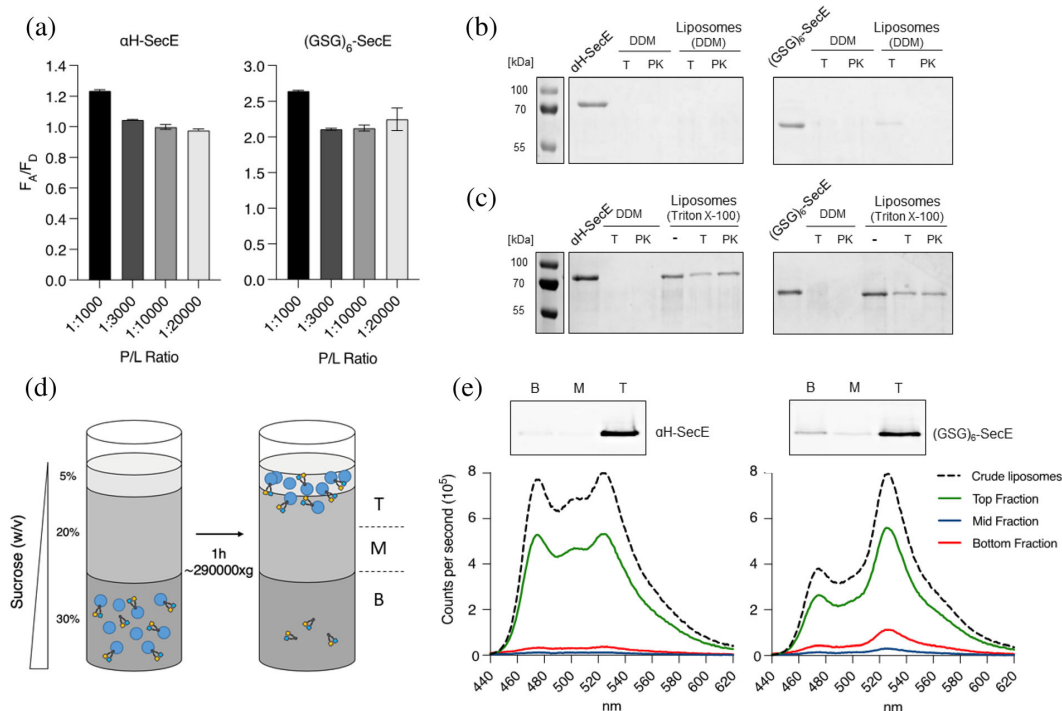


**FIGURE 3** Reconstitution of the crowding sensors in liposomes. (a) Förster's resonance energy transfer (FRET) efficiencies manifested by the sensors reconstituted at indicated protein-to-lipid (P/L) ratios. (b) Topology determination of the liposome-reconstituted sensors via limited proteolysis by trypsin, "T", or proteinase K, "PK". "DDM", detergent-solubilized sensors, "Liposomes (DDM)", sensors in proteoliposomes reconstituted using DDM. (c) Same as (b), but using Triton X-100 for the reconstitution. (d) Scheme of the flotation assay. Fractions collected after centrifugation: T (top), M (middle), B (bottom). (e) In-gel fluorescence and fluorescence emission spectra of the sensors in crude liposomes and in fractions collected from the flotation assay.

fluorescent proteins ( $\epsilon_{mCerulean}^{433nm} = 33,000 \text{ M}^{-1} \text{ cm}^{-1}$ ,  $\epsilon_{mCitrin}^{516nm} = 94,000 \text{ M}^{-1} \text{ cm}^{-1}$ ). The emission spectra of both sensors (Figure 2c) and the ratio between the acceptor and donor fluorescence at 525 and 475 nm, respectively (further indicated as  $F_A/F_D$  ratio), provided the information about the FRET efficiency, and so the sensor conformation.  $F_A/F_D$  ratios measured for the detergent-solubilized sensors were  $0.74 \pm 0.01$  for  $\alpha$ H-SecE, and  $1.56 \pm 0.03$  for  $(GSG)_6$ -SecE (Figure 2d). Thus, the folded helices within the linker domains of  $\alpha$ H-SecE ensured wider spacing between the fluorescent moieties. Interestingly, the values correlated with those previously measured for soluble sensors with comparable linker architectures manifested  $F_A/F_D$  ratios of 0.55 for the sensor GE (analog of  $\alpha$ H-SecE) and 1.4 for the sensor G12 (analog of  $(GSG)_6$ -SecE).

The detergent-solubilized sensors were examined for their propensity to respond to crowding upon increasing concentrations of PEG 6000 in solution (Suppl. Figure 5). PEG is an inert synthetic polymer commonly used as a mimetic crowding agent (Aumiller et al., 2014;

Kuznetsova et al., 2015; Liu et al., 2017). The hydrodynamic radius of PEG 6000 is 2.5 nm (Armstrong et al., 2004) that can be compared to the dimensions of lysozyme (2.2 nm) or GFP (2.8 nm) (Elowitz et al., 1999; Nemzer et al., 2013). Increasing PEG 6000 concentration from 0% to 30% (w/v) led to the substantial increase of the acceptor fluorescence, and so the FRET efficiency for both sensors (Suppl. Figure 5). In the presence of 30% PEG, the  $F_A/F_D$  ratio reached  $1.85 \pm 0.04$  for  $\alpha$ H-SecE and  $3.20 \pm 0.06$  for  $(GSG)_6$ -SecE, suggesting compression of the flexible sensor molecules under the steric forces. Diluting PEG 6000 from 20% to 10% caused a decrease of  $F_A/F_D$  ratios, so both sensors possessed sufficient flexibility to reversibly react to the crowding levels.

### 2.3 | Reconstitution of the sensors into lipid membranes

To characterize the performance of the sensors at the lipid interface, they were reconstituted into liposomes

composed of DOPC:DOPG lipids (molar ratio 7:3). Varying the sensor-to-lipid ratio allowed determining the effect of intermolecular FRET between the reconstituted sensors: The  $F_A/F_D$  values measured in liposomes at the ratios 1:3000, 1:10,000 and 1:20,000 were comparable with each other, with variations typically within 5% (Figure 3a). However, when the sensor-to-lipid ratio reached 1:1000, the FRET efficiency rapidly increased by approximately 20% for each sensor. Similar concentration dependence was observed for mCerulean-SecE and SecE-mCitrine co-reconstituted in liposomes (Suppl. Figure 6A, B), thus pointing to intermolecular FRET at elevated protein-to-lipid ratios, either due to random contacts or due to clustering of the sensors in the lipid membrane. Based on those insights and the optimal signal-to-noise level, further experiments were conducted at the reconstitution ratio of 1:3000, where a single sensor molecule would occur on average over 1000 nm<sup>2</sup> area of the lipid bilayer (Hills & McGlinchey, 2016; Kamel et al., 2022).

Next, we examined the topology of the reconstituted sensors, and so, their accessibility to the crowding agents, which could be added in the following steps. Aiming to incorporate the sensors with their fluorescent domains facing out of the liposomes, a mild detergent DDM was added to swell the liposomes, so the SecE hairpin could be inserted into transient pores within the membrane (Suppl. Figure 7A) (Knol et al., 1996). After removing the detergent, the topology was determined based on the sensor susceptibility to trypsin and proteinase K, two proteases with a broad specificity, which could completely degrade the detergent-solubilized sensors (Figure 3b and Suppl. Figure 8). For the reconstituted sensors, the proteases can only process the accessible parts of the molecule exposed to the exterior of the liposome, such as the linker domains, and the degradation may be monitored via SDS-PAGE. Upon the proteolytic treatment of the liposome-anchored sensors, the bands for the full-size proteins disappear for all samples, with an exception for the (GSG)<sub>6</sub>-SecE FRET sensor treated with trypsin. Here, the digest has not been accomplished completely. While the lysine-containing  $\alpha$ -helices in the  $\alpha$ H-SecE construct offer multiple cleavage sites, those not present within the linkers of (GSG)<sub>6</sub>-SecE, resulting in the partial proteolysis. The results implied that the majority of the liposome-reconstituted sensors had the outward-facing orientation. As a control, we performed the same experiment with proteoliposomes where the lipids were treated with 0.5% Triton X100 detergent prior to reconstitution (Figure 3c). Under these conditions, the liposomes were not swelled, but solubilized (Suppl. Figure 7B), which favored dual, stochastically-driven orientation of the sensor in the liposomes upon their re-assembly (Geertsma et al., 2008;

Knol et al., 1996). The pattern of the protected bands observed on SDS-PAGE after the protease treatment suggested that 30%–50% of sensors indeed acquired the inward-facing orientation (Figure 3c and Suppl. Figure 8). Thus, DDM-based reconstitution protocol was used for further experiments.

Notably, even at low sensor-to-lipid ratios  $F_A/F_D$  values in liposomes was by 25%–30% higher than those recorded for the detergent-solubilized sensors (Figure 2d). To examine whether the increased FRET signal is caused by the off-pathway aggregation, we analyzed the sensor reconstitution efficiency. Once loaded into the sucrose gradient, the liposomes could float to the top due to the density difference between the aqueous interior and the external solution (Figure 3d). Only reconstituted sensors were able to co-migrate with the liposomes, while the non-reconstituted and aggregated proteins remained at the bottom of the gradient. The analysis of the collected fractions by SDS-PAGE showed that both sensor variants predominantly appeared in the top fraction (Figure 3e). The reconstitution efficiency reached 96% for  $\alpha$ H-SecE and 84% for (GSG)<sub>6</sub>-SecE sensors. The proteins remaining in the minor bottom fraction manifested a high FRET efficiency, as  $F_A/F_D$  ratio reached  $2.59 \pm 0.10$  for (GSG)<sub>6</sub>-SecE sensor (not determined for  $\alpha$ H-SecE due to the low concentration in the bottom fraction), as could be expected from the clustered/aggregated molecules. The FRET efficiency of (GSG)<sub>6</sub>-SecE sensor in the top fraction was  $2.08 \pm 0.01$ , that matched closely the value measured for the crude reconstituted sensor,  $2.13 \pm 0.02$ . For  $\alpha$ H-SecE sensor prior and after the flotation assay the values were nearly identical,  $1.03 \pm 0.02$  and  $1.012 \pm 0.004$ , respectively (Figure 3d). Thus, we concluded that the sensors were successfully reconstituted into liposomes, and the resulting relatively high FRET efficiencies were due to altered conformations of the sensors in presence of the proximate lipid interface.

## 2.4 | Sensitivity of the sensors to crowding at the membrane interface

Increased FRET efficiency for the liposome-reconstituted sensors suggested that the proteins acquired more compact conformations at the membrane interface. We questioned whether the sensors remained sufficiently dynamic to respond to the changes in the proximate crowding. To test that, soluble PEG 2000 and 6000 were added to the proteoliposome suspension. Upon increasing PEG 6000 concentration up to 30% (v/v), FRET efficiency increased up to  $3.00 \pm 0.03$  for  $\alpha$ H-SecE (increase by 175%, Figure 4a–c) and to  $3.78 \pm 0.04$  for (GSG)<sub>6</sub>-SecE

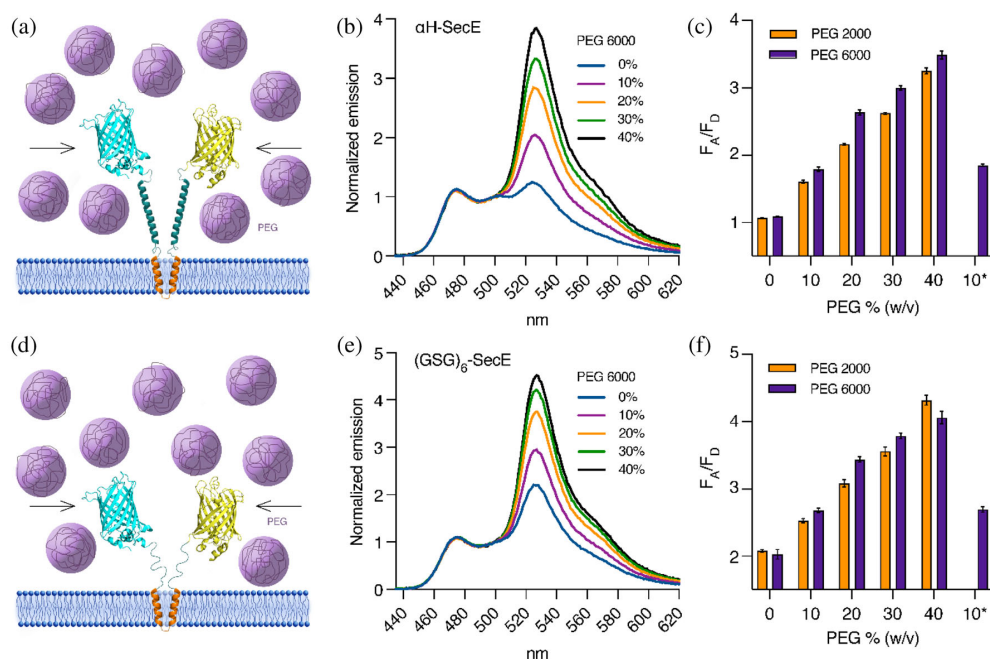


**FIGURE 4** Sensitivity of the membrane-anchored sensors to soluble crowders. (a) Scheme of the reconstituted  $\alpha$ H-SecE sensor in presence of polyethylene glycol (PEG) molecules in solution. (b) Fluorescence emission spectra of  $\alpha$ H-SecE in presence of PEG 6000 at indicated concentrations (w/v). The spectra are normalized at 500 nm. (c) Förster's resonance energy transfer (FRET) efficiencies of  $\alpha$ H-SecE in presence of PEG 6000 or PEG 2000 (mean  $\pm$  SD,  $n = 2$ ). Samples "10\*" correspond to two-fold dilution of 20% PEG 6000 for testing the reversibility of the sensor compaction. (d–f) Same as (a–c), for the liposome-reconstituted  $(\text{GSG})_6$ -SecE sensor.

(increase by 87%; Figure 4d–f), and the change in FRET was reversible for both sensors, when the crowders were diluted back to 10%. To examine the potential contribution of the sensor clustering, which may be stimulated within the two-dimensional membrane (Grasberger et al., 1986), the response of co-reconstituted individual fluorophores to soluble PEG was measured (Suppl. Figure 6C). As the FRET efficiency showed substantially weaker dependence on the crowders and even in presence of 30% PEG 6000 the increase did not exceed 50% (to be compared with the full-length  $\alpha$ H-SecE,  $F_A/F_D$  ratio increase by 175%), we concluded that the effect of the protein clustering was rather limited. Thus, despite the constraints set by the membrane interface, both  $\alpha$ H-SecE and  $(\text{GSG})_6$ -SecE sensors were responsive to the crowding levels, and the response was largely ensured by the intramolecular conformational changes.

In the next step, the performance of the sensors was studied in the presence of the interfacial polymer crowding. For this purpose, PEG-grafted lipids (DOPE-PEG 2000) were incorporated into the liposomes. PEG 2000 at the interface should render the lateral pressure (Marsh et al., 2003), which may cause steric compression of the membrane-anchored sensors (Figure 5a). Indeed, both

sensors responded to the changes in the interfacial crowding, as the FRET efficiency increased nearly linearly with increasing concentration of DOPE-PEG 2000 (Figure 5b–e). In presence of 10 mol% DOPE-PEG 2000, the FRET efficiency reached  $1.20 \pm 0.02$  for the  $\alpha$ H-SecE (increase by 16%), and  $2.86 \pm 0.17$  for the  $(\text{GSG})_6$ -SecE construct (increase by 33%).

Synthetic polymers, such as PEG, are commonly employed as inert crowders, which render steric repulsive forces. However, the proteins found at the cellular membranes are heterogeneous in their physico-chemical properties, such as size, shape and charge distribution, and so the physiological crowding goes beyond the "exclusion volume" effect, but also involves quinary interactions (Guseman et al., 2018; Kuznetsova et al., 2015; Speer et al., 2022). Thus, we set out to analyze the response of the developed crowding sensors to proteins coupled to the membrane interface. To generate protein-based crowding, proteins of choice ranging in their sizes and properties could be anchored at the membrane interface in a controlled way via either  $\text{Ni}^{2+}$ -NTA:histidine or biotin:streptavidin coupling. To ensure anchoring of various poly-histidine-tagged proteins, 18:1 DGS-NTA lipids were incorporated into liposomes, while the tag-less

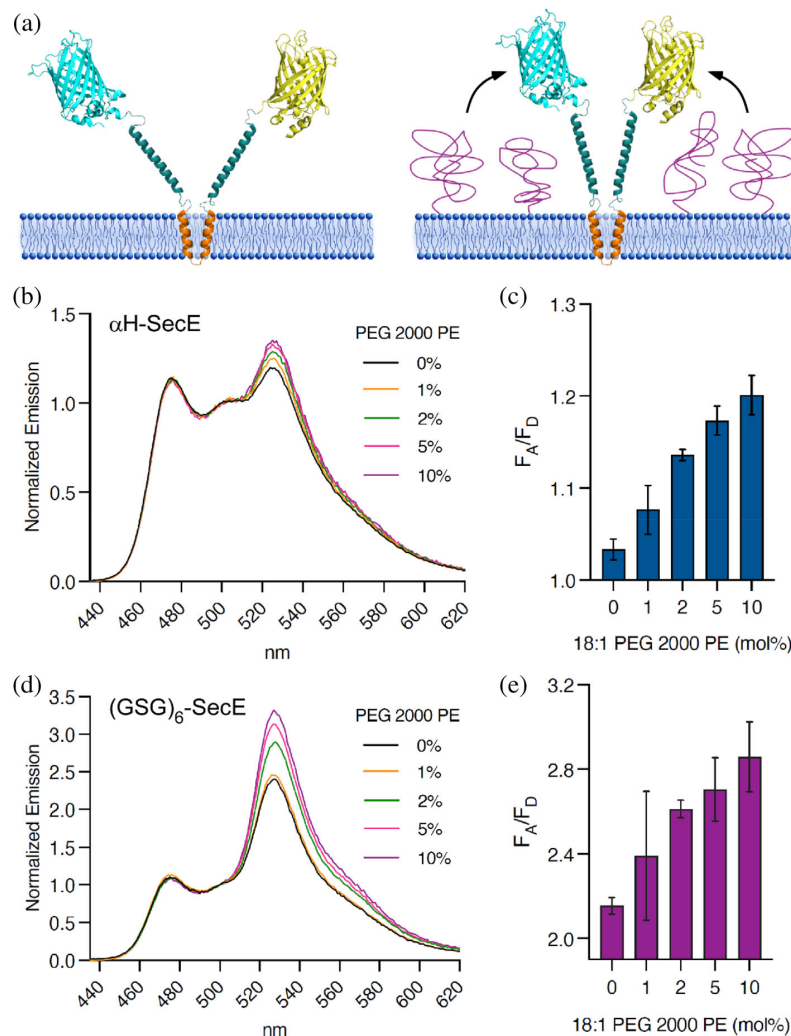


**FIGURE 5** Sensitivity of the membrane-anchored sensors to interfacial polymer crowding. (a) Scheme of the reconstituted  $\alpha$ H-SecE sensor upon compaction induced by a polymer at the membrane interface. (b and c) Fluorescence emission spectra and corresponding Förster's resonance energy transfer (FRET) efficiencies (mean  $\pm$  SD;  $n = 2$ ) of  $\alpha$ H-SecE sensor in presence of DOPE-PEG 2000 lipids at indicated concentrations (mol%). (d, e) Same as (b, c), for the reconstituted  $(\text{GSG})_6$ -SecE sensor.

sensors were employed for the reconstitution. The following poly-histidine-tagged proteins were used then as crowders: monomeric streptavidin (mSA; molecular mass 15.5 kDa) (Demonte et al., 2014), SecB chaperone (monomer size 20.3 kDa), and SecA ATPase with either N- or C-terminal poly-histidine-tags ( $\text{SecA}^{\text{N}}$  and  $\text{SecA}^{\text{C}}$ , monomer size  $\sim 100$  kDa) (Figure 6a, b). Among those, SecB forms a stable tetramer, thus reaching approximately 80 kDa mass (Smith et al., 1996), while SecA may exist both in monomeric and dimeric forms, but predominantly monomeric once it is bound to the membrane (Roussel & White, 2020).

Various amounts of the crowders were incubated with proteoliposomes to achieve either partial or complete coverage of the surface-exposed  $\text{Ni}^{2+}$ -NTA groups (Figure 6c) (Raghunath & Dyer, 2019). All the examined

protein crowders induced the concentration-dependent response of the  $\alpha$ H-SecE sensor, but the measured FRET efficiencies were protein-specific. Thus, titration of the ATPase SecA, the largest examined crowder, induced a rapid increase in the  $F_A/F_D$  ratio followed by a plateau, indicating saturation of the liposome surface with the bound crowder. Notably, different FRET efficiencies were achieved when using SecA variants, with the maximal increase of 14% for  $\text{SecA}^{\text{N}}$  and 8% for  $\text{SecA}^{\text{C}}$ . Strikingly, the relatively small protein mSA induced an equal increase in the FRET efficiency as the N-terminally bound  $\text{SecA}^{\text{N}}$  ATPase, while the tetrameric SecB caused the minimal change in the FRET signal (Figure 6c). Thus, although the sensor was responsive to all tested crowders, their molecular weights were not the decisive factor for the intensity of the response. At the end of the

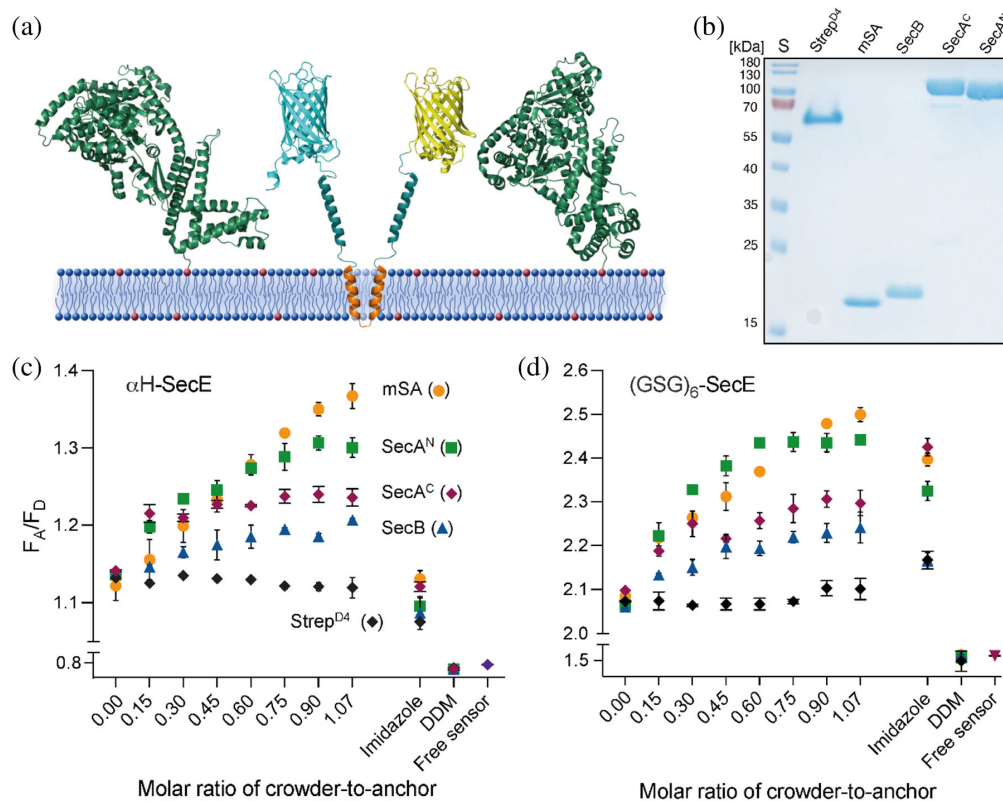


**FIGURE 6** Sensitivity of the membrane-anchored sensors to interfacial protein crowding. (a) Scheme of the reconstituted  $\alpha$ H-SecE sensor in presence of protein crowders, for example, SecA (green) anchored at the membrane interface via specific protein: lipid contact sites (red dots). (b) SDS-PAGE of purified proteins applied as crowders. (c) Förster's resonance energy transfer (FRET) efficiencies of the sensors in presence of increasing concentrations of the protein crowders. "Imidazole", FRET signal after adding 300 mM imidazole to detach the crowders. "DDM", FRET signal after adding detergent to extract the sensor from the membrane. "Free sensor", FRET signal of the sensor prior to the liposome reconstitution.

experiment, the proteoliposomes were incubated with imidazole to dissociate the crowders from the surface, and the FRET efficiency dropped to the initial crowder-free values. Disrupting the proteoliposomes with 1% DDM caused further decrease of the  $F_A/F_D$  ratio to 0.74, matching the value measured for the detergent-isolated sensor (Figure 2d). The non-tagged streptavidin variant Strept<sup>D4</sup> of 60 kDa served as a negative control, which did not affect the fluorescence, and so the sensor conformation (Howarth et al., 2006).

Qualitatively similar results were obtained when employing proteoliposomes with (GSG)<sub>6</sub>-SecE sensor, as the N-terminally anchored SecA<sup>N</sup> and mSA induced the most prominent increase in FRET (Figure 6d). However, addition of imidazole could only partially restore the FRET signal of the sensor, and not for all tested crowders. Notably, the signal even increased for the Strept<sup>D4</sup> protein that served as a negative control. Since the reversibility of

the sensor dynamics in response to changes in crowding was previously confirmed (Figure 4f), we suspect that the elevated imidazole concentration caused unpredicted conformational rearrangements within the flexible linkers, not related to the crowding per se. Nevertheless, excess of the detergent added to proteoliposomes triggered the decay in the FRET efficiency to the level of membrane-free sensor (Figure 6d).

In an alternative approach, the liposomes with  $\alpha$ H-SecE sensor were supplemented with 18:1 biotinyl cap PE lipids, so the crowder proteins could be deposited at the lipid membrane interface via biotin: streptavidin coupling (Suppl. Figure 9). Here, mSA played the role of the crowding agent, and its effect on the sensor conformation could be compared for two binding modes, that is, via NTA and biotin anchoring, as the protein contained a poly-histidine tag (Figure 6c). For the biotin-functionalized liposome containing  $\alpha$ H-SecE sensors,

continuous increase in the FRET efficiency was observed upon titrating mSA suggesting compression of the sensor (Suppl. Figure 10). At the highest examined mSA concentration, the  $F_A/F_D$  reached  $1.37 \pm 0.03$ , which indicates increase of the FRET efficiency by 22%, and the response of the sensor to the increasing mSA concentration was similar between biotin and  $\text{Ni}^{2+}$ -NTA surface anchors.

Finally, we examined whether  $\alpha\text{H-SecE}$  or  $(\text{GSG})_6\text{-SecE}$  are responsive to the crowding within the lipid bilayer. For this purpose, the sensors were reconstituted into liposomes (protein-to-lipid ratio 1:3000) in presence of the membrane protein complex SecYEG (Suppl. Figures 1 and 11A). *E. coli* SecYEG consists of 15 TMs connected by relatively short loops, and it lacks large extramembrane domains, so the protein should not render substantial interfacial crowding. Indeed, even at the molar ratio of SecYEG to lipids of 1:300 that corresponds to mass ratio of 1:3 neither of the crowding sensors manifested higher FRET efficiency (Suppl. Figure 11B). The observation does match the initial intuitive prediction, but it also suggests that the crowding within the membrane does not induce clustering of the sensors, that otherwise would result in high inter-molecular FRET.

## 2.5 | Crowding analysis in cellular membranes

The broad interest in genetically-encoded sensors arises from the opportunity to probe the conditions within the native cellular environments. Characterization of the crowding sensors in synthetic membranes provided above demonstrates their fitness for the proposed task, and we further set out to employ them for measuring the interfacial crowding in a physiologically relevant environment, the inner membrane of *E. coli*. As unambiguous analysis in the living cell would be complicated at this stage due to the intrinsically high crowding in the cytoplasm, we pursued measurements in isolated bacterial membranes.

While the low density of the sensors, and so minimal intermolecular FRET in model liposomes could be achieved by adjusting the protein: lipid ratio upon the membrane assembly (Figure 3a), the density of the sensors in the cellular membrane may be controlled by tuning their expression level. For this purpose, expression of both  $\alpha\text{H-SecE}$  and  $(\text{GSG})_6\text{-SecE}$  sensors was carried out using a tightly regulated arabinose-inducible promoter in presence of 0.001% L-arabinose. To validate the membrane localization of the expressed sensors, *E. coli* host cells were imaged by super-resolution structured illumination microscopy (SR-SIM) (Figure 7a). For both sensors, fluorescence signal of the acceptor fluorophore

mCitrine was observed along the contour of individual bacteria verifying the localization of the proteins at the membrane. Though the expression level was notably higher for  $\alpha\text{H-SecE}$ , the fluorescence signal of both variants was homogeneously distributed over the cell surface without cluster formation or accumulation at the poles.

The presence of both sensor in the membrane was further confirmed by SDS-PAGE in-gel fluorescence of the crude membrane extracts, and the fluorescence intensities correlated with SR-SIM results (Figure 7b). The inner and outer membrane vesicles (IMVs/OMVs) were then separated from each other by sucrose density gradient, and the sensors were predominantly found in the IMV-containing fractions (Figure 7c). To estimate the relative amount of the expressed sensors, we determined the total inner membrane protein concentration by a colorimetric assay, and the concentration of the sensor by SDS-PAGE in gel-fluorescence, where the independently purified sensor served for the signal calibration (Suppl. Figure 12).  $\alpha\text{H-SecE}$  sensor constituted 3.3% of the total inner membrane protein mass, and the fraction of weakly expressed  $(\text{GSG})_6\text{-SecE}$  did not exceed 2% of the total protein content.

For the extracted IMVs, the  $F_A/F_D$  ratios were  $1.17 \pm 0.01$  and  $2.19 \pm 0.03$  for  $\alpha\text{H-SecE}$  and  $(\text{GSG})_6\text{-SecE}$  sensors, respectively (Figure 7d), being within the value range measured previously for the synthetic membranes, either in the presence of PEG or proteinaceous crowders (Figures 5 and 6). To test whether intermolecular FRET had substantial contribution, we analyzed the signal of  $\alpha\text{H-SecE}$  sensor expressed upon varying arabinose concentration (Suppl. Figure 13). While the sensor amount scaled with the arabinose concentration, the FRET efficiencies between the samples differed by less than 5%. Importantly, in each sample the sensors were equally responsive to soluble crowders (10% PEG), while treatment of IMVs with sodium carbonate reduced  $F_A/F_D$  ratio by nearly 10%, as may be expected from forced dissociation of peripheral membrane proteins. With that relatively low abundance of the sensors, and absence of the aggregation clusters in the cells (Figure 7a), we assumed that the intermolecular FRET would not substantially contribute to the fluorescence read-out, and the FRET signal could be related to the crowding-dependent conformations of the sensors. Addition of Strep<sup>D4</sup> did not influence the sensor conformation, as the  $F_A/F_D$  ratios were not affected ( $1.15 \pm 0.01$  for  $\alpha\text{H-SecE}$  and  $2.21 \pm 0.01$  for  $(\text{GSG})_6\text{-SecE}$ ; Figure 7d), and the protein was not expected to interact with the membrane surface. To induce the interfacial crowding, we employed the ATPase SecA, as the protein contains an amphipathic N-terminal helix essential for docking SecA at the membrane interface (Kamel et al., 2022). Addition of SecA had a weak,

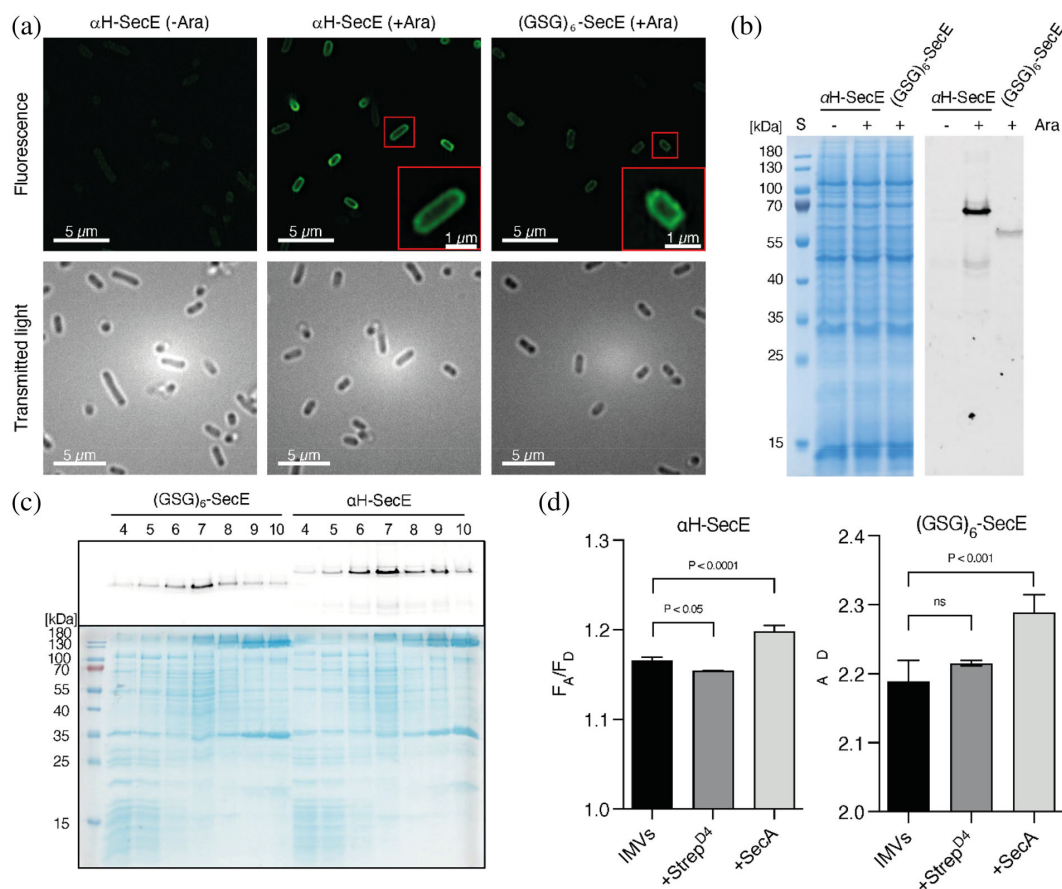


**FIGURE 7** Crowding sensors in cellular membranes. (a) Super-resolution fluorescence (top) and corresponding transmitted microscopy images (bottom) of the *Escherichia coli* cells expressing  $\alpha$ H-SecE and (GSG)<sub>6</sub>-SecE Förster's resonance energy transfer (FRET) sensors. Uninduced cells bearing  $\alpha$ H-SecE expression plasmid served as control ("–Ara"). (b) SDS-PAGE of total cell protein extracts with and without sensor overexpression. Left: Coomassie stained gel; right: in-gel fluorescence. (c) SDS-PAGE of sucrose density gradient fractions to separate inner and outer bacterial membranes. Top: in-gel fluorescence; bottom: Coomassie stained gel. Fractions 4 and 5 demonstrate the characteristic pattern of ribosomal proteins, followed by inner membrane vesicles (IMVs) (fractions 6–8). (d) FRET efficiencies of the crowding sensors recorded in IMVs and in presence of either Step<sup>D4</sup> or membrane-binding SecA (mean  $\pm$  SD,  $n = 3$ ).

but reproducible effect on both sensors, as the FRET efficiencies increased to  $1.20 \pm 0.01$  and  $2.29 \pm 0.03$  for  $\alpha$ H-SecE and (GSG)<sub>6</sub>-SecE, respectively (Figure 7d). Thus, we concluded that the developed sensors achieve membrane localization in living cells, and may be implemented for studying the dynamics of the macromolecular crowding at the biological interface.

### 3 | DISCUSSION

Macromolecular crowding is a physiological cellular condition, where the high density of proteins and nucleic acids inevitably induces steric repulsion between those,

but may also build transient quinary interactions based on their surface properties, thus affecting thermodynamic and kinetic properties of cellular processes. While the effects of the macromolecular crowding on biological membranes are ubiquitous and diverse (Guigas & Weiss, 2016; Löwe et al., 2020), the methods to study the crowding in living cells and reconstituted systems are currently limited (Chen et al., 2010; Houser et al., 2020). In this work, we designed and characterized first genetically encoded FRET-based sensors for the quantification of the crowding at the membrane interfaces and showed that a straightforward reconstitution into model membranes renders the sensors suitable for the assigned task. The difference in the structure of the sensors' linker

domains, that is, flexible Gly-Ser-Gly repeats vs. folded  $\alpha$ -helical domains, had a clear impact on the fluorescence read-out, and so the sensor conformations: The  $\alpha$ -helices within the linkers of  $\alpha$ H-SecE served as spacers within the FRET pair in the absence of crowders, while the unstructured Gly-Ser-Gly repeats rendered a rather compact initial conformation, in agreement with the earlier study (Liu et al., 2017).

Both sensors were sufficiently dynamic to respond to the changes in macromolecular crowding induced with either soluble or membrane-associated molecules. When synthetic PEG was utilized as a non-charged inert crowder that renders hard repulsion, prominent concentration-dependent response of both sensors was observed due to their compression in presence of the steric forces. Interested in the perspective to measure physiological crowding in cellular membranes, we analyzed the sensor performance in presence of the membrane-anchored proteins, which possess unique sizes, shapes and surface properties. Both sensors manifested elevated FRET signal upon increasing the protein abundance, as could be expected from solely steric repulsion. Notably though, the increase in FRET efficiency did not correlate with the molecular sizes of the crowders, as the small protein mSA (16 kDa) and the large motor protein SecA<sup>N</sup> (~100 kDa) triggered comparable responses. As the FRET signal commonly reached saturation within the probed crowders concentration range, incomplete binding could be ruled out, though the amount of crowders bound to the surface may differ due to the steric repulsion between them at the membrane surface (Minton, 2010). Alike, the geometry of the crowder binding may affect the response, as implied by two SecA variants anchored via either N- or C-terminal end, and the tetrameric SecB protein that may acquire planar orientation at the membrane surface when building three or four His:Ni<sup>2+</sup>-NTA contacts. Complementary, the shape and surface charges of the crowders may play roles in quinary interactions with the sensor molecules, both within their linker domains and the bulky fluorescent protein, so their effect may go beyond the excluded volume (Guseman et al., 2018; Kuznetsova et al., 2015; Sarkar et al., 2014; Speer et al., 2022). It should be noted though, that the broad variety of the surface-associated proteins in a living cell, and their unique interaction profiles, cannot not be mimicked in a simple in vitro system. Thus, it is the most important that the presented sensors appear responsive to all tested crowders, including the crude membrane proteome isolated with the inner membrane vesicles, suggesting the dominant effect of the steric forces and hard repulsion. Determining the complex interactions of various crowders with the sensors is a

task for further analysis, where experimental approaches may be combined with computational modeling.

Understanding the mechanisms of sensor:crowder interactions at the membrane interface may be more challenging than for the extensively studied soluble sensors (Groen et al., 2015; Liu et al., 2017; Pittas et al., 2021). While the membrane itself affects the sensor dynamics and favors a relatively compact conformation, the effect of crowders is dependent on their localization. Thus, our in vitro experiments employing PEG variants revealed moderate change in FRET when the crowder was anchored to the membrane in comparison to the free-floating state. On one hand, the conformational dynamics of the PEG chains may play a role, as the polymer undergoes an entropy-induced elongation at the surface, known as “mushroom-to-brush” transition (Marsh et al., 2003), which may reduce the steric pressure on the sensor. Other reason could be the interface of crowder:sensor interactions: While the membrane-attached crowders, both PEG chains and folded proteins, will primarily interact with the linker domains, the bulky fluorescent proteins will be more accessible for the crowders floating above the membrane plane.

The sensor response to the soluble crowders may be utilized in particular applications, for example, if studying dynamics of the actin cytoskeleton or assembly of macromolecular condensates proximate to the membrane (Bokvist & Grobner, 2007; Wang et al., 2023). However, it may also challenge potential measurements of the intrinsic membrane crowding in living cells. Although the cytoplasmic crowding levels in eukaryotic cells are substantially lower than those in bacteria (Speer et al., 2022), unambiguous analysis would require further developments to uncouple the sensor dynamics from the solvent conditions. Here, modifications of the linker architecture may be envisioned, that the linkers determine the dynamic range of the sensors, and so the achievable resolution in crowding measurements. Structured domains, such as  $\alpha$ -helices in  $\alpha$ H-SecE sensor, appear more suitable for design and controlled modifications. Here, introducing amphipathic helices may be a potent strategy, as their crowding-sensitive interactions with the membrane may be employed for switching the sensor conformations (Prévost et al., 2018), while variations in the length, charge distribution and flanking elements will serve for further fine-tuning, for example, to enhance the effects of the steric compression while minimizing the crowder-specific quinary interactions. Furthermore, modifications within the fluorescent domains may benefit the sensor performance in the cellular environments. Here, fast-maturing fluorescent proteins may be introduced (Höfig et al., 2018), but also orthogonal moieties, such as

HaloTag and SNAP-Tag (Hellweg et al., 2023; Zhang et al., 2023), which ensure higher photostability and brightness, and would reduce the sensor propensity to form oligomers at the membrane.

Shown ability of the sensors to target and insert into cellular membranes, together with their functionality within the native membrane vesicles implies applications of the sensors to study membrane proteostasis *in vivo*. Once established in eukaryotic cells, crowding levels may be measured within distinct cellular compartments, and modification of the membrane anchor, that is, size and hydrophobicity may be used for targeting the sensors to specific organelles or the membrane nanodomains (Sezgin et al., 2017; Sharpe et al., 2010). Temporarily-resolved experiments may reveal changes in the crowding levels, for example, due to protein over-expression, membrane stress and cell aging (Karagöz et al., 2019; Mouton et al., 2020), but may be also applied to study the density and dynamics of the cell surface glycocalyx or bacterial lipopolysaccharides. For the latter purpose, synthetic sensors have been recently introduced by Takatori and co-workers (Arnold et al., 2023; Takatori et al., 2023), who combined extensive *in vitro* analysis of the polymer-based sensor dynamics with the measurements on the surface of living cells, where the sensors could be easily delivered once added externally. The studies provide unique insights on organization of the glycocalyx of various cell types, as well as the heterogeneity within the plasma membrane structure, and offer a complementary approach to the genetically-encoded sensors described here.

Studying organization and dynamics of cellular membranes in a non-invasive manner remains a great challenge in biology, but the recent technical developments, first of all in advanced fluorescence microscopy and membrane-specific probes are providing new tools and opportunities (Collot et al., 2022; Sezgin, 2017). We envision that the protein-based sensors for crowding in cellular membranes will be a valuable add-on for characterizing the environment of the cell membrane interfaces, and will also find their applications in crowding analysis in reconstituted systems.

## 4 | MATERIALS AND METHODS

### 4.1 | Expression and purification of the membrane crowding sensors

Gene fragments encoding for TMHs 1–2 of SecE *E. coli* were introduced into the plasmid pRSET-A-FRET (Boersma et al., 2015) via Gibson assembly (New England Biolabs), so the encoded membrane anchor substituted

the flexible linker between the mCerulean and mCitrine. Additionally, a cleavage site for 3C protease (sequence LEVLFQGP) was added to each construct after the N-terminal hexa-histidine tag. A soluble sensor contained a polypeptide of 14 amino acids (AHIVMVDAYKPTK) (Zakeri et al., 2012) instead of the anchor domain. Cloning results were validated by sequencing analysis (Eurofins Genomics). Resulting plasmids containing genes for (GSG)<sub>6</sub>-SecE and  $\alpha$ H-SecE sensors were transferred into the *E. coli* C43(DE3) strain. For the protein over-expression, the cultures were grown at 30°C in LB medium (10 g/L tryptone, 10/L g NaCl and 5 g/L yeast extract) supplemented with 100  $\mu$ g/mL ampicillin till OD<sub>600</sub> of 0.6 was reached. The expression of the sensors was induced with 0.1 mM IPTG and carried out overnight at 25°C (Boersma et al., 2015). For tunable expression of sensors, the constructs were re-cloned into pBAD<sub>His</sub> vector, and expression was induced with 0.001% L-arabinose. Expression of mCerulean-SecE (pBAD-based vector) and SecE-mCitrine (pRSET-A) was performed using the same protocol.

The cells were harvested by centrifugation at 5000 $\times$  g for 15 min (SLC-6000, Thermo Fisher/Sorvall), resuspended in 20 mM NaH<sub>2</sub>PO<sub>4</sub>/Na<sub>2</sub>HPO<sub>4</sub> pH 7.4 and 100 mM NaCl supplemented with 0.1 mM PMSF and lysed by Microfluidizer (M-110P, Microfluidics Corp). Cell debris was removed by subsequent centrifugation at 12,000 $\times$  g for 15 min (SS34, Thermo Fisher/Sorvall). The membrane fraction was collected by centrifugation for 45 min at 235,000 $\times$  g (45 Ti rotor, Beckman Coulter). The pellet was resuspended in 20 mM NaH<sub>2</sub>PO<sub>4</sub>/Na<sub>2</sub>HPO<sub>4</sub> pH 7.4, 100 mM NaCl, 5% glycerol and 0.1 mM PMSF. Further, the membranes were solubilized in 1% DDM (Glycon Biochemicals GmbH), 50 mM NaH<sub>2</sub>PO<sub>4</sub>/Na<sub>2</sub>HPO<sub>4</sub>, 500 mM NaCl, 200  $\mu$ M TCEP and 0.2 mM PMSF. The proteins were purified via metal ion affinity chromatography (IMAC). The solubilized material was loaded on the Ni<sup>2+</sup>-NTA-agarose resin (either QIAGEN or Macherey-Nagel) and the resin was washed with 50 mM NaH<sub>2</sub>PO<sub>4</sub>/Na<sub>2</sub>HPO<sub>4</sub> pH 8.0, 300 mM NaCl, 0.1% DDM and 20 mM imidazole. The proteins were eluted with 50 mM NaH<sub>2</sub>PO<sub>4</sub>/Na<sub>2</sub>HPO<sub>4</sub> pH 8.0, 300 mM NaCl, 0.1% DDM and 250 mM imidazole. The elution fraction was loaded on the Superdex 200 Increase GL 10/300 column (Cytiva) in 10 mM NaH<sub>2</sub>PO<sub>4</sub>/Na<sub>2</sub>HPO<sub>4</sub> pH 7.4, 50 mM NaCl and 0.05% DDM. Peak elution fractions of SEC were pooled, aliquoted and stored at –80°C. The expression of the sensor and each purification stage were controlled via SDS-PAGE, followed by in-gel fluorescence imaging and Coomassie staining (Quick Coomassie® Stain, SERVA). To remove the N-terminal tag, 3C protease was added to the IMAC resin-bound sensors after washing steps and incubated for 2 h. Afterwards, the

released protein was eluted with the wash buffer followed by SEC, as described above. For the spectrophotometric analysis, the following extinction coefficients were used to calculate the concentration of fluorescent proteins, and the total protein concentration: mCerulean3 of  $\epsilon_{433} = 33,000 \text{ M}^{-1} \text{ cm}^{-1}$ , mCitrine of  $\epsilon_{516} = 94,000 \text{ M}^{-1} \text{ cm}^{-1}$  (Lambert, 2019). Both sensors, which differ only by the linker sequence, had the extinction coefficient  $\epsilon_{280} = 56,520 \text{ M}^{-1} \text{ cm}^{-1}$ . The calculated molar ratio of individual fluorescent proteins to the sensor concentration provided an estimate for the folding efficiency. mCerulean and mCitrine of (GSG)<sub>6</sub>-SecE were folded with the efficiency of  $61\% \pm 15\%$  and  $73\% \pm 7\%$ , respectively (three independent expression/isolation experiments). Within the  $\alpha$ H-SecE sensor, the folding efficiency of the fluorescent domains reached  $78\% \pm 9\%$  and  $87\% \pm 1\%$ , respectively ( $n = 3$ ), suggesting more efficient folding within the construct with the elongated and structured linkers.

#### 4.2 | Sensor expression for measurements *in vesicula*

The protein expression using pBAD-based plasmids was conducted as described above, using 0.001% L-arabinose (67  $\mu\text{M}$ ) as the inducer. The isolated crude membrane extract was loaded on the continuous 20%–70% sucrose density gradient in 20 mM  $\text{NaH}_2\text{PO}_4/\text{Na}_2\text{HPO}_4$  pH 7.4 and 100 mM NaCl prepared by the Gradient Station (BioComp Instruments) and centrifuged for 16 h at 30,000 rpm (rotor SW 40 Ti, Beckman Coulter). The gradients were collected with the Gradient Station, and the fractions were analyzed on SDS-PAGE. Selected fractions were pooled together, diluted 5-fold with 20 mM  $\text{NaH}_2\text{PO}_4/\text{Na}_2\text{HPO}_4$  and 100 mM NaCl, and pelleted via centrifugation for 45 min at 235,000 g (45 Ti rotor, Beckman Coulter) to remove sucrose. The pellet was resuspended in 20 mM  $\text{NaH}_2\text{PO}_4/\text{Na}_2\text{HPO}_4$  pH 7.4, 100 mM NaCl, 5% glycerol and cComplete™ EDTA-free protease inhibitor cocktail (Roche).

To determine the total inner membrane protein content, the membrane preparations were solubilized with 1% DDM and the total protein content was measured using Pierce™ 660 nm Protein Assay Reagent (Thermo Scientific) against the BSA standard curve (Thermo Scientific) in concentration range between 0.025 and 2 mg/mL. The concentration of the sensor in the IMVs was determined from SDS-PAGE in-gel fluorescence with ImageQuant TL (Cytiva), using titrations of the purified sensors with known concentrations for the calibration.

#### 4.3 | Size exclusion chromatography coupled to multi-angle light scattering

The oligomeric state of the purified sensor constructs was analyzed by SEC coupled to multi-angle light scattering (SEC-MALS) using Superdex 200 Increase GL 10/300 column coupled to connected to miniDAWN TREOS II light scattering device and Optilab-TrEX Ri-detector (Wyatt Technology Corp.). The sensors were applied at 0.55 mg/mL concentrations in 10 mM  $\text{NaH}_2\text{PO}_4/\text{Na}_2\text{HPO}_4$  pH 7.4, 50 mM NaCl and 0.05% DDM. Experiments with the soluble sensor construct lacking the transmembrane SecE domain were conducted at the same conditions in the buffer without DDM. The data analysis was performed with ASTRA 7.3.2 software (Wyatt Technology Corp.).

#### 4.4 | Expression and characterization of the crowder proteins

The protein crowding agents were expressed and purified as described elsewhere: mSA (Demonte et al., 2014; Lim et al., 2011), Strep<sup>D4</sup> (Howarth et al., 2006), SecB (Fekkes et al., 1998), SecA<sup>N</sup> and SecA<sup>C</sup> (Kamel et al., 2022). As mSA was expressed as inclusion bodies and had to be refolded, its functionality was additionally analyzed by differential scanning fluorimetry (nanoDSF, Prometheus NT48). 1  $\mu\text{M}$  mSA was optionally incubated with 10  $\mu\text{M}$  biotin and the thermal denaturation of the protein was examined between 25 and 85°C (heating ramp 1°C/min) upon monitoring the intrinsic fluorescence at 330 and 350 nm, and the protein stabilization upon ligand binding was analyzed.

#### 4.5 | Reconstitution of the crowding sensors into model membranes

Lipids were purchased in chloroform-solubilized form (Avanti Polar Lipids, Inc.) and were mixed together to obtain required lipid compositions. For PEG-based crowding experiments, liposomes composed of DOPC (63 mol%) and DOPG (27 mol%) were supplemented with 10 mol% of 1,2-dioleoyl-sn-glycero-3-phosphatidylethanolamine (DOPE) and 1,2-dioleoyl-sn-glycero-3-phosphoethanolamine-N-[methoxy(polyethylene glycol)-2000] (DOPE-PEG 2000) at various ratios. For protein-based crowding experiments, 20 mol% of anchor lipids, 1,2-dioleoyl-sn-glycero-3-[(N-(5-amino-1-carboxypentyl) iminodiacetic acid)succinyl] (18:1 DGS-NTA(Ni)) or 1,2-dioleoyl-sn-glycero-3-phosphoethanolamine-N-(cap biotinyl) (sodium salt) (18:1 Biotinyl Cap PE), were added to DOPC:DOPG mixture

(53 mol%: 27 mol%) were used for titration experiments. Lipids were mixed in defined ratios, chloroform was removed via vacuum evaporation (rotary evaporator RV 8, IKA) while incubating the samples at 40°C in a water bath. Formed lipid film was subsequently rehydrated and resuspended with 20 mM Tris-HCl pH 7.5 and 150 mM KCl to achieve final lipid concentration of 5 mM.

The liposome suspensions were extruded with the Mini-Extruder set (Avanti Polar Lipids, Inc.) via 0.2 µm polycarbonate membranes (Nuclepore, Whatman) and liposomes were swelled with 0.2% DDM at 40°C for 15 min (Suppl. Figure 7). Unless other is indicated, the purified crowding sensors were added at the protein: lipid molar ratio of 1:3000 and incubated for 30 min on ice. Afterwards the samples were incubated with Bio-Beads SM-2 sorbent (Bio-Rad Laboratories) overnight on the rolling bank at 4°C to remove the detergent (Rigaud et al., 1997). Proteoliposomes with the reconstituted sensor were pelleted at 162,000× g for 30 min (S120-AT3 rotor, Discovery M120 SE, Thermo Fisher/Sorvall) and then resuspended in 50 mM Tris-HCl pH 7.5 and 150 mM KCl to the final lipid concentration of 5 mM.

The reconstitution efficiency of the membrane-anchored crowding sensors was examined upon centrifugation in the sucrose density gradient. A 50 µL of reconstituted proteoliposomes were mixed together with 60% sucrose (w/v), 50 mM Tris-HCl pH 7.5 and 150 mM KCl to final sucrose concentration of 30% in 200 µL, and loaded at the bottom of the centrifugation tube. A 250 µL of 20% sucrose solution and 50 µL of 5% sucrose solution were loaded on top, thus forming a step gradient of sucrose. The samples were centrifuged for 1 h at 29,000× g (S120-AT3 rotor, Discovery M120 SE, Thermo Fisher/Sorvall) and then harvested from the bottom into 3 fractions (bottom) of 250 µL, “middle” 125 µL, and “top” of 125 µL. The presence of the sensor in each fraction was analyzed by SDS-PAGE: The intensity of fluorescent bands in SDS-PAGE was quantified (ImageQuant TL, Cytiva) and the relative amount of the reconstituted sensor was calculated by dividing band intensity of the individual fractions by the cumulative intensity of all fractions. Flotation experiments were carried independently at least two times for each sensor construct.

For studying the topology of the membrane-embedded sensors, DOPC:DOPG liposomes were incubated with 0.2% DDM or 0.5% Triton X-100, and  $\alpha$ H-SecE or (GSG)<sub>6</sub>-SecE sensors were reconstituted as described above. Formed proteoliposomes were mixed with either 42 µM trypsin (from porcine pancreas, Sigma-Aldrich) or 17 µM proteinase K (Thermo Fisher Scientific). Detergent-solubilized sensors were equally incubated with proteases and served as controls in this experiment. The proteolysis reaction proceeded for 2 h at 22°C, then

the samples were incubated for 5 min at 90°C to inactivate the proteases and were analyzed by SDS-PAGE.

#### 4.6 | Fluorescence spectroscopy

Purified and optionally reconstituted sensors were diluted in 20 mM Tris-HCl pH 7.4 and 150 mM KCl, and the emission spectrums of the probes were recorded on either Fluorolog-3 or FluoroMax-Plus (Horiba™ Scientific). The excitation wavelength was set to 420 nm, slit width 5 nm, so only the donor fluorophore mCerulean was excited, and the fluorescence emission spectra were recorded in the range of 435–620 nm, where the emission of mCerulean (donor) was measured at 475 nm, and mCitrine (acceptor) at 525 nm. Dilution series of PEG 6000 as a soluble crowder were prepared in 20 mM Tris-HCl pH 7.4 and 150 mM KCl based on 50% stock solution (w/v). For measurements that included the detergent-solubilized sensors, 0.05% DDM was additionally supplemented. To induce protein crowding at the liposome surface, crowdiers were titrated stepwise to the liposomes with reconstituted sensors until the crowder/ligand-lipid ratio of 1.1 was reached. To probe crowding in IMVs, Strep<sup>D4</sup> and SecA were added to vesicle suspension in concentrations of 13 µM for  $\alpha$ H-SecE and 8 µM for (GSG)<sub>6</sub>-SecE samples. For all the samples the background spectrum of the corresponding buffer or crowder solution was subtracted.

#### 4.7 | Super-resolution structured illumination microscopy

Cells transformed with pBAD-based plasmids containing genes for either (GSG)<sub>6</sub>-SecE or  $\alpha$ H-SecE sensors were grown as described earlier, and the expression was induced by 0.001% L-arabinose. Additional cell culture with  $\alpha$ H-SecE sensor was prepared as a control and was not induced with arabinose. The harvested cells were resuspended in PBS and the OD<sub>600</sub> was adjusted to 1.2. Cover glasses for the microscopy were cleaned with 70% ethanol and coated by 0.1% (w/v) poly-L-lysine solution. Next, the cover glasses were placed into 12-well plates with 1 mL PBS and 5 µL of bacterial cell suspension and centrifuged at 1500 rpm (ROTOR) for 15 min at 4°C. The supernatant was removed and the attached cells were washed with 1 mL of fresh PBS. Structured illumination microscopy was performed using the Zeiss ELYRA PS.1 microscope system (Zeiss Microscopy GmbH, Oberkochen, Germany) equipped with a Plan-Apochromat 63×/1.4 oil immersion objective lens. For excitation of the sensors, a 488 nm diode laser was used at 1.5%–2.5%

emission intensity. Signals were detected by a front illuminated Andor iXon3 DU-885K camera, a BP 495–575 + LP 750 emission filter, exposure time of 100 ms and an EMCCD gain of 100–200. Individual stacks of  $256 \times 256$  px (pixel) and a Z-axis interval of 110 nm were acquired at  $542 \mu\text{m}$  SIM-grid rotations and with no averaging. Each acquired z-stack was processed internally with the ZEN black SIM feature with the same 3D signal-to-noise filter of  $-3.3$  for all data.

#### AUTHOR CONTRIBUTIONS

**Maryna Löwe:** Conceptualization; Investigation; Writing–original draft; Methodology; Visualization; Formal analysis. **Sebastian Hänsch:** Conceptualization; Methodology; Data curation; Investigation; Formal analysis. **Eymen Hachani:** Investigation; Formal analysis. **Lutz Schmitt:** Supervision; Project administration; Writing–review & editing; Funding acquisition. **Stefanie Weidtkamp-Peters:** Supervision; Project administration; Writing–review & editing; Funding acquisition. **Alexej Kedrov:** Conceptualization; Investigation; Funding acquisition; Writing–review & editing; Project administration; Supervision; Data curation.

#### ACKNOWLEDGMENTS

The work was supported by the German Research Foundation (Deutsche Forschungsgemeinschaft, DFG) via the Research Grant Ke1879/3 and the Collaborative Research Center 1208 “Identity and Dynamics of Membrane Systems”. We thank Prof. Arnold J. Boersma (University of Utrecht), Dr. Jens Reiners (Center for Structural Studies, HHU Düsseldorf), and Dr. Jakub Kubiak for technical advice and discussions along the project. Funding for the instrumentation: DFG- INST 208/613-1 FUGG. Open Access funding enabled and organized by Projekt DEAL.

#### CONFLICT OF INTEREST STATEMENT

The authors declare no conflicts of interest.

#### ORCID

Sebastian Hänsch  <https://orcid.org/0000-0002-7762-2516>

Eymen Hachani  <https://orcid.org/0000-0001-5810-170X>

Lutz Schmitt  <https://orcid.org/0000-0002-1167-9819>

Stefanie Weidtkamp-Peters  <https://orcid.org/0000-0001-7734-3771>

Alexej Kedrov  <https://orcid.org/0000-0001-9117-752X>

#### REFERENCES

- Armstrong JK, Wenby RB, Meiselman HJ, Fisher TC. The hydrodynamic radii of macromolecules and their effect on red blood cell aggregation. *Biophys J*. 2004;87:4259–70.

- Arnold DP, Xu Y, Takatori SC. Antibody binding reports spatial heterogeneities in cell membrane organization. *Nat Commun*. 2023;14:2884.
- Aumiller WM, Davis BW, Hatzakis E, Keating CD. Interactions of macromolecular crowding agents and cosolutes with small-molecule substrates: effect on horseradish peroxidase activity with two different substrates. *J Phys Chem B*. 2014;118:10624–32.
- Bai J, Liu M, Pielak GJ, Li C. Macromolecular and small molecular crowding have similar effects on alpha-synuclein structure. *ChemPhysChem*. 2017;18:55–8.
- Boersma AJ, Zuhorn IS, Poolman B. A sensor for quantification of macromolecular crowding in living cells. *Nat Methods*. 2015;12:227–9.
- Bokvist M, Grobner G. Misfolding of amyloidogenic protein at membrane surfaces: impact of macromolecular crowding. *J Am Chem Soc*. 2007;129:14848–9.
- Breyton C, Haase W, Rapoport TA, Kühlbrandt W, Collinson I. Three-dimensional structure of the bacterial protein-translocation complex SecYEG. *Nature*. 2002;418:662–5.
- Chen L, Novicky L, Merzlyakov M, Hristov T, Hristova K. Measuring the energetics of membrane protein dimerization in mammalian membranes. *J Am Chem Soc*. 2010;132:3628–35.
- Collot M, Pfister S, Klymchenko AS. Advanced functional fluorescent probes for cell plasma membranes. *Curr Opin Chem Biol*. 2022;69:102161.
- Demonte D, Dundas CM, Park S. Expression and purification of soluble monomeric streptavidin in *Escherichia coli*. *Appl Microbiol Biotechnol*. 2014;98:6285–95.
- Dupuy AD, Engelman DM. Protein area occupancy at the center of the red blood cell membrane. *Proc Natl Acad Sci USA*. 2008;105:2848–52.
- Elowitz MB, Surette MG, Wolf PE, Stock JB, Leibler S. Protein mobility in the cytoplasm of *Escherichia coli*. *J Bacteriol*. 1999;181:197–203.
- Engelman DM. Membranes are more mosaic than fluid. *Nature*. 2005;438:578–80.
- Engelman DM, Steitz TA. The spontaneous insertion of proteins into and across membranes: the helical hairpin hypothesis. *Cell*. 1981;23:411–22.
- Fekkes P, De Wit JG, Van Der Wolk JPW, Kimsey HH, Kumamoto CA, Driessen AJM. Preprotein transfer to the *Escherichia coli* translocase requires the co-operative binding of SecB and the signal sequence to SecA. *Mol Microbiol*. 1998;29:1179–90.
- Fotiadis D, Liang Y, Filipek S, Saperstein DA, Engel A, Palczewski K. Rhodopsin dimers in native disc membranes. *Nature*. 2003;421:127–8.
- Geertsma ER, Nik Mahmood NAB, Schuurman-Wolters GK, Poolman B. Membrane reconstitution of ABC transporters and assays of translocator function. *Nat Protoc*. 2008;3:256–66.
- Grasberger B, Minton AP, DeLisi C, Metzger H. Interaction between proteins localized in membranes. *Proc Natl Acad Sci*. 1986;83:6258–62.
- Groen J, Foschepoth D, Te Brinke E, Boersma AJ, Imamura H, Rivas G, et al. Associative interactions in crowded solutions of biopolymers counteract depletion effects. *J Am Chem Soc*. 2015;137:13041–8.
- Guigas G, Weiss M. Effects of protein crowding on membrane systems. *Biochim Biophys Acta Biomembr*. 2016;1858:2441–50.

- Guseman AJ, Perez Goncalves GM, Speer SL, Young GB, Pielak GJ. Protein shape modulates crowding effects. *Proc Natl Acad Sci USA*. 2018;115:10965–70.
- Hellweg L, Edenhofer A, Barck L, Huppertz MC, Frei MS, Tarnawski M, et al. A general method for the development of multicolor biosensors with large dynamic ranges. *Nat Chem Biol*. 2023;19:1147–57.
- Hills RD, McGlinchey N. Model parameters for simulation of physiological lipids. *J Comput Chem*. 2016;37:1112–8.
- Höfig H, Otten J, Steffen V, Pohl M, Boersma AJ, Fitter J. Genetically encoded Förster resonance energy transfer-based biosensors studied on the single-molecule level. *ACS Sensors*. 2018;3:1462–70.
- Houser JR, Hayden CC, Thirumalai D, Stachowiak JC. A Förster resonance energy transfer-based sensor of steric pressure on membrane surfaces. *J Am Chem Soc*. 2020;142:20796–805.
- Howarth M, Chinnapen DJF, Gerrow K, Dorrestein PC, Grandy MR, Kelleher NL, et al. A monovalent streptavidin with a single femtomolar biotin binding site. *Nat Methods*. 2006;3:267–73.
- Kamel M, Löwe M, Schott-Verdugo S, Gohlke H, Kedrov A. Unsaturated fatty acids augment protein transport via the SecA:SecYEG translocon. *FEBS J*. 2022;289:140–62.
- Karagöz GE, Acosta-Alvear D, Walter P. The unfolded protein response: detecting and responding to fluctuations in the protein-folding capacity of the endoplasmic reticulum. *Cold Spring Harb Perspect Biol*. 2019;11:a033886.
- Kater L, Frieg B, Berninghausen O, Gohlke H, Beckmann R, Kedrov A. Partially inserted nascent chain unzips the lateral gate of the sec translocon. *EMBO Rep*. 2019;20:e48191.
- Kedrov A, Janovjak H, Sapra KT, Müller DJ. Deciphering molecular interactions of native membrane proteins by single-molecule force spectroscopy. *Annu Rev Biophys Biomol Struct*. 2007;36:233–60.
- Kirchhoff H. Molecular crowding and order in photosynthetic membranes. *Trends Plant Sci*. 2008;13:201–7.
- Knol J, Veenhoff LM, Liang WJ, Henderson PJF, Leblanc G, Poolman B. Unidirectional reconstitution into detergent-stabilized liposomes of the purified lactose transport system of *Streptococcus thermophilus*. *J Biol Chem*. 1996;271:15358–66.
- Kuznetsova IM, Turoverov KK, Uversky VN. What macromolecular crowding can do to a protein. *Int J Mol Sci*. 2014;15:23090–140.
- Kuznetsova IM, Zaslavsky BY, Breydo L, Turoverov KK, Uversky VN. Beyond the excluded volume effects: mechanistic complexity of the crowded milieu. *Molecules*. 2015;20:1377–409.
- Lambert TJ. FPbase: a community-editable fluorescent protein database. *Nat Methods*. 2019;16:277–8.
- Lim KH, Huang H, Pralle A, Park S. Engineered streptavidin monomer and dimer with improved stability and function. *Biochemistry*. 2011;50:8682–91.
- Liu B, Åberg C, van Eerden FJ, Marrink SJ, Poolman B, Boersma AJ. Design and properties of genetically encoded probes for sensing macromolecular crowding. *Biophys J*. 2017;112:1929–39.
- Liu LN, Scheuring S. Investigation of photosynthetic membrane structure using atomic force microscopy. *Trends Plant Sci*. 2013;18:277–86.
- Löwe M, Kalacheva M, Boersma AJ, Kedrov A. The more the merrier: effects of macromolecular crowding on the structure and dynamics of biological membranes. *FEBS J*. 2020;287:5039–67.
- Marsh D, Bartucci R, Sportelli L. Lipid membranes with grafted polymers: physicochemical aspects. *Biochim Biophys Acta Biomembr*. 2003;1615:33–59.
- Minton AP. Analysis of membrane binding equilibria of peripheral proteins: allowance for excluded area of bound protein. *Anal Biochem*. 2010;397:247–9.
- Minton AP, Wilf J. Effect of macromolecular crowding upon the structure and function of an enzyme: Glyceraldehyde-3-phosphate dehydrogenase. *Biochemistry*. 1981;20:4821–6.
- Mouton SN, Thaller DJ, Crane MM, Rempel IL, Terpstra O, Steen A, et al. A physicochemical perspective of aging from single-cell analysis of pH, macromolecular and organellar crowding in yeast. *Elife*. 2020;9:e54707.
- Nawrocki G, Wang PH, Yu I, Sugita Y, Feig M. Slow-down in diffusion in crowded protein solutions correlates with transient cluster formation. *J Phys Chem B*. 2017;121:11072–84.
- Nemzer LR, Flanders BN, Schmit JD, Chakrabarti A, Sorensen CM. Ethanol shock and lysozyme aggregation. *Soft Matter*. 2013;9:2187–96.
- Pittas T, Zuo W, Boersma AJ. Engineering crowding sensitivity into protein linkers. *Methods Enzymol*. 2021;647:51–81.
- Prévost C, Sharp ME, Kory N, Lin Q, Voth GA, Farese RVJ, et al. Mechanism and determinants of amphipathic helix-containing protein targeting to lipid droplets. *Dev Cell*. 2018;44:73–86.
- Raghunath G, Dyer RB. Kinetics of histidine-tagged protein association to nickel-decorated liposome surfaces. *Langmuir*. 2019;35:12550–61.
- Rigaud JL, Mosser G, Lacapere JJ, Olofsson A, Levy D, Ranck JL. Bio-beads: an efficient strategy for two-dimensional crystallization of membrane proteins. *J Struct Biol*. 1997;118:226–35.
- Rivas G, Minton AP. Toward an understanding of biochemical equilibria within living cells. *Biophys Rev*. 2018;10:241–53.
- Rivas G, Minton AP. Influence of nonspecific interactions on protein associations: implications for biochemistry in vivo. *Annu Rev Biochem*. 2022;91:321–51.
- Robertson JL. The lipid bilayer membrane and its protein constituents. *J Gen Physiol*. 2018;150:1472–83.
- Rohwer JM, Postma PW, Kholodenko BN, Westerhoff HV. Implications of macromolecular crowding for signal transduction and metabolite channeling. *Proc Natl Acad Sci USA*. 1998;95:10547–52.
- Roussel G, White SH. The SecA ATPase motor protein binds to *Escherichia coli* liposomes only as monomers. *Biochim Biophys Acta Biomembr*. 2020;1862:183358.
- Sarkar M, Lu J, Pielak GJ. Protein-crowder charge and protein stability. *Biochemistry*. 2014;53:1601–6.
- Sezgin E. Super-resolution optical microscopy for studying membrane structure and dynamics. *J Phys Condens Matter*. 2017;29:273001.
- Sezgin E, Levental I, Mayor S, Eggeling C. The mystery of membrane organization: composition, regulation and roles of lipid rafts. *Nat Rev Mol Cell Biol*. 2017;18:361–74.
- Sharpe HJ, Stevens TJ, Munro S. A comprehensive comparison of transmembrane domains reveals organelle-specific properties. *Cell*. 2010;142:158–69.

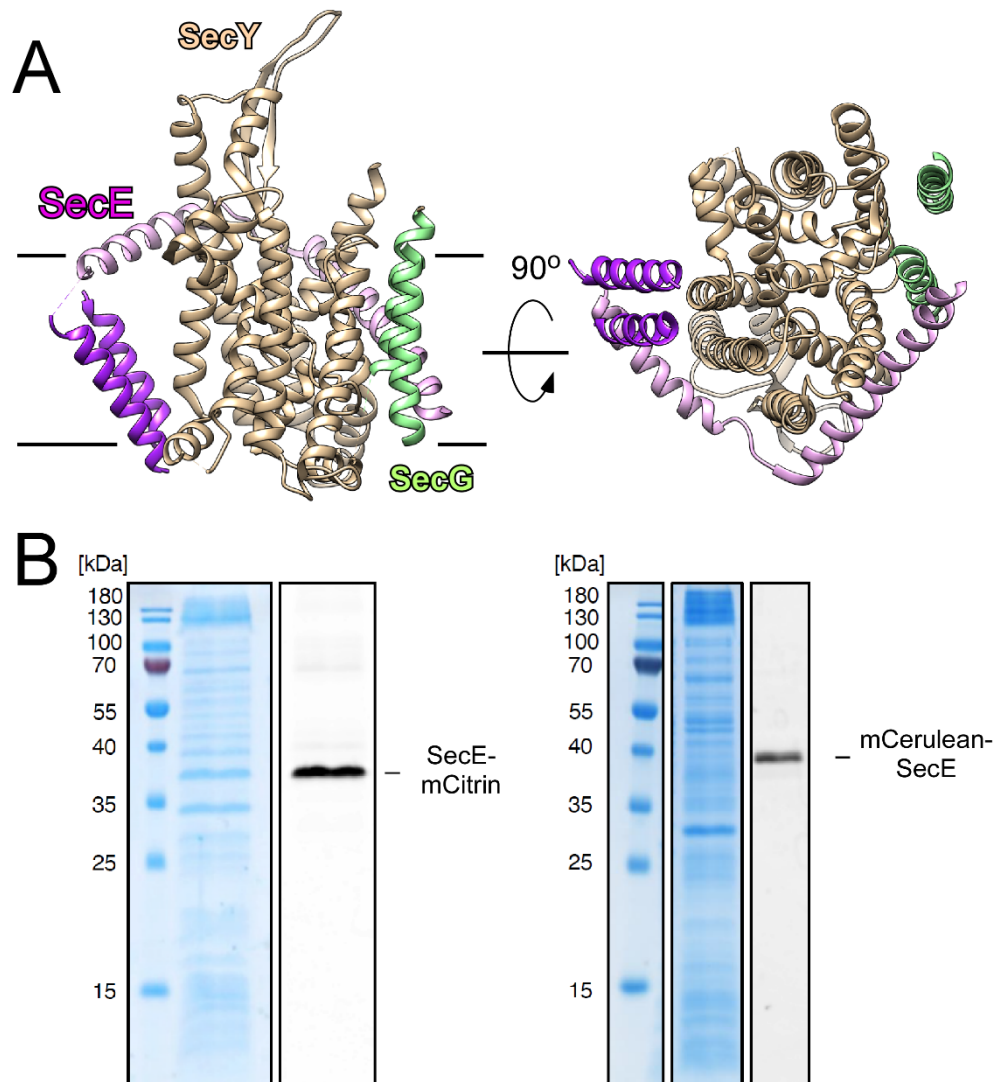
- Smith VF, Schwartz BL, Randall LL, Smith RD. Electrospray mass spectrometric investigation of the chaperone SecB. *Protein Sci.* 1996;5:488–94.
- Speer SL, Stewart CJ, Sapir L, Harries D, Pielak GJ. Macromolecular crowding is more than hard-Core repulsions. *Annu Rev Biophys.* 2022;51:267–300.
- Srere PA. The infrastructure of the mitochondrial matrix. *Trends Biochem Sci.* 1980;5:120–1.
- Strop P, Brunger AT. Refractive index-based determination of detergent concentration and its application to the study of membrane proteins. *Protein Sci.* 2005;14:2207–11.
- Takatori SC, Son S, Lee DSW, Fletcher DA. Engineered molecular sensors for quantifying cell surface crowding. *Proc Natl Acad Sci.* 2023;120:e2219778120.
- van den Berg B, Ellis RJ, Dobson CM. Effects of macromolecular crowding on protein folding and aggregation. *EMBO J.* 1999;18:6927–33.
- Wang H, Chan SH, Dey S, Castello-serrano I, Rosen MK, Ditlev JA, et al. Coupling of protein condensates to ordered lipid domains determines functional membrane organization. *Sci Adv.* 2023;9:eadf6205.
- Zakeri B, Fierer JO, Celik E, Chittock EC, Schwarz-Linek U, Moy VT, et al. Peptide tag forming a rapid covalent bond to a protein, through engineering a bacterial adhesin. *Proc Natl Acad Sci.* 2012;109:E690–7.
- Zhang D, Chen Z, Du Z, Bao B, Su N, Chen X, et al. Design of a palette of SNAP-tag mimics of fluorescent proteins and their use as cell reporters. *Cell Discov.* 2023;9:56.
- Zimmerman SB, Pfeiffer BH. Macromolecular crowding allows blunt-end ligation by DNA ligases from rat liver or *Escherichia coli*. *Proc Natl Acad Sci USA.* 1983;80:5852–6.
- Zimmerman SB, Trach SO. Estimation of macromolecule concentrations and excluded volume effects for the cytoplasm of *Escherichia coli*. *J Mol Biol.* 1991;222:599–620.

### SUPPORTING INFORMATION

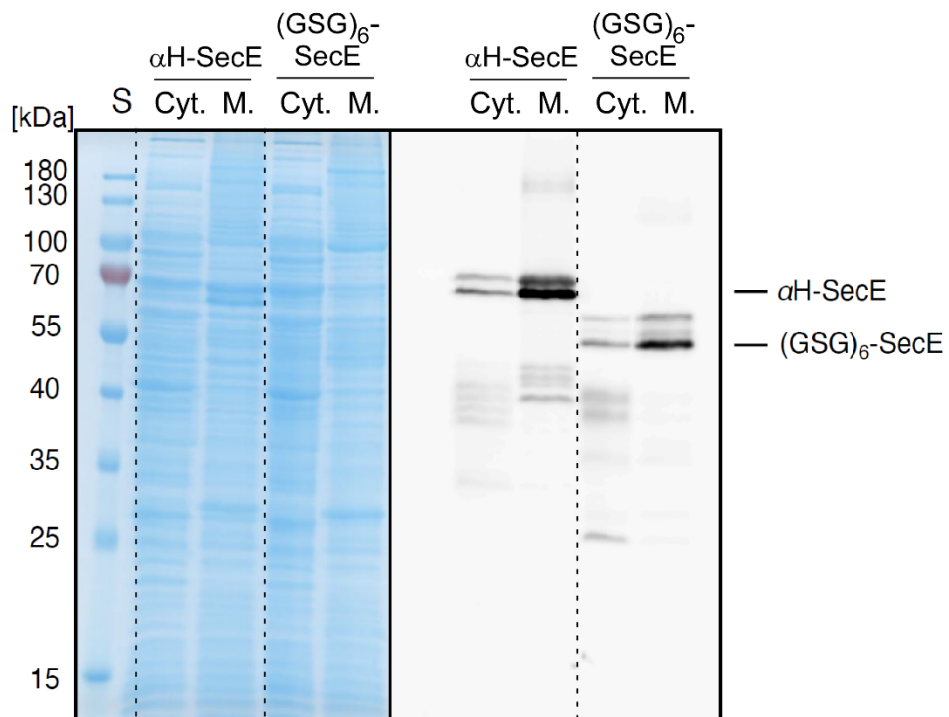
Additional supporting information can be found online in the Supporting Information section at the end of this article.

**How to cite this article:** Löwe M, Hänsch S, Hachani E, Schmitt L, Weidtkamp-Peters S, Kedrov A. Probing macromolecular crowding at the lipid membrane interface with genetically-encoded sensors. *Protein Science.* 2023;32(11): e4797. <https://doi.org/10.1002/pro.4797>

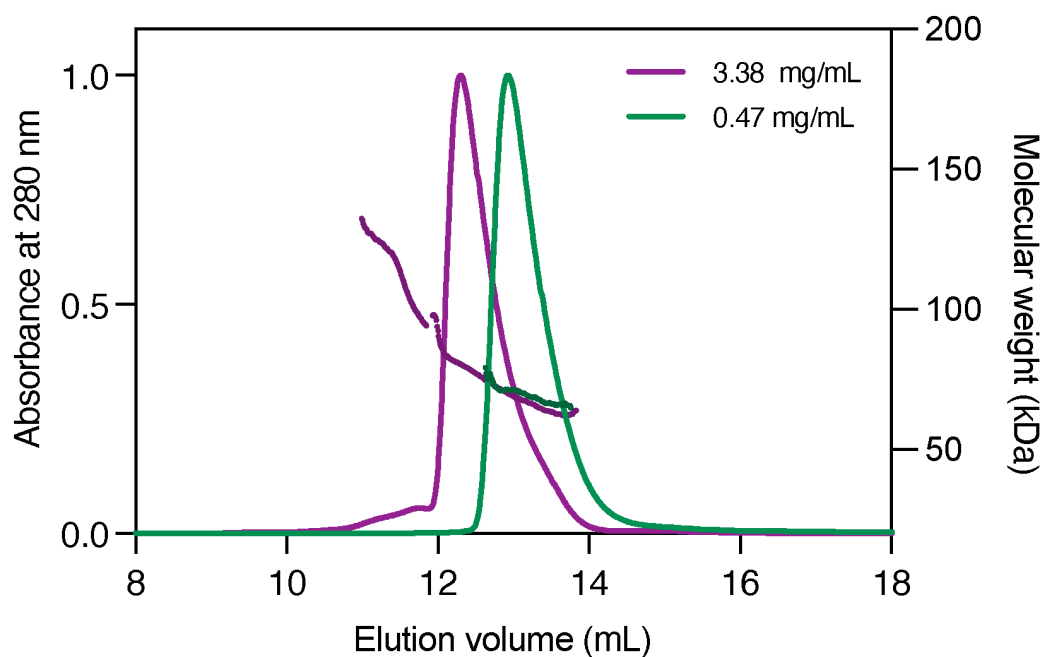
## 3.2.1 Supplemental figures



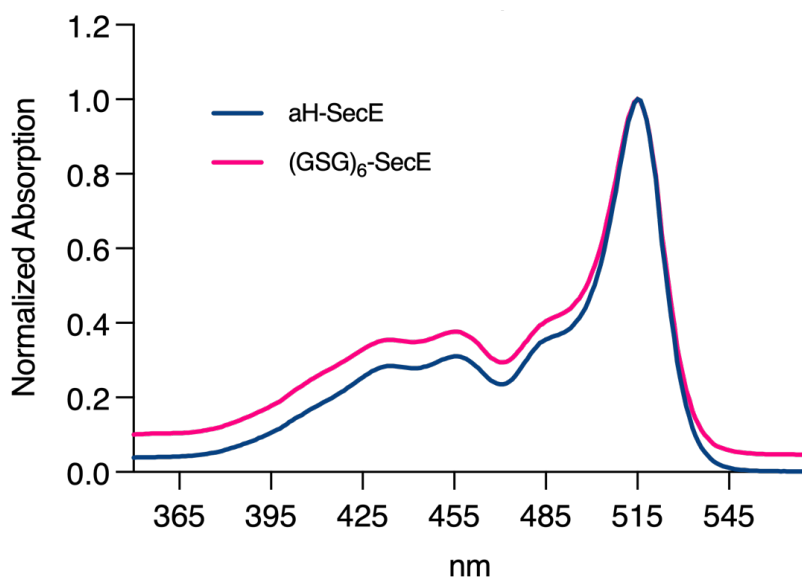
**Supplemental Figure 1. Transmembrane anchor for the crowding sensors.** (A) SecYEG translocon in the lipid membrane (PDB: 6R7L), view in the membrane plane (left) and from the periplasm (right). The membrane plane is shown by red lines, as resolved by cryo-EM. Individual subunits are indicated and color-coded. SecE TMHs 1-2 used for anchoring the crowding sensors are shown in dark purple. The connecting periplasmic loop of four amino acids is not resolved in the cryo-EM structure. (B) SDS-PAGE of crude membrane extracts containing SecE-mCitrine and mCerulean-SecE fusion proteins. Left: Coomassie stained gels; right: In-gel fluorescence.



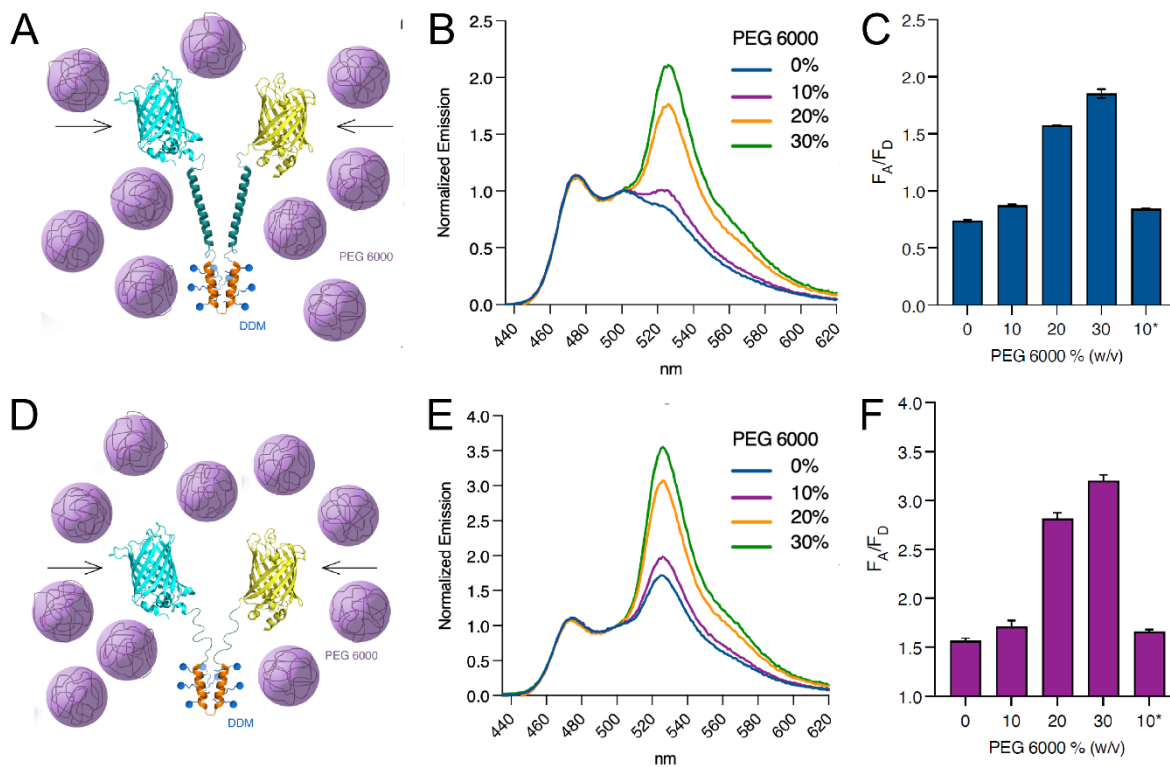
**Supplemental Figure 2. Expression of the crowding sensors.** SDS-PAGE (left) and in-gel fluorescence (right) of the cytoplasmic (“Cyt.”) and crude membrane (“M.”) fractions of the cells expressing the indicated crowding sensor.



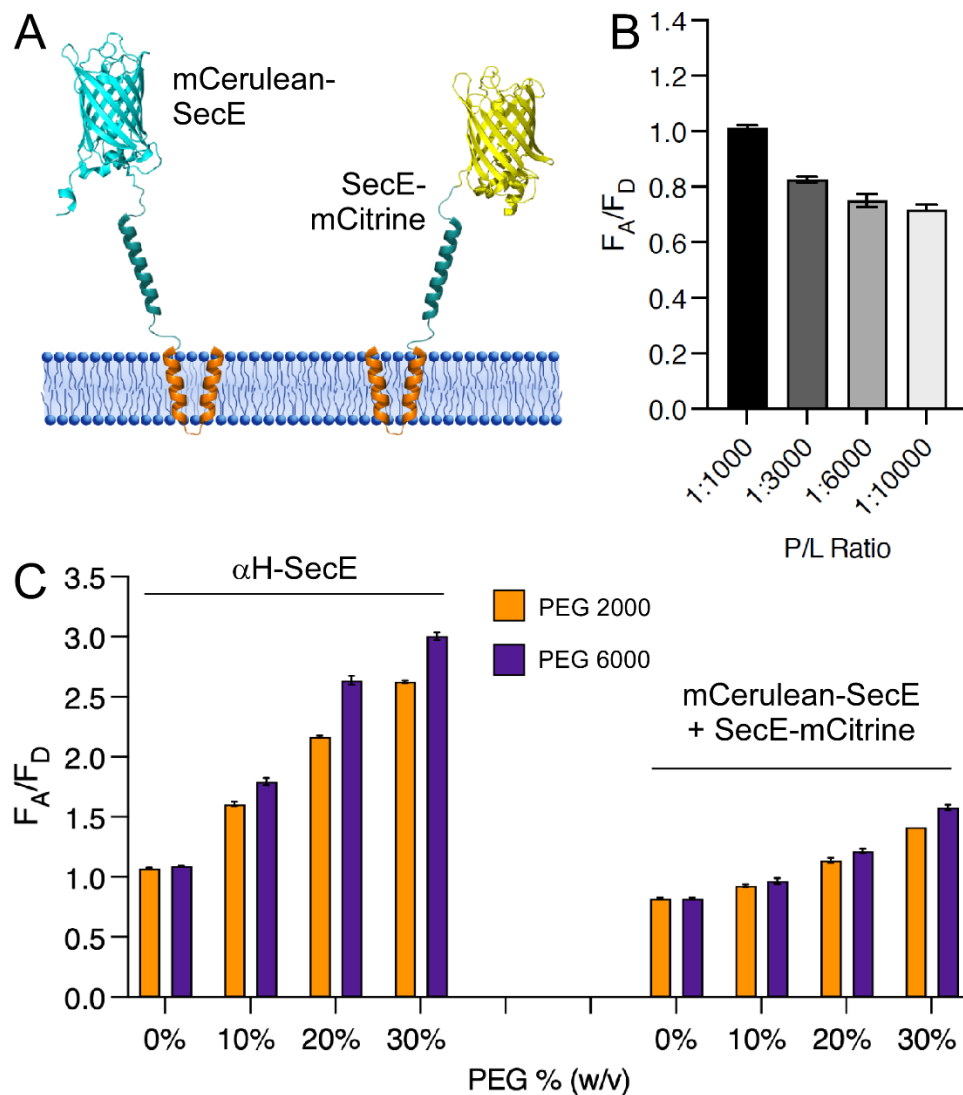
**Supplemental Figure 3. Soluble sensor undergoes concentration-dependent oligomerization.** SEC-MALS profiles of the membrane anchor-free sensor at 0.47 and 3.38 mg/mL concentrations reveals a shift towards higher molecular mass at the elevated concentration. For the sample injected with 0.47 mg/mL (green), only one peak in MALS with  $70.4 \pm 1.5$  kDa was measured. For the elevated concentration (purple), several peaks were detected at  $269 \pm 16$  kDa,  $110 \pm 1$  kDa and  $75 \pm 1$  kDa, thus showing a concentration-dependent oligomerization of the sensor in absence of the hydrophobic anchor.



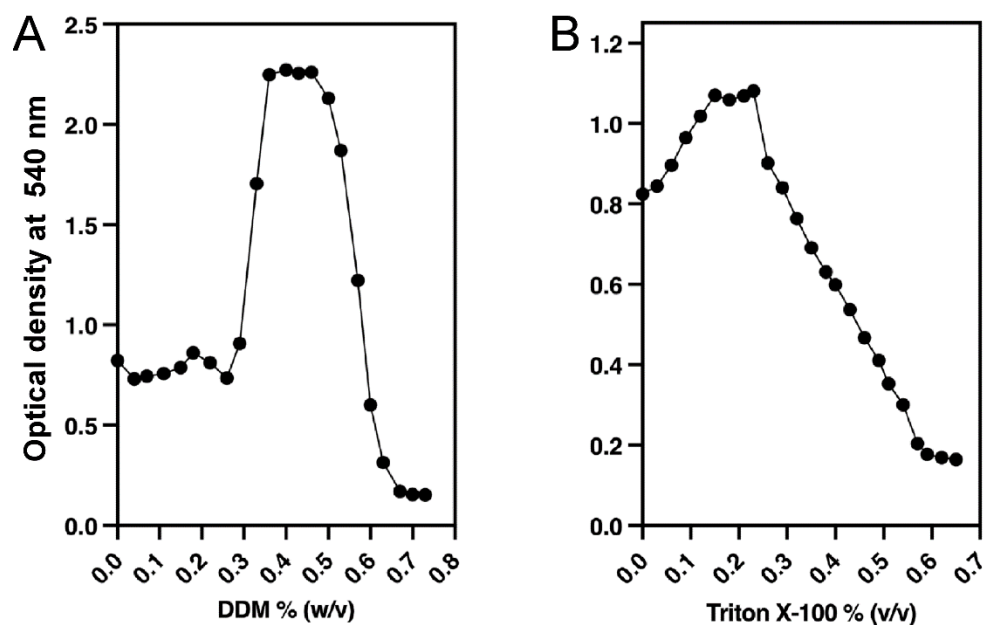
**Supplemental Figure 4. Absorption spectra of the purified crowding sensors.** The characteristic absorption spectra confirm presence of two fluorescent proteins with specific peaks for mCerulean (~430 nm) and mCitrine (515 nm).



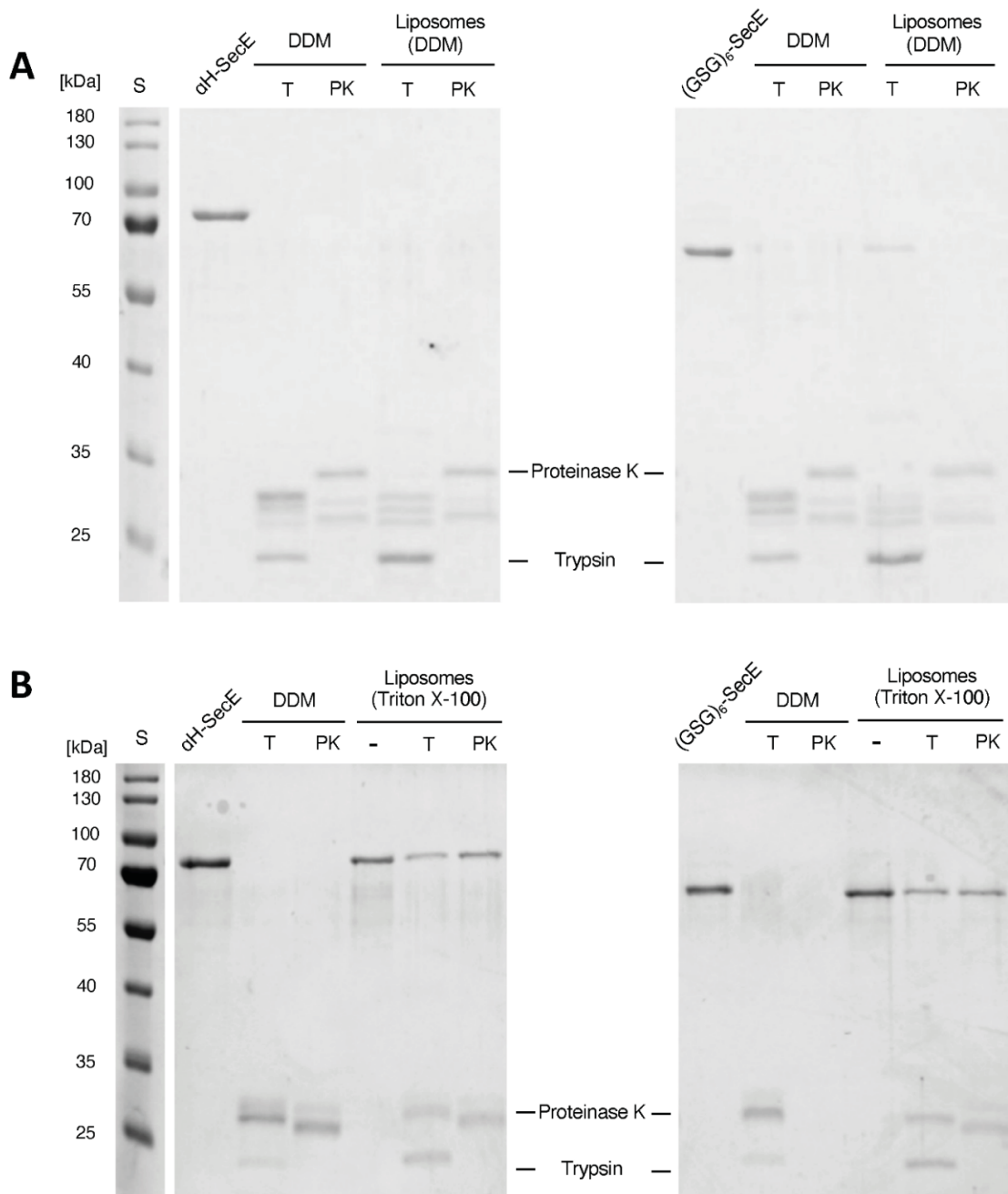
**Supplemental Figure 5. Sensitivity of the detergent-solubilized sensors to the polymer-induced crowding.** (A) Scheme of the  $\alpha$ H-SecE sensor in detergent micelle upon compaction induced by the polymer in solution. (B) Fluorescence emission spectra of  $\alpha$ H-SecE sensor in presence of PEG 6000 at indicated concentrations (w/v). (C) Corresponding FRET efficiencies of  $\alpha$ H-SecE sensor (mean  $\pm$  SD,  $n = 2$ ). Sample “10%\*” correspond to two-fold dilution of 20% PEG 6000 for testing the reversibility of the sensor compaction. (D-F) Same as (A-C), for the detergent-solubilized (GSG)<sub>6</sub>-SecE sensor.



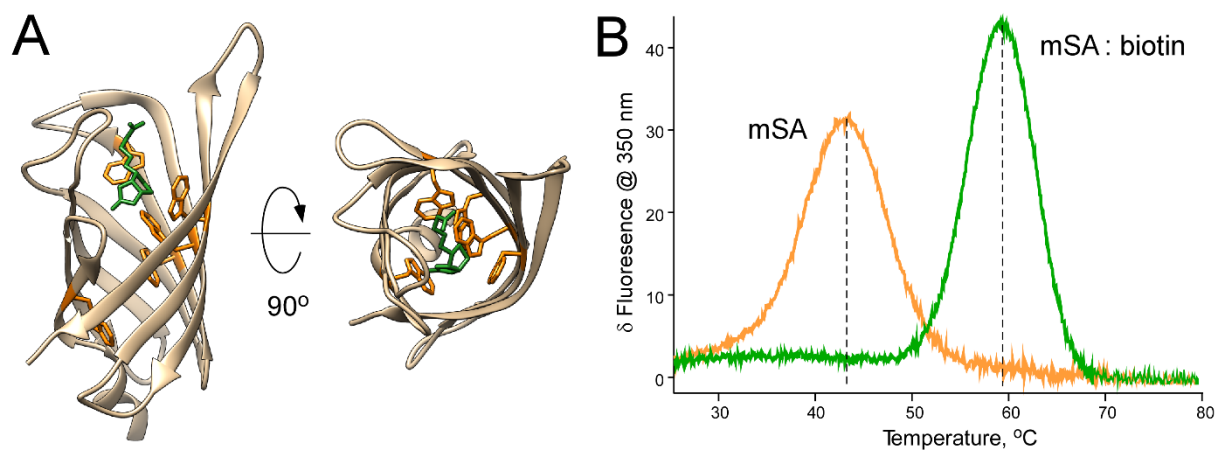
**Supplemental Figure 6. Individual membrane-anchored fluorophores manifest weak dependence of FRET on macromolecular crowding.** (A) Scheme of co-reconstituted fluorophores fused with individual membrane anchors. (B) FRET efficiency is dependent on the protein-to-lipid ratio used for reconstitution. Elevated protein density facilitates intermolecular FRET. (C) FRET efficiency of the crowding sensor  $\alpha$ H-SecE vs. individual co-reconstituted fluorophores at P/L ratio of 1:3,000 in response to soluble crowders PEG 2000 and PEG 6000.



**Supplemental Figure 7. Destabilization of liposomes prior reconstitution of the crowding sensors.** Optical density for DOPC:DOPG (70:30 mol%) liposomes in presence of DDM (A) and Triton X-100 (B). The liposomes were titrated with detergents and the optical density at 540 nm was recorded after each step until the suspension was completely solubilized. At the beginning of the titrations the liposome swelling is observed for both detergents resulting in increase of the optical density, followed by disintegration/solubilization of liposomes and decrease in the optical density.

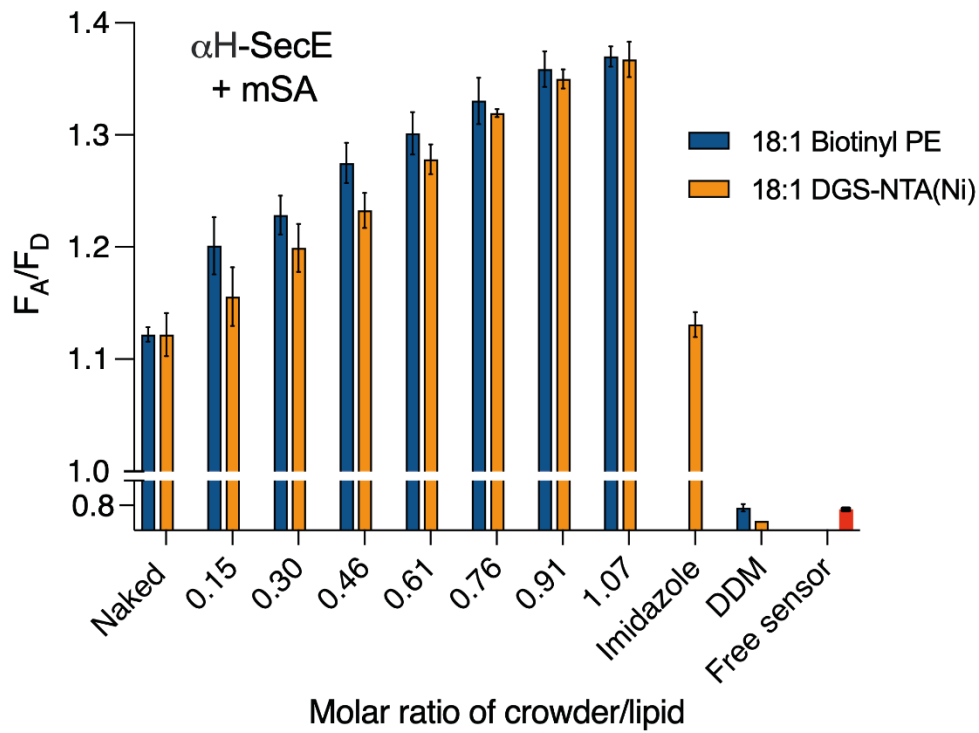


**Supplemental Figure 8. Topology determination of the liposome-reconstituted sensor using limited proteolysis.** Topology determination of the liposome-reconstituted sensors via limited proteolysis by trypsin (T), or proteinase K, (PK) for DDM-based reconstitution. “DDM”, detergent-solubilized sensors. (B) Same as (A), but using Triton X-100 for the liposome reconstitution.

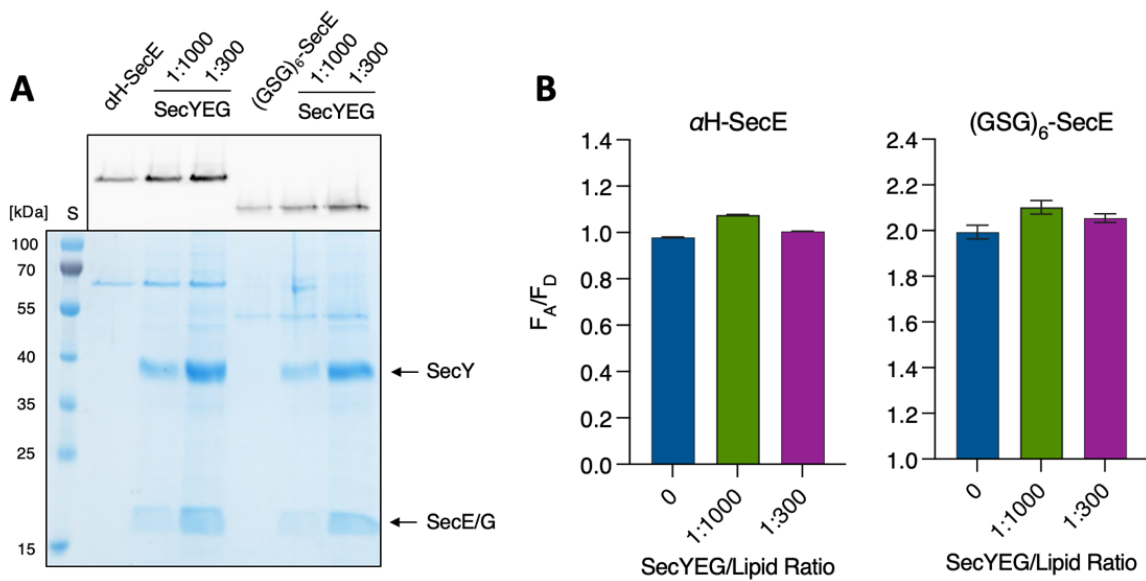


**Supplemental Figure 9. Functional test of the refolded monomeric streptavidin (mSA).**

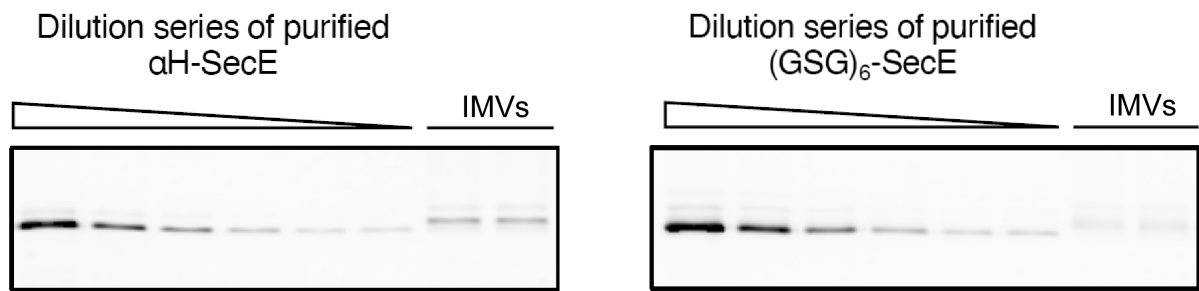
(A) Structure of mSA with bound biotin molecule (PDB ID: 4JNJ). Tryptophan residues are shown in orange, biotin in green. (B) Differential scanning fluorometry of mSA and mSA:biotin complex. Biotin binding induces prominent thermodynamic stabilization of mSA, as the thermal denaturation point shifts from 43 °C to 59 °C. Complete shift to the higher denaturation temperature indicates that all mSA molecules were competent for the ligand binding.



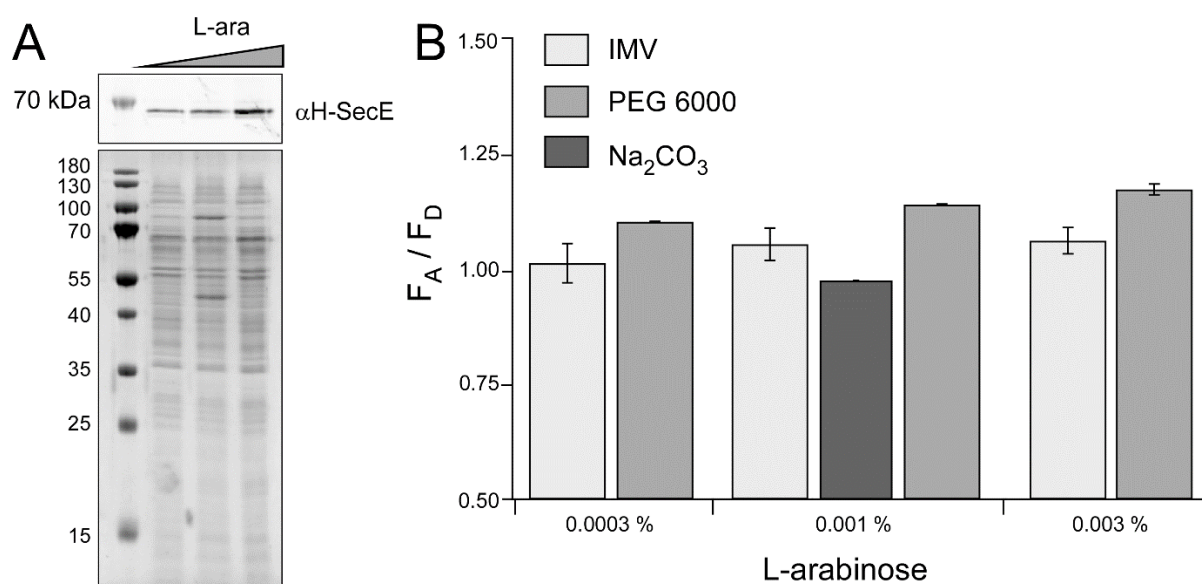
**Supplemental Figure 10. mSA-induced crowding at the membrane interface is detected by the sensor.** Two approaches for binding mSA to the membrane surface, either via biotinyl cap PE lipids or DGS-NTA lipids resulted in nearly identical response of the reconstituted sensor  $\alpha$ H-SecE.



**Supplemental Figure 11. Interfacial sensors do not respond to the crowding within the membrane.** (A) Protein content of the proteoliposomes with either sensors alone or also SecYEG translocon added at the indicated protein-to-lipid molar ratios. (B) FRET efficiencies of both sensors in each type of proteoliposomes.



**Supplemental Figure 12. Determination of the sensor abundance in the bacterial membrane.** In-gel fluorescence images of SDS-PAGE show IMVs containing the sensors loaded next to the serial dilutions of the purified sensors of known concentrations (range 166  $\mu\text{g}/\text{mL}$  to 5  $\mu\text{g}/\text{mL}$ ).



**Supplemental Figure 13. Dynamics of the crowding sensor in native membrane vesicles.**

(A) Increasing arabinose concentration promoted expression of the  $\alpha$ H-SecE sensor in *E. coli* C41(DE3). Bottom: Coomassie-stained SDS-PAGE of isolated IMVs; top: in-gel fluorescence. (B) Expression levels of  $\alpha$ H-SecE had minimal influence on the FRET signal (light grey bars). At all conditions, the sensors were responsive to the crowding in solution rendered by 10 % PEG 6000 (grey bars). Incubation of IMVs (0.001 % arabinose as inducer) with 0.2 M sodium carbonate reduced the FRET signal (dark grey bar), likely due to dissociation of peripheral proteins and so decrease in the interfacial crowding.

**$\alpha$ H-SecE sensor amino acid sequence:**

MHHHHHHLEVLFFQGPVSKGEELFTGVVPILVELDGDVNGHKFSVSGEGEGDATYGKLT  
 FICTTGKLPVPWPTLVTTLSWGVQCFARYPDHMKQHDFFKSAMPEGYVQERTIFFKDDGNY  
 KTRAEVKFEGDTLVNRIELKGIDFKEDGNILGHKLEYNAIHGNVYITADKQKNGIKANFGLNC  
 NIEDGSVQLADHYQQNTPIGDGPVLLPDNHYLSTQSKLSKDPNEKRDHMLLEFVTAAGITL  
 GMDELYKSGSGSGSGSGSGSGSGSGSGAEAAAKEAAAKEAAAKEAAAKEAAAKEAAAKAGS  
 GSGSGSGSGSGANTEAQSGRGLEAMKWWVVALLLVAIVGNLYRDIMLPLRALAVVILIAA  
 AGGVALLTTKKGSGSGSGSGSGSGSGAEAAAKEAAAKEAAAKEAAAKEAAAKEAAAKAGSG  
 GSGSGSGSGSGSGSMVSKGEELFTGVVPILVELDGDVNGHKFSVSGEGEGDATYGKLT  
 FICTTGKLPVPWPTLVTTFGYGLMCFARYPDHMKQHDFFKSAMPEGYVQERTIFFKDDGNY  
 KTRAEVKFEGDTLVNRIELKGIDFKEDGNILGHKLEYNYNSHNVYIMADKQKNGIKVNFKIRH  
 NIEDGSVQLADHYQQNTPIGDGPVLLPDNHYLSYQSALS KDPNEKRDHMLLEFVTAAGITL  
 GMDELYK

**(GSG)<sub>6</sub>-SecE sensor amino acid sequence:**

MHHHHHHLEVLFFQGPVSKGEELFTGVVPILVELDGDVNGHKFSVSGEGEGDATYGKLT  
 FICTTGKLPVPWPTLVTTLSWGVQCFARYPDHMKQHDFFKSAMPEGYVQERTIFFKDDGNY  
 KTRAEVKFEGDTLVNRIELKGIDFKEDGNILGHKLEYNAIHGNVYITADKQKNGIKANFGLNC  
 NIEDGSVQLADHYQQNTPIGDGPVLLPDNHYLSTQSKLSKDPNEKRDHMLLEFVTAAGITL  
 GMDELYKSGSGSGSGSGSGSGSGSGSGSANTEAQSGRGLEAMKWWVVALLLVAIVGNLY  
 YRDIMLPLRALAVVILIAAAGGVALLTTKKGSGSGSGSGSGSGSGSMVSKGEELFTGVV  
 PILVELDGDVNGHKFSVSGEGEGDATYGKLT FICTTGKLPVPWPTLVTTFGYGLMCFARY  
 PDHMKQHDFFKSAMPEGYVQERTIFFKDDGNYKTRAEVKFEGDTLVNRIELKGIDFKEDGNI  
 LGHKLEYNYNSHNVYIMADKQKNGIKVNFKIRHNIEDGSVQLADHYQQNTPIGDGPVLLPDN  
 HYLSYQSALS KDPNEKRDHMLLEFVTAAGITLGMDELYK

mCerulean is highlighted in blue, mCitrine in orange, SecE in red,  $\alpha$ -helices of the linker region in green

### 3.3 Development of anchoring strategies and other sensor designs

#### 3.3.1 Transmembrane anchor domains for the crowding sensors

##### 3.3.1.1 Introduction

To characterize the membrane properties, e.g. macromolecular crowding, efficient targeting of the sensor molecules is an essential prerequisite. In the Chapter 3.2 we accomplished that task by utilizing the transmembrane helical hairpin of SecE. Besides the SecE hairpin, several other anchors were tested within the project, aiming to increase the robustness of the approach and also avoid pitfalls, such as anchor-mediated clustering.

Among the tested anchors were Mistic (Membrane-Integrating Sequences for Translation of Inter-membrane protein Constructs) from *Bacillus subtilis* and RseC protein from *E. coli*. Intrinsically, Mistic plays a role in the biofilm formation (Lundberg *et al.*, 2013), while it is a quite peculiar protein with hydrophilic properties due to a high abundance of polar and charged amino acids on the surface but remains associated with membranes when expressed in *E. coli* (Roosild *et al.*, 2005). The protein consists of 110 amino acids that form a four-helix bundle structure in detergent micelles (figure 3.1), however the structure in the membrane remains unknown and changes of the protein conformation upon the membrane insertion are hypothesized (Roosild *et al.*, 2005). Mistic can assist the membrane targeting and insertion of inner membrane proteins: When used as a fusion tag on the N-terminus of the protein of interest of either prokaryotic or eukaryotic origin, it allows for the high expression yield in *E. coli* potentially avoiding the known translocation machineries (Chowdhury *et al.*, 2012; Dvir and Choe, 2009; Ji-Ann Lee and Dien *et al.*, 2010; Roosild *et al.*, 2005). The spontaneous association with the membrane makes Mistic a potential candidate for anchoring of the membrane sensors.

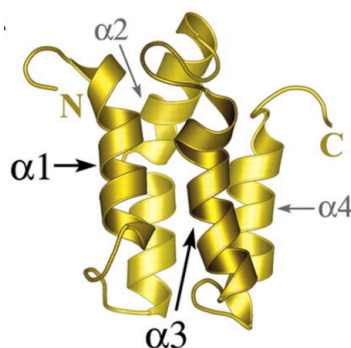


Figure 3.1: Ribbon diagram of the Mistic structure from Roosild *et al.* (2005)

Another potential candidate for the sensor membrane anchoring was the RseC protein, a positive regulator of  $\sigma^E$  (RpoE) transcription factor. The  $\sigma^E$ -mediated system regulates the

gene expression as a stress response to accumulation of unfolded/aggregated outer membrane proteins in periplasm (Mitchell and Silhavy, 2019). RseC is one of the four proteins encoded in the gene operon containing RpoE (De Las Peñas *et al.*, 1997). RseA and RseB proteins were shown to be negative regulators of RpoE transcription activity (Missiakas *et al.*, 1997), while RseC may be also involved in reduction of iron-sulfur center of SoxR system after its activation upon oxidative stress response (Lee *et al.*, 2022). The structure of RseC protein is currently unsolved, but models generated by the AlphaFold2 (figure 3.2) and sequential analysis predicts the presence of two transmembrane helices forming a tight hairpin in the lipid bilayer. Experimental evidences suggest that RseC is an inner membrane protein involved in modulation of  $\sigma^E$  activity (Missiakas *et al.*, 1997) and in reduction of SoxR (Lee *et al.*, 2022).

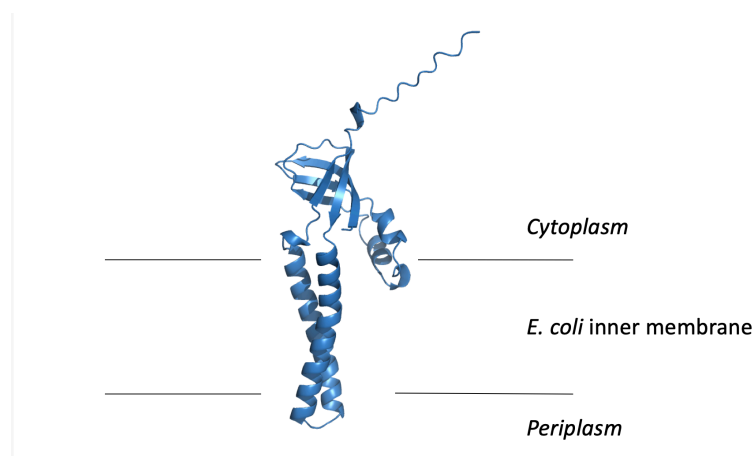


Figure 3.2: AlphaFold model of RseC protein (UniProt ID:P46187). Topology of the RseC protein is shown accordingly to the proposed model (Lee *et al.*, 2022)

For characterization of Mystic as a potential candidate for the membrane anchoring, the SecE transmembrane domain of  $\alpha$ H-SecE sensor was replaced, and the new sensor  $\alpha$ H-Mistic was characterized. The sequence of potential helical hairpin of RseC protein was encoded instead of SecE transmembrane domain of (GSG)<sub>6</sub>-SecE sensor resulting in (GSG)<sub>6</sub>-RseC construct. Both sensors,  $\alpha$ H-Mistic and (GSG)<sub>6</sub>-RseC, were examined on their association with the membrane upon expression, purification and reconstitution efficiency into model membranes as well as the ability to respond to the macromolecular crowding.

### 3.3.1.2 Materials and Methods

#### Expression and purification of sensor constructs

##### *$\alpha$ H-Mistic*

Gene fragments containing sequence encoding  $\alpha$ H-Mistic construct bearing N-terminal poly-histidine tag were cloned via Gibson Assembly into plasmid pRSET-A, which was transferred into *E. coli* C43(DE3) strain. The cells were grown in LB medium (Carl Roth) supplemented with 100  $\mu$ g/mL ampicillin till  $OD_{600}$  of 0.55 and the expression of the protein was induced upon addition of 0.1 mM IPTG and proceeded overnight at 25°C and 180 rpm. The cells were harvested for 10 min at 5000xg (SLC-6000 fixed angle rotor, Thermo Fisher/Sorvall). The cell pellet was resuspended in 10 mM  $NaH_2PO_4/Na_2HPO_4$  pH 7.4, 100 mM NaCl and 0.1 mM PMSF and lysed by Microfluidizer (M-110P, Microfluidics Corp). The first centrifugation at 12000xg for 15 min (SS34, Thermo Fisher/Sorvall) was applied to remove cell debris and the second at 235000xg for 45 min (Ti45 rotor, Beckman Coulter) was used to collect the membrane fraction, which was resuspended in 10 mM  $NaH_2PO_4/Na_2HPO_4$  pH 7.4, 100 mM NaCl, 5% glycerol and 0.1 mM PMSF. The solubilization of the membranes was performed in 50 mM  $NaH_2PO_4/Na_2HPO_4$  pH 7.4, 500 mM NaCl, 200  $\mu$ M TCEP, 1 mM AEBSF and 1% LDAO. The solubilized material was centrifuged at 5000xg for 10 min and the supernatant was loaded at  $Ni^{2+}$ -NTA agarose resin (Macherey-Nagel). The resin was washed with 50 mM  $NaH_2PO_4/Na_2HPO_4$  pH 7.4, 500 mM NaCl, 200  $\mu$ M TCEP, 1 mM AEBSF, 10 mM imidazole and 0.1% LDAO and the sensor was eluted with 50 mM  $NaH_2PO_4/Na_2HPO_4$  pH 7.4, 500 mM NaCl, 200  $\mu$ M TCEP, 1 mM AEBSF, 300 mM imidazole and 0.1% LDAO. The eluted protein fraction was loaded on the Superdex 200 Increase GL 10/300 column (Cytiva) in 10 mM  $NaH_2PO_4/Na_2HPO_4$  pH 7.4, 50 mM NaCl and 0.1% LDAO. The peak elution fractions containing the sensor were pooled, supplemented with 5% glycerol and stored at -80°C for further experiments. The purification process was analyzed with SDS-PAGE by in-gel fluorescence and subsequent staining with Coomassie (Quick Coomassie® Stain, SERVA).

##### *(GSG)<sub>6</sub>-RseC*

The (GSG)<sub>6</sub>-RseC construct was purified by the identical protocol described for (GSG)<sub>6</sub>-SecE sensor from the Chapter 3.2.

#### Reconstitution of the sensor constructs into liposomes

Chloroform-solubilized stocks of lipids (Avanti Polar Lipids, Inc.) were used to prepare two different types of liposomes – either DOPC (70 mol %) and DOPG (30 mol %) or DOPC (54 mol %), DOPG (26 mol %) and 18:1 Biotinyl Cap PE (20 mol %). The lipids were mixed in defined ratios, the chloroform was evaporated at 40°C (rotary evaporator RV 8, IKA) and the lipid film was rehydrated and resuspended in 20 mM Tris/HCl pH 7.5 and 150 mM KCl to a

final lipid concentration of 5 mM. The vesicle suspensions were extruded via 200 nm polycarbonate membranes with mini-extruder lipids (Avanti Polar Lipids, Inc.) to obtain unilamellar liposomes. For the reconstitution the liposomes were mixed with either 0.3% LDAO for  $\alpha$ H-Mistic or 0.2% DDM for (GSG)<sub>6</sub>-RseC constructs, incubated for 15 min at 40°C and then mixed with purified and detergent solubilized sensors with protein:lipid molar ratio of 1:3,000.

#### *Detergent removal by sorbent beads*

After the 30 min incubation period on ice, the protein:lipid:detergent mixtures were transferred on pre-washed Bio-Beads SM-2 sorbent (Bio-Rad Laboratories) and the detergents were removed overnight on the rolling bank at 4°C. The proteoliposomes were pelleted at 162000xg for 30 min (S120-AT3 rotor, Discovery M120 SE, Thermo Fisher/Sorvall) and resuspended in 20 mM Tris/HCl pH 7.5 and 150 mM KCl to the final lipid concentration of 5 mM.

#### *Dialysis*

After 30 min incubation period on ice, the protein:lipid:detergent mixtures were loaded into the 3 mL Slide-A-Lyzer dialysis cassettes with 3.5 MWCO (Thermo Fischer Scientific) and the samples were dialyzed against 2 L of fresh 20 mM Tris/HCl pH 7.5 and 150 mM KCl buffer for 24h. The proteoliposomes were pelleted and resuspended as described above.

#### *Dilution*

The protein:lipid:detergent mixtures (500  $\mu$ L) were incubated on ice for 2 h and then diluted with 20 mL fresh 20 mM Tris/HCl pH 7.5 and 150 mM KCl in 1 mL steps under continuous stirring. The proteoliposomes were pelleted at 160000xg for 30 min (50.2 Ti rotor, Beckman Coulter) and resuspended in 20 mM Tris/HCl pH 7.5 and 150 mM KCl to the final lipid concentration of 5 mM.

### **Sensor reconstitution efficiency and fluorescence spectroscopy**

The reconstitution efficiency was analyzed via the flotation assay described in Chapter 3.2. Recording the emission spectra and calculation of corresponding  $F_A/F_D$  ratios were performed as described in Chapter 3.2.

### 3.3.1.3 Results

#### A. $\alpha$ H-Mistic as a potential candidate for the sensor anchoring

The  $\alpha$ H-Mistic construct was expressed and the membrane fraction was extracted via ultracentrifugation. The  $\alpha$ H-Mistic sensor was found to be present in both the cytoplasmic and the membrane fractions (data not shown). The collected membrane fraction was solubilized with lauryldimethylamine N-oxide (LDAO), since the protein requires ionic detergent (Roosild *et al.*, 2005) and the solubilized material was subsequently purified with IMAC. The resulting sensor construct (theoretical molecular weight of 77 kDa) appeared in the elution fraction as a single band of approx. 70 kDa and it was further purified with size exclusion chromatography (figure 3.3).

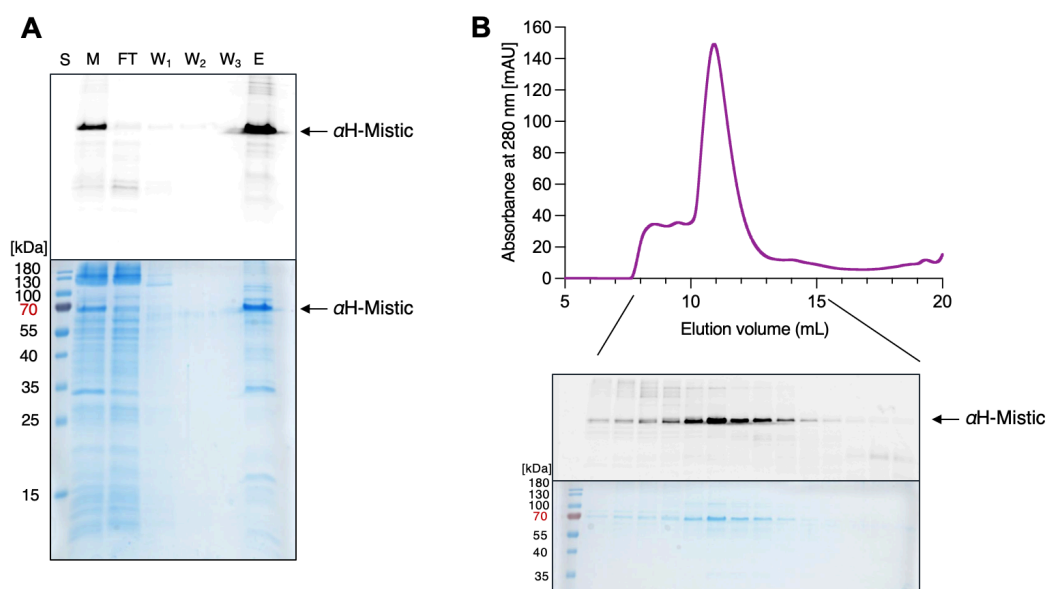


Figure 3.3: SDS-PAGE analysis with corresponding in-gel fluorescence of (A) IMAC purification with applied crude membranes (M, flow through (FT) after protein binding, wash ( $W_1$ - $W_3$ ) and elution fraction (E) and (B) size exclusion of  $\alpha$ H-Mistic sensor construct.

The purified  $\alpha$ H-Mistic was reconstituted into liposomes consisting of either DOPC/PG (70:30 mol %) or 18:1 biotinyl cap PE:DOPC:DOPG (20:54:26 mol %) using Bio-Beads to remove the detergent. The emission spectra of LDAO-solubilized as well as liposome-reconstituted sensor construct were recorded (figure 3.4). The  $F_A/F_D$  ratios upon reconstitution increased from  $0.692 \pm 0.002$  to  $1.21 \pm 0.02$  for DOPC/PG liposomes, but only  $0.90 \pm 0.01$  for the liposomes containing 20 mol % biotinyl cap PE.

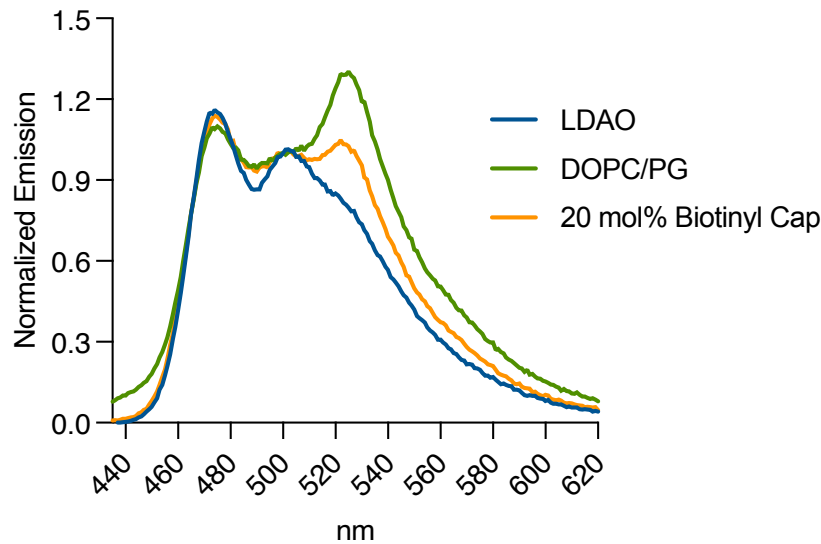


Figure 3.4: Emission spectra of  $\alpha$ H-Mistic solubilized in LDAO and reconstituted to the liposomes with different lipid compositions

The reconstitution efficiency was analyzed via the flotation assay, as described in Chapter 3.2. After centrifugation,  $\alpha$ H-Mistic was found in the top and the bottom fractions for both types of liposomes, and the estimated reconstitution efficiency was around 60% (figure 3.5-A). The emission spectra of the top fraction showed a decreased  $F_A/F_D$  ratio of  $0.868 \pm 0.001$  in comparison to the crude liposomes after reconstitution in DOPC/PG (figure 3.5-B) and a slight decrease of  $F_A/F_D$  ratio of  $0.81 \pm 0.02$  for liposomes containing 20 mol % biotinyl cap PE (data not shown). To probe  $\alpha$ H-Mistic sensitivity to the macromolecular crowding in the solution, the collected top fraction of DOPC/PG reconstitution was mixed with PEG 6000 to achieve the crowder concentration of 10% (w/v). The  $F_A/F_D$  ratio increased by 14%, so the resulting construct was able to detect crowding in solution.

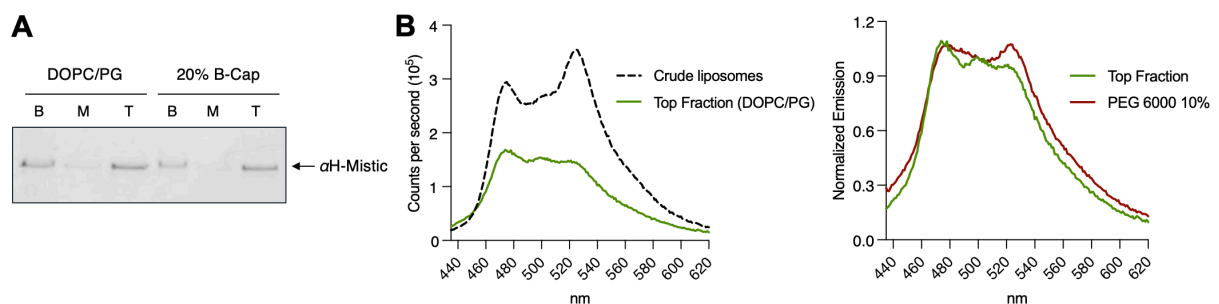


Figure 3.5: (A) Flotation assay with reconstituted  $\alpha$ H-Mistic proteoliposomes and (B) corresponding emission spectra of the crude DOPC:DOPG liposomes and the top fraction with and without 10% (w/v) PEG 6000

Relatively low reconstitution efficiency of  $\alpha$ H-Mistic was likely accompanied by aggregation of the sensor, thus resulting in remarkable changes of  $F_A/F_D$  ratios recorded for the crude

liposomes. The removal of the detergent with Bio-Beads in the reconstitution protocol may be not suitable for this type of the sensor construct, so alternative reconstitution strategies were tested, i.e. dialysis and rapid dilution methods. The liposomes were mixed with 0.3% LDAO and the solubilized  $\alpha$ H-Mistic, incubated for 2 h and were left for dialysis for 24 h. Another method tested was the proteoliposomes formation using rapid dilution. After incubation of the protein with the liposomes, the solution is diluted with fresh detergent-free buffer under stirring, so LDAO concentration falls below CMC (0.023 %). Afterwards, the liposomes were pelleted via ultracentrifugation, resuspended in fresh buffer to achieve back the concentration of the lipids employed in this experiment and analyzed via flotation assay (figure 3.6-A). In the proteoliposomes formed with rapid dilution method, the amount of  $\alpha$ H-Mistic was very low: only faint bands with residual protein were detected in the bottom fraction of the flotation assay and even less was found in top fraction, which implies that this method is not suitable for  $\alpha$ H-Mistic reconstitution.

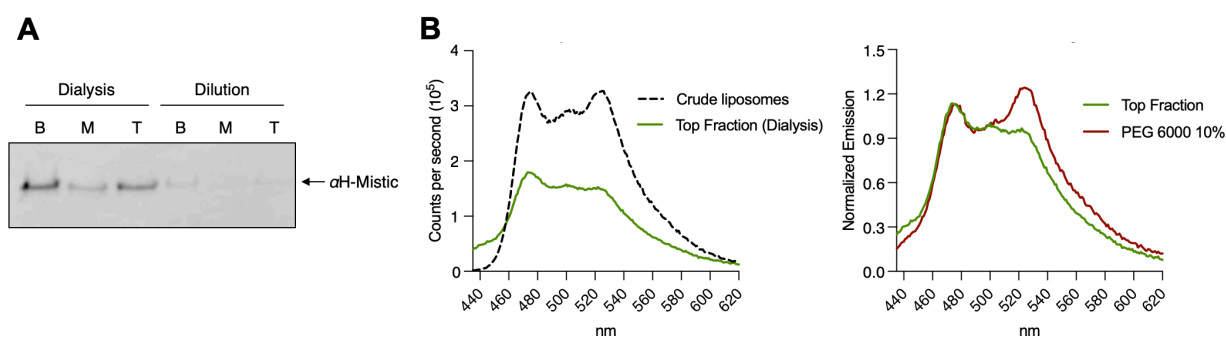


Figure 3.6: (A) Flotation assay with  $\alpha$ H-Mistic proteoliposomes reconstituted with either dialysis or dilution method and (B) corresponding emission spectra of the crude dialyzed DOPC:DOPG liposomes and the top fraction with and without 10% (w/v) PEG 6000 (right graph).

The dialyzed  $\alpha$ H-Mistic sample have shown same result as in the initial sorbent-based reconstitution trial. Remarkably, the  $F_A/F_D$  ratio of the crude liposomes was smaller -  $1.01 \pm 0.01$  upon reconstitution with dialysis compared to Bio-Beads reconstitution with  $1.21 \pm 0.02$  with the same liposome composition. Still in the top fraction the  $F_A/F_D$  ratio was found to be  $0.86 \pm 0.04$ . Notably, upon mixing of the sample with PEG 6000 (final concentration 10% (w/v)), the response of the sensor reached  $1.07 \pm 0.04$  which is higher than by reconstitution with Bio-Beads, possibly due to the reduced tendency to aggregation and/or clustering of the construct during slower detergent removal.

### B. RseC as a potential candidate for the sensor anchoring

The transmembrane domain from RseC protein composed of two TMHs was introduced into the  $(GSG)_6$ -SecE sensor. The *E. coli* BL21(DE3), C41(DE3) and C43(DE3) strains were transformed with pBAD-based plasmid containing the sequence for the new  $(GSG)_6$ -RseC sensor. The expression of the protein induced with 0.02% w/v arabinose was comparable

between all tested strains and resulted in the formation of multiple fluorescent species with different molecular weights (figure 3.7)

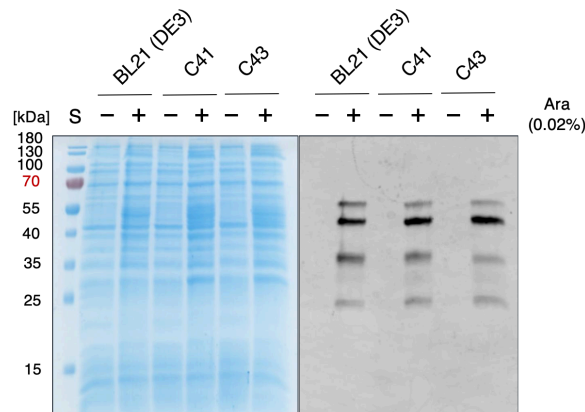


Figure 3.7: Expression test of  $(GSG)_6$ -SecE sensor in the different *E. coli* strains upon 0.02% arabinose induction

BL21(DE3) strain expression was employed for further tests, where the concentration of arabinose was varied, which affected the synthesized product (figure 3.8-A). While two-fold reduction of the arabinose did not affect the sensor expression, further reduction to 0.001% (w/v) lowered the formation of degradation products (figure 3.8-A). The cells from this expression condition were lysed, the cell debris was removed and the membrane fraction was separated from the lysate via ultracentrifugation. The sensor appeared in the membrane fraction as a single band on SDS-PAGE (figure 3.8-B), whereas in the cytoplasmic fraction the degradation products and a low amount of the full-size sensor were detected.

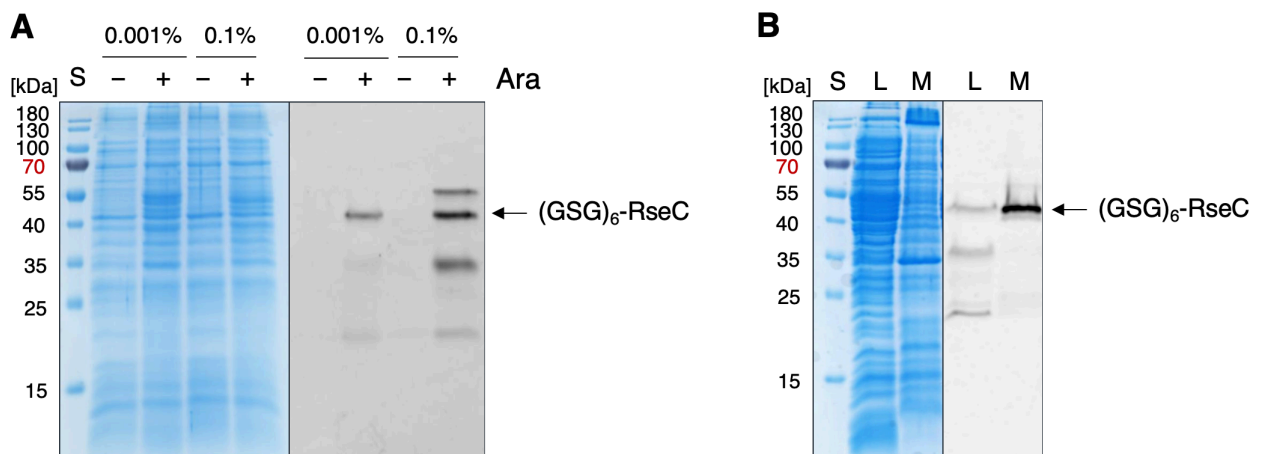


Figure 3.8: (A) SDS-PAGE analysis of the expression of  $(GSG)_6$ -SecE sensor in *E. coli* BL21 (DE3) strain upon 0.001% and 0.1% arabinose induction. (B) Analysis of the separated cytoplasmic (L) and membrane fraction (M) with overexpressed  $(GSG)_6$ -SecE construct.

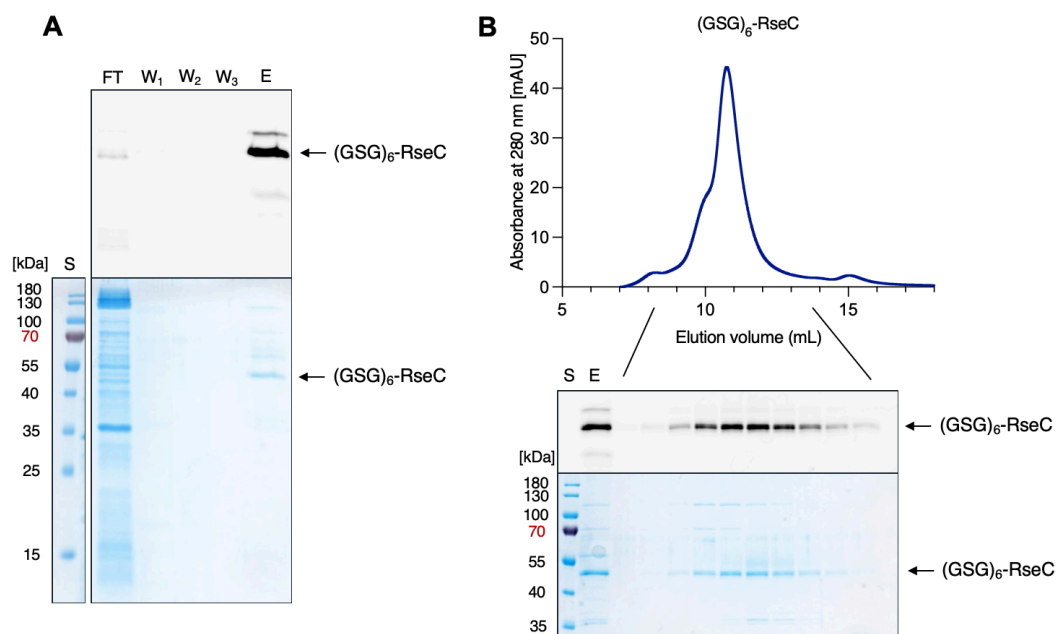


Figure 3.9: SDS-PAGE analysis with corresponding in-gel fluorescence of (A) IMAC purification, where flow-through (FT) after protein binding, wash (W<sub>1</sub>-W<sub>3</sub>) and elution fraction (E) are applied and (B) size exclusion chromatography of (GSG)<sub>6</sub>-SecE sensor.

Next, the membranes containing (GSG)<sub>6</sub>-RseC sensor were solubilized with DDM. The His-tagged sensor construct was purified with IMAC (figure 3.9-A) and the elution fraction (E) was applied on SEC. The main peak at 10.75 mL manifested a shoulder at around 10 mL, which is possibly coming from the impurities after Ni<sup>2+</sup>-NTA purification. The purest fractions were collected and employed for reconstitution experiments.

(GSG)<sub>6</sub>-RseC sensor was reconstituted into liposomes consisting of DOPC/PG (70:30 mol %) with P/L ratio of 1:3,000 upon Bio-Beads assisted detergent removal. The emission spectra of DDM-solubilized and reconstituted (GSG)<sub>6</sub>-RseC were recorded (figure 3.10) and the  $F_A/F_D$  ratios were calculated to be  $1.17 \pm 0.01$  and  $3.02 \pm 0.02$ , respectively. The addition of PEG 6000 with final concentration of 10% (w/v) led to minor decrease of the acceptor fluorescence intensity.

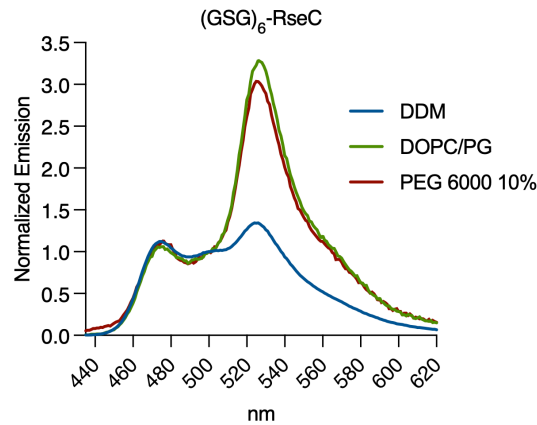


Figure 3.10: (A) Recorded emission spectra of  $(GSG)_6$ -SecE DDM-solubilized sensor and reconstituted to the liposomes consisting out of DOPC/PG. Addition of PEG to the proteoliposomes resulted in decrease of the acceptor fluorescence.

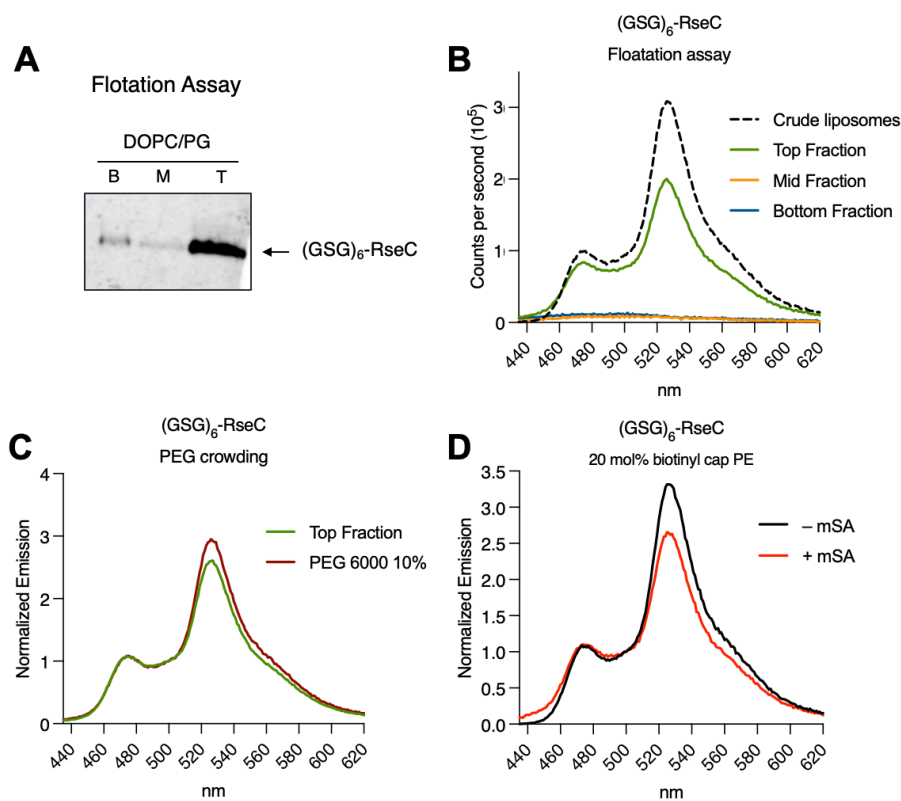


Figure 3.11: (A) Flotation assay with reconstituted  $(GSG)_6$ -SecE proteoliposomes and (B) corresponding emission spectra of the crude DOPC:DOPG liposomes and collected fractions. (C) Reaction of the sensor in the top fraction on solution crowding induced by 10% (w/v) PEG 6000. (D) Reaction of the membrane reconstituted of  $(GSG)_6$ -SecE sensor upon interfacial crowding with mSA.

Such an intensive increase of the  $F_A/F_D$  ratio upon reconstitution may be an indication on sensor aggregation, so the reconstitution efficiency was verified with flotation assay (figure 3.11-A). As can be seen on the SDS-PAGE, the  $(GSG)_6$ -RseC sensor was predominantly found in the top fraction suggesting the high reconstitution efficiency. The emission spectra of

the top fraction manifested a decrease of the acceptor fluorescence intensity with corresponding  $F_A/F_D$  ratio of  $2.34 \pm 0.01$  (figure 3.11-B), and the reconstituted sensor responded to the crowding mimicked by PEG 6000 in solution (increase of 8%, figure 3.11-C). Upon the reconstitution of the sensor construct into liposomes containing 20 mol % biotinyl cap PE, the calculated  $F_A/F_D$  ratio was  $3.090 \pm 0.002$ . After addition of mSA protein to mimic the crowding on the interface of the membrane, the  $F_A/F_D$  ratio suddenly dropped to  $2.40 \pm 0.04$  (figure 3.11-D). The reconstitution efficiency for 20 mol % biotinyl cap PE liposomes was comparable to the DOPC/PG and the  $F_A/F_D$  ratio of the top fraction also decreased to  $2.53 \pm 0.02$  (data not shown).

Same as for the  $\alpha$ H-Mistic, the dialysis and dilution method were tested for the reconstitution of the  $(GSG)_6$ -RseC sensor construct, and the reconstitution efficiency was examined (figure 3.12). The reconstitution efficiency within both reconstitution methods was comparable, but the  $F_A/F_D$  ratios of the collected top fractions showed a significant difference to each other and also to the firstly tested method which involved Bio-Beads detergent removal. In comparison to the Bio-Beads method, the  $F_A/F_D$  ratios of the top fractions decreased to 50% for the dialyzed sample and increased to 19% for the diluted sample: For the dialyzed sample the calculated values were  $3.40 \pm 0.01$  and  $1.17 \pm 0.01$  for the crude liposomes and top fractions, respectively, and for the diluted sample  $3.22 \pm 0.04$  and  $2.79 \pm 0.02$ .

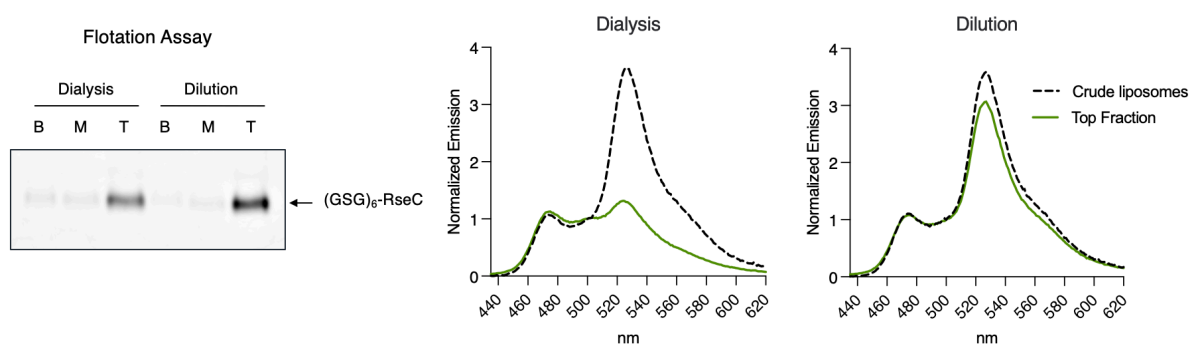


Figure 3.12: SDS-PAGE analysis of flotation assay with  $(GSG)_6$ -SecE proteoliposomes reconstituted with either dialysis or dilution method with corresponding emission spectra of the crude liposomes and collected top fractions

### 3.3.1.4 Discussion

A prerequisite for accurate crowding sensor readout on the membrane surface is the correct and stable insertion into the membrane. For this, several candidates for the anchoring domain were tested, among them Mystic protein and the transmembrane helical hairpin of RseC protein. Both generated constructs,  $\alpha$ H-Mistic and (GSG)<sub>6</sub>-RseC were expressed and purified from *E. coli* membranes and their reconstitution efficiency and the ability to respond to crowding-induced environment were examined. Additionally, anchors like PgaD and EmrE were examined within the Bachelor projects of Samet Kurt (2019, Appendix, Supervised student projects) and Anastasiia Romenska (2022, Appendix, Supervised student projects).

$\alpha$ H-Mistic sensor construct faced two major problems. First, upon expression of this construct in *E. coli* a large fraction of the protein was found in the cytoplasm. Quantification of macromolecular crowding *in vivo* with this type of the sensor would be ambiguous, as the signal from the membrane-anchored population would be perturbed by the uninserted protein in the cytoplasm. Second, the purified  $\alpha$ H-Mistic showed relatively low reconstitution efficiency, as approximately 50% of the protein remained in the bottom fraction in flotation assay experiments. Additionally, the recorded emission spectra of the sensor in liposomes with different compositions (DOPC:DOPG versus DOPC:DOPG:biotinyl cap PE) reported varying  $F_A/F_D$  ratios. Different reconstitution strategies beyond the conventional Bio-Beads detergent removal, i.e. rapid dilution and dialysis, were tested for this construct improve the reconstitution efficiency. In the rapid dilution approach, the mixture of detergent, protein and lipids is diluted with fresh detergent-free buffer below critical micelle concentration (CMC) of the detergent which leads to a spontaneous insertion of the protein and formation of proteoliposomes (Wang and Tonggu, 2015). Although the rate of the detergent removal can be controlled, the diluted sample has to be concentrated. The amount of  $\alpha$ H-Mistic detected in the pellet was substantially lower than the initial protein input, suggesting the limited applicability of the method. Alternatively, slow detergent removal may be achieved via the dialysis-based approach, where the detergent-solubilized protein is mixed with the liposomes and after incubation the mixture is dialyzed against a detergent-free buffer (Skrzypek *et al.*, 2018). In the case of  $\alpha$ H-Mistic, the dialysis approach did not improve the reconstitution efficiency, as was shown in flotation assay (figure 3.6-A). Notably, the resulting  $F_A/F_D$  ratio of the crude liposomes was smaller in comparison to the Bio-Beads-based reconstitution trial. As the  $F_A/F_D$  ratios of the top fractions were comparable between these reconstitutions, less aggregates were likely formed upon the dialysis. Moreover, the sensitivity of the reconstituted  $\alpha$ H-Mistic to PEG-induced crowding was approximately 8% higher than of the Bio-Beads reconstituted sample under identical conditions.

In case of the (GSG)<sub>6</sub>-RseC construct, expression of the sensor cloned into pBAD vector could be modulated by the inducer concentration. At high arabinose concentration several fluorescent entities differing by their molecular weights were observed, which could represent degradation products, as it was the case for SecE-based sensors upon high overexpression (Suppl. Information, figure 2, Chapter 3.2, Löwe *et al.*, 2023). Appearance of those species was substantially reduced for (GSG)<sub>6</sub>-RseC at arabinose concentration of 0.001%, resulting in a dominant fluorescent band of the full-length sensor on SDS-PAGE. After the membrane extraction the degradation products were found in the cytoplasm, whereas the (GSG)<sub>6</sub>-RseC sensor was present in the membrane fraction. After purification, the proteoliposomes with the sensor were formed and the reconstitution efficiency in model membranes consisting of DOPC/PG was comparable to the original (GSG)<sub>6</sub>-SecE sensor described in Chapter 3.2. The  $F_A/F_D$  ratios in the crude liposomes increased to 159% in comparison to the DDM-solubilized sample. This striking increase in the FRET efficiency and the absence of response to PEG crowding implied that the protein aggregated or clustered within the model membranes. Different reconstitution methods allowed for high yields, but also resulted in substantially different acceptor/donor ratios in the top fractions. Thus, the reconstitution conditions should be carefully analyzed for this sensor construct, and the detergent screen for the sensor isolation and handling may be required.

Comparison of the expression, isolation and performance of  $\alpha$ H-Mistic, (GSG)<sub>6</sub>-RseC and SecE-based sensors in terms of response upon crowding is summarized in the Table 1. As can be seen, Mistic is not optimal for the anchoring of the sensors due to the problematic expression in the cells and challenged reconstitution. On one hand, the expression yield can be tuned by the choice of different vector or by altering the expression conditions, as shown for other constructs. But on the other hand, the low reconstitution efficiency of the purified construct makes Mistic a bad candidate for the evaluation of the sensor performance *in vitro*. Additionally, the conformation of the anchor domain in the membrane not known. As already mentioned above, the outer surface of Mistic is more hydrophilic than an average transmembrane domain of many IMP (Roosild *et al.*, 2005), which can be the reason for a poor reconstitution efficiency. The response of the sensor upon PEG crowding was achieved only after separation of liposomes with reconstituted  $\alpha$ H-Mistic from the crude liposomes.

The same behavior upon PEG-crowding was observed for (GSG)<sub>6</sub>-RseC sensor, whereas a decrease of the  $F_A/F_D$  ratio was observed upon mSA attachment to the biotinylated liposomes even after flotation assay. It can be concluded, that among the tested transmembrane domains for the sensor anchoring, SecE-based constructs from Chapter 3.2 revealed as the best candidates for the further sensor development because of the tight association with the membranes and synthetic liposomes, reproducible reconstitution and sensor response.

Table 1: Comparison of the tested single-chain sensors

Sensor	Expression	Isolation	Aggregation	Response to crowders	
				In solution (10% w/v PEG 6000)	At the interface (mSA)
$\alpha$ H-Mistic	Present in cytoplasm and in membrane	good	Moderate upon reconstitution, low reconstitution efficiency	14 % increase after flotation assay	n/a*
(GSG) <sub>6</sub> -RseC	Present in the membrane, degradation products	good	High upon reconstitution	8 % increase after flotation assay	22 % decrease
$\alpha$ H-SecE (Chapter 3.2)	Present in the membrane	good	Transient contacts and/or minor clustering	22 % increase	22 % increase
(GSG) <sub>6</sub> -SecE (Chapter 3.2)	Present in the membrane	good	Transient contacts and/or minor clustering	14 % increase	20 % increase

\* not assessed

### 3.3.2 Two-component crowding sensor design development

#### 3.3.2.1 Introduction

Upon the development of the sensor for the interfacial crowding quantification, various designs and membrane-docking approaches were tested. Next to the single-chain constructs encoding the fluorescent moieties and the membrane anchor as one protein (Chapters 3.2 and 3.3.1), we also aimed to apply the sensor to the membrane interface in a flexible modular manner. Here, we proposed a membrane anchor which is able to bind the soluble sensor externally added in the aqueous phase. For that purpose, the SpyTag-SpyCatcher assembly was utilized as it spontaneously forms a covalent isopeptide bond upon mixing two components, SpyTag peptide and SpyCatcher globular domain (Keeble and Howarth, 2019; Zakeri *et al.*, 2012). SpyTag and the binding partner SpyCatcher were initially derived from *Streptococcus pyogenes* fibronectin-binding protein FbaB by splitting its CnaB2 domain into a peptide and the remaining part of the domain combined with rational protein engineering of resulting products. SpyTag is composed of 13 amino acids with the sequence AHIVMVDAYKPTK that can be introduced at either C- or N-terminal ends or within the protein sequence. The reaction with the binding partner SpyCatcher, a small protein of approx. 15 kDa, results in the isopeptide bond formation between aspartic acid of SpyTag and  $\epsilon$ -amino group of lysin from SpyCatcher catalyzed by adjacent glutamic acid. The reaction is robust and may be performed in conventional buffer and a broad pH range, being also compatible with detergents and efficiently working inside of the cytosol of a living cell (Zakeri *et al.*, 2012).

The previously developed FRET-based sensor for quantification of macromolecular crowding in solution (Boersma *et al.*, 2015) was modified by introducing the SpyTag-peptide between the two fluorescent proteins, either instead of the helices or between them, resulting in (GSG)<sub>6</sub>-SpyTag and  $\alpha$ H-SpyTag sensors, respectively (figure 3.13). In its turn, SpyCatcher was fused via flexible (GSG)<sub>6</sub>-linker to a transmembrane anchor consisting of the SecE helical hairpin of the *E. coli* SecYEG translocon (Löwe *et al.*, 2023) resulting in SecE-SpyCatcher membrane anchor.

The modified sensor constructs alone as well as the resulting complexes with SpyCatcher and SecE-SpyCatcher were expressed, purified and characterized on their ability to respond to macromolecular crowding *in vitro*. Additionally, the structures of soluble sensors with and without bound SpyCatcher were analyzed by SAXS.

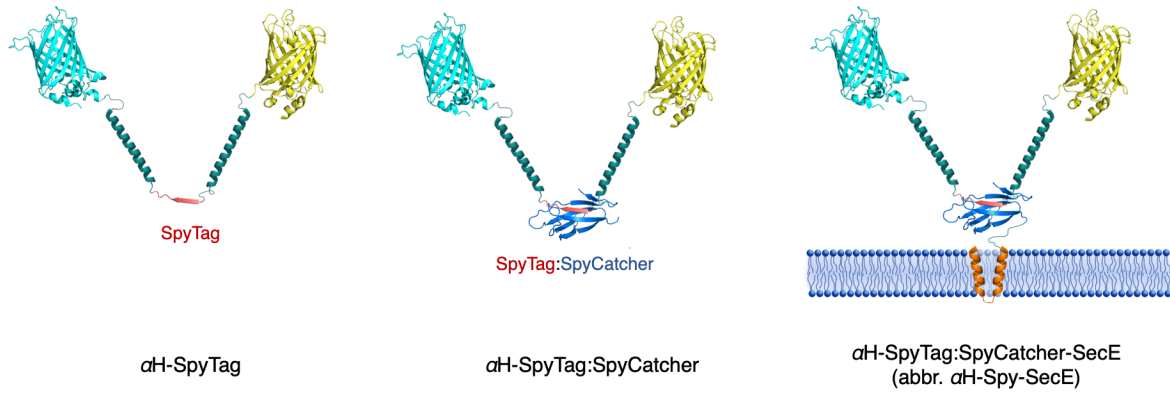


Figure 3.13:  $\alpha$ H-SpyTag FRET-based sensor (left), fused with SpyCatcher (middle) and the design of membrane-anchored sensor with SecE fused to SpyCatcher via GSG-repeats. Protein structures adopted from PDB: mCerulean in cyan (4ENI), mCitrine in yellow (3DPW), SpyTag in red and SpyCatcher in blue (4MLI), SecE (in orange) and the linker helices (green) are free drawn in Pymol and Adobe Photoshop.

### 3.3.2.2 Materials and Methods

#### Expression and purification of SpyTag-sensor constructs

The constructs bearing SpyTag, as well as N-terminal poly-His-tag and 3C cleavage site were cloned into pRSET-A vector and expressed in *E. coli* C41(DE3). The overnight cultures were grown from a single picked colony in 20 mL LB medium (Carl Roth) supplemented with 1% glucose and 100 µg/mL ampicillin at 30°C. The expression of the sensors was performed in 2 L LB-medium (Carl Roth) supplemented with 100 µg/mL ampicillin inoculated with the saturated overnight cultures via dilution 1:100. The cells were grown on 30°C till OD<sub>600</sub> of 0.6 was reached and the expression of the proteins was induced with 0.1 mM IPTG and proceeded overnight at 25°C to achieve proper folding of both mCerulean and mCitrine domains. The cells were harvested at 5000xg for 10 min (SLC-6000 fixed angle rotor, Thermo Fisher/Sorvall), resuspended in 20 mM NaH<sub>2</sub>PO<sub>4</sub>/Na<sub>2</sub>HPO<sub>4</sub> pH 7.4, 100 mM NaCl and 0.1 mM PMSF and lysed by Microfluidizer (M-110P, Microfluidics Corp). Cell debris was removed by subsequent centrifugation at 12000xg for 10 min. The clarified lysate was supplemented with 10 mM imidazole and loaded on the pre-washed Ni<sup>2+</sup>-NTA agarose resin (Qiagen). After 1 h incubation at 4°C the beads were washed with 50 mM NaH<sub>2</sub>PO<sub>4</sub>/Na<sub>2</sub>HPO<sub>4</sub> pH 8.0, 300 mM NaCl, 20 mM imidazole and both types of sensor were then eluted with 50 mM NaH<sub>2</sub>PO<sub>4</sub>/Na<sub>2</sub>HPO<sub>4</sub> pH 8.0, 300 mM NaCl and 250 mM imidazole. The elution fraction was loaded on Superdex 200 Increase 10/300 column (Cytiva) in 10 mM NaH<sub>2</sub>PO<sub>4</sub>/Na<sub>2</sub>HPO<sub>4</sub> pH 7.4. The peak fractions containing the purified sensor were pooled, supplemented with 5% glycerol, aliquoted and stored at -80°C. The purity of the sensors was examined by 15% SDS-PAGE by the in-gel fluorescence followed by Coomassie staining (Quick Coomassie® Stain, SERVA).

#### Expression and purification of SpyCatcher-based constructs

Soluble SpyCatcher was expressed in *E. coli* BL21(DE3) from the plasmid pDEST14 (Addgene). The cultures were grown at 37°C in LB medium (Carl Roth) supplemented with 100 µg/mL ampicillin till OD<sub>600</sub> of 0.6 was reached. The expression was induced by addition of 0.5 mM IPTG and proceeded for 3 h. The cells were harvested at 5000xg for 10 min (SLC-6000 fixed angle rotor, Thermo Fisher/Sorvall) and resuspended in 50 mM Tris/HCl, pH 7.4, 150 mM KCl and 1 mM AEBSF. After cell lysis (Microfluidizer M-110P, Microfluidics Corp) the cell lysate was clarified by centrifugation for 30 min at 23500xg (Rotor 45Ti, Beckman Coulter). Next, the lysate was loaded on the pre-washed Ni<sup>2+</sup>-NTA agarose resin (Qiagen) and incubated on the rolling bench at 4°C for 1 h. The beads were washed with buffer containing 50 mM Tris/HCl, pH 8.0, 150 mM KCl and 10 mM imidazole. SpyCatcher was eluted with 50 mM Tris/HCl, pH 8.0, 150 mM KCl and 300 mM imidazole and loaded on Superdex 200 10/300 column (Cytiva) in 20 mM Tris/HCl, pH 7.4, 150 mM KCl. The peak fraction containing

SpyCatcher was collected, supplemented with 5% glycerol, aliquoted and stored at -80°C. Aliquots from each step of purification were collected and analyzed by 15% SDS-PAGE.

The SecE-SpyCatcher construct, a modified version of SpyCatcher for the membrane anchoring, was cloned via Gibson assembly into pRSET-A vector and was expressed in *E. coli* C43(DE3) strain. The cells were grown in 2L LB medium (Carl Roth) supplemented with 100 µg/mL ampicillin till OD<sub>600</sub> of 0.6 was reached and the expression was induced by addition of 0.1 mM IPTG. The cells were harvested at 5000xg for 10 min (SLC-6000 fixed angle rotor, Thermo Fisher/Sorvall), resuspended in 50 mM HEPES, pH 7.4, 150 mM KCl and 0.2 mM PMSF and lysed by Microfluidizer (M-110P, Microfluidics Corp). The cell debris was removed by centrifugation at 12000xg for 15 min (SS34, Thermo Fisher/Sorvall) and the membranes were collected by subsequent centrifugation at 235000xg for 45 min (45 Ti rotor, Beckman Coulter). The membrane fraction was solubilized in 50 mM HEPES, pH 7.4, 500 mM KCl, 200 µM TCEP, 0.1 mM PMSF and 1% DDM for 1 h at 4°C on the rolling bench. The solubilized material was loaded on the Ni<sup>2+</sup>-NTA-agarose resin (Macherey-Nagel), incubated for 1 hour at 4°C and then washed with 50 mM HEPES, pH 7.4, 150 mM KCl, 200 µM TCEP, 0.1 mM PMSF, 10 mM imidazole and 0.1% DDM. SecE-SpyCatcher was eluted with buffer containing with 50 mM HEPES, pH 7.4, 150 mM KCl, 200 µM TCEP, 0.1 mM PMSF, 300 mM imidazole and 0.1% DDM and then loaded on Superdex 200 10/300 column (Cytiva) in 50 mM HEPES, pH 7.4, 150 mM KCl and 0.05% DDM. The fractions with purified protein were collected, supplemented with 5% glycerol, aliquoted and stored at -80°C.

### **Purification and characterization of monomeric streptavidin**

The pRSET-A plasmid containing encoded monomeric streptavidin (mSA) with N-terminal His<sub>6</sub>-tag and C-terminal FLAG tag (DYDDDDK) was purchased by Addgene (Cat. Nr.: 39860) and transferred into *E. coli* BL21(DE3). The expression and purification of the target protein was done by modified version of previously published protocol (Lim *et al.*, 2011) as follows. The overexpression of the mSA in inclusion bodies was induced with 0.1 mM IPTG at OD<sub>600</sub> of 0.9 and proceeded for 4 h at 37°C in 2 L LB medium (Carl Roth). Cells were harvested as described above and the cell pellet was lysed in B-PER solution (Thermo Fischer Scientific) supplemented with 100 µg/mL lysozyme (Carl Roth) and 20 µg/mL DNase I (Bio-Rad) upon incubation for 15 min and vortexing. The inclusion bodies were pelleted upon centrifugation at 17000xg for 15 min (SS34, Thermo Fisher/Sorvall), the pellet was resuspended in inclusion bodies wash buffer (50 mM Tris/HCl pH 8.0, 100 mM KCl and 0.5% Triton X-100) and vortexed until the suspension became homogeneous. The inclusion bodies were pelleted and the washing procedure was repeated in total for three times. The resulting pellet was solubilized in 6 M guanidine hydrochloride, 50 mM Tris/HCl pH 8.0 and 100 mM KCl. The non-solubilized

portion was pelleted upon centrifugation at 17,000 $\times g$  for 15 min and the supernatant was applied on pre-washed Ni<sup>2+</sup>-NTA-agarose resin (Macherey-Nagel). After 1 h incubation on the rolling bank at room temperature the agarose resin was extensively washed with 6 M guanidine hydrochloride, 50 mM Tris/HCl pH 8.0 and 150 mM KCl and 10 mM imidazole, and mSA was eluted with the buffer supplemented with 300 mM imidazole. The target protein was refolded in PBS under rapid dilution at 4°C, as the denatured mSA was added dropwise to the upper part of the vortex of the stirring buffer. The aggregated material was removed by centrifugation at 46,000 $\times g$  for 20 min (45 Ti rotor, Beckman Coulter). It was not possible to concentrate the mSA using centrifugal filters (Amicon Ultra, Millipore) since the protein aggregated on the membrane. To concentrate the refolded mSA, the protein was loaded again on the PBS pre-washed Ni<sup>2+</sup>-NTA-agarose resin and eluted with buffer supplied with 0.5 M imidazole. The eluate was loaded on the Superdex 200 Increase 10/300 GL column (Cytiva) in 50 mM Tris/HCl pH , pH 7.4 and 150 mM KCl. Peak fractions with the purified protein were pooled, supplemented with 5% glycerol, flash-frozen in liquid nitrogen and stored at -80°C for the further experiments. mSA concentration was determined from the protein absorbance at 280 nm ( $\epsilon_{280} = 38,000 \text{ M}^{-1}\cdot\text{cm}^{-1}$ ). Samples from every purification stage were examined via SDS-PAGE. The activity of the purified mSA was tested with ITC (Microcal ITC-200, GE) upon biotin binding. 10  $\mu\text{M}$  mSA in the sample cell was titrated stepwise with 100  $\mu\text{M}$  biotin stock (Carl Roth) loaded into the injection syringe. The raw data was fitted and the  $K_d$  as well as the other parameters were calculated with the software supplied by manufacturer.

#### **Small angle X-ray scattering (SAXS)**

Measurements were performed in collaboration with Dr. Jens Reiners in the Center for Structural Studies (CSS) in Heinrich Heine University Düsseldorf. “All SAXS data was collected on our Xeuss 2.0 Q-Xoom system from Xenocs, equipped with a PILATUS 3 R 300K detector (Dectris) and a GENIX 3D CU Ultra Low Divergence x-ray beam delivery system. The chosen sample to detector distance for the experiment was 0.55 m, results in an achievable q-range of 0.05 - 6  $\text{nm}^{-1}$ . All measurements were performed at 15°C with a protein concentration range of 3.04 - 7.72 mg/ml. Samples were injected in the Low Noise Flow Cell (Xenocs) via autosampler. For each sample, 18 frames with an exposur time of ten minutes were collected. Data were scaled to absolute intensity against water.

All used programs for data processing were part of the ATSAS Software package (Version 3.0.2) (Manalastas-Cantos *et al.*, 2021). Primary data reduction was performed with the program PRIMUS (Konarev *et al.*, 2003). With the Guinier approximation (Guinier, 1939), we determine the forward scattering  $I(0)$  and the radius of gyration ( $R_g$ ). The program GNOM (Svergun, 1992) was used to estimate the maximum particle dimension ( $D_{max}$ ) with the pair-

distribution function  $p(r)$ . Low resolution *ab initio* models were calculated with GASBOR (Svergun *et al.*, 2001) (P1 symmetry). Superimposing of the predicted model was done with the program SUPCOMB (Kozin and Svergun, 2001).”

### **Liposome preparation**

The lipid stocks solubilized in chloroform (Avanti Polar Lipids, Inc.) were mixed to achieve desired concentrations and the solvent was removed with a rotary evaporator (RV 8, IKA) at 40°C and 200 mbar. The resulting lipid film was rehydrated in 20 mM Tris/HCl, pH 7.4 and 150 mM KCl to achieve the final lipid concentration of 5 mM. The extrusion of lipid vesicles was done using 0.2 µm polycarbonate membranes (Nuclepore, Whatman) with the Mini-Extruder set (Avanti Polar Lipids, Inc.). For the reconstitution of SecE-SpyCatcher anchor or the pre-formed sensor:anchor complexes, DOPC:DOPG (70:30 mol %) liposomes were prepared. In the case of the application of PEG to the surface of the liposomes, mixtures of lipids with varying molar concentrations of PEG 1000 and PEG 2000 (1, 2, 5, 10 mol %) with constant DOPC and DOPG and varying DOPE concentration (according to the amount of the PEGylated lipids, in order to keep the negative charge constant) were produced, whereas the non-crowded liposomes were made of DOPC:DOPG:DOPE (60:30:10 mol %) mixture. For binding mSA to the liposomal surface, 20 mol % 18:1 biotinyl cap PE lipids in combination with DOPC (54 mol %) and DOPG (26 mol %) were used.

### **Extraction of IMVs containing overexpressed SecE-SpyCatcher**

The crude membranes with overexpressed SecE-SpyCatcher construct were applied on the continuous sucrose density gradient (20-70%, w/v) in 20 mM NaH<sub>2</sub>PO<sub>4</sub>/Na<sub>2</sub>HPO<sub>4</sub> pH 7.4 and 100 mM NaCl (Gradient Station, BioComp) and centrifuged for 16h at 30,000 rpm (SW 40Ti swinging-bucket rotor, Beckman Coulter). After centrifugation, the gradient was fractionated (Gradient Station, BioComp) and the protein content of each fraction was analyzed via SDS-PAGE. Fractions containing IMVs were pooled together, diluted at least five-fold with 10 mM NaH<sub>2</sub>PO<sub>4</sub>/Na<sub>2</sub>HPO<sub>4</sub> and 50 mM NaCl and centrifuged at 235000xg for 40 min at 4°C (45 Ti rotor, Beckman Coulter). The pelleted IMVs were resuspended in 200 µL fresh buffer (10 mM NaH<sub>2</sub>PO<sub>4</sub>/Na<sub>2</sub>HPO<sub>4</sub>, 50 mM NaCl, EDTA-free inhibitors, 5% glycerol), aliquoted and stored at -80°C until further analysis.

To quantify the protein content of the extracted IMVs, the samples were diluted 1:2 and 1:10 with buffer containing 1 % DDM to the total volume of 10 µL and loaded into the 96-well plate together with serial dilutions of BSA standard (Pierce™ BSA, 2 mg/mL, Thermo Fischer Scientific) supplemented with DDM. The samples were mixed with 150 µL of Pierce™ 660 nm Protein Assay reagent (Thermo Fischer Scientific). After 5 min incubation at room temperature the absorbance of the standards and the diluted samples was measured at 655 nm with iMark Microplate Absorbance Reader (Bio-Rad) and the total protein content was quantified.

### **Binding of the soluble sensor constructs to liposomes and IMVs**

To test binding of the soluble sensor constructs to liposomes, SecE-SpyCatcher was reconstituted into DOPC:DOPG (70:30 mol %) liposomes, as described above, at P/L ratio of 1:3,000. Resulted proteoliposomes were incubated overnight at 4°C with two-fold lower molar amount of the SpyTag-sensors, ensuring an excess of reconstituted SecE-SpyCatcher.

In the case of IMVs with overexpressed SecE-SpyCatcher, 10 µl of extracted IMVs were mixed with 0.2, 0.5, 1 and 5 µL of 15,5 µM of  $\alpha$ H-SpyTag or 17,1 µM (GSG)<sub>6</sub>-SpyTag sensors and the samples were incubated overnight at 4°C. The binding of the sensor to proteoliposomes and IMVs was analyzed with SDS-PAGE. Afterwards the emission spectra of the IMVs-bound sensor samples were recorded as described in Chapter 3.2.

### 3.3.2.3 Results

#### A. Purification and assembly of the sensor components

The SpyTag-modified soluble sensors were overexpressed with high yields, purified with IMAC and analyzed with size exclusion chromatography (figure 3.14). The elution volumes for  $\alpha$ H-SpyTag and (GSG)<sub>6</sub>-SpyTag modified sensors were 11.7 mL and 12.8 mL, respectively. As this was the case for SecE-containing sensors (Chapter 3.2), the elution for the SpyTag-modified soluble sensors was surprisingly fast for the proteins with the theoretical mass of 65.9 kDa for  $\alpha$ H-SpyTag and 58.4 kDa for (GSG)<sub>6</sub>-SpyTag. For the sensor constructs with the fused transmembrane domain this fast migration could be potentially explained by the presence of the DDM micelle around the hydrophobic section (Löwe *et al.*, 2023). For the soluble sensors, this unusual migration can be the consequence of the protein conformation and/or oligomerization at high protein concentrations, as was shown in the analysis with SEC-MALS dependent (Suppl. Information, figure 3, Chapter 3.2, Löwe *et al.*, 2023). Also, the migration of the sensors on SDS-PAGE was observed to be faster than expected from the theoretical protein mass. Upon heating at 95°C for 5-10 min the proteins were fully denaturated, lost their fluorescence and migrated on expected mass levels.

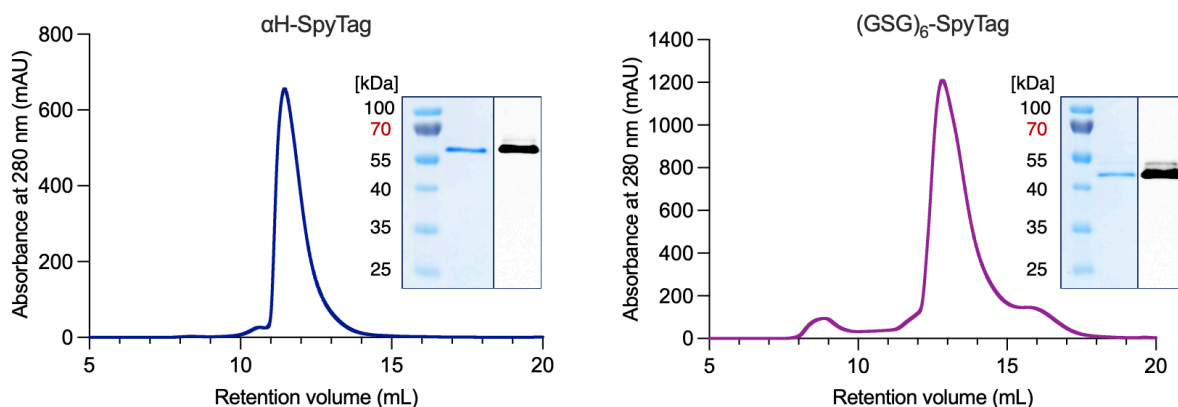


Figure 3.14: Size exclusion profiles of purified  $\alpha$ H-SpyTag and (GSG)<sub>6</sub>-SpyTag sensor constructs and corresponding SDS-PAGE analysis of collected peak fractions with recorded in gel-fluorescence and stained in Coomassie.

In the first step, the soluble SpyCatcher domain was used for the evaluation of the binding to the soluble SpyTag-sensor constructs. The domain was purified with IMAC from the cleared lysate (figure 3.15-A) and applied on size exclusion chromatography (Superdex 200 Increase 10/300 GL, Cytiva), where it eluted at 17.36 mL, in agreement with the calculated mass of 15.4 kDa (figure 3.15-B). For membrane anchoring, SpyCatcher was fused via flexible (GSG)<sub>6</sub>-linker to the helical hairpin consisting of TMHs 1 and 2 of the SecE subunit from SecYEG translocon, that was previously utilized in  $\alpha$ H-SecE and (GSG)<sub>6</sub>-SecE sensors (Chapter 3.2). Anchored in the membrane bilayer, SpyCatcher-SecE may serve for covalent attachment of

SpyTag-modified sensors (figure 3.13). The SecE-SpyCatcher with encoded His<sub>8</sub>-tag on the C-terminal side was purified from the extracted membranes. For this, the membranes were solubilized with 1% DDM and the target protein construct was purified with IMAC and SEC. On SDS-PAGE the protein appeared as a single band matching its calculated mass of 22 kDa (figure 3.16-A). The purified anchor was reconstituted into liposomes consisting of 18:1 biotinyl cap PE, DOPC and DOPG mixture (20:54:26 mol %) and the reconstitution efficiency was tested with the flotation assay (Chapter 3.2). The SecE-SpyCatcher was found in the top fraction validating the efficient reconstitution, as required for the docking of SpyTag-modified sensors (figure 3.16-B).

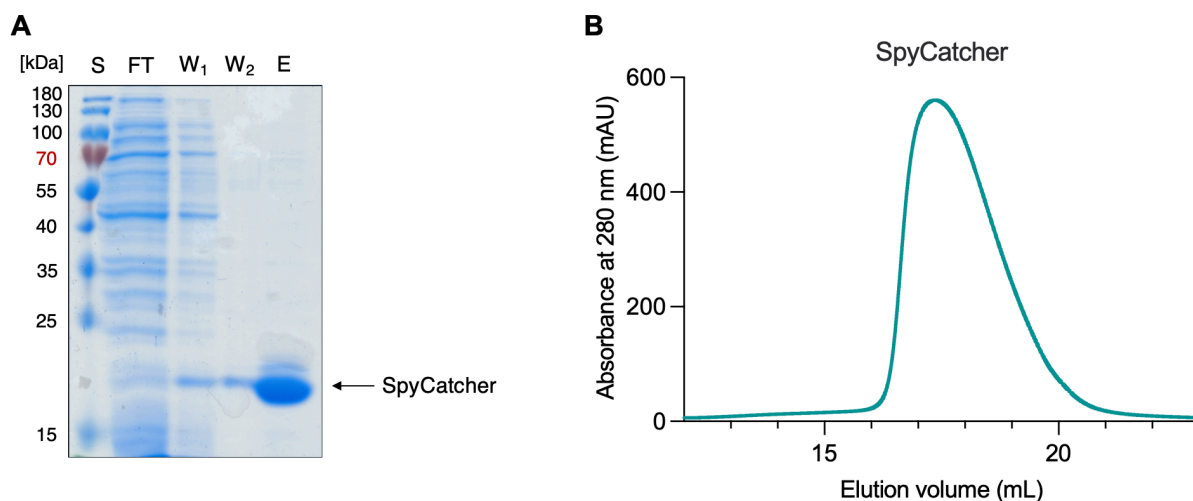


Figure 3.15: SDS-PAGE analysis of the Ni-NTA purification, where FT represents the flow through fraction after binding to Ni<sup>2+</sup>-NTA resin, W<sub>1</sub> and W<sub>2</sub> are the collected samples from resin wash, E is the elution fraction with SpyCatcher protein (A) and subsequent size exclusion chromatography of SpyCatcher (B).

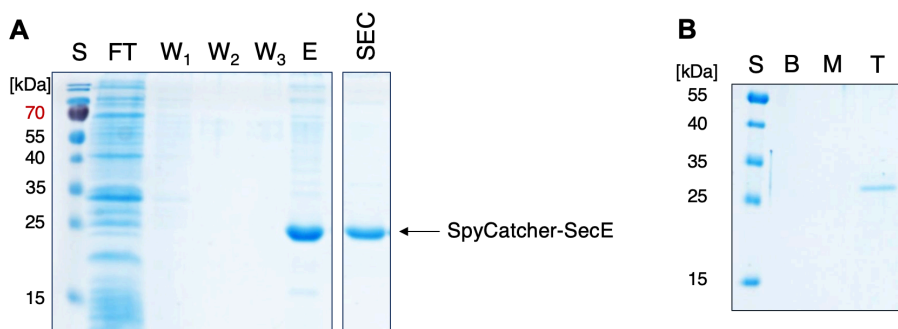


Figure 3.16: (A) Purification of SecE-SpyCatcher, where FT represents the collected flow through fraction after binding to Ni<sup>2+</sup>-NTA resin, W<sub>1</sub>, W<sub>2</sub>, and W<sub>3</sub> are the collected samples from resin wash, E is the elution fraction with target protein and SEC represents the pooled peak fractions after size exclusion chromatography. (B) Flotation assay of reconstituted SecE-SpyCatcher in liposomes with 20 mol % biotinyl cap PE with collected bottom (B), middle (M) and top (T) fractions.

Binding of SpyTag-modified sensors with the purified SpyCatcher and SecE-SpyCatcher were tested. The proteins were mixed and incubated for at least one hour at room temperature. The mixtures were applied on the SEC and the distinct fractions were collected and analyzed via SDS-PAGE (figures 5 and 6). Addition of SpyCatcher to either  $\alpha$ H-SpyTag or (GSG)<sub>6</sub>-SpyTag sensors should result in the mass changes due to formation of complexes referred as  $\alpha$ H-SpyTag:SC and (GSG)<sub>6</sub>-SpyTag:SC with calculated masses of 82.2 kDa and 73.8 kDa, respectively. SEC elution peaks showed a shift by approx. 0.5 mL towards higher molecular weight species for both sensor types when bound to SpyCatcher: 11.15 mL for  $\alpha$ H-SpyTag:SC and 12.43 mL for (GSG)<sub>6</sub>-SpyTag:SC (figures 3.17-A and 3.18-A). Free SpyCatcher added in excess to ensure the complete binding to the soluble sensor constructs eluted in both cases at around 17 mL. SDS-PAGE analysis of the collected peak fractions confirmed the complex formation between two proteins, as a new band of higher molecular mass was observed in each reaction (figures 3.17-B and 3.18-B).

Same behavior was observed for the complexes formed from mixtures of the SecE-SpyCatcher with corresponding SpyTag-modified sensors resulted in formation of complexes referred as  $\alpha$ H-Spy-SecE or (GSG)<sub>6</sub>-Spy-SecE with calculated masses of 88.7 kDa and 81.2 kDa respectively. The reaction was performed with excess of the sensor molecules to achieve better separation on SEC. As expected, two peaks appeared in the chromatograms (shown in red), and the peak fractions of these particular SEC runs were additionally analyzed via SDS-PAGE (data not shown) to identify the proteins. The  $\alpha$ H-Spy-SecE complex and free  $\alpha$ H-SpyTag eluted at 10.53 mL and 12.48 mL, whereas the (GSG)<sub>6</sub>-Spy-SecE and free (GSG)<sub>6</sub>-SpyTag eluted at 11.19 mL and 14.01 mL, respectively. Independent SEC runs with same complex formations were highly reproducible, as characterized before (Samet Kurt, Bachelor thesis 2019, Appendix, Supervised student projects)

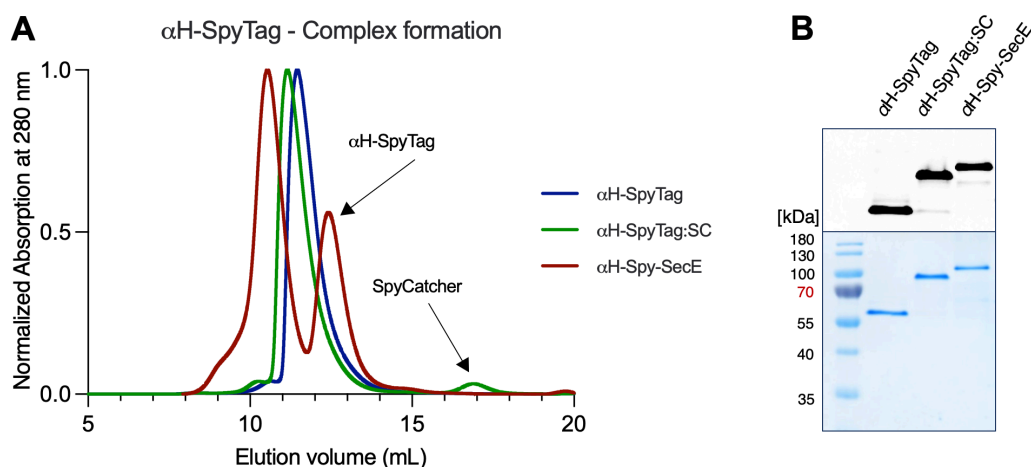


Figure 3.17: (A) Size exclusion chromatography of  $\alpha$ H-SpyTag alone (blue) or coupled with either SpyCatcher (green) or SecE-SpyCatcher (red). (B) Resulting complexes  $\alpha$ H-SpyTag:SC and  $\alpha$ H-Spy-SecE, as well as free  $\alpha$ H-SpyTag were analyzed via SDS-PAGE.

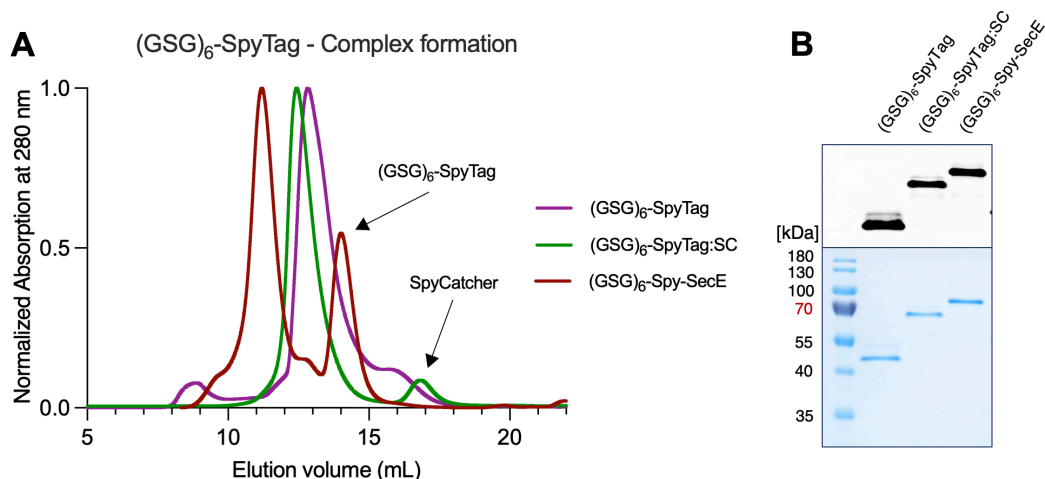


Figure 3.18: (A) Size exclusion chromatography of the reaction mixes of  $(\text{GSG})_6\text{-SpyTag}$  with either SpyCatcher or SecE-SpyCatcher. (B) Resulting complexes  $(\text{GSG})_6\text{-SpyTag:SC}$  and  $(\text{GSG})_6\text{-Spy-SecE}$  as well as free  $(\text{GSG})_6\text{-SpyTag}$  were analyzed with SDS-PAGE.

Notably, the elution volume of free  $\alpha\text{H-Spy-SecE}$  and  $(\text{GSG})_6\text{-Spy-SecE}$  on the size exclusion column shifts in concentration-dependent manner, as was previously shown via SEC-MALS (Suppl. Information, figure 3, Chapter 3.2, Löwe *et al.*, 2023). For the size exclusion chromatography (figure 3.17-A and 3.18-A) of pre-formed  $\alpha\text{H-Spy-SecE}$  or  $(\text{GSG})_6\text{-Spy-SecE}$  complexes (in red) a low concentration of reactants was used because of lower yield of SecE-SpyCatcher purified from the crude membranes in comparison to the soluble sensor (in blue and lilac), which explains the shift of the unbound sensor towards low molecular weight elution.

### B. Structural analysis of the sensor with and without SpyCatcher

Free and SpyCatcher-bound sensors were further characterized via small-angle X-ray scattering (SAXS). Obtained peak fractions from SEC were collected and the structure of the soluble constructs were subject to SAXS analysis (figure 3.19). The molecular masses determined from the forward scattering  $I(0)$  were slightly higher than the theoretical masses of 69.2 kDa for  $\alpha\text{H-SpyTag}$  and 63.7 kDa for  $(\text{GSG})_6\text{-SpyTag}$ . This may be a consequence of the partial oligomerization of the sensors at elevated protein concentrations of  $\approx 6$  g/L employed in the SAXS measurements. Upon SpyCatcher binding the estimated  $D_{max}$  increased from 21.25 to 23.56 nm for  $\alpha\text{H-SpyTag}$  and from 15.75 to 19.05 nm for  $(\text{GSG})_6\text{-SpyTag}$  sensors. Additionally, structural models obtained from these measurements indicated the change of the sensor conformation upon SpyCatcher binding, from an elongated to V-shaped configuration (figure 3.19). The molecular masses of the SpyCatcher-bound sensors determined in SAXS were higher than the theoretical masses of the complexes and were measured in the independent experiments to be identical for both types of the sensor constructs with 96.9 kDa. There is a chance that the presence of bound SpyCatcher and the high concentrations of the complexes used in this experiment ( $\approx 4$  g/L) led to a partial di- or oligomerization of the proteins,

as was described above, and requires further investigation. However, high protein concentrations in SAXS greatly exceed those employed in the spectroscopic measurements, and therefore the likelihood that the oligomerization of soluble constructs significantly influences the results is low.

The solubilized  $\alpha$ H-Spy-SecE or (GSG)<sub>6</sub>-Spy-SecE complexes were not subjected for SAXS measurement due to the presence of DDM micelles in the buffer, which would interfere in the measurement setup and affect the evaluation.

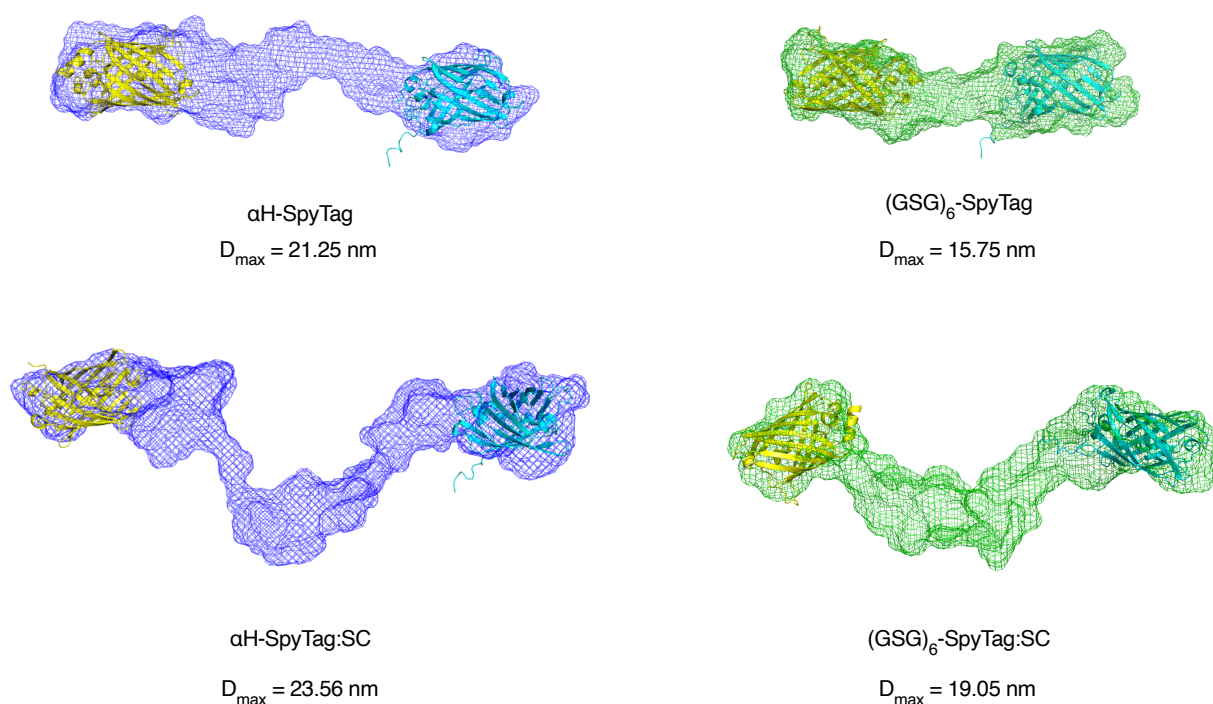


Figure 3.19.: Results of the SAXS analysis of  $\alpha$ H-SpyTag (purple) and (GSG)<sub>6</sub>-SpyTag (green) in their free and SpyCatcher-bound states. The structure model obtained on SAXS are superimposed with the protein structures of mCerulean in cyan (PDB: 4ENI), mCitrine in yellow (PDB: 3DPW) with PyMOL.

### C. Sensitivity of the SpyTag-sensors in crowded solutions

#### Soluble sensors

As the initial test for the sensor dynamics, the response of the soluble sensors to macromolecular crowding in solutions were tested. Steric confinement provided by the crowders changes the sensor conformation bringing the fluorescent proteins closer to each other, which can be quantified by changes in FRET. The ratio of corresponding fluorescence intensities of acceptor (mCitrine, 525 nm) and donor (mCerulean, 475 nm) were used to calculate the FRET efficiency, further termed as  $F_A/F_D$  ratio. The performance of the FRET-

sensor derivatives containing SpyTag sequence was systematically analyzed in solution in the presence of PEG 2000 and 6000 in the range of 0-40% (w/v). Compression of the sensor was observed by monitoring the changes in acceptor fluorescence, as increasing the crowder fraction in the solution led to increasing  $F_A/F_D$  ratios. In the absence of the crowders the acceptor/donor ratio was  $0.80 \pm 0.01$  and  $1.73 \pm 0.02$  for  $\alpha$ H-SpyTag and (GSG)<sub>6</sub>-SpyTag, respectively, whereas in the 40 % PEG 6000 the  $F_A/F_D$  ratio shifted to  $1.35 \pm 0.01$  for  $\alpha$ H-SpyTag (68% increase) and to  $2.17 \pm 0.01$  for (GSG)<sub>6</sub>-SpyTag sensor (26 % increase). Moreover, sensors were also responsive to crowders of different size. The  $F_A/F_D$  ratio was measured smaller in the same setup when using PEG 2000:  $1.16 \pm 0.02$  for  $\alpha$ H-SpyTag (46% increase) and  $1.914 \pm 0.005$  (GSG)<sub>6</sub>-SpyTag sensors (11% increase), as shown in figure 3.20.

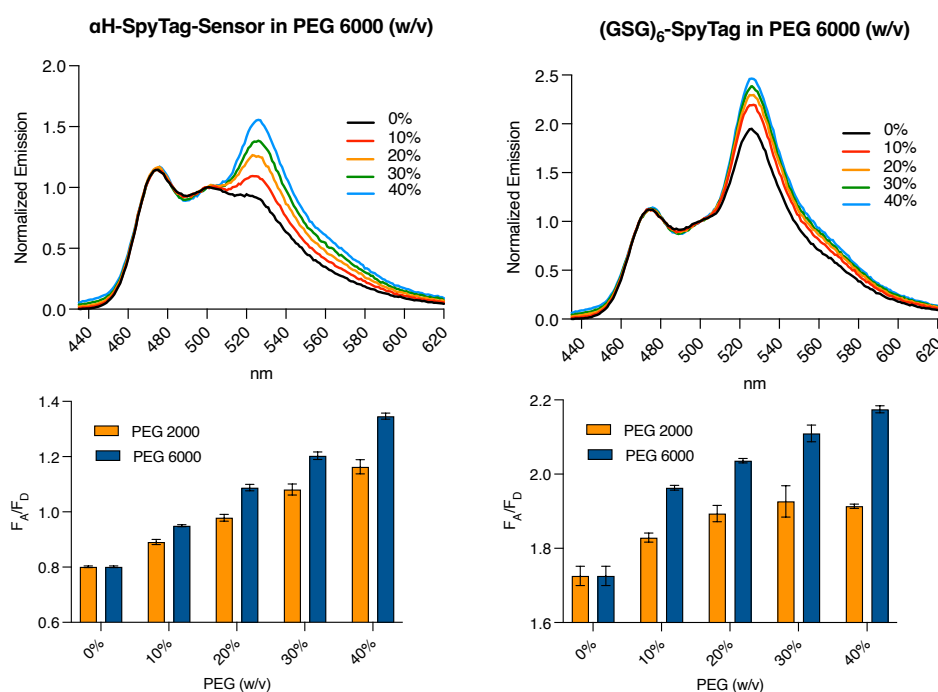


Figure 3.20: Performance of the  $\alpha$ H-SpyTag and (GSG)<sub>6</sub>-SpyTag in PEG 2000 and PEG 6000 solutions. Upper graphs: FRET sensor emission spectra recorded by increasing crowder concentrations. Acceptor fluorescence increases with the increasing PEG 6000 (w/v) concentration. Lower Graphs: calculated acceptor/donor ratios ( $F_A/F_D$ , 525nm/475 nm) of soluble FRET sensors in presence of PEG 2000 and 6000.

### SpyTag-sensors bound to SpyCatcher

Next, the ability of the soluble sensors with the covalently bound SpyCatcher to respond to macromolecular crowding changes in solution was examined. As described above, the soluble SpyTag-based sensors were incubated with SpyCatcher to allow a covalent bond formation between them. The isolated soluble complexes showed a slight decrease their  $F_A/F_D$  ratios

compared to the free SpyTag-modified sensors:  $0.76 \pm 0.01$  for the  $\alpha$ H-SpyTag:SC construct (decrease of 5%) and  $1.15 \pm 0.03$  for the  $(\text{GSG})_6$ -SpyTag:SC sensor (decrease of 33%) indicating wider distance between the fluorescent proteins. The structural data obtained with SAXS may explain the significant change in acceptor/donor ratios of  $(\text{GSG})_6$ -SpyTag and the less pronounced effect for  $\alpha$ H-SpyTag upon SpyCatcher binding. Whereas the helices in the linker of  $\alpha$ H-SpyTag sensor contribute to increased spacing between the fluorescent proteins of the FRET pair, the flexible linker in the  $(\text{GSG})_6$ -SpyTag construct allows mCitrine and mCerulean to come closer to each other (Liu *et al.*, 2017; Löwe *et al.*, 2023). The covalent attachment of SpyCatcher, the protein of approx. 15 kDa, between the fluorescent proteins introduces a steric hindrance which results in a larger distance and the lower  $F_A/F_D$  ratio.

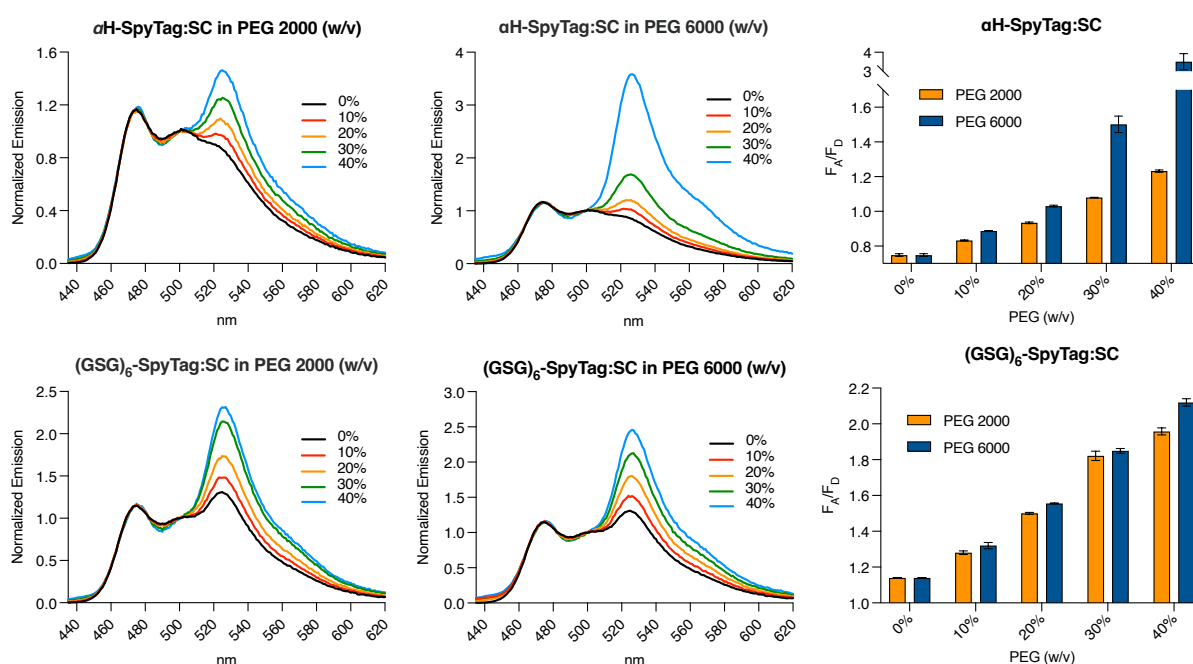
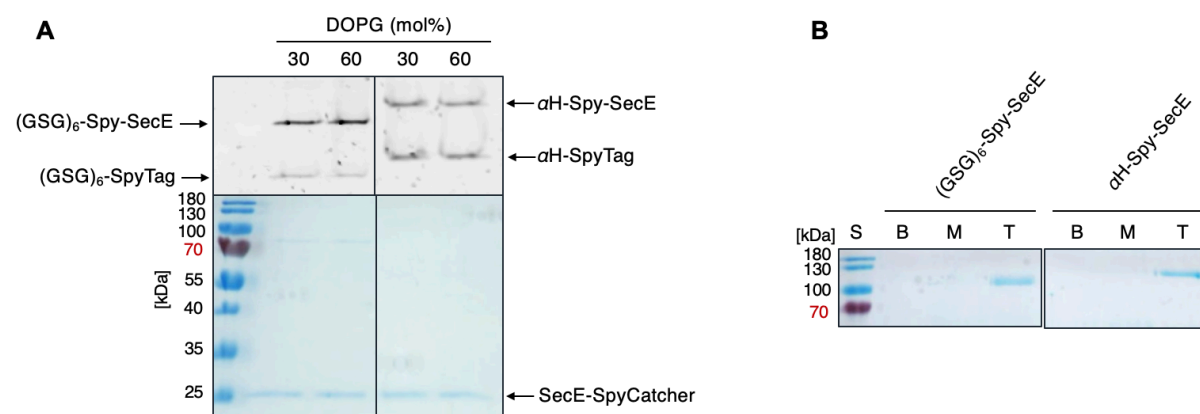


Figure 3.21: Emission spectra of the complexes  $\alpha$ H-SpyTag:SC and  $(\text{GSG})_6$ -SpyTag:SC in PEG 2000 and PEG 6000 solutions recorded by increasing concentrations of PEG 2000 and PEG 6000 and corresponding bulk diagrams with calculated acceptor/donor ratios ( $F_A/F_D$ , 525nm/475 nm).

The resulting complexes were tested on their ability to sense the macromolecular crowding simulated with PEG 2000 and PEG 6000, as in the previous experiment (figure 3.21). Surprisingly, the  $(\text{GSG})_6$ -SpyTag:SC sensor showed lower sensitivity upon crowder size change in this experiment: At 40 % (w/v) PEG 2000 and PEG 6000 the  $F_A/F_D$  ratios were calculated to be  $1.96 \pm 0.02$  (increase of 70 %) and  $2.12 \pm 0.02$  (increase of 84 %), whereas the acceptor/donor ratios of  $\alpha$ H-SpyTag:SC increased by 62 % for PEG 2000 ( $1.23 \pm 0.01$ ) and more than four-fold ( $3.29 \pm 0.21$ , increase of 334 %) in presence of 40 % (w/v) PEG 6000.

### **SpyTag-sensors bound to SecE-SpyCatcher**

The assembly of the soluble SpyTag-sensor with SecE-SpyCatcher was tested on the liposomes. SecE-SpyCatcher serving as an anchor was reconstituted with P/L ratio of 1:3,000 into liposomes consisting of DOPC:DOPG lipids with varying DOPG content, either 10, 30 or 60 mol %. The reconstitution for 10 mol % DOPG was not successful as was analyzed by SDS-PAGE: The protein was present in the liposomes in a very small amount in comparison to other samples and was not used for binding experiment. The soluble sensor was added to the proteoliposomes in approx. ten-fold lower concentration than SecE-SpyCatcher. The binding proceeded overnight on the rolling bench and the complex formation was analyzed via SDS-PAGE (figure 3.22-A). Appearance of a distinct high molecular weight band for each sample indicated the complex formation. However, a fraction of the unbound sensor was still detectable despite the excess of the SecE-SpyCatcher. No significant differences in the binding efficiency was observed by different DOPG concentrations: The increased abundance of negative charges on the liposomal surface with 60 mol % DOPG had no effect on the sensor binding.



*Figure 3.22: (A) Binding of the soluble  $\alpha$ H-SpyTag and (GSG)<sub>6</sub>-SpyTag to SecE-SpyCatcher reconstituted into the model membranes with different DOPG content (either 30 mol % or 60 mol %). The bound and unbound fractions of the sensors are visualized by in-gel fluorescence. (B) Determination of the reconstitution efficiency of the pre-formed  $\alpha$ H-SpyTag-SecE and (GSG)<sub>6</sub>-SpyTag-SecE complexes via flotation assay. The collected fractions: bottom (B), middle (M) and top (T).*

In order to ensure the accuracy of the measurement and to prevent the influence of the free-floating sensor,  $\alpha$ H-SpyTag and (GSG)<sub>6</sub>-SpyTag were first incubated with the detergent-solubilized SecE-SpyCatcher and the resulting  $\alpha$ H-Spy-SecE and (GSG)<sub>6</sub>-Spy-SecE sensors were then purified via SEC. The isolated complexes were subsequently reconstituted into liposomes made of DOPC/DOPG (70:30 mol %) with the identical protocol used in the Chapter 3.2. The reconstitution efficiency of the crowding sensors was examined with flotation assay (figure 3.22-B), as was described above. The protein constructs were found in the top fractions

denoting the efficient insertion of  $\alpha$ H-Spy-SecE and (GSG)<sub>6</sub>-Spy-SecE into the vesicles. Upon reconstitution, the acceptor/donor ratio increased for both sensor types:  $1.12 \pm 0.01$  for  $\alpha$ H-Spy-SecE (increase of 47 %) and  $1.87 \pm 0.01$  for (GSG)<sub>6</sub>-Spy-SecE (increase of 63 %) in comparison to the soluble sensor constructs bound to SpyCatcher (figure 3.23). This can be a result of two factors: Firstly, reduced degree of freedom of the sensor linker arms and as a consequence changed sensor conformation on the membrane, which results in the decreased distance between the fluorophores, and secondly, due to the partial clustering and random contacts of the sensor in the membrane.

The membrane reconstituted sensors showed response to crowding in the solution induced by PEGs (figure 3.23).  $F_A/F_D$  ratios for  $\alpha$ H-Spy-SecE at 40 % (w/v) PEG 6000 increased to  $3.72 \pm 0.06$  (increase of 128%) and at 30 % PEG 2000 to  $2.90 \pm 0.05$  (increase of 160%), but suddenly dropped to  $1.59 \pm 0.08$  at 40 % PEG 2000. Similar response upon crowding in solution was observed for the reconstituted (GSG)<sub>6</sub>-Spy-SecE sensor: In presence of 40% PEG 6000 the  $F_A/F_D$  ratio reached  $4.26 \pm 0.06$  (increase of 128%) and  $3.42 \pm 0.03$  in 30 % PEG 2000 3 (increase of 83 %), followed by a sudden drop to  $1.61 \pm 0.07$  at 40 % PEG 2000. Notably, the net FRET efficiency of  $\alpha$ H-Spy-SecE construct was higher with the increasing PEG 6000 concentrations in comparison to (GSG)<sub>6</sub>-Spy-SecE sensor. Probably, the presence of two  $\alpha$ -helices in the linker region led to the improvement of sensors conformational dynamics and higher sensitivity of the reconstituted  $\alpha$ H-Spy-SecE construct.

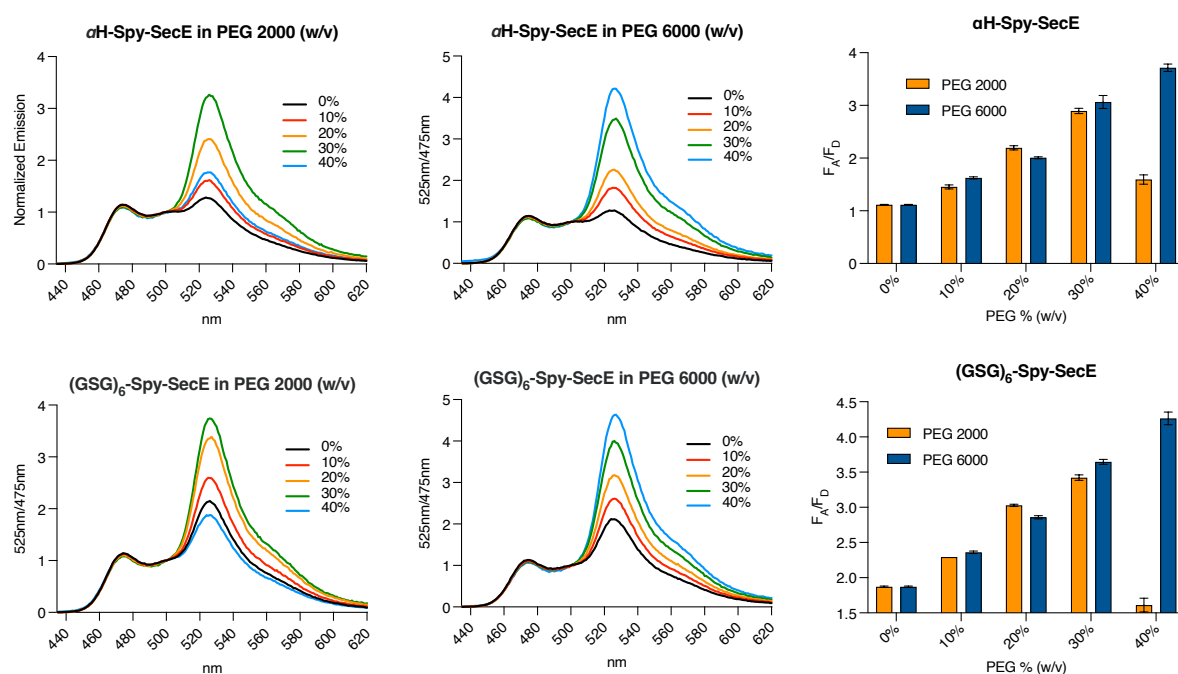


Figure 3.23: Sensitivity of the reconstituted  $\alpha$ H-Spy-SecE and (GSG)<sub>6</sub>-Spy-SecE sensor constructs in solutions with increasing PEG 2000 and PEG 6000 concentrations with corresponding bulk diagrams with calculated  $F_A/F_D$  ratios.

#### D. Crowding at the membrane interfaces with synthetic and proteinaceous crowders

The response of the membrane-reconstituted  $\alpha$ H-Spy-SecE and (GSG)<sub>6</sub>-Spy-SecE sensors to synthetic and proteinaceous crowders at the interface was characterized. Crowding on the liposomal surface was rendered and controlled by varying the molar fraction of PEGylated lipids (1, 2, 5 and 10 mol %). With the increasing abundance of PEG 1000 and PEG 2000 the lateral pressure on the surface increases thus leading to the compression of the membrane-anchored sensors (figure 3.24).

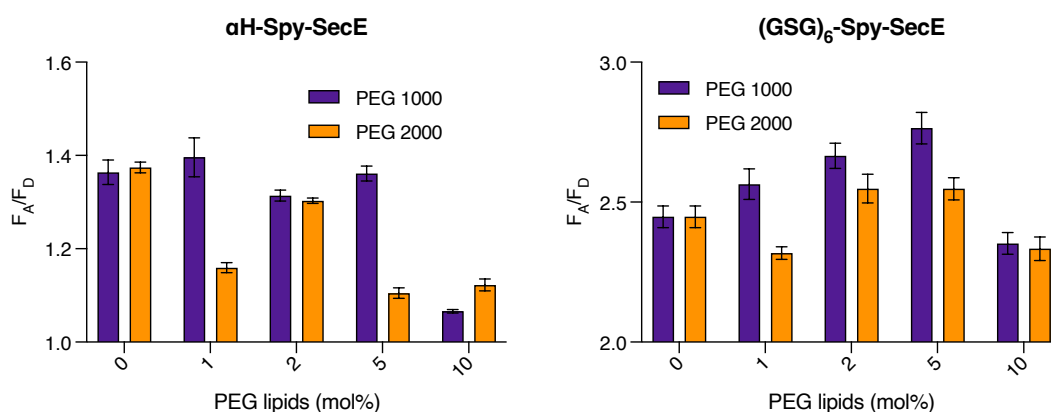


Figure 3.24: Sensitivity of the reconstituted  $\alpha$ H-Spy-SecE and (GSG)<sub>6</sub>-Spy-SecE sensor constructs in the model membranes with different concentrations (0, 1, 2, 5 or 10 mol %) of either PEG 1000 or PEG 2000 conjugated lipids.

Upon reconstitution of  $\alpha$ H-Spy-SecE and (GSG)<sub>6</sub>-Spy-SecE complexes into PEG-free liposomes DOPC:DOPG:DOPE (60:30:10 mol %), the resulting  $F_A/F_D$  ratios were  $1.36 \pm 0.02$  and  $2.45 \pm 0.03$ , respectively. The values were higher than in previous reconstitution using DOPC:DOPG liposomes, indicating that the sensor may undergo clustering during reconstitution. The  $\alpha$ H-Spy-SecE showed no response to the crowding on the surface induced by PEGylated lipids. Only for the (GSG)<sub>6</sub>-Spy-SecE a weak trend for both crowder types could be observed: Here, the increase of the  $F_A/F_D$  ratios was estimated to be 5%, 9% and 13% for the 1, 2 and 5 mol % of PEG 1000 PE compared to the non-crowded sample. However, this trend was not reproduced in presence of PEG 2000 PE resulting in the decrease of the  $F_A/F_D$  ratio of the sensors at 1 mol % of PEGylated lipids and a slight increase of 4 % for 2 mol % and 5 mol % PEG 2000 PE. Moreover, in presence of 10 mol % of PEGylated lipids, the  $F_A/F_D$  ratios substantially decreased for both sensors.

Inert in their nature, synthetic crowders cannot represent the natural complexity of biomacromolecules, but can be applied for the simulation of the excluded volume effect. Unlike synthetic ones, protein-based crowders allow for a native-like simulation of the crowding effects on the membrane interfaces. One of the tested candidates was a monomeric mutant of

streptavidin, mSA. Binding of the purified mSA to biotin was initially tested with ITC (figure 13). The quantified  $K_D$  of mSA:biotin interaction was 10 nM with number of binding sites  $n=0.822$ , which was comparable with previously published data measured with fluorescence polarization spectroscopy ( $K_D = 2.8$  nM) (Lim *et al.*, 2013).

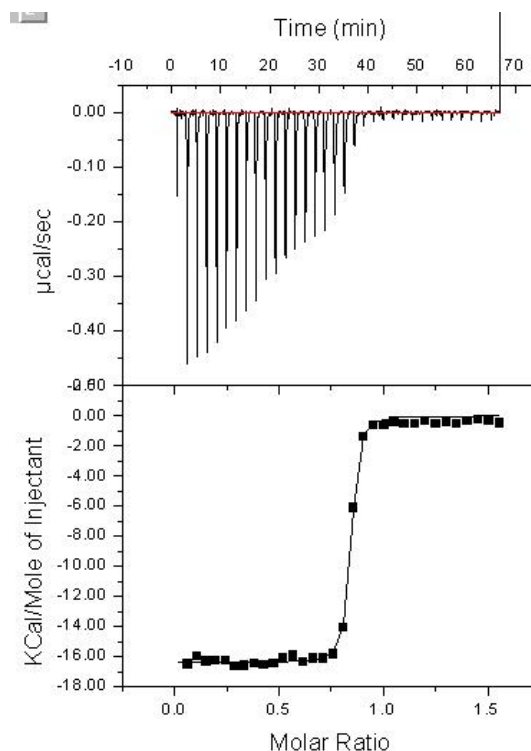


Figure 3.25: Binding of purified mSA to biotin analyzed with ITC.

Binding of the soluble SpyTag-sensors to the membrane-reconstituted SecE-SpyCatcher was tested on the liposomes containing 20 mol % biotinyl cap PE lipids. Formation of the Spy-complex between two proteins occurred with a limited efficiency, as it was already shown for DOPC:DOPG liposomes, as fractions of soluble  $(GSG)_6$ -SpyTag and  $\alpha$ H-SpyTag sensors were present after incubation (figure 3.26). Due to the incomplete binding, the pre-formed complexes  $\alpha$ H-Spy-SecE and  $(GSG)_6$ -Spy-SecE were reconstituted into the liposomes. Upon reconstitution of the sensor, the  $F_A/F_D$  ratio was  $1.13 \pm 0.01$  for  $\alpha$ H-Spy-SecE, being comparable to previous reconstitution into DOPC:DOPG with  $1.12 \pm 0.01$ , whereas the  $(GSG)_6$ -Spy-SecE sensor constructs have shown a decrease in the initial  $F_A/F_D$  ratio: From  $1.87 \pm 0.01$  in DOPC:DOPG to  $1.30 \pm 0.01$  in the liposomes with 20 mol % 18:1 biotinyl cap PE. Both types of proteoliposomes were titrated then with mSA protein to achieve saturation of the surface-exposed biotin groups.  $F_A/F_D$  ratios were increasing with the increasing mSA concentration reaching  $1.24 \pm 0.01$  for the  $\alpha$ H-Spy-SecE (increase of 10 %) and  $1.37 \pm 0.01$  for  $(GSG)_6$ -Spy-SecE (increase of 6 %) (figure 3.27)

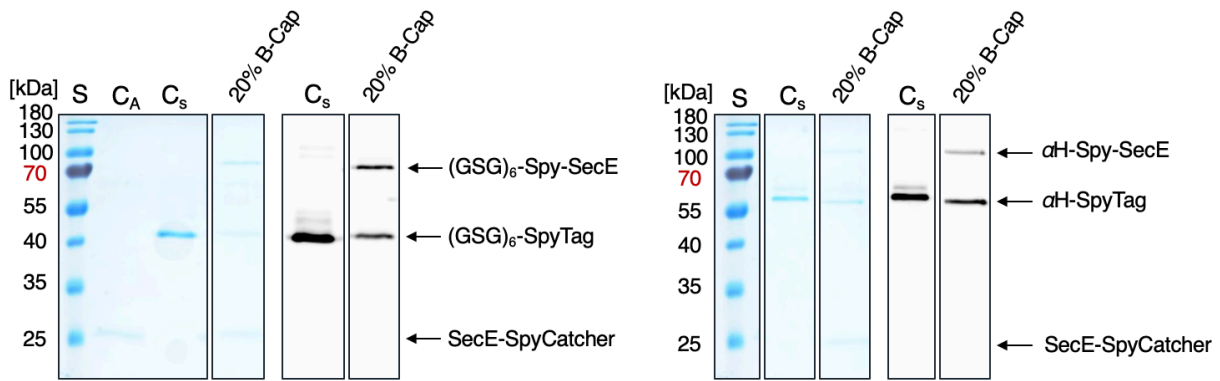


Figure 3.26: Binding of soluble  $(GSG)_6$ -SpyTag (left) and  $\alpha H$ -SpyTag (right) to the reconstituted membrane anchor SecE-SpyCatcher incorporated into liposomes containing 20% biotinyl cap PE lipids in DOPC:DOPG background.

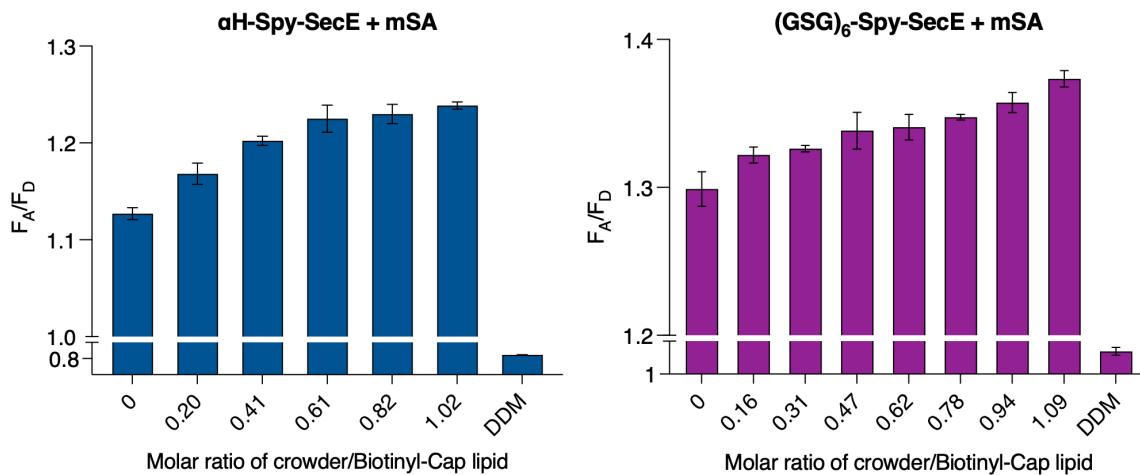


Figure 3.27: Response of  $\alpha H$ -Spy-SecE (left) and  $(GSG)_6$ -Spy-SecE (right) sensor reconstituted into liposomes containing 20 mol % biotinyl cap PE lipids upon interfacial crowding mimicked by mSA.

### E. Binding of the SpyTag-sensors to SecE-SpyCatcher in IMVs

Binding of the soluble SpyTag-modified sensors to the reconstituted SecE-SpyCatcher anchor in the synthetic liposomes was only partially successful since not all soluble counterparts formed the complex. To test binding of the soluble sensors to the physiologically relevant samples, the inner membrane vesicles (IMVs) with overexpressed SpyCatcher were isolated from the crude membranes using continuous sucrose density gradient (20-70 % w/v). The gradient was collected and a recorded profile with absorbance at 280 nm is shown in figure 3.28. In the eleven fractions of gradient the separation of ribosomes (fractions 2-5), inner membranes (fractions 6-8) and outer membranes (fractions 8-10) are visualized.

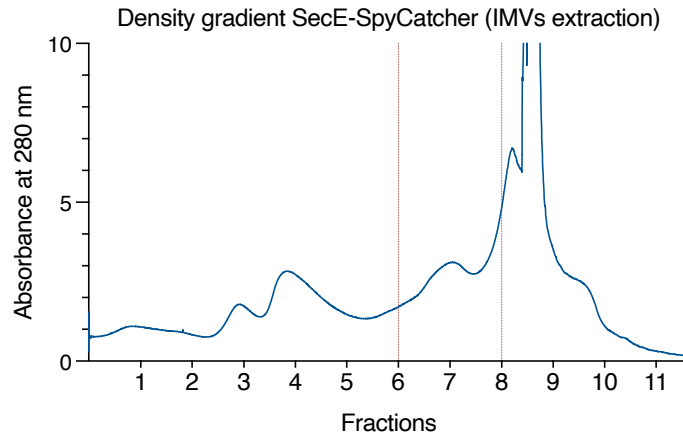


Figure 3.28: Sucrose density gradients (20-70%) profile performed with extracted bacterial crude membranes for the isolation of the IMVs with membrane-incorporated SecE-SpyCatcher construct. Fractions 6-8 (highlighted in red) containing the IMVs were collected for further experiments.

The fractions containing IMVs (highlighted in red) were collected, diluted at least five-fold to reduce the sucrose concentration and then centrifuged again to pellet the IMVs. The pellet was resuspended in fresh buffer and the total protein concentration was estimated using a colorimetric assay to be 2.4 mg/mL. Varying amounts of either  $\alpha$ H-SpyTag or (GSG)<sub>6</sub>-SpyTag sensors were pipetted resulting in different IMVs/sensor ratios ( $\mu$ g/ $\mu$ g) and incubated overnight, as it was done with synthetic membranes. The sensor abundance ranged between 0.9 and 20 % with respect to the total protein in IMVs. Differently to the synthetic liposomes, no free SpyTag-modified sensor was detected after incubation, as can be judged from SDS-PAGE (figure 3.29).

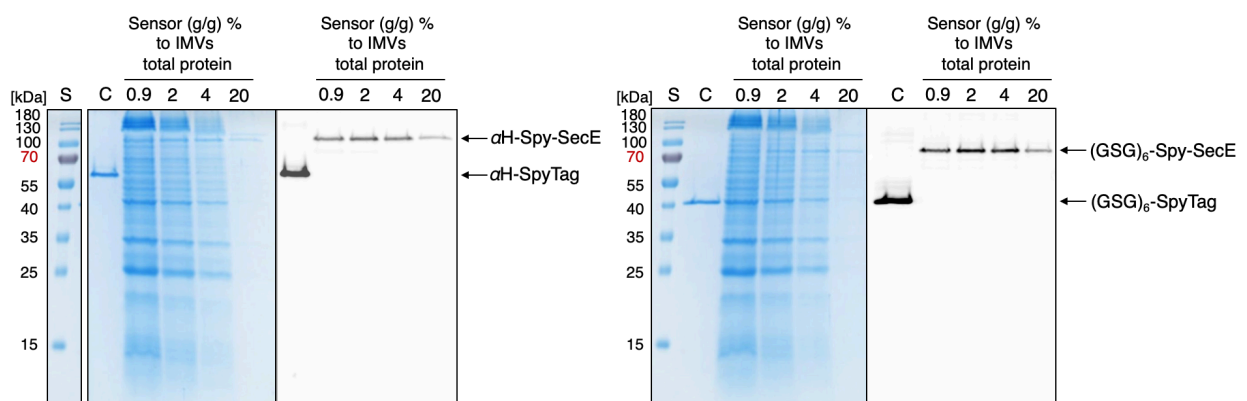


Figure 3.29: Binding of the soluble  $\alpha$ H-SpyTag (left) and (GSG)<sub>6</sub>-SpyTag (right) to extracted IMVs with overexpressed SecE-SpyCatcher and formation of corresponding  $\alpha$ H-Spy-SecE and (GSG)<sub>6</sub>-Spy-SecE complexes with different sensor/IMVs ratios (g/g) expressed in sensor amount (%) to the total protein mass quantified in IMVs. In order to maintain a uniform sensor concentration and to avoid signal overload, the sample size for SDS-PAGE was adjusted accordingly.

The emission spectra of the IMV samples with either of sensors were recorded. The calculated  $F_A/F_D$  ratios for the  $\alpha$ H-Spy-SecE constructs within 0.9 % and 2 % sensor stayed constant with  $0.89 \pm 0.01$  and slightly increased to  $0.92 \pm 0.01$ , when the sensor abundance reached 4% IMVs (figure 3.30). In the sample with the highest sensor concentration (20%), the  $F_A/F_D$  ratio was  $1.17 \pm 0.01$  which implied the intermolecular FRET between multiple sensor molecules in direct neighborhood. The same is observed for the  $(GSG)_6$ -Spy-SecE sensor bound to the surface of IMVs. Here the  $F_A/F_D$  ratio increased slowly from  $1.29 \pm 0.01$  in the sample with 0.9% sensor to  $1.34 \pm 0.01$  and  $1.38 \pm 0.01$  for 2% and 4%, respectively, and the highest signal of  $1.73 \pm 0.01$  was measured at 20% sensor, suggesting strong contribution of intermolecular FRET.

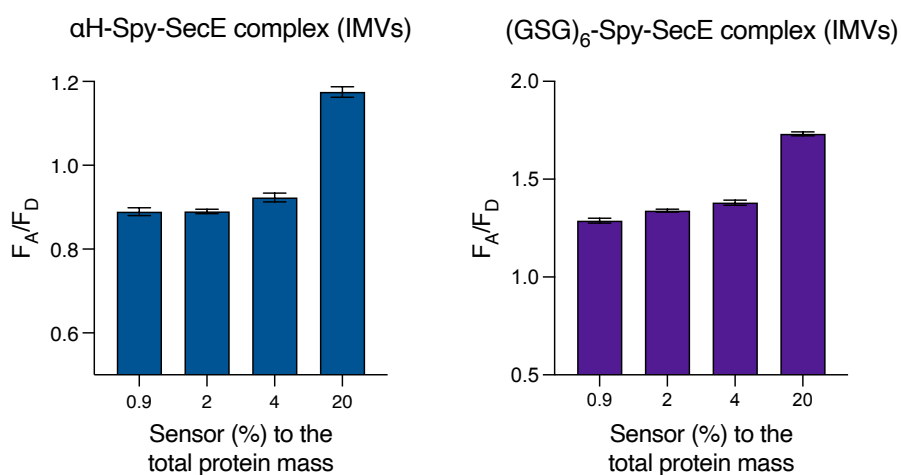


Figure 3.30: Estimated  $F_A/F_D$  ratios for the  $\alpha$ H-Spy-SecE and  $(GSG)_6$ -Spy-SecE constructs formed on the surface of extracted IMVs with overexpressed SecE-SpyCatcher anchors.

### 3.3.2.4 Discussion

This chapter introduces a membrane-anchoring strategy for the crowding sensor that would complement the approach described in Chapter 3.2. There, the transmembrane helices 1 and 2 of SecE were genetically fused to the fluorescent proteins via linkers, resulting in a single-chain protein. The design of the constructs developed in this chapter is based on the SpyTag:SpyCatcher interaction and consists of two parts, i.e. SpyCatcher protein fused via a flexible linker with the membrane-anchoring TMHs from SecE, termed as SecE-SpyCatcher anchor, and the soluble sensor with the SpyTag-peptide in the central linker region. This design allows binding of the soluble crowding sensor to the membrane interface in the robust manner using an independent membrane anchor. The SpyTag-modified sensors,  $\alpha$ H-SpyTag and (GSG)<sub>6</sub>-SpyTag, as well as the complex formation of the sensor with the soluble SpyCatcher, a precursor of the membrane anchoring domain SecE-SpyCatcher, were characterized in solution as well as their sensitivity to macromolecular crowding mimicked by PEG of different sizes.

The initial  $F_A/F_D$  ratios for  $\alpha$ H-SpyTag and (GSG)<sub>6</sub>-SpyTag sensors were  $0.80 \pm 0.01$  and  $1.73 \pm 0.02$ , respectively, i.e. slightly higher compared to the analogous sensor constructs GE with around 0.6 and G12 with 1.4 (Liu *et al.*, 2017) despite the elongation of the region between the fluorescent proteins by the SpyTag peptide. Upon binding of the soluble SpyCatcher, the  $F_A/F_D$  ratio of (GSG)<sub>6</sub>-SpyTag:SC decreased, suggesting larger distance within the FRET pair. The decrease was also observed, though with a less extent, for the  $\alpha$ H-SpyTag:SC complex, where the presence of the  $\alpha$ -helices in the linker region already provided an enlarged spacing (Liu *et al.*, 2017; Löwe *et al.*, 2023). Additionally, the structural data obtained by SAXS showed an elongation of the sensor upon SpyCatcher binding and the change of the sensors three-dimensional conformation from an elongated, cylinder-like form to a V-shaped structure. Still, the determined molecular weight of  $\alpha$ H-SpyTag and (GSG)<sub>6</sub>-SpyTag were higher than expected from their theoretical masses and moreover in the case of complexes  $\alpha$ H-SpyTag:SC and (GSG)<sub>6</sub>-SpyTag:SC were found to be surprisingly identical for both sensor despite their molecular mass difference. High concentrations employed in the SAXS measurements may be the reason for the partial formation of oligomeric species by interaction of the fluorescent proteins, as was discussed in the Chapter 3.2, that would explain the increase of the estimated molecular weights. However, the identical result for the SpyCatcher:FRET-sensor complexes could serve as indication for the interaction between SpyCatcher molecules at high concentrations and should be further analyzed.

The  $\alpha$ H-SpyTag and (GSG)<sub>6</sub>-SpyTag sensors showed the response to crowding mimicked in solution by PEG molecules of two different sizes resulting in the continuous increase of  $F_A/F_D$  ratios with increasing crowder fraction in solution. For the complexes  $\alpha$ H-SpyTag:SC and

(GSG)<sub>6</sub>-SpyTag:SC, the binding of SpyCatcher not only preserved the structural dynamics of the sensory domains, but also improved the sensors readout in terms of their FRET efficiency. In the presence of PEG 2000 and PEG 6000 at 40% the FRET efficiency of the (GSG)<sub>6</sub>-SpyTag:SC increased from 11% to 70% and from 26% to 84%, respectively, as compared to the free (GSG)<sub>6</sub>-SpyTag. The FRET efficiency of the  $\alpha$ H-SpyTag:SC complex in crowded solution increased from 46% to 62% and from 68% to 334% at 40% PEG 2000 and PEG 6000, respectively, in comparison to the unbound  $\alpha$ H-SpyTag.

To anchor the soluble SpyTag-sensor to the membrane interface, the SecE-SpyCatcher construct was generated and reconstituted into liposomes. However, binding of the soluble  $\alpha$ H-SpyTag and (GSG)<sub>6</sub>-SpyTag to the reconstituted membrane anchor occurred at relatively low efficiency, as the fraction of the unbound sensor remained at 50%. Modulating the negative net charge at the membrane interface did not affect the binding efficiency between  $\alpha$ H-SpyTag and (GSG)<sub>6</sub>-SpyTag and the membrane-incorporated SecE-SpyCatcher. Despite this negative result, the experiment conducted on liposomes with neutral charge e.g. only DOPC to exclude of the role of the negative surface charge should be considered in future.

To avoid that further measurement results are impaired by the unbound crowding sensor, the pre-formed  $\alpha$ H-Spy-SecE and (GSG)<sub>6</sub>-Spy-SecE complexes were reconstituted into the liposomes. Both sensor types demonstrated the ability to respond to PEG 2000 and PEG 6000 added to the solution. The  $F_A/F_D$  ratios were increasing with increasing crowder concentration except for the sample with 40% PEG 2000: Here, the acceptor fluorescence suddenly decreased and the reason for this phenomenon remains currently unknown. Possibly the interaction of the current PEG stock with the sensor itself or with the model membranes can play a role, since it is known that PEG polymers are not completely inert and may interfere with the probe (Wu *et al.*, 2014).

A bottleneck for the sensor application was observed when employing the PEG-conjugated lipids to mimic the crowding on the interfaces. In this experiment, only (GSG)<sub>6</sub>-Spy-SecE incorporated into liposomes with PEG 1000 PE manifested a weak response. The (GSG)<sub>6</sub>-linker together with SpyCatcher increases the distance from the sensor to the membrane surface and thereby limits the effect of relatively small crowders, which are not able to generate lateral compression that is required to bring the sensor to a more compact form. The response of the (GSG)<sub>6</sub>-Spy-SecE can be most likely be explained to the more flexible nature of the linker domains. However, already in the non-crowded liposomes, deviating  $F_A/F_D$  ratios were observed after reconstitution upon addition of DOPE lipid (10 mol %), suggesting the need for further research on influence of lipid composition on the sensor's dynamics. Furthermore, both employed sensor types the decreased acceptor/donor ratios at 10 mol % PEGylated lipids were observed. Synergistic effect of the sensor clustering upon reconstitution and the

presence of PEG on the surface of the liposome can impair the insertion of the sensor and accurate sensor readout. Further research on optimization of reconstitution conditions and characterization of the reconstitution efficiency is necessary for this type of the experiment.

To surpass the reconstitution constraint described above and to simulate physiologically relevant environment on the liposomal surface, proteins were employed for the characterization of  $\alpha$ H-Spy-SecE and (GSG)<sub>6</sub>-Spy-SecE upon crowding. In this thesis, one of the strategies for the attachment of the proteins to the membrane surfaces relied on 18:1 biotinyl cap PE lipids included in the liposomal formulations and streptavidin as a crowder of proteinaceous origin. Streptavidin is a well-studied protein from *Streptomyces avidinii* and is widely used in research since the interaction of streptavidin and biotin shows a strongest known binding affinity with  $K_d$  of approx. 10 fM (Dundas *et al.*, 2013; Green, 1990). The wildtype streptavidin is a tetramer, where each of the monomers binds a single biotin molecule. The molecule was not applicable for this study, since it led to clustering and aggregation of the biotin-containing liposomes. To overcome this limitation mutants of streptavidin were applied and tested, i.e. the monovalent tetrameric streptavidin with a single biotin binding site A1D3 (composed of one functional “Alive” subunit and three inert “Dead” subunits) (Howarth *et al.*, 2006) and monomeric streptavidin mSA (Lim *et al.*, 2013). The studies with monovalent A1D3 streptavidin were not included in this thesis, even though the binding to the biotinylated lipid was achieved. The application of A1D3 led to controversial and non-reproducible responses of the crowding sensor. Several experiments (data not shown) have indicated that A1D3 generally can be bound to the surface of biotin-functionalized liposomes, but is most probably pulled out the bound lipid species from the vesicle making A1D3 not suitable for the current applications. On the other side, the monomeric version of streptavidin (mSA) revealed as a good candidate for the surface crowding experiments. Binding of mSA to the liposome interface was observed and confirmed with developed SecE-based crowding sensor with high degree of reproducibility.

Upon mSA titration of the liposomes consisting of 20 mol % biotinylated PE lipids, the  $F_A/F_D$  ratios increased upon binding of mSA to the liposomal surface, but the response was weak in comparison to the single-chain FRET-sensor described in the Chapter 3.2. The possible explanation of these observations could be the final size and geometry of the FRET-sensor constructs, as it was discussed before. SpyCatcher anchor increases the distance from the sensor to the membrane surface and the small size of the mSA with 15.5 kDa led to a loss of the sensor sensitivity to the crowding in the membrane proximity.

## 3.4 Effects of macromolecular crowding on transport activity and translocation via SecYEG

### 3.4.1 Introduction

The excluded volume effect induced by soluble crowders and the high abundance of proteins within the membrane and at the membrane interfaces may significantly influence the membrane-associated processes (Löwe *et al.*, 2020). Transport across the cellular cytoplasm and translocation of proteins across the membrane in the crowded environment of a living cell can be significantly different in comparison to the diluted solutions due to the altered diffusion and emerging quinary interactions between the target protein and the crowders. To study the effects of the macromolecular crowding on targeting, complex assembly and transport processes, we have to distinguish between three types of crowding, i.e. crowding in solution, on the membrane surface and within the membrane itself, and characterize their effects on a particular biological process to gain a more in-depth knowledge of the interplay between highly confined environment and vital biological processes. Well-characterized membrane constituents offer a useful platform for studying the macromolecular crowding effects in the model systems with induced confinement.

The translocon SecYEG performs transport of proteins across the cytoplasmic membrane and mediates the insertion of the  $\alpha$ -helical membrane proteins. The complex consists of three subunits SecY, SecE and SecG forming a dynamic channel that spans through the cytoplasmic membrane. In *E. coli* the motor ATPase SecA is required for the post-translational transport of unfolded preproteins via SecYEG. SecA associates with SecYEG at the cytoplasmic side and is known to interact with anionic lipids even in the absence of the translocon. In the highly crowded cytoplasmic environment, aggregation or premature folding of preproteins are likely scenarios, but they can be stabilized in their largely unfolded state by chaperones. Especially SecB demonstrated a specialized role by stabilization of the freshly synthesized preproteins, preventing their folding and aggregation, and delivering the secretory preproteins to SecA:SecYEG machinery (Bechtluft *et al.*, 2010).

In this chapter, we employ Sec machinery as a model system to examine the effect of macromolecular crowding on the complex process of protein translocation. The translocation activity and kinetics of preprotein pOmpA via SecYEG channel and interactions between SecA, lipids and SecYEG are studied under following conditions: (i) solution crowding rendered by synthetic polymers and (ii) crowding of membrane interfaces rendered either by PEGylated lipids or by attachment of proteinaceous model crowder mSA.

### 3.4.2 Materials and methods

#### Expression and purification of proteins

##### *SecYEG*

Overexpression of the cysteine-less SecYEG and SecY<sup>C148</sup>EG translocons encoded in plasmids pEK20 and pEK20-L148C, respectively, was induced in *E. coli* C41(DE3) upon addition of 0.5 mM IPTG as the culture reached OD<sub>600</sub> of around 0.6 and was conducted for 3 h and 180 rpm. The cells were harvested, resuspended in cell buffer (CB, 20 mM Hepes, 150 mM KOAc, 5 mM Mg(OAc)<sub>2</sub>, 5% glycerol and 1 mM DTT, 0.2 mM PMSF), lysed (Microfluidizer, M-110P, Microfluidics Corp) and centrifuged for 15 min at 12000xg (SS-34 fixed angle rotor, Sorvall) to remove the cell debris. The crude membranes were pelleted upon subsequent centrifugation of the supernatant for 50 min at 235000xg (rotor 45 Ti, Beckman Coulter) and were resuspended in CB. Membranes were flash-frozen in liquid nitrogen and stored in -80°C.

The purification of SecYEG from the membrane crude started with solubilization. For this 1 mL of the membrane suspension were mixed with 9 mL solubilization buffer (50 mM Hepes pH 7.2, 500 mM KCl, 1% DDM, 200 μM TCEP and EDTA-free protease inhibitor cocktail (cOmplete™, Roche)) and were incubated on the rolling bench for 1 h at 4°C. The sample was centrifuged for 15 min at 4000xg to remove the non-solubilized material. The supernatant was supplied with 5 mM imidazole to avoid non-specific binding, loaded on pre-washed Ni<sup>2+</sup>-NTA agarose resin (Qiagen) and incubated on the rolling bench for 1 h at 4°C. The flow-through was collected, the resin was washed with wash buffer (WB, 50 mM Hepes pH 7.2, 150 mM KCl, 0.1% DDM, 200 μM TCEP, 10 mM imidazole and EDTA-free protease inhibitor cocktail) and SecYEG was eluted with elution buffer (EB, 50 mM Hepes pH 7.2, 150 mM KCl, 0.1% DDM, 200 μM TCEP, 300 mM imidazole and EDTA-free protease inhibitor cocktail). Next, the sample was applied on the size exclusion column (SEC) Superdex 200 Increase GL 10/300 (Cytiva). Samples from expression and every purification stage as well as the peak fraction from SEC were analyzed via SDS-PAGE. The purified protein was supplemented with 5% glycerol and flash-frozen in liquid nitrogen and stored in -80°C for the further experiments. The concentration was determined from protein absorbance at 280 nm ( $\epsilon_{280} = 70,945 \text{ M}^{-1}\text{cm}^{-1}$ ).

For the labeling procedure, purification was conducted as described. After the washing step, Ni<sup>2+</sup>-NTA resin with bound SecY<sup>C148</sup>EG was supplied with 0.5 mL of WB and 100 μM of the fluorescent dye ATTO 643-maleimide. The sample was incubated for 3 h at room temperature on the rolling bank. The unbound dye was washed with fresh WB and the labeled protein was eluted and further analyzed as described above.

To remove the N-terminal His-tag, purification was proceeded until washing steps were completed. The beads in the gravity flow column were supplied with 0.5 mL of WB and the in-house produced 3C protease was added (80 µg/mL). The cleavage was performed for 2 h on the rolling bank at 4°C. The tag-less target protein was collected in the flow-through fraction and further analyzed as described above.

#### *SecA*

The gene encoding for *E. coli* SecA was cloned into pET21a vector to contain C-terminal His-tag. SecA was overexpressed in *E. coli* BL21(DE3) in 2 L LB-medium (Carl Roth) supplemented with 100 µg/mL ampicillin. Expression was induced with 0.5 mM IPTG (at OD<sub>600</sub> around 0.6) and was proceeded for 3 h. The cells were harvested upon centrifugation at 5000xg for 10 min (SLC-6000 Fixed Angle Rotor, Sorvall) and resuspended in cell buffer (50 mM Tris/HCl pH 7.6, 200 mM KOAc, 5 mM Mg(OAc)<sub>2</sub>, 20% glycerol and EDTA-free protease inhibitor cocktail). Cells were lysed as described above and the lysate was clarified for 30 min 235000xg (rotor Ti45, Beckman Coulter). The supernatant was loaded on the pre-washed Ni<sup>2+</sup>-NTA agarose resin and incubated for at least 45 min on the rolling bench at 4°C. The resin with bound SecA was washed with 20 mM Tris/HCl pH 7.6, 500 mM KOAc, 5 mM Mg(OAc)<sub>2</sub>, 20% glycerol, 200 µM TCEP and EDTA-free protease inhibitor cocktail. SecA was eluted using same buffer supplemented with 300 mM imidazole and then applied on Superose 6 Increase 10/300 GL column (Cytiva) equilibrated with 20 mM Tris/HCl pH 7.6, 50 mM KOAc, 5 mM Mg(OAc)<sub>2</sub>, 20% glycerol and 200 µM TCEP. Peak fractions containing SecA were pooled, analyzed with SDS-PAGE, aliquoted and stored at -80°C. The concentration of the protein was obtained from the measured absorbance at 280 nm ( $\epsilon_{280} = 76,000 \text{ M}^{-1}\text{cm}^{-1}$ ). For the removal of the His-tag, the 0.5 mL aliquot with purified protein was mixed with 3C protease (80 µg/mL) and incubated for 3 h. The solution was applied on Superdex 200 Increase GL 10/300 (Cytiva) to remove the protease. Collected peak fractions with SecA protein were applied on pre-washed Ni<sup>2+</sup>-NTA agarose resin (either Qiagen or Merck) and the flow-through fraction with the tag-less SecA was collected.

#### *SecB*

The gene encoding for *E. coli* SecB was cloned into pRSFDuet plasmid to contain N-terminal His-tag. The chaperone SecB was overexpressed in *E. coli* BL 21(DE3) upon induction with 0.5 mM IPTG (culture OD<sub>600</sub> around 0.6) in 2 L LB-medium (Carl Roth) supplemented with 50 µg/mL kanamycin and the expression was carried out for 2 h. The cells were harvested as described above and were resuspended in buffer containing 20 mM Hepes pH 7.2, 50 mM KCl, 5 mM Mg(OAc)<sub>2</sub>, 1 mM DTT and 0.1 mM PMSF and lysed with Microfluidizer (M-110P,

Microfluidics Corp) and centrifuged for 15 min at 12000 $\times$ g (SS-34 fixed angle rotor, Sorvall) to remove the cell debris. For the purification, the supernatant supplemented with 5 mM imidazole was applied on pre-washed Ni<sup>2+</sup>-NTA resin and incubated for 1 h. The resin was washed with 20 mM Hepes pH 7.2, 50 mM KCl, 5 mM Mg(OAc)<sub>2</sub>, 40 mM imidazole, 1 mM DTT and 0.1 mM PMSF, and the protein was eluted with the identical buffer, but with 300 mM imidazole concentration. The eluted sample was subsequently applied on Superdex 200 Increase GL 10/300 (Cytiva) in 20 mM Hepes pH 7.2, 50 mM KCl, 5 mM Mg(OAc)<sub>2</sub>. Peak fractions with SecB were pooled and supplemented with 5% glycerol. The protein concentration was determined from the absorbance at 280 nm ( $\epsilon_{280,monomer} = 14,690 \text{ M}^{-1}\text{cm}^{-1}$ ) and the protein was flash-frozen in liquid nitrogen and stored in -80°C

### *mSA*

The overexpression and purification of *mSA* was performed with identical procedure described in Material and Methods in Chapter 3.3.2.

### **Liposome formation and reconstitution of SecYEG**

Lipids stocks solubilized in chloroform (Avanti Polar Lipids, Inc.) were mixed together in desired lipid compositions. For the experiments involving soluble crowders, the DOPC:DOPG (70:30 mol %) mixture was used. For simulation of the interfacial crowding with synthetic crowders, the liposomes were composed of 1,2-dioleoyl-sn-glycero-3-phosphoethanolamine-N-methoxy(polyethylene glycol)-1000, -2000 and 5000 referred as PEG 1000 PE, PEG 2000 PE and PEG 5000 PE respectively with different concentrations (0, 1, 3 and 10 mol %) with DOPC (63 mol %), DOPG (27 mol %) and varying DOPE concentrations according to the amount of PEGylated lipids, whereas the non-crowded liposomes were composed of DOPC:DOPG:DOPE (63:27:10 mol %). For simulation of the interfacial crowding with proteins, the 1,2-dioleoyl-sn-glycero-3-[(N-(5-amino-1-carboxypentyl) iminodiacetic acid)succinyl] (referred as 18:1 DGS-NTA(Ni<sup>2+</sup>)) and 1,2-dioleoyl-sn-glycero-3-phosphoethanolamine-N-(cap biotiny) (sodium salt) (referred as 18:1 biotiny cap PE) in final concentration of 10 mol % in DOPC (63 mol %), DOPG (27 mol %) were used. After the lipid mixtures were prepared, the chloroform was evaporated at 40°C (rotary evaporator RV 8, IKA) and the resulting lipid film was rehydrated and resuspended to a final lipid concentration of 5 mM in 20 mM Tris/HCl pH 7.5 and 150 mM KCl. Alternatively, 20 mM Tris/HCl pH 7.5 and 50 mM KCl buffer composition was used for flotation assays, where indicated. The unilamellar liposomes were homogenized via extrusion through 200 nm polycarbonate membranes (Whatman).

For the SecYEG reconstitution, the liposomes were swelled with 0.2% DDM (Löwe *et al.*, 2023) and incubated for 30 min on ice with the detergent-solubilized SecYEG at the molar

protein/lipid ratio of 1:1,000. The detergent was removed overnight with the adsorbent medium (Bio-Beads SM-2, Bio-Rad). The proteoliposomes were pelleted for 30 min at 162000 $\times$ g (S120-AT3 fixed angle rotor, Thermo Scientific™) and resuspended back to the initial 5 mM lipid concentration. The reconstitution of SecYEG was controlled via SDS-PAGE.

### Translocation assay of pOmpA via SecYEG

*In vitro* translocation assay with the fluorescently labeled preprotein OmpA was performed as described previously (Kamel *et al.*, 2022; De Keyzer *et al.*, 2002) with minor modifications. The components for the translocation assay were mixed together to the final volume of 50  $\mu$ L in 20 mM Tris/HCl pH 7.4 and 150 mM KCl: either 10  $\mu$ L or 20  $\mu$ L of SecYEG proteoliposomes (5 mM lipid concentration with molar protein/lipid ratio of 1:1,000), 0.5  $\mu$ M of fluorescein-maleimide labeled pOmpA-FM as a substrate, SecB chaperone, 5 mM ATP, 0.1 mg/mL BSA, 10 mM DTT, 5 mM MgCl<sub>2</sub>, energy mix (0.05 mg/mL phosphocreatine kinase and 10 mM phosphocreatine) and Ficoll PM70 as crowder in desired amounts. The reaction mixture was placed at 37°C for 2 min and the translocation of the substrate was induced upon addition of SecA (0.8  $\mu$ M). The reaction was kept at 37°C for 15 min and was stopped by transferring the samples on ice. 5  $\mu$ L of the reaction volume was set aside as a reference. The non-translocated pOmpA-FM was degraded with 0.2 mg/mL proteinase K (Thermo Fisher Scientific), whereas the translocated substrate remained protected within the liposome lumen. Next, the samples were precipitated using trichloroacetic acid (TCA) with the final concentration of 15% (w/v) for 30 min on ice. The samples were centrifuged for 15 min at 21000 $\times$ g (table-top Eppendorf 5417 R centrifuge). The supernatant was carefully removed and the pellet was washed with 0.5 mL ice-cold acetone. After second centrifugation for 5 min at 21000 $\times$ g acetone was removed and the pellets were dried at 37°C. The pellets were resuspended in 2x SDS-PAGE sample buffer, incubated for 5 min at 90°C and analyzed via SDS-PAGE together with the untreated reference samples, which contained 10% of the total pOmpA-FM in the reaction. The intensity of the bands ( $I$ ) was quantified from in-gel fluorescence of pOmpA-FM (ImageQuant TL, Cytiva) with the “Local Average” background subtraction algorithm. The translocation activity was determined using following equation:

$$\text{Translocation activity}(\%) = \frac{I_T}{10 \times I_R} \times 100\% \quad (\text{Eq. 4})$$

where  $I_T$  represents the portion of translocated substrate and  $I_R$  the intensity of the reference sample. Translocation assay was carried at least two times for each sample type.

### Real-time translocation assay

The translocation of the synthetic substrate pOmpA-DHFR, a fusion of the precursor protein OmpA and dihydrofolate reductase (DHFR), via SecYEG was analyzed with real-time assay in accordance to the previously published protocol (Kamel *et al.*, 2022; Kedrov *et al.*, 2011; Koch *et al.*, 2016). Upon the translocation, the folded DHFR domain blocks the protein translocation and traps the unfolded pOmpA in the SecYEG channel. Formed translocation intermediate allows for FRET between fluorophores on pOmpA and SecY, which come closer together, and the increase of the acceptor fluorescence may be monitored in a real-time manner. The urea-denatured pOmpA-DHFR was labeled with Cyanine3-maleimide (FRET donor) at the unique cysteine position 282 within pOmpA, whereas the DDM-solubilized SecY<sup>C148</sup>EG with a cysteine at position 148 of SecY subunit was labeled with ATTO 643-maleimide (FRET acceptor). Prior to the translocation experiment, the DHFR domain of pOmpA-DHFR-Cy3 was folded and stabilized with methotrexate (MTX) and NADPH (Arkowitz *et al.*, 1993), whereas the unfolded pOmpA was stabilized with chaperone SecB. The proteoliposomes with SecYEG were mixed with SecA (1  $\mu$ M) either in 25 mM Hepes pH 7.4 and 150 mM KCL or in the crowder solutions (5%, 10%, 15% and 25% (w/v) Ficoll PM70, PEG 1500, PEG 4000 and PEG 8000 dissolved in the same buffer). The quartz cuvette with the reaction mixture was incubated at 37°C for 5 min and the reaction was started upon addition of ATP (5 mM) and the acceptor fluorescence was recorded for 800 s at 37°C with Fluorolog-3 (Horiba Scientific) with 510 nm excitation wave length and the emission was recorded at 690 nm with slit of 3 nm for both. The baseline recorded prior to the ATP addition was subtracted and the data points were normalized with respect to the initial value of reaction start to obtain  $Y_0=1$ . Translocation rate constants were estimated with GraphPad Prism software using the one-phase association function for the curve fitting:

$$Y = Y_0 + A(1 - e^{-kt}) \quad (\text{Eq. 5})$$

where  $Y_0$  is the starting point of the reaction,  $A$  is the amplitude (Plateau- $Y_0$ ),  $k$  is the association constant and  $t$  is the time (s).

### Flotation assay

The liposome binding assay or flotation assay was performed by adapted version of previously published protocol (Tronchere and Boal, 2017) as follows. The empty liposomes or proteoliposomes with SecYEG were mixed with SecA at 1:5,000 molar protein/lipid ratio in 100  $\mu$ L of buffer (20 mM Tris/HCl pH 7.4, 5 mM MgCl<sub>2</sub> with either 50 mM or 150 mM KCl). Samples were incubated for 20 min at 25°C and mixed with 60% sucrose (w/v). The reaction was loaded into the centrifugation tube and sequentially layered with 250  $\mu$ L and 50  $\mu$ L of

buffers, containing 20% and 5% sucrose, respectively. The tubes were centrifuged for 1 h at 289000 $xg$  (Rotor S120-AT3, Thermo Scientific™) and the samples were carefully collected in total to three fractions with Hamilton syringe starting with the bottom fraction (250  $\mu\text{L}$ ), followed by middle (125  $\mu\text{L}$ ) and top fraction (125  $\mu\text{L}$ ). The proteins in the collected fractions were precipitated upon addition of 300  $\mu\text{L}$  of 20% TCA followed by incubation on ice for 30 min. After centrifugation for 15 min at 21000 $xg$  (table-top Eppendorf 5417 R centrifuge) the resulting pellets were washed with acetone as was described for the translocation assay and finally resuspended in the diluted sample buffer and analyzed with SDS-PAGE. The intensity of the bands was quantified with ImageQuant TL (Cytiva) with the “Local Average” background subtraction algorithm. The recovery of the SecA or SecYEG associated with liposomes in the top fraction was calculated by dividing the determined band intensity by the sum of band intensities in all 3 fractions. Flotation assay was carried at least two times for each sample type.

#### **Surface plasmon resonance analysis of SecA binding**

SecA binding was tested on two-channel surface plasmon resonance system (Reichert® 2SPR) with three types of vesicles: Empty non-crowded liposomes composed of DOPC:DOPG:DOPE (63:27:10 mol %), surface-crowded empty liposomes composed of DOPC:DOPG:DOPE:PEG 2000 PE (63:27:7:3 mol %), and surface-crowded proteoliposomes with reconstituted SecYEG. For each measurement, the reference channel was coated with DOPC liposomes. Prior the immobilization, the vesicles were homogenized using mini-extruder with 50 nm polycarbonate membranes (Avanti Polar Lipids, Inc.). The system was pre-equilibrated with SPR buffer (20 mM Tris/HCl pH 7.4, 150 mM KCl and 5 mM  $\text{MgCl}_2$ ), the surface of the LP chip (Xantec Bioanalytics) was activated with three injections 40 mM CHAPS at the flow-rate of 10  $\mu\text{l}/\text{min}$  for 1 min. For immobilization of the vesicles on the first channel, solution with 2 mM liposomes or proteoliposomes was injected at the flow-rate of 10  $\mu\text{l}/\text{min}$  for 10 min. For DOPC:DOPG:DOPE:PEG 2000 PE liposomes the injection time was 15 min because of the slow accumulation on the chip surface. On the second channel, DOPC vesicles were applied at the flow-rate of 10  $\mu\text{l}/\text{min}$  for 10 min. Both channels were washed with 50 mM NaOH (10  $\mu\text{l}/\text{min}$ , 1 min), to wash-off the unbound vesicles followed by injection of 0.1 mg/mL BSA (10  $\mu\text{l}/\text{min}$ , 1 min) to reduce the unspecific binding. After the baseline was stabilized, 1  $\mu\text{M}$  SecA was injected over both chip channels (10  $\mu\text{l}/\text{min}$ , 3 min), followed by dissociation phase of 10 min. The SecA binding response was referenced by subtraction of the signal obtained on the reference channel and the data was processed with Trace Drawer software. After every measurement, the surface of the chip was regenerated injection of 1% DDM (10  $\mu\text{l}/\text{min}$ , 3 min) and fresh vesicles were immobilized for the next measurement round.

### 3.4.3 Results

#### A. Effects of the solution crowding on protein targeting and translocation via SecYEG

The translocation activity of the SecYEG using the model substrate pOmpA-FM, precursor of the outer membrane protein A, was determined in presence of Ficoll PM70 as crowder in different concentrations ranging from 0 to 30% (w/v). The translocation was initiated upon addition of SecA and the formed complex of SecA:SecYEG performed active transport of the substrate into the interior of the liposomes upon ATP consumption. After 15 min, the non-translocated substrate was degraded with the proteinase K, whereas the full-size translocated pOmpA-FM remains protected in the liposomal interior. The fraction of translocated pOmpA-FM was determined with respect to the reference taken prior the protease degradation. The effect of Ficoll PM70 present as crowder on translocon activity is shown in figure 4.1-A.

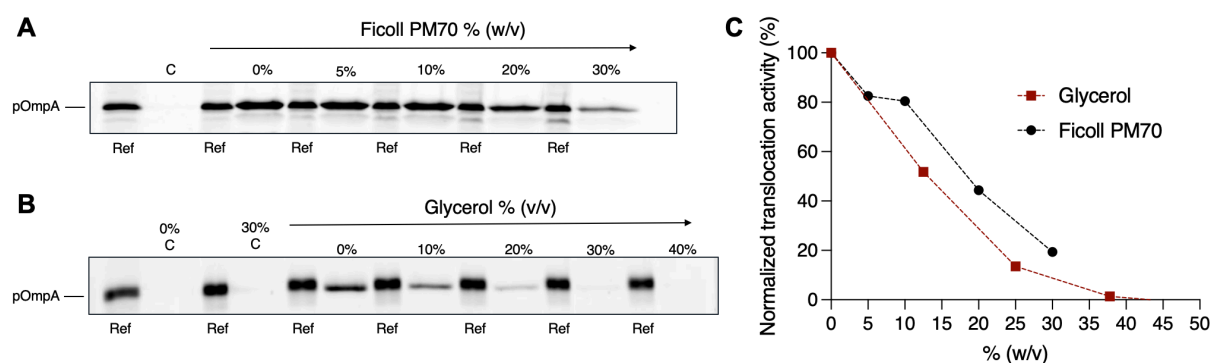


**Figure 4.1:** Translocation assay of pOmpA-FM via SecYEG in presence of different concentrations of (A) Ficoll PM 70 (% w/v) and (B) glycerol (% v/v) analyzed with SDS-PAGE. Samples C, 0%C and 30%C represent control samples without addition of SecA. (C) Quantified and normalized translocation activity in presence of either Ficoll PM70 (black circles) or glycerol (red squares) applied with different concentrations (% w/v)

The assay revealed that the translocation activity was inhibited upon increasing Ficoll PM70 concentration. The effect could be due to the macromolecular crowding, but also due to the increased viscosity of the solution. To characterize the impact of the viscosity on the translocation activity, the same assay was performed in presence of glycerol (figure 4.1-B). The translocation activity dropped drastically in the samples with 10%, 20% and 30% (v/v) glycerol and no translocation activity was observed 40% glycerol. To compare the results from both translocation activity experiments, the glycerol concentrations were re-calculated from v/v to w/v concentrations and the quantitated band intensity was normalized and plotted in figure 4.1-C. The viscosity of 10% (w/v) glycerol solution is 1.3 cP, while it is 2.1 cP for 10% Ficoll PM70. For 30% solutions, the viscosity of Ficoll PM70 reaches over 20 cP, but remains at 2.5 cP for glycerol at room temperature (Acosta *et al.*, 2017; Lecinski *et al.*, 2022; Rashid *et al.*,

2015; Segur and Oberstar, 1951). Thus, even though Ficoll PM70 shows significantly higher viscosity compared to glycerol, the translocation activity measured in the polymer solution was enhanced in comparison to the glycerol solution. The detected effect on the translocation activity is more likely attributed to the excluded volume effect induced by Ficoll PM70 and not to the increase of the viscosity, since the probe in crowded environment represented by synthetic polymers experience not the overall bulk viscosities, but micro-viscosity and the diffusion of the translocation components behave differently than predicted by Stokes law (Eq.1).

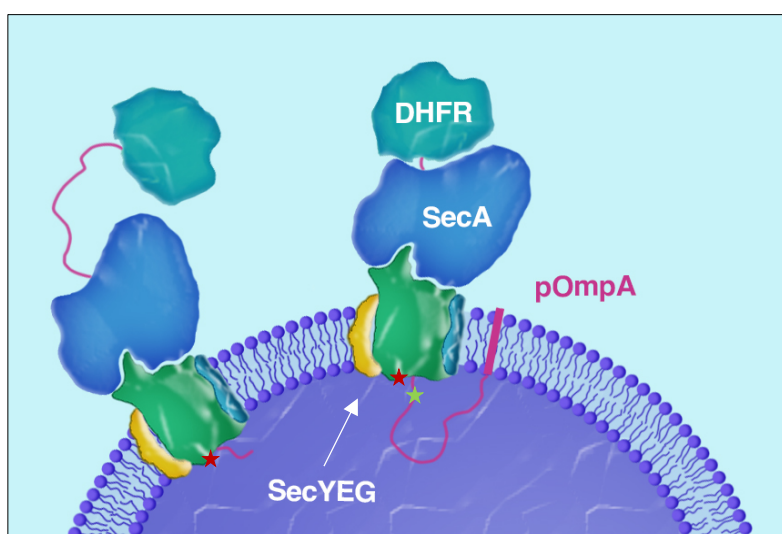


Figure 4.2: Schematic representation of FRET-based translocation assay

The type of the crowder used for rendering the excluded volume and its physico-chemical properties may have an impact on the studied biological process (Harrison and Zimmerman, 1984; Jiang and Guo, 2007). Translocation assays using PEG as a crowder, another commonly used crowding agent, was not possible due to precipitation of PEG upon addition of TCA in the assay protocol. To study the effects of macromolecular crowding with PEG, the FRET-based assay was used. Differently to the protease-protection assay, where multiple substrate molecules may be sequentially translocated by single SecYEG, the FRET assay measures the translocation of the single substrate pOmpA via the SecA:SecYEG complex (figure 4.2). The translocation is interrupted and blocked by the folded domain of DHFR resulting in the formation of translocation intermediate (Kamel *et al.*, 2022; Kedrov *et al.*, 2011). The real-time manifestation of the intermediate formation is given by the increase of the acceptor emission (ATTO 643-maleimide conjugated on the periplasm-facing position 148 of SecY subunit), as the acceptor (Cyanine3-maleimide conjugated at position 282 of pOmpA-DHFR fusion protein) is positioned close enough in the stalled translocation intermediate to allow for FRET. FRET-based assay was performed with SecY<sup>C148</sup>EG-ATTO-643

proteoliposomes in presence of Ficoll PM70 and PEG (1500, 4000, 8000) at different concentrations. The resulting curves displaying the formation of translocation intermediate were baseline-corrected, normalized, and fitted with one-phase association function (figure 4.3).

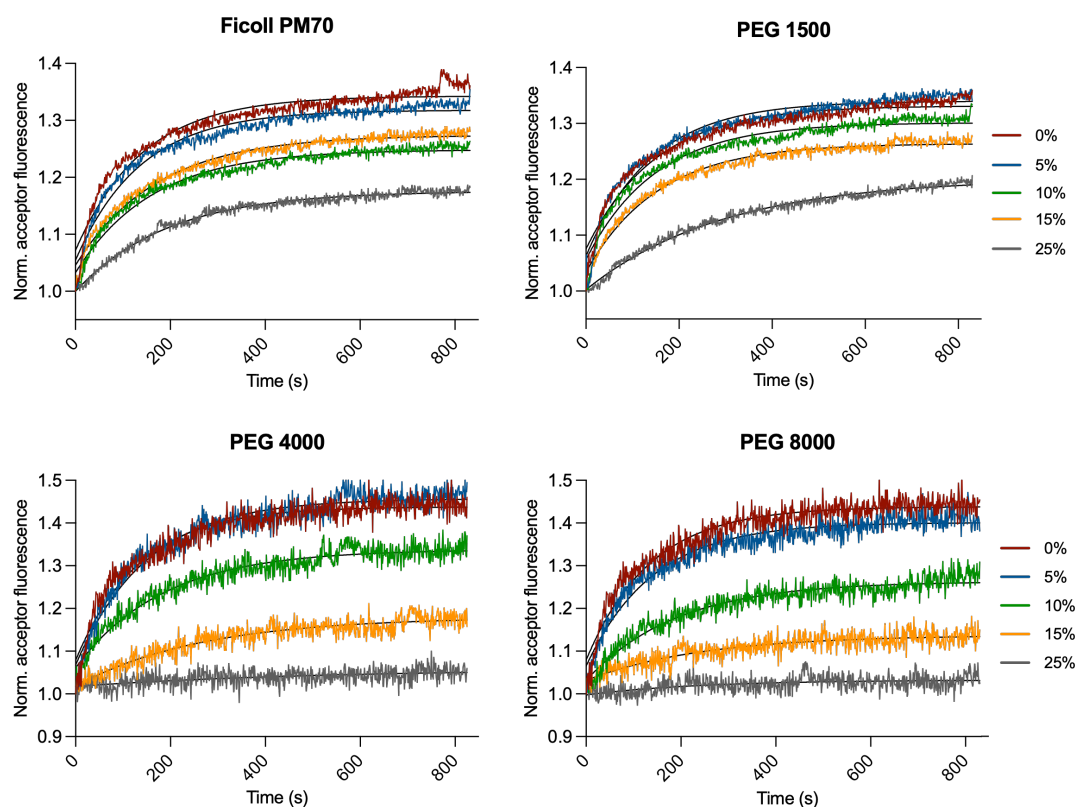


Figure 4.3: DHFR-FRET real-time kinetics analysis of assembly of the SecYEG:pOmpA-DHFR-Cy5 translocation intermediate in solution with crowders (Ficoll PM70, PEG 1500, PEG 4000, PEG 8000) with different concentrations.

The presence of the crowders of different types, concentrations and sizes slows down the formation of the intermediate complex. With the 25% Ficoll PM70 (w/v) as crowder the complex formation can be still observed, but the amplitude is decreased more than two-fold in comparison to the crowder-free sample, which is consistent with the previous results obtained with the protease-protection assay (figure 4.1-A). PEG 1500 with hydrodynamic radius of about 1 nm (Adams *et al.*, 2019), a small crowder in comparison to Ficoll PM70 with 5.5 nm (Chung *et al.*, 2019; Junker *et al.*, 2019), showed comparable influence on the formation of the translocation intermediate. PEG 4000 and 8000 with hydrodynamic radius 1.6 nm (Dong *et al.* 2018) and 2.7 nm, respectively (Ling *et al.* 2013), showed no pronounced effect at 5% concentration, but led to a decrease of amplitude of the curve at 10% and 15%, whereas at 25% no intermediate formation was observed. The translocation rates (1/min) were determined for each reaction and plotted against the corresponding crowder concentration (figure 4.4).

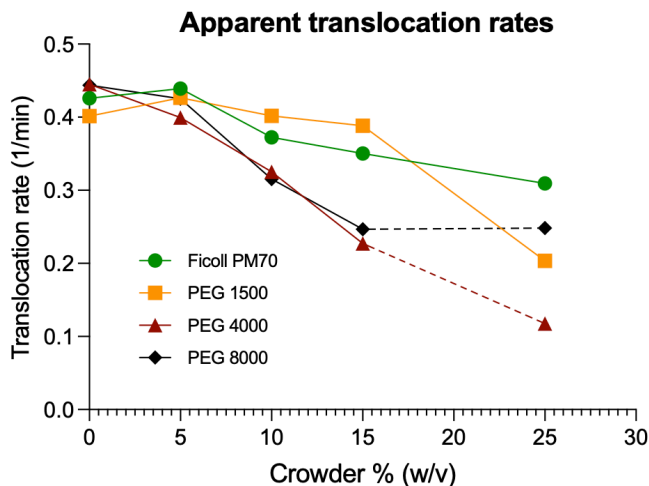


Figure 4.4: Determined translocation rates (1/min) in presence of soluble crowders of different type, size and concentrations.

The intermediate formation rate decreased with the increasing crowder concentration and it was depended on the crowder type. Increasing concentrations of Ficoll PM70 and PEG 1500 had a moderate effect on the translocation rates, which even resulted in a slight stimulation at 5%, but decreased further with increasing crowder concentration, whereas the presence of 25% PEG 1500 had a stronger effect in comparison to the Ficoll PM70 at same concentration. No significant difference was seen between PEG 4000 and 8000, but the overall effect of both was larger than that of Ficoll PM70 and PEG 1500, leading to faster decay of the translocation rates. The coefficient of determination ( $R^2$ ) indicated poor curve fit at the highest crowder concentration, with 25% for PEG 4000 and 25% for PEG 8000. Moreover, visual inspection of the recordings in figure 4.3 shows no translocation intermediate formation, which suggests that the translocation rates of this reactions are tending toward zero and therefore are marked with dashed line on the figure 4.4.

### B. Crowding on the membrane interface: Effects on protein targeting and translocation via SecYEG

As described in previous chapters, the most straightforward approach to induce crowding at the lipid membrane interface is to supplement the membranes with defined amounts of commercially available PEG-conjugated lipids. PEG is an inert synthetic polymer and is widely used for simulation of excluded volume effect in the macromolecular crowding research. The SecYEG translocon was reconstituted into the liposomes carrying different molar fractions of PEGylated lipids for rendering crowding on the surface of model membranes (figure 4.5). PEG-conjugated lipids with different concentrations (0, 1, 3 and 10 mol %) and polymer sizes (1000, 2000 and 5000 Da) were tested. The translocon reconstitution efficiency was examined via

SDS-PAGE with regard of the protein amount in harvested proteoliposomes (figure 4.6). Visual inspection suggested a uniform reconstitution between the presented samples which were subsequently employed for the translocation assay.

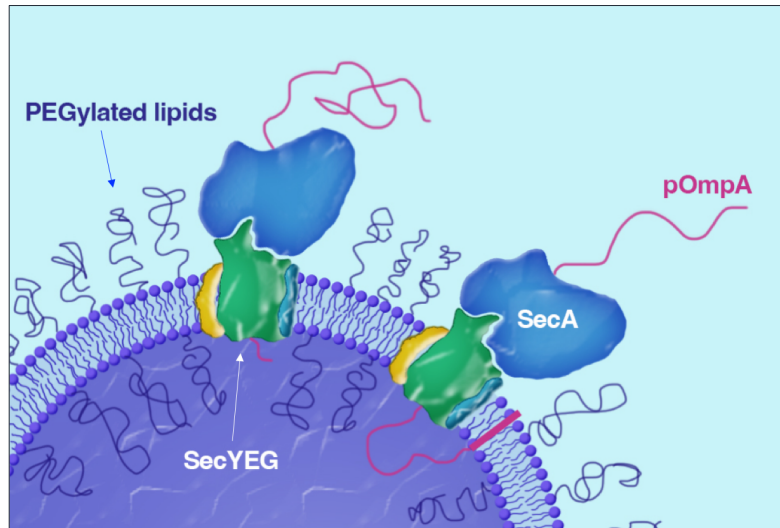


Figure 4.5: Schematic representation of translocation assay in SecYEG proteoliposomes with interfacial crowding rendered with PEGylated lipids.

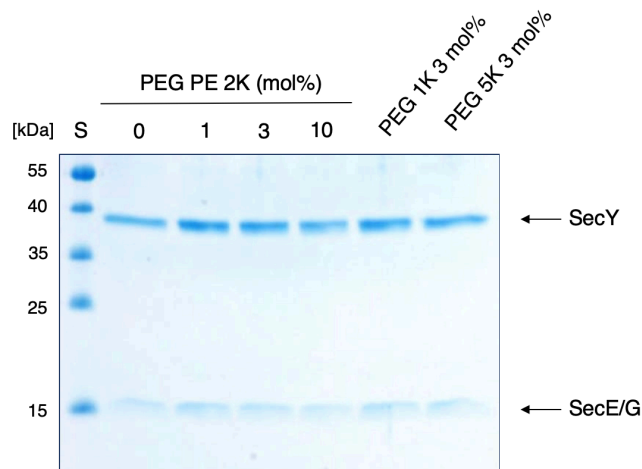


Figure 4.6: Reconstitution of the SecYEG translocon to liposomes with different amount and sizes of PEGylated lipids.

After mixing the components needed for the translocation, the reaction was started upon addition of SecA. The amount of translocated substrate (pOmpA-FM) was analyzed via SDS-PAGE as described above (figure 4.1). The intensity of the reference and corresponding bands were quantified and the translocation plotted in the figure 4.7.

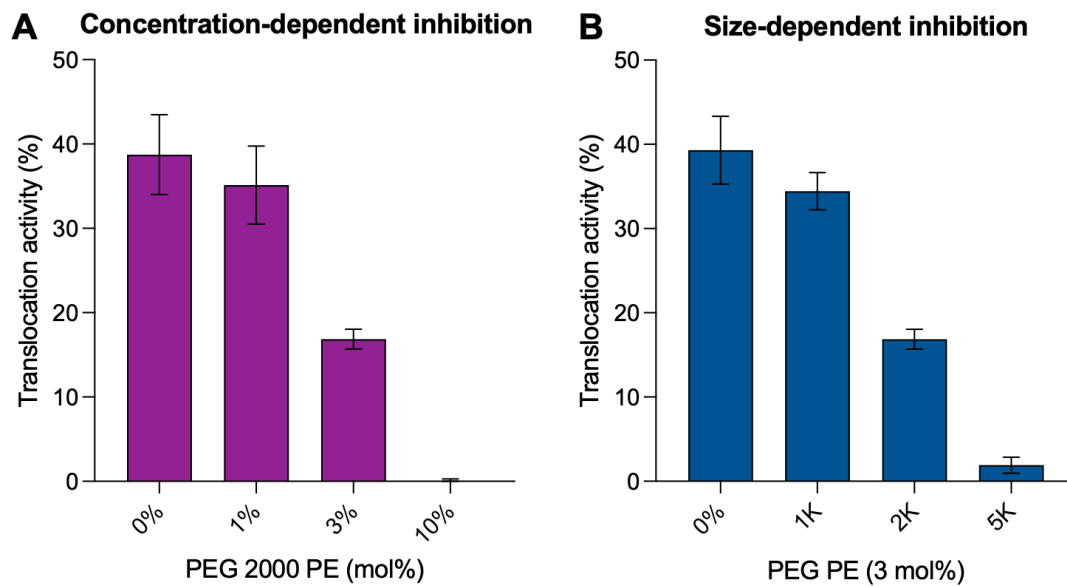


Figure 4.7: Translocation of *pOmpA* via *SecYEG* reconstituted into liposomes with PEGylated with different concentrations and sizes ( $n=3$ ). (A) Concentration-dependent inhibition of translocation activity with PEG 2000 at different mol %. (B) Size-dependent inhibition of translocation activity using PEG 1000 (1K), PEG 2000 (2K) and PEG 5000 (5K) at 3 mol %.

The decrease in *SecA:SecYEG* translocation activity was observed and was dependent on both the concentration and the size of the crowder on the liposomal surface. The translocation efficiency in the non-crowded liposomes reached  $39\% \pm 4\%$ . In the presence of PEG 2000 PE at 1 mol % and PEG 1000 PE at 3 mol % was comparable and shown a minor decrease of translocation activity. At 3 mol % PEG 2000 PE the translocation activity decreased two-fold to  $17\% \pm 1\%$  and no translocation activity was observed at the highest abundance of PEG 2000 PE lipids (10 mol %). The residual activity of  $1.9 \pm 0.3\%$  was measured in the liposomes with the largest crowder PEG 5000 PE with 3 mol %. The decrease in the translocation activity can be related to two possible events: The accessibility of the *SecYEG* translocon for the *SecA* is impaired due to the presence of the crowder and/or the *SecA*:lipid interaction is inhibited, which were described to be crucial for modulation of translocation activity (Kamel *et al.*, 2022; Koch *et al.*, 2016, 2019; Lill *et al.*, 1990; de Vrije *et al.*, 1988)

### SecA:lipid interactions in surface-crowded membranes

The *SecA*:lipid interactions in presence of interfacial crowding were further examined. To test the association of *SecA* with PEGylated liposomes, previously established flotation assay was employed (Kamel *et al.*, 2022). *SecA* was mixed with empty liposomes containing either different concentrations or sizes of PEGylated lipids. The suspension was applied on the bottom of the centrifugation tube and the discontinuous sucrose gradient was layered above (figure 4.8). Upon centrifugation, the liposomes float upwards to the environment with the lower

sucrose concentration, while carrying the membrane-associated SecA. Thus, membrane-associated SecA can be detected in the top fraction, whereas the bottom fraction contains the unbound fraction of SecA. The fractions were analyzed via SDS-PAGE (figure 4.9), and the bands were subsequently quantified to estimate the amount of the liposome-associated SecA.

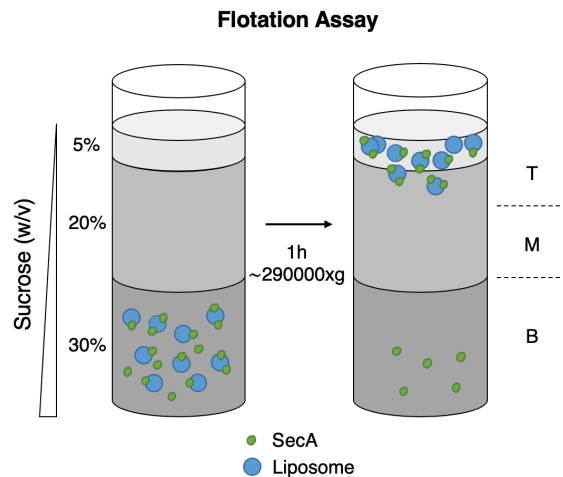


Figure 4.8: Schematic representation of the flotation assay in discontinuous sucrose density gradient for study the SecA:lipid interactions in empty and SecA:lipid:SecYEG interactions in proteoliposomes.

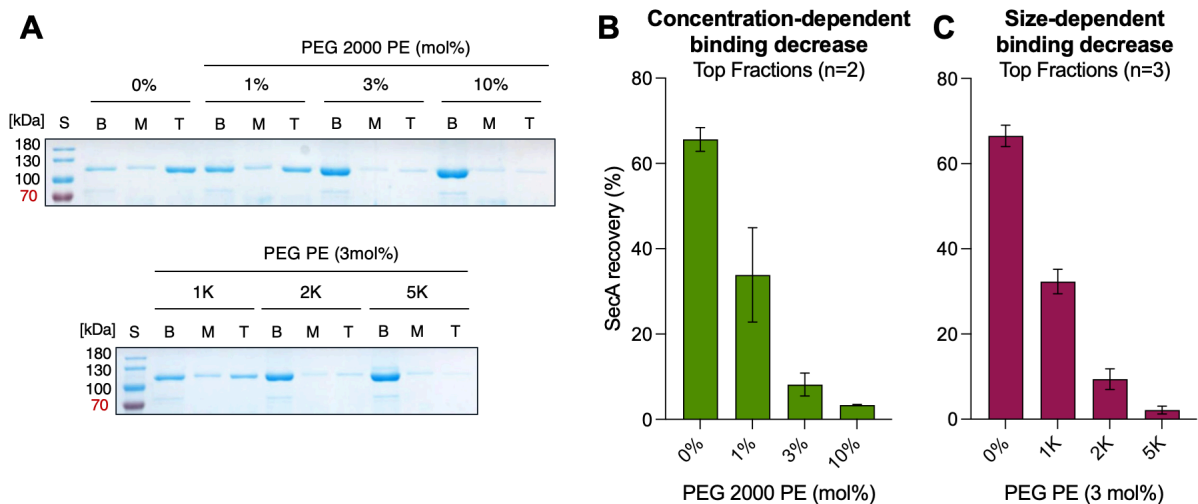


Figure 4.9: (A) SDS-PAGE analysis of flotation assay of SecA with liposomes with different concentrations and sizes of PEGylated lipids. (B) Quantified band intensity shows concentration-dependent inhibition with PEG 2000 at different mol % and (C) size-dependent inhibition of SecA interactions with liposomes containing either PEG 1000 (1K), PEG 2000 (2K) or PEG 5000 (5K) at 3 mol %.

SecA:lipid binding was strongly dependent on the degree of crowding on the liposomal surface. In the non-crowded liposomes, the recovery of SecA in the top fraction was  $66\% \pm 2\%$  (figure 4.9-B and 4.9-C). The association of SecA with PEGylated membranes decreased with

increasing abundance of PEG 2000 PE on the surface: Already at 1 mol % the two-fold decrease of SecA in the top fraction was observed ( $34\% \pm 8\%$ ). A high standard deviation of the obtained results is most likely related to the transition of the surface-conjugated PEG from so called “mushroom” to a “brush” configuration, which is expected to occur at 1.4 mol % PEG 2000 (Marsh *et al.*, 2003) and influences the SecA:lipid interaction. At 3 mol % and 10 mol % PEG 2000, binding of SecA decreased to  $8.2\% \pm 1.9\%$  and  $3.4 \pm 0.1\%$ , respectively. By varying the size of the surface-grafted PEG crowder at a constant molar concentration (3 mol %), a size-dependent decrease of the SecA interaction with liposomes was observed. Again, the interaction with non-crowded vesicles was reproducible, as was quantified in the previous experiment, and decreased two-fold for liposomes with 3 mol % PEG 1000 PE and continued to decrease with larger crowder PEG 2000 PE to  $9.4\% \pm 2.0\%$  and with PEG 5000 to  $2.2\% \pm 0.8\%$ .

However, SecA:lipid interaction alone does not explain the decrease of translocation activity, since the interaction of SecA with the PEGylated vesicles at 3 mol % PEG 2000 decrease around seven-fold whereas the translocation activity decreased only two-fold in the same type of the membrane. Same is for the liposomes with PEG 2000 PE at 1 mol % and PEG 1000 PE at 3 mol %, where binding of SecA to the membranes decreased two-fold, whereas translocation activity was barely affected. Additionally, the salt concentration used in flotation assay was shown to affect the SecA:lipid interactions (Kamel *et al.*, 2022). The binding of SecA in this experiment involving 50 mM KCl is predicted to decrease further in 150 mM KCl, which is applied in translocation assay.

#### **SecA:SecYEG interactions in surface-crowded membranes**

To address the question to which extend SecYEG presence in the crowded membranes would influence the SecA interactions in flotation assay, the proteoliposomes with the SecYEG translocon were produced, incubated with SecA in the same manner, as in the previous experiment with empty liposomes. Indeed, the SecA recovery in the top fraction with SecYEG in the non-crowded proteoliposomes was improved from  $66.5\% \pm 2.0\%$  to  $88.5\% \pm 5.5\%$  in comparison to the empty vesicles, and even for the PEGylated liposomes the SecA binding was restored by the presence of incorporated SecYEG to  $86.2\% \pm 7.6\%$  for PEG 1000 PE (3 mol %),  $55.7\% \pm 1.5\%$  for PEG 2000 PE (3 mol %) and  $34.5\% \pm 4.7\%$  for PEG 5000 PE (3 mol %) (figure 4.10):

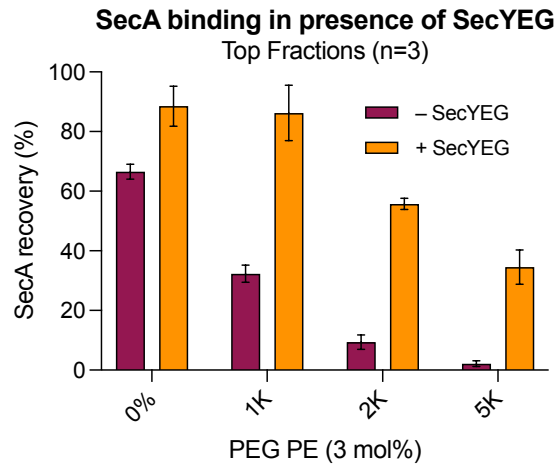


Figure 4.10: Comparison of the SecA binding to empty liposomes and SecYEG proteoliposomes with PEGylated lipids of different size at 3 mol %.

To evaluate how the elevated salt concentration influences SecA:lipid and SecA:SecYEG interactions in surface-crowded liposomes, the flotation assay was performed in presence of 150 mM KCl (figure 4.11-A). The bands of SecA were quantified and the SecA binding in 150 mM KCl (n=2) and 50 mM KCl (n=3) was compared (figure 4.11-B).

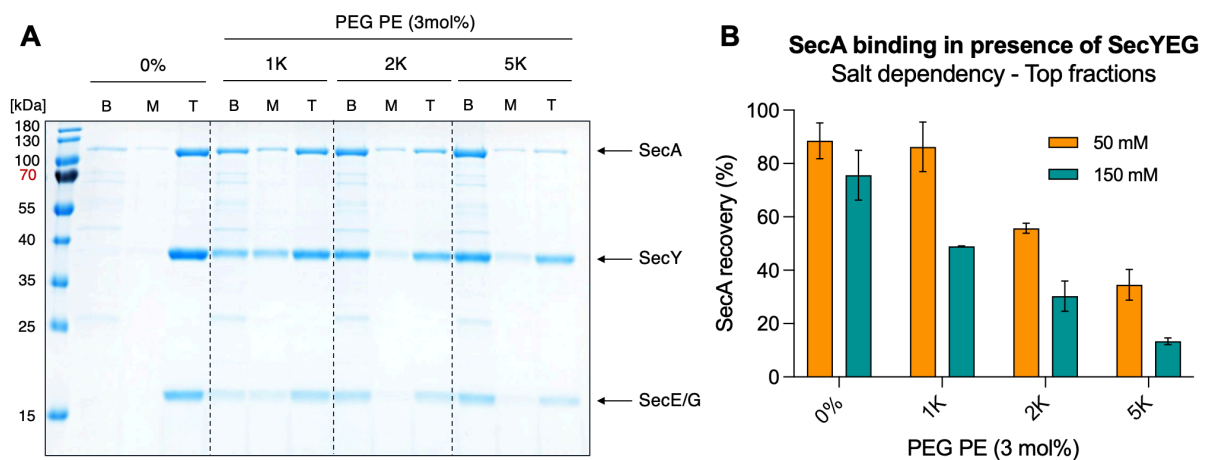


Figure 4.11: (A) SDS-PAGE analysis of collected flotation assay fractions in 150 mM KCl buffer. (B) Influence of 50 mM and 150 mM KCl on SecA association with SecYEG proteoliposomes with PEGylated lipids of different size at 3 mol %.

As expected, the elevated salt concentration decreased the SecA recovery in the top fractions to  $75.6\% \pm 6.6\%$  in the non-crowded liposomes,  $49.9\% \pm 0.1\%$  in PEG 1000 PE (3 mol %),  $30.3\% \pm 4.0\%$  in PEG 2000 PE (3 mol %) and  $13.4\% \pm 0.9\%$  in PEG 5000 PE (3 mol %). Same experiment was performed with SecYEG-proteoliposomes containing PEG 2000 PE at different molar concentrations (figure 4.12).

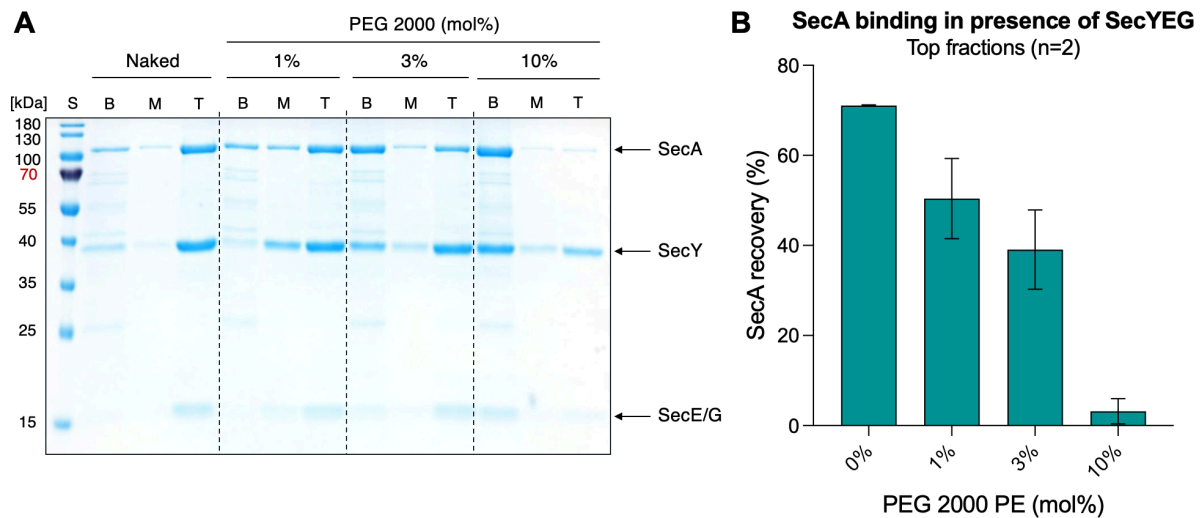
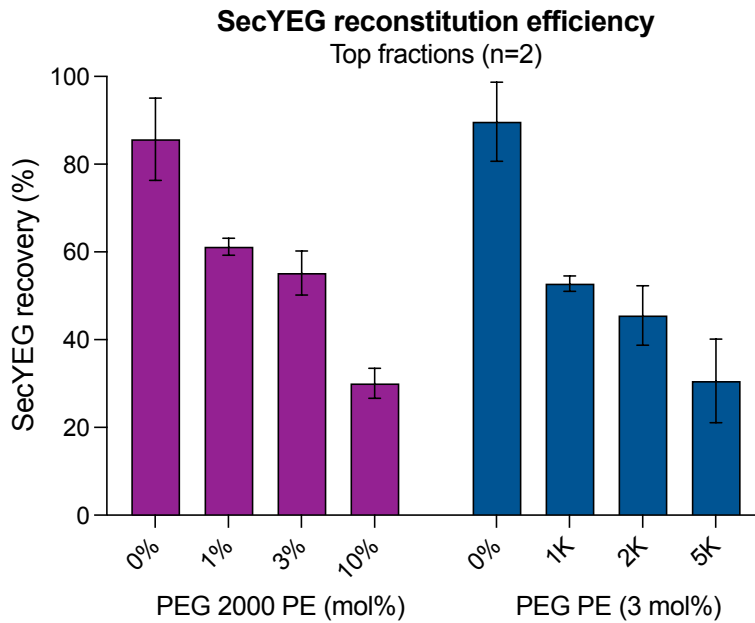


Figure 4.12: SDS-PAGE analysis (A) and quantified corresponding band intensities (B) of SecA interactions with liposomes containing PEG 2000 at different mol %.

Even though the SecYEG was reconstituted in the liposomes with 10 mol % PEG 2000 PE on the membrane surface and residual SecA was found in the top fraction of the flotation assay, no translocation activity was observed. Notably, the amount of SecYEG in the top fractions of the flotation assay varied between reconstitutions, when using different size and concentrations of PEGylated lipids (figure 4.13). The decrease of SecYEG reconstitution efficiency was dependent on the type and the size of the crowder. In the non-crowded liposomes, the reconstitution efficiency was in the range of 85% and 89%, whereas in the PEG 2000 PE with 1 mol % and 3 mol %, as well as in PEG 1000 PE and PEG 5000 PE with 3 mol % it varied between 46% and 61%. The lowest reconstitution efficiency of 30% was observed in the liposomes with 10 mol % PEG 2000 PE and for the largest crowder PEG 5000 PE at 3 mol %. The abundance of PEG on the liposomal surface hinders the efficient insertion of the SecYEG during reconstitution. The non-reconstituted SecYEG can lead to incorrect readout of the translocation assay since only reconstituted translocons can transport the substrate into the vesicles interior and shelter it from the protease degradation. Nevertheless, in the binding experiments with SecA the non-reconstituted or non-floated SecYEG can reduce the actual amount of bound SecA in the top fraction



*Figure 4.13: Quantified reconstitution efficiency of SecYEG in liposomes with different size and amount of PEGylated lipids in previously performed flotation assays.*

Under assumption that SecYEG may be indeed poorly reconstituted in the PEGylated lipids, the translocation assays were repeated (n=2), but now in the presence of the control, where the amount of the non-crowded proteoliposomes, and so the amount of active SecYEG, was decreased two-fold (referred as 1/2 0% sample) in order to study the influence of the decreased SecYEG abundance on the translocation activity outcome. The band with translocated substrate were quantified, the translocation activity was calculated and normalized to 100% with respect to the non-crowded sample with maximum possible reconstituted amount of SecYEG (figure 4.14). As can be seen, the half-reduced amount of the proteoliposomes and so a decreased amount of SecYEG in the reaction had no influence on the final amount of the translocated substrate possibly due the limitation of the reaction by amount of SecA protein and the saturation of the translocation reaction after 15 min reaction time.

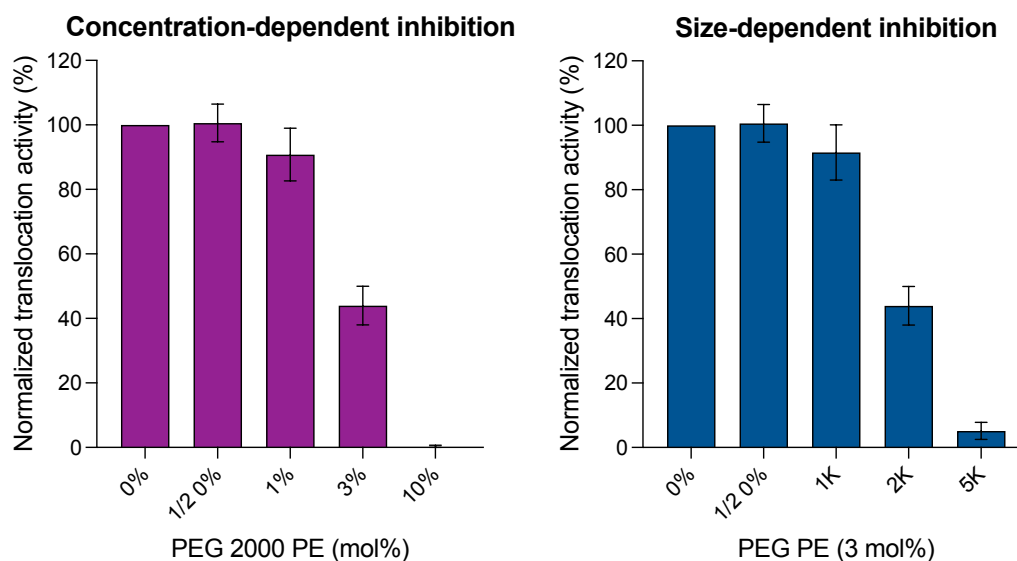


Figure 4.14: Normalized translocation activity of pOmpA via SecYEG in PEGylated proteoliposomes with different crowder concentrations and sizes. Sample 1/2 0% represents the reaction with half-amount of proteoliposomes used in 0% sample to decrease the number of active SecYEG translocons.

### SecA:lipid and SecA:SecYEG interactions in surface-crowded membranes: SPR-based analysis

For the verification of the results obtained by flotation assays, i.e. the ability of the reconstituted SecYEG to restore the SecA binding in the presence of interfacial crowding, the experiment surface plasmon resonance (SPR) was established with selected membrane compositions. SPR allows the analysis of protein:lipid as well as membrane protein:protein interactions in the real-time manner. The crowder-free liposomes composed of DOPC:DOPG:DOPE (63:27:10 mol %), PEG-covered liposomes DOPC:DOPG:DOPE:PEG 2000 PE (63:27:7:3 mol %), or crowded liposomes with reconstituted SecYEG were immobilized on the surface of LP chip (XanTec bioanalytics GmbH). The LP chip carries a planar carboxymethyl dextran layer with coupled alkyl chains providing lipophilic anchors for stable liposome immobilization. In every round of measurement one type of liposomes was immobilized on one of the two available channels in the instrument, the second channel carried the liposomes consisting of DOPC serving as a reference, since previous experiments shown no interaction between DOPC lipids and SecA (Kamel *et al.*, 2022). The liposome suspensions were applied on the corresponding chip channel until the plateau with maximum possible saturation of the chip surface was reached. The immobilization levels for each type of liposomes was observed to be different due to the physico-chemical properties of the resulting liposomes (figure 4.15). Immobilization of DOPC liposomes was reproducible in each immobilization round and was found to be the highest, reaching 8500 response units, whereas the immobilization of

DOPC:DOPG:DOPE (63:27:10 mol %) resulted in 5500 response units. The reason for the different immobilization levels is likely the presence of negative charges from DOPG lipids on the surface of the vesicles contributing to electrostatic repelling of the liposomes and less dense immobilization compared to zwitterionic DOPC in the reference channel. The lowest immobilization level with 5000 response units was observed for the liposomes carrying PEG 2000 PE lipids: The presence of the synthetic crowder on the surface provided another steric barrier around each vesicle thereby limiting the amount of possible immobilized liposomes. Furthermore, the saturation of the chip surface was slower and required a longer contact phase to archive saturation (figure 4.15). Notably, the same type of the liposomes but with reconstituted SecYEG led to higher immobilization response. Attachment of the proteo-liposomes resulted in immobilization levels around 7500 response units, probably due to higher mass or divergency in the refractive index as a result of the reconstitution of SecYEG.

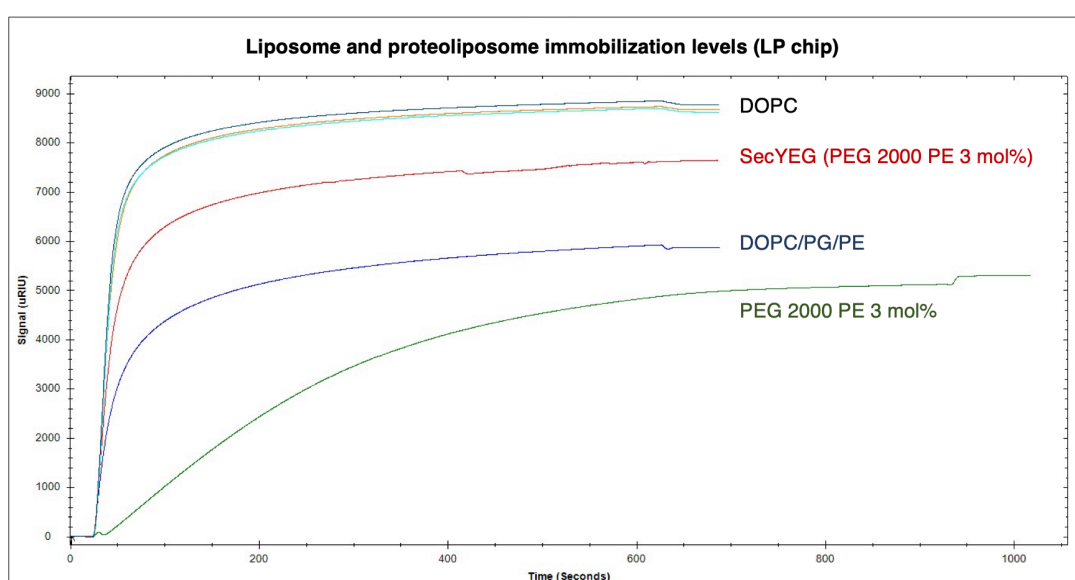


Figure 4.15: Immobilization levels of empty liposomes and SecYEG proteoliposomes on LP chip for SPR measurement of SecA binding.

For each measurement 1  $\mu$ M SecA was injected for 180 s on both chip channels followed by 600 s dissociation phase. In each measurement round, binding of SecA to the reference channel was found to be reproducible (figure 4.16). Since SecA protein does not interact with DOPC lipids (Kamel *et al.*, 2022), the unspecific binding to the carboxymethyl dextran layer is assumed. In the independent preliminary tests, SecA flow over the bare sensor surface resulted in high response supporting this hypothesis (data not shown). The reference channel with DOPC was therefore subtracted from the actual measurement on the neighboring chip channel to account for the unspecific interaction with the matrix of the sensor.

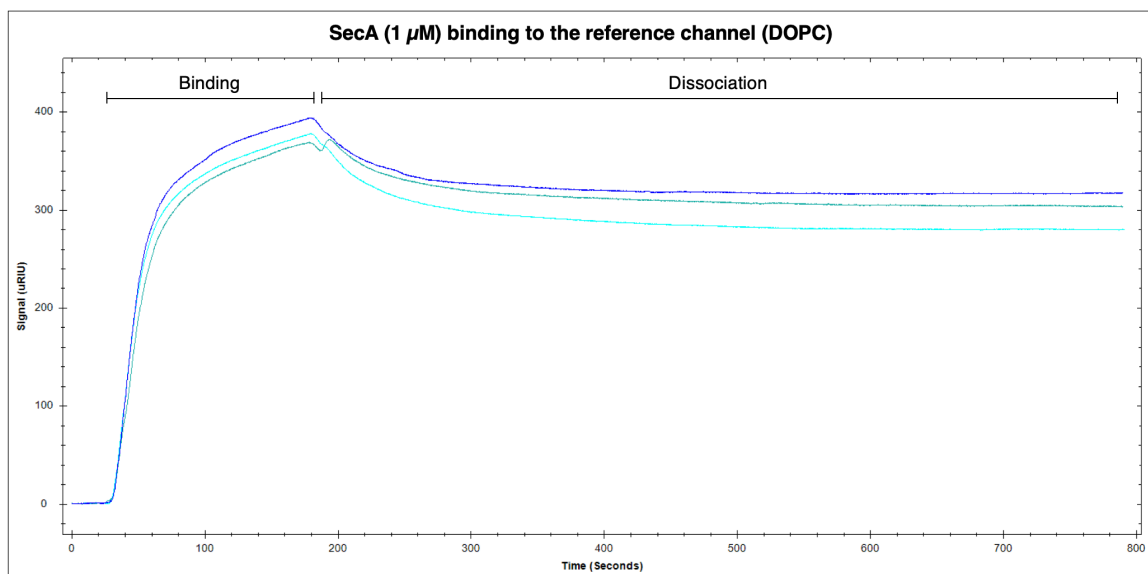


Figure 4.16: Injection of SecA ( $1 \mu\text{M}$ ) on the reference channel with immobilized DOPC vesicles characterized by association (180s) and dissociation (600 s) phases.

Corrected SPR sensorgram of SecA binding to the immobilized liposomes are shown in the figure 4.17. The highest response of approx. 580 units was measured with the non-crowded liposomes consisting of DOPC:DOPG:DOPE (indicated as DOPC/PG/PE). The interaction of SecA with the PEG-coated liposomes was suppressed, as the maximal response of this binding reached only 240 response units. Binding of SecA to SecYEG reconstituted in liposomes with PEG 2000 PE showed the elevated response of around 400 response units.

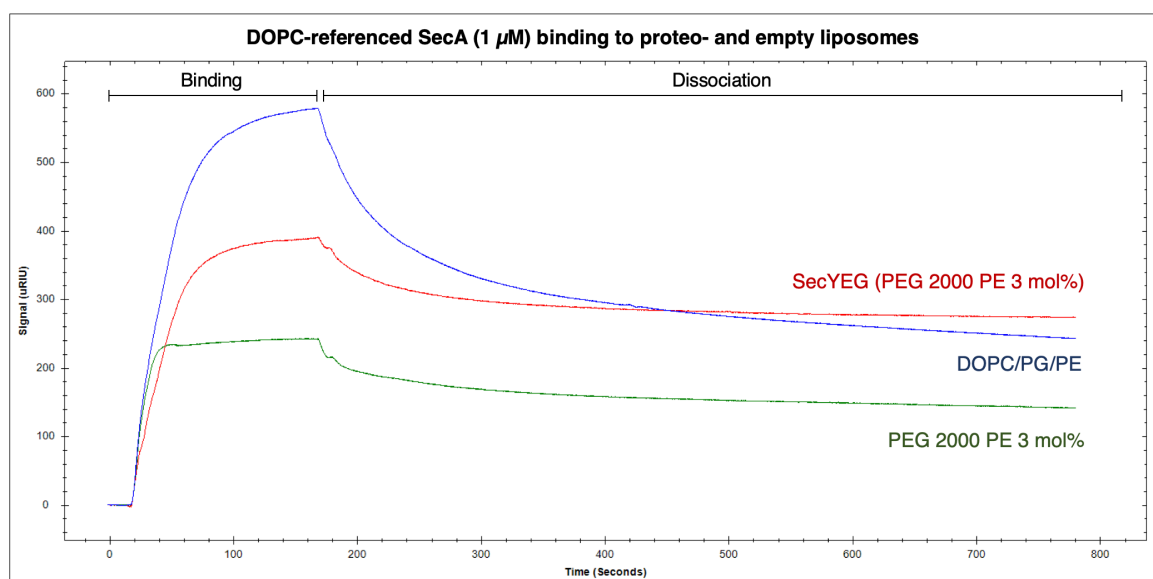


Figure 4.17: Interaction of SecA ( $1 \mu\text{M}$ ) with non-crowded and PEG 2000 PE (3 mol %) crowded liposomes as well as with SecYEG proteoliposomes in presence of 3 mol % PEG 2000 PE.

This experiment provides a qualitative information on the SecA binding yet delivers an independent confirmation for the results observed in the flotation assay indicating that the presence of SecYEG can restore the association of SecA with vesicles in presence of crowders.

### C. Proteinaceous crowding at the membrane interface

While the synthetic polymers are commonly used in the macromolecular crowding research for simulation of excluded volume effect, it is important to keep in mind that the native environment of the living cell is represented by various biological molecules, first of all proteins and nucleic acids. Employment of the proteins as crowding agents creates a native-like, physiologically relevant environment for the investigation of effects of macromolecular crowding on biological systems. For simulation of the crowding on the liposome interface, the recombinant mSA protein with molecular mass of 15.5 kDa was chosen as a proteinaceous model crowder. mSA can be conveniently coupled to the liposomal surface via two different binding modes, i.e. via mSA:biotin interaction through the biotinylated lipids or via complexation of His-tag with DGS-NTA( $\text{Ni}^{2+}$ ) lipids incorporated into model liposomes, as described in Chapters 3.2 and 3.3.2. For coupling mSA to the liposomal surface, lipid mixtures were prepared containing 10 mol % of either 18:1 biotinyl cap PE or 18:1 DGS NTA( $\text{Ni}^{2+}$ ) lipids in combination with DOPC (63 mol %) and DOPG (27 mol %) mixture and reconstituted SecYEG translocon.

The translocation assays were performed with the SecYEG-liposomes with different concentrations of biotinylated lipids (0, 2, 5 and 10 mol %) to study the influence on the translocation activity. Surprisingly, the translocation activity in liposomes was strongly depended on amount of the biotinylated lipids even in the absence of crowder (figure 4.18), and it was completely abolished in presence of 10 mol % of biotinyl cap PE lipids. Thus, this crowding strategy appeared not suitable for the study.

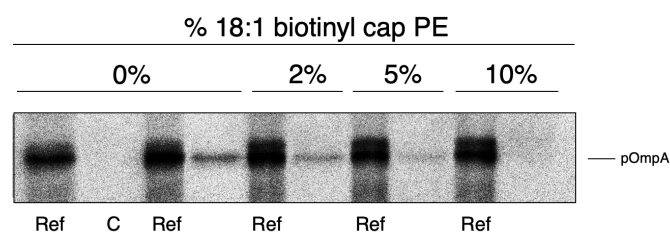


Figure 4.18: Translocation assay in non-crowded liposomes with different concentrations of 18:1 biotinyl cap PE lipids.

However, the liposomes composed of 10 mol % 18:1 DGS NTA(Ni<sup>2+</sup>) have shown a residual activity (data not shown) and were applied for probing the effects of interfacial crowding on protein translocation via SecYEG using mSA as crowder. Prior the experiments, His-tags of purified SecYEG and SecA were proteolytically removed to prevent non-physiological interactions of the translocation machinery with the NTA(Ni<sup>2+</sup>) lipids. The cleavage of the tag present on SecB failed in multiple attempts, so it was considered to exclude SecB from the translocation experiment. Lack of the stabilization of pOmpA by a chaperone can be also the reason why the translocation activity recorded in the following experiments was lower than expected.

Binding of mSA to the liposomal surface was confirmed using  $\alpha$ H-SecE crowding sensor from the Chapter 3.2. Three identical reconstitutions were performed resulting in the proteoliposomes containing either SecYEG translocon alone,  $\alpha$ H-SecE alone or in co-reconstitution of translocon with  $\alpha$ H-SecE crowding sensor. The molar P/L-ratio for the reconstitution was applied for the sensor with 1:3,000 and for SecYEG translocon with 1:1,000 and the reconstitution of both proteins was controlled via SDS-PAGE (figure 4.19-A). By the visual inspection the samples containing either SecYEG alone or in co-reconstitution with the crowding sensor showed similar reconstitution efficiency. Same was observed for the  $\alpha$ H-SecE sensor and upon its reconstitution with SecYEG. Emission spectra of the crowding sensor with and without addition of mSA as crowder agent were recorded in both types of liposomes. Next, the samples with the co-reconstituted translocon and the sensor, as well as the sample with the sensor only were mixed with an appropriate amount of mSA needed to saturate the available functional NTA(Ni<sup>2+</sup>) groups on the outer surface of the vesicles. The emission spectra were recorded prior and after addition of mSA and the ratios of fluorescence intensities of acceptor and donor (525 nm/475 nm) were estimated. The initial FRET  $F_A/F_D$  ratio was comparable in both samples:  $1.05 \pm 0.01$  and  $1.08 \pm 0.01$  for liposomes containing either  $\alpha$ H-SecE sensor alone or co-reconstituted with SecYEG respectively. Co-reconstitution of SecYEG with the sensor did not affect the signal of the sensor since SecYEG lacks large extramembrane domains. Upon addition of mSA an increase of approx. 6% of  $F_A/F_D$ -ratio in both samples indicating successful attachment of protein to the liposomal surface.

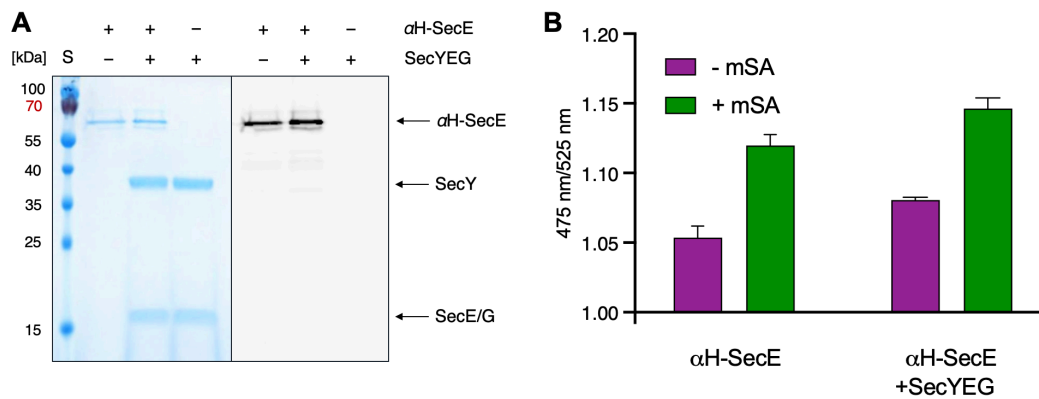


Figure 4.19: (A) SDS-PAGE analysis with corresponding in-gel fluorescence of (co-)reconstitution of  $\alpha$ H-SecE crowding sensor from the Chapter 3.2 and Tag-less SecYEG in liposomes. (B) Response of the  $\alpha$ H-SecE sensor in proteoliposomes with and without SecYEG upon addition of mSA for mimicking of native-like proteinaceous interfacial crowding.

In the next step, the translocation assay was performed in presence of mSA using non-crowded liposomes as control. As already mentioned, the translocation activity drastically dropped in presence of 10 mol % DGS-NTA( $\text{Ni}^{2+}$ ) lipid in the model membranes. Upon quantification of in-gel fluorescence for the control without mSA addition the residual translocation activity was estimated to be  $3.1\% \pm 0.5\%$ . The amount of mSA protein added to the reaction tube was varied to reach a specific coverage of the liposomal surface (figure 4.20).

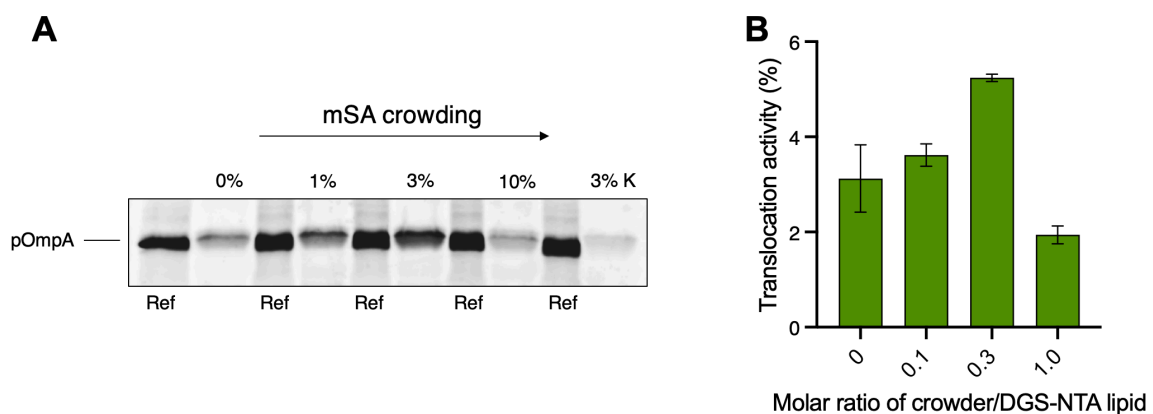


Figure 4.20: (A) SDS-PAGE analysis and (B) subsequent quantification ( $n=2$ ) of translocation assay in presence of proteinaceous interfacial crowding represented by mSA attached to the surface via His-tag to DGS-NTA( $\text{Ni}^{2+}$ ) lipids.

Surprisingly, the translocation activity increased to  $3.6\% \pm 0.2\%$  and  $5.2\% \pm 0.1$  in the samples with crowder/DGS-NTA lipid of 0.1 and 0.3 %, respectively, but once the mSA/ DGS-NTA lipid ratio of 1.0 was reached, the translocation activity decreased to  $1.9\% \pm 0.1$ . The estimated varying positive and negative effect on translocation activity upon different amounts of mSA on the surface of the proteoliposomes can be seen as a consequence from the crowding simulation.

### 3.4.4 Discussion

Existing scientific research literature demonstrates the significant impact of macromolecular crowding on diverse vital biological processes occurring in the dynamic environment of the living cell. In this chapter the effects of crowding in solution and interfacial crowding on the membrane were evaluated in regard to their ability to influence one of the most fundamental processes, translocation of preprotein via the SecA:SecYEG machinery. The translocation activity was shown to decrease monotonically with the increasing concentrations of Ficoll PM70 in solution and was attributed to the exclusion volume effect, rather than the rise of the viscosity, as suggested by the control experiment using glycerol to modulate the viscosity. Similar experiments using PEG as a crowder faced a methodological limitation due to the precipitation step involving TCA that led to co-precipitation of PEG in course of procession of established protocol (Kamel *et al.*, 2022; De Keyzer *et al.*, 2002). Instead, FRET-based assay was employed, which allows for the measurement of the real-time kinetics of the pOmpA-DHFR translocation intermediate formation at SecA:SecYEG. This assay was applicable only till around 25% (w/v) PEG concentration due to the increased solution viscosities, which led to the difficulties by homogeneous mixing of the sample. The reaction was performed in the presence of Ficoll PM70 and showed similar results to the translocation assay, where the Sec machinery manifested a two-fold decrease in activity at 25% Ficoll PM 70 (w/v), whereas the number of formed translocation intermediate in the FRET-based assay was also approximately halved, as concluded from the maximal signal intensity.

By the involvement of PEGs as crowders, the size-dependent and concentration-dependent decrease of the translocation intermediate formation was observed. Notably, the results obtained with PEG 1500 and Ficoll PM70 were comparable despite a smaller hydrodynamic radius and more compact conformation of PEG 1500. A minor increase of the translocation rates at low PEG 1500 and Ficoll PM70 were observed, followed by decrease at emerging crowder concentrations, presumably due to the limited diffusion (Minton, 2001). With increasing PEG size and concentrations, e.g. PEG 4000 and PEG 8000, the translocation rates were further decreased, and no formation of the SecYEG:pOmpA-DHFR translocation intermediate was observed at 25%, as no increase in the acceptor emission was detected. The decrease of the amplitude of the measured FRET signal and the decrease of the translocation rates suggests the inhibition of protein transport. Solution viscosity, which increases with the increasing size and concentration of PEG (González-Tello *et al.*, 1994; Junker *et al.*, 2019; Regupathi *et al.*, 2009) can play a role by the association of the translocation intermediate, however to the lesser extent. As was mentioned before, the translational and rotational diffusion of the biomacromolecules in the crowded environment does not depend on the bulk viscosity of the solution, how it is predicted by Stokes law (Eq. 1 and 2). Instead they experience a so-called micro-viscosity, which in turn depends on the size

relation of the target protein and the crowder. With the increasing crowder size, the emerging excluded volume effect in presence of the PEG crowders restricts the mobility and leads to the anomalous diffusion of probes. As a result, the effective interaction between the reactants are hindered by means of sieving effect (Junker *et al.*, 2019; Lavalette *et al.*, 2006).

Our experiments on interfacial crowding with synthetic crowders at the lipid membrane revealed a decrease of the translocation activity via SecYEG, which was analyzed in the membranes upon varying the size or the molar concentration of PEG-conjugated lipids. Application of the PEG 1000 PE at 3 mol % barely affected the translocation activity, whereas the doubling of the crowder size by involvement of PEG 2000 PE led to a two-fold decrease, and the largest crowder PEG 5000 PE at the same concentration induced more than 20-fold decrease of translocation activity. Same was observed by varying the molar concentration of PEG 2000 PE in the proteoliposomes, so at the highest abundance of the PEGylated lipids (10 mol %) no translocation activity could be detected.

To identify the reason for the observed experimental outcome, interactions of SecA with the surface-crowded liposomes and SecYEG-containing proteoliposomes were studied. SecA and SecYEG complex have to form a functional unit in order to translocate the substrate across the membrane, and SecA:lipid interaction can modulate the translocation activity (Kamel *et al.*, 2022; Koch *et al.*, 2016; Lill *et al.*, 1990; de Vrije *et al.*, 1988). Binding of SecA to the surface-crowded liposomes was strongly hindered by PEGylated lipids, and the effect correlated with their concentration and size. Presence of the SecYEG translocon partially restored SecA binding in the presence of the crowders, which explained the residual translocation activity. However even though the translocon was present in the membranes with 10 mol % of PEG 2000 PE and the SecA was shown to be associated with the proteoliposomes no translocation activity was observed, due to the induced surface crowding.

Binding of SecA to the crowded and non-crowded membrane vesicles as well as SecA:lipid:SecYEG interactions were additionally analyzed using SPR. Upon injection of SecA on the sensor chip surface coated with 3 mol % PEG 2000 PE crowded liposomes the reduction of approx. 60% of the binding response was observed, which suggests more efficient SecA binding to the vesicles than analyzed with flotation assay. It should be noted that the binding experiments in SPR were performed with higher salt concentration (150 mM KCl) as it was done in flotation assay (50 mM KCl, figure 4.9-B and 4.9-C). Still, it is predicted that increase of the ionic strength would weaken the association of SecA with membranes as it was reported previously (Kamel *et al.*, 2022) and was observed in flotation assay with SecYEG proteoliposomes (figure 4.10). The reason for elevated binding in SPR needs further characterization, but it may owe to the unspecific interactions of SecA with the dextran matrix exposed upon lower immobilization levels of PEGylated vesicles. Although the liposomal

suspensions were injected until the maximal saturation of chip surface, they all have shown different immobilization levels due to their alternating physico-chemical nature. The reason for this was briefly discussed in the Result chapter. Despite the differences in the immobilization levels, it is still reasonable to maintain the described measurement approach. Under assumption, that the same immobilization levels are applied for all the vesicles types and some of them would not reach the saturation on the chip surface, it is possible that the dextran coating would become more accessible to non-specific SecA binding, resulting in false-positive sensor response. However, the binding of SecA to SecYEG reconstituted in liposomes was restored, consistent with the results in flotation assay.

In addition to the results provided in the chapter, the performance of LD chip for the liposome mobilization was tested. In contrast to the used LP chip the LD chip is more suitable for the capturing of the vesicles and allows more efficient immobilization of liposomes on the chip surface. However, the 3D-like surface consisting of carboxymethyl dextran was more assessible for the unspecific SecA interaction. The same experiments were performed with this type of chip (data not shown) and were found to be qualitatively same, besides more pronounced binding of SecA to the reference channel covered with DOPC. On the other side, the immobilization of the liposomes on the LP chip led to a more efficient coverage of the chip surface thus “hiding” the chip matrix and restrain the unspecific SecA interaction. As an alternative method, the supported bilayers can be formed and the SecA binding can be measured with QCM (Kamel *et al.*, 2022). However, application of the PEGylated lipids for the formation of the supported bilayer may be challenging, since the steric effect of PEG may hinder the liposome rupture on the chip surface. Another approach for the introduction interfacial crowding has to be probed, and some options for this will be discussed below (Chapter 4).

Application of the proteinaceous crowders to the membrane interface for studying their effect on protein translocation via SecYEG proved to be challenging task. For the application of mSA crowder on the proteoliposomes surface two strategies were employed, via introduction of either 18:1 biotinyl cap PE or 18:1 DGS-NTA(Ni<sup>2+</sup>) lipids for binding mSA via mSA:biotin interaction or via complexation with mSA His<sub>6</sub>-tag, respectively. Unfortunately, the translocation activity decreased with increasing abundance of 18:1 biotinyl cap PE lipids in the synthetic membranes and no translocation of pOmpA was observed for the proteoliposomes containing 10 mol % 18:1 biotinyl cap PE, making this crowder coupling strategy unsuitable for the study. Presence of the biotin on the surface disturbed the translocation whereas the reason to this phenomenon remains currently unknown. However, the proteoliposomes with 10 mol % 18:1 DGS-NTA(Ni<sup>2+</sup>) lipids have shown residual translocation activity, even though the chaperone holdase SecB had to be omitted from the assay because of failed attempts to

---

remove the encoded His-tag by enterokinase cleavage, possibly due to a poor accessibility of the cleavage site.

The binding of mSA to the vesicle surface was confirmed upon employment of  $\alpha$ H-SecE crowding sensor from Chapter 3.2. Sensor response was similar on non-crowded liposomes with or without co-reconstituted SecYEG and increased upon addition of mSA, as it was already characterized before (Löwe *et al.*, 2023). At the low abundance of mSA on the proteoliposomal surface, crowder to DGS-NTA(Ni<sup>2+</sup>) lipid of 0.1 and 0.3, an increase in translocation activity was observed, whereas at the highest possible vesicle saturation (ratio of crowder to DGS-NTA(Ni<sup>2+</sup>) lipid of 1) the translocation activity decreased in comparison to the non-crowded sample. The mSA protein in this sample saturates the surface of the liposomes, thus is it possible that the binding of SecA is hindered. It is not clear what exactly led to the increase of translocation activity at low mSA levels. One of the possible explanations could be the partial shielding of positively charged NTA(Ni<sup>2+</sup>) groups, which may negatively influence the translocation machinery. However, it can be clearly seen that application of proteins to induce the interfacial crowding modulates translocation of pOmpA via SecYEG translocon.

## 4 Discussion and Outlook

### 4.1 Crowding sensors for macromolecular confinement in membranes

Studying the macromolecular crowding at membrane interfaces and its effects on biological processes requires mimicking the crowded environment *in vitro* in physiologically relevant ranges and systematic studies of crowding effects *in vivo*. However, the characterization of the macromolecular confinement at and near the biological membranes remains challenging. Developing sensors that allow a simple readout from *in vivo* and *in vitro* crowded systems would offer non-invasive tools helping to measure and accurately replicate the confinement in physiologically relevant range (Löwe *et al.*, 2020). So far, there is a limited number of approaches, that would allow this (Arnold *et al.*, 2023; Houser *et al.*, 2020; Takatori *et al.*, 2023). To facilitate the quantification of the interfacial crowding, we adapted the previously published version of the FRET-based crowding sensors (Boersma *et al.*, 2015). To apply the sensor for the analysis at biological interfaces, a membrane-anchoring strategy was developed and optimized. Transmembrane helices (TMHs) forming a helical hairpin or a helical bundle were perceived as suitable candidates for being the anchors since they demonstrate remarkable stability upon the lipid bilayer insertion (Engelman and Steitz, 1981) and their N- and C-termini face the same side with in respect to the membrane for correct positioning of the FRET fluorophores. Among possible candidates, THMs 1 and 2 of the translocon subunit SecE of *E. coli*, Mistic from *B. subtilis* and the THMs of *E. coli* RseC protein were evaluated. The helical hairpin of SecE proved to be the most suitable candidate for the current study and was applied for the further sensor development with two principally different sensor designs described in Chapter 3.2 and 3.3.2. Other tested anchoring domains were not able to fulfill the requirements regarding either efficient membrane insertion *in vivo* or reconstitution into synthetic vesicles *in vitro*, as well as the ability to respond to the crowding in solution or at the membrane interfaces. Further search for optimal anchoring domains may enable robust sensor application in different cell lines, e. g. for controlled targeting to specific organelles or plasma membrane compartments in eukaryotic cells.

To this point, two types of membrane-anchored sensors differing by design and distinct linker architectures connecting the fluorescent proteins to the anchor have been developed. The first type of sensors, described in Chapter 3.2, is built of SecE-based membrane anchor introduced between the fluorescent moieties of the sensor, that allows direct anchoring of the sensor in the membrane as a single-chain protein. The second type, described in Chapter 3.3.2, consists of two separate parts, the soluble sensory part and the SecE-based anchor. Both components can be coupled together via SpyTag:SpyCatcher interaction forming a covalent bond (Zakeri *et al.*, 2012), thus allowing a robust application of the sensor to the membrane interfaces from

the aqueous phase. The formation of the complexes with the SecE-SpyCatcher was successful in solution and in IMVs, while lower efficiency was observed at the interfaces of the liposomes. It remained not clear why the complexes formed with higher efficiency in the native membranes in comparison to the synthetic vesicles. Potentially, the SpyCatcher domain anchored in the IMVs is more exposed towards the aqueous phase, but also soft interactions with the endogenous proteins could attract the soluble sensor closer to the membrane thus allowing a more efficient reaction. A bottleneck of this sensor type, however, was the broad variation of  $F_A/F_D$  ratios upon reconstitution. For the *in vitro* calibration of this sensor type, improved binding between SpyTag-sensors and SecE-SpyCatcher should be achieved and the reconstitution protocol for the sensor complex should be adjusted.

In contrast, the single-chain sensors  $\alpha$ H-SecE and (GSG)<sub>6</sub>-SecE from the Chapter 3.2 yielded reliable and robust experimental data regardless of the lipid composition of the tested liposomes or type of crowder applied, i.e. synthetic or proteinaceous origin. The FRET signal of the sensor increased upon increasing the crowder abundance, as would be expected from the steric repulsion. We demonstrated the ability of  $\alpha$ H-SecE and (GSG)<sub>6</sub>-SecE constructs to fulfil the expected functions, being able to sense the confinement induced not only by PEGylated lipids, but also by different proteins attached on the liposomal surface. Moreover, the sensors in extracted IMVs manifested a signal within the range of values previously measured upon titration with different proteinaceous crowders. In addition, they were responsive to the surface crowding induced by addition of SecA protein, crowding in solution rendered by PEG, and also to forced dissociation of peripheral proteins (Suppl. Information, figure 13, Chapter 3.2).

The sensitivity of the single-chain sensors was estimated to be higher compared to the SpyTag:SpyCatcher-based sensors. The higher response is possibly due to the architecture of sensor, which minimizes the sensor elevation above the membrane. In contrast, for the SpyTag:SpyCatcher-based constructs, additional spacing is provided by the coupling element, so the crowder on the surface is not able to induce sufficient compression of the sensor. This may also explain the absence of the response of  $\alpha$ H-Spy-SecE and only a minor response of (GSG)<sub>6</sub>-Spy-SecE complexes upon crowding with PEGylated lipids, since the synthetic polymers have smaller molecular sizes with hydrodynamic radius of 0.9 nm for PEG 1000 (Chung *et al.*, 2019; Dong *et al.*, 2018) and PEG 2000 with 1.15 nm (Zhu *et al.*, 2016) compared to mSA with around 2.1 nm and its attached conformation accounting the linker of the biotinylated lipid (Wu and Wong, 2005). Therefore, single-chain and Spy-based sensors can be potentially applied for measuring the lateral confinement on different heights, thus allowing for crowding quantification either directly at the membrane, or within the proximate environment. The SpyTag:SpyCatcher-based system offers a great potential for different applications and should be further optimized and applied for the study of organization on the

cellular surfaces or extracellular space, e.g. dynamics of glycocalyx and bacterial lipopolysaccharides, or for the characterization of the phase-separations in the membrane proximity inside the cell.

However, even in case of the better-performing single-chain sensor constructs, further characterization and optimization is required. In collaboration with the Institute for Physical Chemistry, the steady-state anisotropy of the directly excited mCitrine was measured for the detergent-solubilized and liposome-reconstituted sensors,  $\alpha$ H-SecE and (GSG)<sub>6</sub>-SecE (experiments guided by Dr. Jakub Kubiak). The preliminary results revealed a decay of the anisotropy for the membrane-anchored sensor compared to the solubilized one. This can be an indicator of intramolecular FRET resulting from sensor's transient contacts within the membrane and/or their partial clustering. The transient contacts of the sensor molecules governed by diffusion within the lipid bilayer can be limited by reducing the sensors concentration. The possible contribution of clustering was further examined by the steady-state anisotropy measurements of mCerulean using a truncated mCerulean-SecE construct, described in Chapter 3.2. The estimated anisotropy of the DDM-solubilized mCerulean-SecE was barely different from the anisotropy measured for the same construct in extracted IMVs, in contradiction to the decreased anisotropy observed for the full-length sensor upon excitation of the mCitrine. That leads to the preliminary conclusion that mCitrine may mediate partial clustering of the sensor, thus affecting the read-out signal. The significance of the intramolecular FRET contribution was examined by varying inducer concentrations during sensor's expression. Although the sensor amount in the extracted IMVs correlated with the inducer concentration, only minor deviations of the sensor's response were observed. In another approach, truncated sensor constructs mCerulean-SecE and SecE-mCitrine were co-reconstituted in liposomes. The resulting  $F_A/F_D$  ratios were dependent on the amount of the reconstituted proteins and increased with higher abundance of the proteins in the membrane. However, the response of the truncated constructs upon induced crowding was significantly weaker in comparison to the full-length sensors. It may be concluded, that the contribution of the clustering is not expected to have significant effect on the measurements, when applied under the characterized conditions for the sensor's expression and reconstitution,

In summary, the presented architectures and designs of the crowding sensors, although functional, are not the endpoint of the research, but should be regarded as foundation for the further applications. They validate the feasibility and can be employed as a simple tool for characterizing crowding conditions *in vitro* and *in vivo*.

## 4.2 Effects of macromolecular crowding on protein targeting and translocation via SecYEG

A large fraction of proteins synthesized in *E. coli* should be either translocated through or inserted into the bacterial membrane. However, the studies of the protein biogenesis are commonly conducted in the oversimplified and minimalistic environment that does not reflect the naturally abundant crowding in the living cell. This thesis aimed to examine the effects of macromolecular crowding in solution and at the membrane interface on post-translational protein targeting and translocation via the SecA:SecYEG machinery. For this purpose, synthetic polymers were utilized to mimic the crowding in solution, and both synthetic and proteinaceous crowders were developed for rendering the confinement on the membrane interfaces. Two previously established methods to address the translocon functionality were applied, i.e. the protease-protection assay which measures the accumulation of multiple translocated substrates in the vesicle lumen, and FRET-based assay for the estimation of translocation kinetics and the effective amount of stalled SecYEG:pOmpA-DHFR translocation intermediates. Both methods revealed their specific limitations when studying effects of solution crowding on the translocation system. However, Ficoll PM70 and PEGs of different sizes at 25% (w/v) could be employed, showing that crowding in solution inhibits the translocation rates, and the transport is dependent on the type of the crowder, its size and the effective concentration. Increasing the volume fraction of the synthetic crowders may affect the translational mobility, thus providing a steric barrier for the assembly of the translocation intermediate and negatively influences the translocation rates. While the synthetic crowders are used mainly to mimic the exclusion volume effect, the interior of the living cell is crowded by biological molecules, where the influence of the quinary interactions gets more pronounced. As it was shown previously, proteins applied as crowders have a different effect on protein translational and rotational mobility in comparison to synthetic polymers (Junker *et al.*, 2019; Wang *et al.*, 2010), so the study of protein translocation in crowded solution should be continued in the presence of proteinaceous crowders, which are not related to the system of interest and can be concentrated to physiologically relevant concentrations.

Next to the crowding in solution, proteins and complexes that interact with membranes, e.g. cytoskeletal proteins, ribosome-nascent chain complexes, chaperone-stabilized secretory preproteins, and membrane-associated proteins, including the ATPase like SecA, experience also the crowding at the membrane interfaces. The interactions of such proteins with membrane surfaces and/or their interaction partners can be characterized *in vitro*. To render the interfacial crowding on the membranes, both synthetic or proteinaceous crowders were considered in this thesis. While PEGylated liposomes differing by the crowder size and the abundance can be routinely prepared using the commercially available PEG-conjugated lipids,

the native-like surface crowding requires proteins as crowding mimetics at the interfaces. Employment of proteins as crowders may lead to alternate experimental outcome, in comparison to the synthetic ones, due to the rise of the quinary interactions at the membrane surface and potential interferences with the targets in the experimental setup and should be studied in addition to the inert synthetic crowders. Proteins can be stably anchored at the membrane interfaces via covalent and non-covalent binding, for example by cross-linking or affinity binding to the modified lipid head groups, or via introduction of fusion proteins, which contain membrane-associate domains, e.g. transmembrane or amphipathic helices (Raghunath and Dyer, 2019; Snead *et al.*, 2017). The method for attachment of the proteinaceous crowders should be chosen carefully and be compatible with the assay used.

Real-time binding methods, such as SPR and QCM, can be used to characterize protein association and dissociation kinetics, and to determine and binding affinity at the crowded membrane surfaces, and can be employed for studying SecA:SecYEG interactions. For this, supported bilayers, but also liposomes or extracted native membrane vesicles can be immobilized on the sensor chip surfaces for the experiments via SPR (Erb *et al.*, 2000; Kamel *et al.*, 2022; De Keyzer *et al.*, 2003; Wu *et al.*, 2012). In a conventional QCM set-up, formation of supported bilayers is achieved upon saturation of the chip surface and subsequent rupture of the vesicles (Kamel *et al.*, 2022; Wang *et al.*, 2018). However, in our trials it was not possible to produce planar bilayer with PEGylated liposomes, since the crowder on the interface hindered fusion of the liposomes. As an alternative approach, lipids with modified head groups, e.g. NTA(Ni<sup>2+</sup>) or biotin, can be employed in QCM/SPR experiments for attachment of the crowders to the pre-formed supported lipid bilayer. Furthermore, the surface crowding may be rendered by synthetic polymers other than PEG, e.g. amphiphilic glycomacromolecules, which can be inserted into pre-formed supported bilayer (Banger *et al.*, 2021). QCM-D experiments should allow then quantifying the amount of the crowder on the surface by measuring the induced frequency shifts in response to the mass changes on the chip surface.

Another robust method described in this thesis is the flotation assay, which is easy to handle, fast and does not require specialized equipment and expertise. The assay may be applied not only for the protein:liposome binding studies, but can be used for estimation of reconstitution efficiency of membrane proteins. Flotation assay was successfully employed for the estimation of SecA interactions with non-crowded and PEG-crowded liposomes, where the suppressed SecA binding was observed upon increasing concentrations and sizes of PEGylated lipids, but was partially restored in the presence of reconstituted SecYEG translocon. Moreover, flotation assays with SecYEG proteoliposomes served for the quality control, as it indicated that the reconstitution efficiency of the translocon was dependent on the concentration and on the size of the surface exposed PEG. Lower reconstitution efficiency could be readily explained by additional steric barrier provided to PEG. However, no significant changes in the translocation

activity were observed, likely due to limited number of available SecA and saturation of the translocation reaction. In the samples with the highest applied surface crowding rendered by PEGylated lipids, SecA was found to be barely associated with the proteoliposomes and no translocation activity was observed despite approximately 30% of SecYEG being reconstituted.

In the trial experiments on protein-based crowding, another complication was encountered. Anchoring of the crowders to the membrane surfaces was achieved by means of either 18:1 biotinyl cap PE or 18:1 DGS-NTA(Ni<sup>2+</sup>) lipids present in the liposomes. However, those lipids severely inhibited the functionality of the SecA:SecYEG machinery. The presence of biotinylated lipids strongly downregulated the preprotein secretion via SecYEG, whereas the modified DGS-NTA(Ni<sup>2+</sup>) head groups reduced the translocation activity for more than 10-fold, possibly due to the added positive charges on the liposomal surface. The translocation activity is known to depend on the lipid composition of the membrane (Kamel *et al.*, 2022; Lill *et al.*, 1990; de Vrije *et al.*, 1988), and it seems also be affected by the modified lipid head groups. However, even with this obstacle, the preliminary experiment with induced surface crowding was performed and was shown to modulate the translocation activity. Notably, the translocation activity increased with the increasing abundance of the crowder, mSA, whereas at the highest possible liposome saturation of mSA on the proteoliposomal surface, the translocation activity was lower compared to the initial levels. While it is tempting to relate the stimulated translocation to crowding effects, it may also originate from partial shielding of NTA(Ni<sup>2+</sup>) groups on the vesicle surface. It is important to note, that the potential contribution of the soft interactions by application of proteins as crowders may have a considerable effect on the experimental outcome and the stimulation of the translocation activity cannot be excluded. To achieve a better understanding of the effects of native-like interfacial crowding on the translocation machinery, another strategy for the proteinaceous crowder attachment should be used for this system. The possible approaches are discussed in the Chapter 4.3.

In conclusion, the existing strategies for studying the translocation activity, as well as the characterization of protein-membrane interactions were adapted to examine the effects of macromolecular crowding on the post-translational translocation via the SecYEG machinery. It was shown that emerging exclusion volume effect in solution and at the membrane interfaces negatively influences both the assembly of the translocation machinery components and their translocation activity, making a first step towards contribution to a more comprehensive understanding on how the complex bioprocesses are influenced by the confined environment of the living cell.

## 4.3 Outlook

### 4.3.1 The future perspectives for the membrane-associated crowding sensor

The  $\alpha$ H-SecE and (GSG)<sub>6</sub>-SecE sensors for the interfacial crowding were characterized *in vitro*, as their ability to respond to changing confinement in native and synthetic membranes was validated. The results *in vivo* suggested that both sensors are inserted in the inner membrane of *E. coli* cells, thus allowing further investigations of the dynamic crowding in living cells. The sensor response *in vivo* may be measured by advanced microscopic methods, such as laser scanning microscopy (LSM) or by fluorescence activated cell sorting (FACS) technique, which was shown to be compatible for FRET measurements in living cells (He *et al.*, 2003). For this goal, expression, membrane insertion and functional characterization of the sensor response should be continued in different bacterial strains and in eukaryotic cells. Also, further exploration of new candidates for anchoring, their characterization and optionally engineering is beneficial for the delivery of the crowding sensor to specific organelles and membrane domains. In their turn, the two-component sensors  $\alpha$ H-SpyTag and (GSG)<sub>6</sub>-SpyTag may be employed for the quantification of crowding confinement at the cellular surfaces, since they can be applied externally to the exposed SpyCatcher-modified anchors, for example for studies of glycocalyx dynamics or measurements of bacterial LPS densities. Also, for this application a suitable transmembrane anchor should be found and evaluated.

As discussed in Chapter 2, the first generation of the membrane crowding sensors can be further improved by substitution of the one of the fluorescent proteins forming the FRET pair for the SNAP-tag (figure 4.1). The enzyme was engineered from human O<sup>6</sup>-alkylguanine-DNA alkyltransferase, a DNA repair protein, that performs a covalent binding with O<sup>6</sup>-benzylguanine derivatives (Dreyer *et al.*, 2023; Juillerat *et al.*, 2003). The benzylguanine substrates for the SNAP-tag are commercially available, allowing for coupling with variety of the fluorescent dyes with a high labeling efficiency, both *in vitro* and *in vivo*. These substrates, depending on the application type, can be used for labeling of SNAP-tag fusion proteins on the cellular surfaces or even inside the cell by employment of specialized cell-permeable substrates. Moreover, the substrates can be designed in the way that fluorescence is switched only after the conjugation with SNAP-tag is achieved, which reduced the background fluorescence from the free substrate. This can be achieved with employment of the quencher, which is then released together with guanine (Sun *et al.*, 2011). Application of a synthetic fluorophore instead of one of the fluorescent proteins may additionally reduce the non-specific soft interactions between the sensor and proteinaceous environment when applied *in vivo* or by calibration of sensor with proteinaceous crowders *in vitro*.

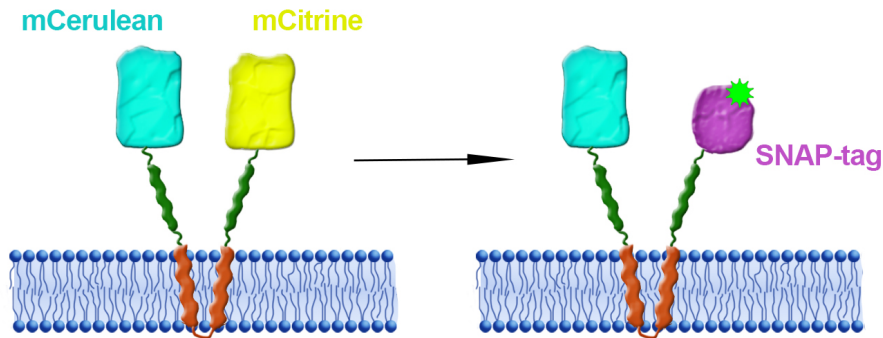


Figure 4. 1: Design of the crowding sensor with SNAP-tag

#### 4.3.2 Overcoming obstacles for the characterizations of crowding effects on protein targeting and translocation via SecYEG

The translocation via the SecA:SecYEG machinery was inhibited by soluble synthetic crowders, and the effect was dependent on the crowders type, size and concentration, while application of proteins as crowders may lead to the divergent results. The translational and rotational mobility of the proteins in the presence of crowders of proteinaceous origin was shown to have complex, crowder-specific effects (Wang *et al.*, 2010). Several proteins, that can be obtained at high concentrations to match the physiological crowding levels, e.g. BSA or lysozyme, could be potentially employed in translocation assays in the further perspective as crowders (figure 4.2-A). However, the conventional methods, such as the protease-protection assay, would be possibly difficult to employ under crowded conditions. As SDS-PAGE is involved to visualize the translocated protein, abundant proteinaceous crowders may disturb the band migration and affect the subsequent quantification. However, for the application of the surface crowders this method will be still suitable, since a low amount of proteoliposomes are required for the translocation which in turn lowers the overall amount of crowder employed in assay. Alternatively, fluorescence-based methods, including FRET, may be utilized to measure translocon activity, while binding of the SecA ATPase to the membrane interfaces can be potentially probed by QCM. The adsorption of SecA on the supported lipid bilayer can be compared in the presence of various crowders of synthetic or proteinaceous origin in the mobile phase. The association and dissociation kinetics may deliver more insights on how confined environments influence SecA:membrane interaction.

As it was shown, the strategy for binding crowders to the surface of the model membranes has to be chosen with care, since it may occur to be incompatible with the studied targets. Here, introduction of lipids with functional head groups, biotinylated or carrying  $\text{Ni}^{2+}$ -NTA, led to decrease of the translocation activity of the SecA:SecYEG machinery. Other approaches to mimic the confinement at the membrane interfaces may be further explored, for example

insertion of custom-designed amphiphilic glycomacromolecules with various sizes into pre-formed proteoliposomes as shown in figure 4.2-B (Banger *et al.*, 2021). This can allow a uniform reconstitution of the translocon in samples with various surface crowding levels, and the crowding may be monitored by  $\alpha$ H-SecE FRET-sensor, as validated in Chapter 3.4. Generation of fusion proteins carrying either self-inserting amphipathic helices, tail-anchored domains or other membrane-targeting elements, e.g. fragments of pore-forming toxins, can be another option for the surface crowding by proteins (figure 4.2-C and 4.2-D). Epsin I ENTH domain can be inserted into membrane bilayer by its amphipathic helix, but requires binding to phosphatidylinositol-4,5- biphosphate lipid and can may cause deformation of the membrane, when present at high surface concentration (Stachowiak *et al.*, 2012). Using this strategy, the occupancy of the membrane surface and compatibility with the studied system should be characterized with care. Another possibility would be co-reconstitution of fusion proteins with introduced transmembrane domain together with the SecYEG translocon. As transmembrane domain the helical hairpin of SecE domain can be used, since it can be reconstituted with high efficiency, as it was shown for the SecE-SpyCatcher protein used as anchor for the FRET-sensor constructs in the Chapter 3.3.2. Instead of SpyCatcher, proteins with various molecular sizes can be encoded and expressed recombinantly. However, the method would be also limited by a low yield of final product extracted from the membranes and the reconstitution efficiency of both, crowder and translocon, has to be characterized for each experiment for example by flotation assay.

Whereas the research in this thesis primarily focused on the post-translational pathway, the effects of the macromolecular crowding on the co-translational transmembrane transport and insertion via SecYEG remain unexplored. Experimental approaches described in this thesis may be further optimized and implemented to get valuable insights on how RNCs and SecYEG interaction is affected in crowded environments.

Another interesting approach would be to characterize the influence of the in-membrane crowding on the translocation activity. LacY protein, the symporter for the H<sup>+</sup> ions and lactose, is an integral membrane protein, that consists of 12 THMs organized in two bundles of six helices bound together by the cytoplasmic loop (Abramson and Wright, 2021; Kaback *et al.*, 2011). The absence of the large extramembrane domains makes this protein for a good candidate for simulation of naturally occurring membrane confinement.

In perspective, the intensively debated oligomeric state of SecYEG can be characterized using the established crowded membrane systems. It was shown that a single translocon can conduct the translocation (Kedrov *et al.*, 2011), however, the stabilization of dimeric structure was observed by interactions with cardiolipin (Gold *et al.*, 2010), as well as SecYEG dimers and higher oligomeric species were observed in extracted IMVs and proteoliposomes.

However, this can be a result of high translocon concentration achieved by overexpression or reconstitution, as only monomers and dimers were observed at naturally abundant concentrations in the wild-type membranes (Bessonneau *et al.*, 2002). The dynamic dimerization of the translocon can be the consequence of the naturally occurring macromolecular crowding conditions that would favor the assembly of the complexes and take part in the sorting processes in heterogenic biological membranes.

Concluding this study, it is important to note that this thesis serves not as a final chapter; instead it can be seen as a starting point for further research. The establishment and validation of current strategies and developed tools has revealed a pathway for optimizing the system for the study of the effects of macromolecular crowding on the vital membrane-related processes.

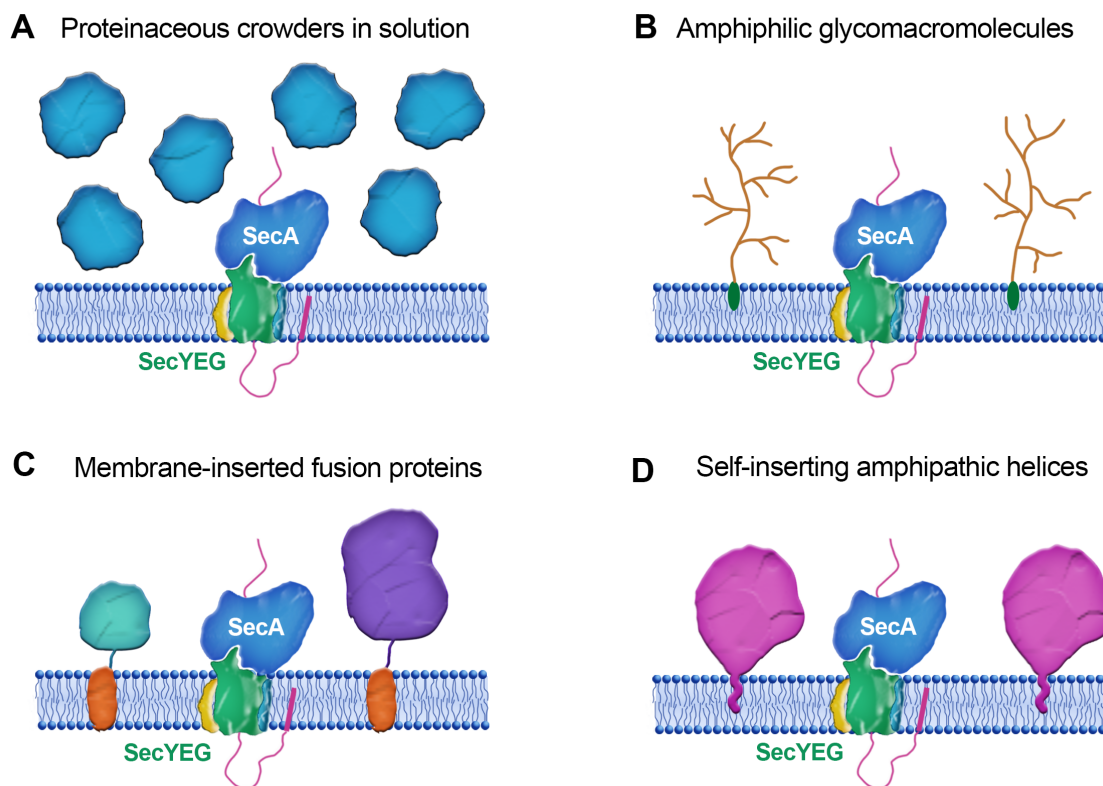


Figure 4.2: Further perspectives for studying of translocation via the SecA:SecYEG machinery: (A) employment of proteinaceous crowders in solution, (B) insertion of custom designed amphiphilic glycomacromolecules, (C) development of membrane-anchored fusion proteins with various sizes or (D) introduction of self-inserting amphipathic helices

## 5 References

- Abramson, J. and Wright, E.M. (2021), “*Function Trumps Form in Two Sugar Symporters, LacY and vSGLT*”, *International Journal of Molecular Sciences*, Vol. 22 No. 7, doi: 10.3390/ijms22073572.
- Acosta, L.C., Perez Goncalves, G.M., Pielak, G.J. and Gorenssek-Benitez, A.H. (2017), “*Large cosolutes, small cosolutes, and dihydrofolate reductase activity*”, *Protein Science*, Vol. 26 No. 12, pp. 2417–2425, doi: 10.1002/pro.3316.
- Adams, L.M., Andrews, R.J., Hu, Q.H., Schmit, H.L., Hati, S. and Bhattacharyya, S. (2019), “*Crowder-Induced Conformational Ensemble Shift in Escherichia coli Prolyl-tRNA Synthetase*”, *Biophysical Journal*, Biophysical Society, Vol. 117 No. 7, pp. 1269–1284, doi: 10.1016/j.bpj.2019.08.033.
- Ádén, J. and Wittung-Stafshede, P. (2014), “*Folding of an unfolded protein by macromolecular crowding in vitro*”, *Biochemistry*, Vol. 53 No. 14, pp. 2271–2277, doi: 10.1021/bi500222g.
- André, A.A.M. and Spruijt, E. (2020), “*Liquid–liquid phase separation in crowded environments*”, *International Journal of Molecular Sciences*, Vol. 21 No. 16, doi: 10.3390/ijms21165908.
- Arkowitz, A.R., Joly, C.J. and Wickner, W. (1993), “*Translocation can drive the unfolding of a preprotein domain*”, *The EMBO Journal*, Vol. 12 No. 1, pp. 243–253, doi: 10.1021/bi00061a021.
- Arnold, D.P., Xu, Y. and Takatori, S.C. (2023), “*Antibody binding reports spatial heterogeneities in cell membrane organization*”, *Nature Communications*, Vol. 14(1):2884, doi: 10.1038/s41467-023-38525-2.
- Banger, A., Sindram, J., Otten, M., Kania, J., Wilms, D., Strzelczyk, A., Miletic, S., *et al.* (2021), “*Synthesis and self-assembly of amphiphilic precision glycomacromolecules*”, *Polymer Chemistry*, Royal Society of Chemistry, Vol. 12 No. 33, pp. 4795–4802, doi: 10.1039/d1py00422k.
- Bechtluft, P., Nouwen, N., Tans, S.J. and Driessen, A.J.M. (2010), “*SecB - A chaperone dedicated to protein translocation*”, *Molecular BioSystems*, Vol. 6 No. 4, pp. 620–627, doi: 10.1039/b915435c.
- Berg, B. van den, Ellis, R.J. and M.Dobson, C. (1999), “*Effects of macromolecular crowding on protein folding and aggregation*”, *The EMBO Journal*, Vol. 18 No. 24, pp. 6927–6933, doi: 10.1016/j.bbrc.2020.06.156.

- Bessonneau, P., Besson, V., Collinson, I. and Duong, F. (2002), "*The SecYEG preprotein translocation channel is a conformationally dynamic and dimeric structure*", *The EMBO Journal*, Vol. 21 No. 5, pp. 995–1003, doi: 10.1093/emboj/21.5.995.
- Boersma, A.J., Zuhorn, I.S. and Poolman, B. (2015), "*A sensor for quantification of macromolecular crowding in living cells*", *Nature Methods*, Vol. 12 No. 3, pp. 227–229, doi: 10.1038/nmeth.3257.
- Bolhuis, A. (2004), "*The archaeal Sec-dependent protein translocation pathway*", *Philosophical Transactions of the Royal Society B: Biological Sciences*, Vol. 359, pp. 919–927, doi: 10.1098/rstb.2003.1461.
- Bramkamp, M. and Lopez, D. (2015), "*Exploring the Existence of Lipid Rafts in Bacteria*", *Microbiology and Molecular Biology Reviews*, Vol. 79 No. 1, pp. 81–100, doi: 10.1128/mnbr.00036-14.
- Breukink, E., Demel, R.A., de Korte-Kool, G. and de Kruijff, B. (1992), "*SecA Insertion into Phospholipids Is Stimulated by Negatively Charged Lipids and Inhibited by ATP: A Monolayer Study*", *Biochemistry*, Vol. 31 No. 4, pp. 1119–1124, doi: 10.1021/bi00119a021.
- Breydo, L., Reddy, K.D., Piai, A., Felli, I.C., Pierattelli, R. and Uversky, V.N. (2014), "*The crowd you're in with: Effects of different types of crowding agents on protein aggregation*", *Biochimica et Biophysica Acta - Proteins and Proteomics*, Vol. 1844 No. 2, pp. 346–357, doi: 10.1016/j.bbapap.2013.11.004.
- Chen, L., Novicky, L., Merzlyakov, M., Hristov, T. and Hristova, K. (2010), "*Measuring the energetics of membrane protein dimerization in mammalian membranes*", *Journal of the American Chemical Society*, Vol. 132 No. 10, pp. 3628–3635, doi: 10.1021/ja910692u.
- Chowdhury, A., Feng, R., Tong, Q., Zhang, Y. and Xie, X.-Q. (2012), "*Mistic and TarCF as fusion protein partners for functional expression of the cannabinoid receptor 2 in Escherichia coli*", *Protein Expression and Purification*, Vol. 83 No. 2, pp. 128–134, doi: 10.1016/j.pep.2012.01.008.
- Chung, S.Y., Lerner, E., Jin, Y., Kim, S., Alhadid, Y., Grimaud, L.W., Zhang, I.X., *et al.* (2019), "*The effect of macromolecular crowding on single-round transcription by Escherichia coli RNA polymerase*", *Nucleic Acids Research*, Oxford University Press, Vol. 47 No. 3, pp. 1440–1450, doi: 10.1093/nar/gky1277.
- Corradi, V., Mendez-Villuendas, E., Ingólfsson, H.I., Gu, R.X., Siuda, I., Melo, M.N., Moussatova, A., *et al.* (2018), "*Lipid-Protein Interactions Are Unique Fingerprints for Membrane Proteins*", *ACS Central Science*, Vol. 4 No. 6, pp. 709–717, doi:

10.1021/acscentsci.8b00143.

Dedmon, M.M., Patel, C.N., Young, G.B. and Pielak, G.J. (2002), "*FlgM gains structure in living cells*", Proceedings of the National Academy of Sciences of the United States of America, Vol. 99 No. 20, pp. 12681–12684, doi: 10.1073/pnas.202331299.

Démery, V. and Lacoste, D. (2018), "*Mechanical factors affecting the mobility of membrane proteins*", Physics of Biological Membranes, Springer, pp. 191–211, doi: 10.1007/978-3-030-00630-3\_8.

Dong, X., Al-Jumaily, A. and Escobar, I.C. (2018), "*Investigation of the use of a bio-derived solvent for non-solvent-induced phase separation (NIPS) fabrication of polysulfone membranes*", Membranes, Vol. 8 No. 2:23, doi: 10.3390/membranes8020023.

Dreyer, R., Pfukwa, R., Barth, S., Hunter, R. and Klumperman, B. (2023), "*The Evolution of SNAP-Tag Labels*", Biomacromolecules, Vol. 24 No. 2, pp. 517–530, doi: 10.1021/acs.biomac.2c01238.

Duncan, A.L., Reddy, T., Koldsø, H., Hélie, J., Fowler, P.W., Chavent, M. and Sansom, M.S.P. (2017), "*Protein crowding and lipid complexity influence the nanoscale dynamic organization of ion channels in cell membranes*", Scientific Reports, Vol. 7 No. 1, pp. 1–15, doi: 10.1038/s41598-017-16865-6.

Dundas, C.M., Demonte, D. and Park, S. (2013), "*Streptavidin-biotin technology: Improvements and innovations in chemical and biological applications*", Applied Microbiology and Biotechnology, Vol. 97 No. 21, pp. 9343–9353, doi: 10.1007/s00253-013-5232-z.

Dupuy, A.D. and Engelman, D.M. (2008), "*Protein area occupancy at the center of the red blood cell membrane*", Proceedings of the National Academy of Sciences of the United States of America, Vol. 105 No. 8, pp. 2848–2852, doi: 10.1073/pnas.0712379105.

Dvir, H. and Choe, S. (2009), "*Bacterial expression of a eukaryotic membrane protein in fusion to various *Mistic* orthologs*", Protein Expression and Purification, Vol. 68(1), pp. 28–33, doi: 10.1016/j.pep.2009.06.007.

Edmond, E. and Ogston, A.G. (1968), "*An approach to the study of phase separation in ternary aqueous systems.*", The Biochemical Journal, Vol. 109(4), pp. 569–576, doi: 10.1042/bj1090569.

Ellis, R.J. (2001), "*Macromolecular crowding: Obvious but underappreciated*", Trends in Biochemical Sciences, Vol. 26 No. 10, pp. 597–604, doi: 10.1016/S0968-0004(01)01938-7.

Ellis, R.J. and Minton, A.P. (2003), "*Join the crowd*", Nature Cell Biology, Vol. 425 (Sept), pp.

---

27–28.

- Engelman, D.M. and Steitz, T.A. (1981), “*The spontaneous insertion of proteins into and across membranes: The helical hairpin hypothesis*”, *Cell*, Vol. 23 (Februa, pp. 135–146, doi: 10.1142/9789811215865\_0012.
- Erb, E.M., Chen, X., Allen, S., Roberts, C.J., Tendler, S.J.B., Davies, M.C. and Forsén, S. (2000), “*Characterization of the surfaces generated by liposome binding to the modified dextran matrix of a surface plasmon resonance sensor chip*”, *Analytical Biochemistry*, Vol. 280, pp. 29–35, doi: 10.1006/abio.1999.4469.
- Flaugh, S.L. and Lumb, K.J. (2001), “*Effects of macromolecular crowding on the intrinsically disordered proteins c-Fos and p27Kip1*”, *Biomacromolecules*, Vol. 2(2), pp. 538–540, doi: 10.1021/bm015502z.
- Frick, M., Schmidt, K. and Nichols, B.J. (2007), “*Report Modulation of Lateral Diffusion in the Plasma Membrane by Protein Density*”, *Current Biology* 17, Vol. 17(5), pp. 462–467, doi: 10.1016/j.cub.2007.01.069.
- Gnutt, D., Gao, M., Brylski, O., Heyden, M. and Ebbinghaus, S. (2015), “*Excluded-volume effects in living cells*”, *Angewandte Chemie - International Edition*, Vol. 54(8), pp. 2548–2551, doi: 10.1002/anie.201409847.
- Gold, V.A.M., Robson, A., Bao, H., Romantsov, T., Duong, F. and Collinson, I. (2010), “*The action of cardiolipin on the bacterial translocon*”, *Proceedings of the National Academy of Sciences of the United States of America*, Vol. 107 No. 22, pp. 10044–10049, doi: 10.1073/pnas.0914680107.
- González-Tello, P., Camacho, F. and Blázquez, G. (1994), “*Density and Viscosity of Concentrated Aqueous Solutions of Polyethylene Glycol*”, *Journal of Chemical and Engineering Data*, Vol. 39, pp. 611–614, doi: 10.1021/jc00018a028.
- Green, M.N. (1990), “*Avidin and Streptavidin*”, *Methods in Enzymology*, Vol. 184, pp. 51–67, doi: 10.1016/0076-6879(90)84259-J.
- Guinier, A. (1939), “*Diffraction of x-rays of very small angles-application to the study of ultramicroscopic phenomenon*”, *Annales de Physique*, Vol. 12, pp. 161–237, doi: 10.1016/0146-3535(89)90023-3.
- Hancock, R. (2007), “*Packing of the polynucleosome chain in interphase chromosomes: Evidence for a contribution of crowding and entropic forces*”, *Seminars in Cell and Developmental Biology*, Vol. 18(5), pp. 668–675, doi: 10.1016/j.semcd.2007.08.006.
- Harder, T., Scheiffele, P., Verkade, P. and Simons, K. (1998), “*Lipid domain structure of the plasma membrane revealed by patching of membrane components*”, *Journal of Cell*

- Biology, Vol. 141 No. 4, pp. 929–942, doi: 10.1083/jcb.141.4.929.
- Harrison, B. and Zimmerman, S.B. (1984), “*Polymer-stimulated ligation: enhanced ligation of oligo- and polynucleotides by T4 RNA ligase in polymer solutions*”, *Nucleic Acids Research*, Vol. 12 No. 21, pp. 8235–8251, doi: 10.1093/nar/gkh100.
- Hatters, D.M., Minton, A.P. and Howlett, G.J. (2002), “*Macromolecular crowding accelerates amyloid formation by human apolipoprotein C-II*”, *Journal of Biological Chemistry*, Vol. 277 No. 10, pp. 7824–7830, doi: 10.1074/jbc.M110429200.
- He, L., Bradrick, T.D., Karpova, T.S., Wu, X., Fox, M.H., Fischer, R., McNally, J.G., *et al.* (2003), “*Flow Cytometric Measurement of Fluorescence (Förster) Resonance Energy Transfer from Cyan Fluorescent Protein to Yellow Fluorescent Protein Using Single-Laser Excitation at 458 nm*”, *Cytometry Part A*, Vol. 53, pp. 39–54, doi: 10.1002/cyto.a.10037.
- Hedin, L.E., Illergård, K. and Elofsson, A. (2011), “*An introduction to membrane proteins*”, *Journal of Proteome Research*, Vol. 10(8), pp. 3324–3331, doi: 10.1021/pr200145a.
- Houser, J.R., Busch, D.J., Bell, D.R., Li, B., Ren, P. and Stachowiak, J.C. (2016), “*The impact of physiological crowding on the diffusivity of membrane bound proteins*”, *Soft Matter*, Royal Society of Chemistry, Vol. 12(7), pp. 2127–2134, doi: 10.1039/c5sm02572a.
- Houser, J.R., Hayden, C.C., Thirumalai, D. and Stachowiak, J.C. (2020), “*A Förster Resonance Energy Transfer-Based Sensor of Steric Pressure on Membrane Surfaces*”, *Journal of the American Chemical Society*, Vol. 142 No. 49, pp. 20796–20805, doi: 10.1021/jacs.0c09802.
- Howarth, M., Chinnapen, D.J.F., Gerrow, K., Dorrestein, P.C., Grandy, M.R., Kelleher, N.L., El-Husseini, A., *et al.* (2006), “*A monovalent streptavidin with a single femtomolar biotin binding site*”, *Nature Methods*, Vol. 3 No. 4, pp. 267–273, doi: 10.1038/nmeth861.
- Hyman, A.A. and Brangwynne, C.P. (2011), “*Forum Beyond Stereospecificity: Liquids and Mesoscale Organization of Cytoplasm*”, *Developmental Cell*, Vol. 21, pp. 14–16, doi: 10.1016/j.devcel.2011.06.013.
- Jancsik, V., Keleti, T., Nagy, M., Fenyvesi, E., Bartha, A., Rudas, A., Kovacs, P., and Wolfram, E. (1979), “*Effect of Soluble Polymers on the Kinetic Properties of Aldolase and D-glyceraldehyde3-phosphate*”, *Journal of Molecular Catalysis*, Vol. 6(1), pp. 41–49, doi: 10.1016/0304-5102(79)85017-8.
- Jancsik, V., Keleti, T., Biczók, G., Nagy, M., Szabó, Z. and Wolfram, E. (1976), “*Kinetic properties of aldolase in polymer solutions*”, *Journal of Molecular Catalysis*, Vol. 1 No. 2, pp. 137–144, doi: 10.1016/0304-5102(76)80007-7.
- Javanainen, M., Martinez-Seara, H., Metzler, R. and Vattulainen, I. (2017), “*Diffusion of*

- 
- Integral Membrane Proteins in Protein-Rich Membranes*", Journal of Physical Chemistry Letters, Vol. 8(17), pp. 4308–4313, doi: 10.1021/acs.jpcclett.7b01758.
- Jeon, J.H., Javanainen, M., Martinez-Seara, H., Metzler, R. and Vattulainen, I. (2016), "*Protein crowding in lipid bilayers gives rise to non-Gaussian anomalous lateral diffusion of phospholipids and proteins*", Physical Review X, Vol. 6 No. 2, pp. 1–17, doi: 10.1103/PhysRevX.6.021006.
- Ji-Ann Lee, and K.C.M.M.V.H. and Dien et al., 2013. (2010), "*The Functionally Active Mistic-Fused Histidine Kinase Receptor, EnvZ*", Biochemistry, Vol. 49(42), pp. 9089–9095, doi: 10.1021/bi1009248.The.
- Jiang, M. and Guo, Z. (2007), "*Effects of macromolecular crowding on the intrinsic catalytic efficiency and structure of enterobactin-specific isochorismate synthase*", Journal of the American Chemical Society, Vol. 129(4), pp. 730–731, doi: 10.1021/ja065064+.
- Juillerat, A., Gronemeyer, T., Keppler, A., Gendreizig, S., Pick, H., Vogel, H. and Johnsson, K. (2003), "*Directed Evolution of O<sup>6</sup>-Alkylguanine-DNA Alkyltransferase for Efficient Labeling of Fusion Proteins with Small Molecules In Vivo*", Chemistry & Biology, Vol. 10 (April), pp. 313–317, doi: 10.1016/S.
- Junker, N.O., Vaghefikia, F., Albarghash, A., Höfig, H., Kempe, D., Walter, J., Otten, J., et al. (2019), "*Impact of Molecular Crowding on Translational Mobility and Conformational Properties of Biological Macromolecules*", Journal of Physical Chemistry B, Vol. 123(21), pp. 4477–4486, doi: 10.1021/acs.jpccb.9b01239.
- Kaback, H.R., Smirnova, I., Kasho, V., Nie, Y. and Zhou, Y. (2011), "*The alternating access transport mechanism in LacY*", Journal of Membrane Biology, Vol. 239, pp. 85–93, doi: 10.1007/s00232-010-9327-5.
- Kamel, M., Löwe, M., Schott-Verdugo, S., Gohlke, H. and Kedrov, A. (2022), "*Unsaturated fatty acids augment protein transport via the SecA:SecYEG translocon*", FEBS Journal, Vol. 289, pp. 140–162, doi: 10.1111/febs.16140.
- Kedrov, A., Kusters, I., Krasnikov, V. V. and Driessen, A.J.M. (2011), "*A single copy of SecYEG is sufficient for preprotein translocation*", The EMBO Journal, Vol. 30 No. 21, pp. 4387–4397, doi: 10.1038/emboj.2011.314.
- Keeble, A.H. and Howarth, M. (2019), "*Insider information on successful covalent protein coupling with help from SpyBank*", Methods in Enzymology, Vol. 617, pp. 443–461, doi: 10.1016/bs.mie.2018.12.010.
- De Keyzer, J., Van der Does, C. and Driessen, A.J.M. (2002), "*Kinetic analysis of the translocation of fluorescent precursor proteins into Escherichia coli membrane vesicles*",

## 5 References

---

- Journal of Biological Chemistry, Vol. 277 No. 48, pp. 46059–46065, doi: 10.1074/jbc.M208449200.
- De Keyzer, J., Van Der Does, C., Kloosterman, T.G. and Driessen, A.J.M. (2003), “*Direct demonstration of ATP-dependent release of SecA from a translocating preprotein by surface plasmon resonance*”, Journal of Biological Chemistry, Vol. 278 No. 32, pp. 29581–29586, doi: 10.1074/jbc.M303490200.
- Kirchhoff, H. (2008), “*Molecular crowding and order in photosynthetic membranes*”, Trends in Plant Science, Vol. 13 No. 5, pp. 201–207, doi: 10.1016/j.tplants.2008.03.001.
- Koch, S., Exterkate, M., López, C.A., Patro, M., Marrink, S.J. and Driessen, A.J.M. (2019), “*Two distinct anionic phospholipid-dependent events involved in SecA-mediated protein translocation*”, Biochimica et Biophysica Acta - Biomembranes, Vol. 1861 No. 11, p. 183035, doi: 10.1016/j.bbamem.2019.183035.
- Koch, S., De Wit, J.G., Vos, I., Birkner, J.P., Gordiichuk, P., Herrmann, A., Van Oijen, A.M., *et al.* (2016), “*Lipids activate SecA for high affinity binding to the SecYEG complex*”, Journal of Biological Chemistry, Vol. 291 No. 43, pp. 22534–22543, doi: 10.1074/jbc.M116.743831.
- Konarev, P. V., Volkov, V. V., Sokolova, A. V., Koch, M.H.J. and Svergun, D.I. (2003), “*PRIMUS: A Windows PC-based system for small-angle scattering data analysis*”, Journal of Applied Crystallography, Vol. 36 No. 5, pp. 1277–1282, doi: 10.1107/S0021889803012779.
- Kozin, M.B. and Svergun, D.I. (2001), “*Automated matching of high- and low-resolution structural models*”, Journal of Applied Crystallography, Vol. 34 No. 1, pp. 33–41, doi: 10.1107/S0021889800014126.
- Kulothungan, S.R., Das, M., Johnson, M., Ganesh, C. and Varadarajan, R. (2009), “*Effect of crowding agents, signal peptide, and chaperone secb on the folding and aggregation of e. coli maltose binding protein*”, Langmuir, Vol. 25 No. 12, pp. 6637–6648, doi: 10.1021/la900198h.
- Kusters, I. and Driessen, A.J.M. (2011), “*SecA, a remarkable nanomachine*”, Cellular and Molecular Life Sciences, Vol. 68, pp. 2053–2066, doi: 10.1007/s00018-011-0681-y.
- Kuznetsova, I.M., Turoverov, K.K. and Uversky, V.N. (2014), “*What macromolecular crowding can do to a protein*”, International Journal of Molecular Sciences, Vol. 15, pp. 23090–23140, doi: 10.3390/ijms151223090.
- De Las Peñas, A., Connolly, L. and Gross, C.A. (1997), “*The  $\sigma(E)$ -mediated response to extracytoplasmic stress in Escherichia coli is transduced by RseA and RseB, two negative*

- 
- regulators of  $\sigma(E)$* ", *Molecular Microbiology*, Vol. 24 No. 2, pp. 373–385, doi: 10.1046/j.1365-2958.1997.3611718.x.
- Laurent, T.C. (1971), "*Enzyme Reactions in Polymer Media*", *European Journal of Biochemistry*, Vol. 21 No. 4, pp. 498–506, doi: 10.1111/j.1432-1033.1971.tb01495.x.
- Laurent, T.C. and Ogston, A.G. (1963), "*The Interaction Between Polysaccharides and Other Macromolecules. Part 4: The Osmotic Pressure of Mixtures of Serum Albumin and Hyaluronic Acid*", *Biochem J.*, Vol. 89, pp. 249–253.
- Lavalette, D., Hink, M.A., Tourbez, M., Tétreau, C. and Visser, A.J. (2006), "*Proteins as micro viscosimeters: Brownian motion revisited*", *European Biophysics Journal*, Vol. 35 No. 6, pp. 517–522, doi: 10.1007/s00249-006-0060-z.
- Lecinski, S., Shepherd, J.W., Bunting, K., Dresser, L., Quinn, S.D., MacDonald, C. and Leake, M.C. (2022), "*Correlating viscosity and molecular crowding with fluorescent nanobeads and molecular probes: in vitro and in vivo*", *Interface Focus*, Vol. 12 No. 6, doi: 10.1098/rsfs.2022.0042.
- Lee, K.L., Lee, K.C., Lee, J.H. and Roe, J.H. (2022), "*Characterization of components of a reducing system for SoxR in the cytoplasmic membrane of Escherichia coli*", *Journal of Microbiology*, Vol. 60 No. 4, pp. 387–394, doi: 10.1007/s12275-022-1667-1.
- Lill, R., Dowhan, W. and Wickner, W. (1990), "*The ATPase activity of SecA is regulated by acidic phospholipids, SecY, and the leader and mature domains of precursor proteins*", *Cell*, Vol. 60, pp. 271–280, doi: 10.1016/0092-8674(90)90742-W.
- Lim, K.H., Huang, H., Pralle, A. and Park, S. (2011), "*Engineered streptavidin monomer and dimer with improved stability and function*", *Biochemistry*, Vol. 50 No. 40, pp. 8682–8691, doi: 10.1021/bi2010366.
- Lim, K.H., Huang, H., Pralle, A. and Park, S. (2013), "*Stable, high-affinity streptavidin monomer for protein labeling and monovalent biotin detection*", *Biotechnology and Bioengineering*, Vol. 110 No. 1, pp. 57–67, doi: 10.1002/bit.24605.
- Ling, K., Jiang, H. and Zhang, Q. (2013), "*A colorimetric method for the molecular weight determination of polyethylene glycol using gold nanoparticles*", *Nanoscale Research Letters*, Vol. 8 No. 1, pp. 1–10, doi: 10.1186/1556-276X-8-538.
- Liu, B., Åberg, C., van Eerden, F.J., Marrink, S.J., Poolman, B. and Boersma, A.J. (2017), "*Design and Properties of Genetically Encoded Probes for Sensing Macromolecular Crowding*", *Biophysical Journal*, Vol. 112 No. 9, pp. 1929–1939, doi: 10.1016/j.bpj.2017.04.004.
- Liu, L.N. and Scheuring, S. (2013), "*Investigation of photosynthetic membrane structure using*

## 5 References

---

- atomic force microscopy*”, Trends in Plant Science, Vol. 18 No. 5, pp. 277–286, doi: 10.1016/j.tplants.2013.03.001.
- Löwe, M., Kalacheva, M., Boersma, A.J. and Kedrov, A. (2020), “*The more the merrier: effects of macromolecular crowding on the structure and dynamics of biological membranes*”, FEBS Journal, Vol. 287 No. 23, pp. 5039–5067, doi: 10.1111/febs.15429.
- Lundberg, M.E., Becker, E.C. and Choe, S. (2013), “*MstX and a Putative Potassium Channel Facilitate Biofilm Formation in Bacillus subtilis*”, PLoS ONE, Vol. 8(5), doi: 10.1371/journal.pone.0060993.
- Manalastas-Cantos, K., Konarev, P. V., Hajizadeh, N.R., Kikhney, A.G., Petoukhov, M. V., Molodenskiy, D.S., Panjkovich, A., et al. (2021), “*ATSAS 3.0: Expanded functionality and new tools for small-angle scattering data analysis*”, Journal of Applied Crystallography, International Union of Crystallography, Vol. 54, pp. 343–355, doi: 10.1107/S1600576720013412.
- Marsh, D. (2008), “*Protein modulation of lipids, and vice-versa, in membranes*”, Biochimica et Biophysica Acta - Biomembranes, Vol. 1778, pp. 1545–1575, doi: 10.1016/j.bbamem.2008.01.015.
- Marsh, D., Bartucci, R. and Sportelli, L. (2003), “*Lipid membranes with grafted polymers: Physicochemical aspects*”, Biochimica et Biophysica Acta - Biomembranes, Vol. 1615, pp. 33–59, doi: 10.1016/S0005-2736(03)00197-4.
- McConkey, E.H. (1982), “*Molecular evolution, intracellular organization, and the quinary structure of proteins.*”, Proceedings of the National Academy of Sciences of the United States of America, Vol. 79 No. 10, pp. 3236–3240, doi: 10.1073/pnas.79.10.3236.
- Minton, A.P. (1981), “*Excluded volume as a determinant of protein structure and stability*”, Biopolymers, Vol. 20, pp. 2093–2120, doi: 10.1016/S0006-3495(80)84917-4.
- Minton, A.P. (2000), “*Implications of macromolecular crowding for protein assembly*”, Current Opinion in Structural Biology, Vol. 10, pp. 34–39, doi: 10.1016/S0959-440X(99)00045-7.
- Minton, A.P. (2001), “*The Influence of Macromolecular Crowding and Macromolecular Confinement on Biochemical Reactions in Physiological Media*”, Journal of Biological Chemistry, Vol. 276 No. 14, pp. 10577–10580, doi: 10.1074/jbc.R100005200.
- Minton, A.P. (2013), “*Quantitative assessment of the relative contributions of steric repulsion and chemical interactions to macromolecular crowding*”, Biopolymers, Vol. 99 No. 4, pp. 239–244, doi: 10.1002/bip.22163.
- Missiakas, D., Mayer, M.P., Lemaire, M., Georgopoulos, C. and Raina, S. (1997), “*Modulation of the Escherichia coli  $\sigma(E)$  (RpoE) heat-shock transcription-factor activity by the RseA,*

- 
- RseB and RseC proteins*", Molecular Microbiology, Vol. 24 No. 2, pp. 355–371, doi: 10.1046/j.1365-2958.1997.3601713.x.
- Mitchell, A.M. and Silhavy, T.J. (2019), "*Envelope stress responses: balancing damage repair and toxicity*", Nature Reviews Microbiology, Vol. 17(7) No. July, pp. 417–428, doi: 10.1053/j.gastro.2016.08.014.CagY.
- Mitchison-Field, L.M. and Belin, B.J. (2023), "*Bacterial lipid biophysics and membrane organization*", Current Opinion in Microbiology, Vol. 74, p. 102315, doi: 10.1016/j.mib.2023.102315.
- Molliex, A., Temirov, J., Lee, J., Coughlin, M., Kanagaraj, A.P., Kim, H.J., Mittag, T., *et al.* (2015), "*Phase Separation by Low Complexity Domains Promotes Stress Granule Assembly and Drives Pathological Fibrillization*", Cell, Vol. 163, pp. 123–133, doi: 10.1016/j.cell.2015.09.015.
- Mueller, N.S., Wedlich-Söldner, R. and Spira, F. (2012), "*From mosaic to patchwork: Matching lipids and proteins in membrane organization*", Molecular Membrane Biology, Vol. 29 No. 5, pp. 186–196, doi: 10.3109/09687688.2012.687461.
- Munishkina, L.A., Cooper, E.M., Uversky, V.N. and Fink, A.L. (2004), "*The effect of macromolecular crowding on protein aggregation and amyloid fibril formation*", Journal of Molecular Recognition, Vol. 17 No. 5, pp. 456–464, doi: 10.1002/jmr.699.
- Murade, C.U. and Shubeita, G.T. (2019), "*A molecular sensor reveals differences in macromolecular crowding between the cytoplasm and nucleoplasm*", ACS Sensors, Vol. 4 No. 7, pp. 1835–1843, doi: 10.1021/acssensors.9b00569.
- Nawrocki, G., Karaboga, A., Sugita, Y. and Feig, M. (2019), "*Effect of protein-protein interactions and solvent viscosity on the rotational diffusion of proteins in crowded environments*", Physical Chemistry Chemical Physics, Royal Society of Chemistry, Vol. 21 No. 2, pp. 876–883, doi: 10.1039/c8cp06142d.
- Ogston, A.G. and Preston, B.N. (1966), "*The Exclusion of Protein by Hyaluronic Acid*", Journal of Biological Chemistry, Vol. 241 No. 1, pp. 17–19, doi: 10.1016/s0021-9258(18)96951-6.
- Oswald, J., Njenga, R., Natriashvili, A., Sarmah, P. and Koch, H.G. (2021), "*The Dynamic SecYEG Translocon*", Frontiers in Molecular Biosciences, Vol. 8 (April), doi: 10.3389/fmolb.2021.664241.
- Patel, C.K., Singh, S., Saini, B. and Mukherjee, T.K. (2022), "*Macromolecular Crowding-Induced Unusual Liquid-Liquid Phase Separation of Human Serum Albumin via Soft Protein-Protein Interactions*", Journal of Physical Chemistry Letters, Vol. 13, pp. 3636–

- 3644, doi: 10.1021/acs.jpcclett.2c00307.
- Peters, R. and Cherry, R.J. (1982), "*Lateral and rotational diffusion of bacteriorhodopsin in lipid bilayers: Experimental test of the Saffman-Delbruck equations*", Proceedings of the National Academy of Sciences of the United States of America, Vol. 79, pp. 4317–4321, doi: 10.1073/pnas.79.14.4317.
- Raghunath, G. and Dyer, R.B. (2019), "*Kinetics of Histidine-Tagged Protein Association to Nickel-Decorated Liposome Surfaces*", Langmuir, research-article, American Chemical Society, Vol. 35 No. 38, pp. 12550–12561, doi: 10.1021/acs.langmuir.9b01700.
- Ralston, G.B. (1990), "*Effects of 'crowding' in protein solutions*", Journal of Chemical Education, Vol. 67 No. 10, pp. 857–860, doi: 10.1021/ed067p857.
- Ramadurai, S., Holt, A., Krasnikov, V., Van Den Bogaart, G., Killian, J.A. and Poolman, B. (2009), "*Lateral diffusion of membrane proteins*", Journal of the American Chemical Society, Vol. 131 No. 35, pp. 12650–12656, doi: 10.1021/ja902853g.
- Rapoport, T.A., Li, L. and Park, E. (2017), "*Structural and mechanistic insights into protein translocation*", Annual Review of Cell and Developmental Biology, Vol. 33, pp. 369–390, doi: 10.1146/annurev-cellbio-100616-060439.
- Rashid, R., Chee, S.M.L., Raghunath, M. and Wohland, T. (2015), "*Macromolecular crowding gives rise to microviscosity, anomalous diffusion and accelerated actin polymerization*", Physical Biology, Vol. 12 No. 3, doi: 10.1088/1478-3975/12/3/034001.
- Ray, S., Singh, N., Kumar, R., Patel, K., Pandey, S., Datta, D., Mahato, J., *et al.* (2020), " *$\alpha$ -Synuclein aggregation nucleates through liquid–liquid phase separation*", Nature Chemistry, Springer US, Vol. 12, pp. 705–716, doi: 10.1038/s41557-020-0465-9.
- Regupathi, I., Govindarajan, R., Amaresh, S.P. and Murugesan, T. (2009), "*Densities and viscosities of polyethylene glycol 6000 + triammonium citrate + water systems*", Journal of Chemical and Engineering Data, Vol. 54 No. 12, pp. 3291–3295, doi: 10.1021/jc9002898.
- Rivas, G., Fernandez, J.A. and Minton, A.P. (1999), "*Direct observation of the self-association of dilute proteins in the presence of inert macromolecules at high concentration via tracer sedimentation equilibrium: Theory, experiment, and biological significance*", Biochemistry, Vol. 38 No. 29, pp. 9379–9388, doi: 10.1021/bi990355z.
- Rollauer, S.E., Soorshjani, M.A., Noinaj, N. and Buchanan, S.K. (2015), "*Outer membrane protein biogenesis in Gram-negative bacteria*", Philosophical Transactions of the Royal Society B: Biological Sciences, Vol. 370(1679), doi: 10.1098/rstb.2015.0023.
- Roosild, T.P., Greenwald, J., Vega, M., Castronovo, S., Riek, R. and Choe, S. (2005), "*NMR*

- 
- structure of mistic, a membrane-integrating protein for membrane protein expression*", Science, Vol. 307 No. 5713, pp. 1317–1321, doi: 10.1126/science.1106392.
- Ross, P.D. and Minton, A.P. (1977), "*Analysis of non-ideal behavior in concentrated hemoglobin solutions*", Journal of Molecular Biology, Vol. 112 No. 3, pp. 437–452, doi: 10.1016/S0022-2836(77)80191-5.
- Sarkar, M., Li, C. and Pielak, G.J. (2013), "*Soft interactions and crowding*", Biophysical Reviews, Vol. 5 No. 2, pp. 187–194, doi: 10.1007/s12551-013-0104-4.
- Sasahara, K., McPhie, P. and Minton, A.P. (2003), "*Effect of dextran on protein stability and conformation attributed to macromolecular crowding*", Journal of Molecular Biology, Vol. 326 No. 4, pp. 1227–1237, doi: 10.1016/S0022-2836(02)01443-2.
- Schavemaker, P.E., Boersma, A.J. and Poolman, B. (2018), "*How important is protein diffusion in prokaryotes?*", Frontiers in Molecular Biosciences, Vol. 5(93), doi: 10.3389/fmolb.2018.00093.
- Segur, J.B. and Oberstar, H.E. (1951), "*Viscosity of Glycerol and Its Aqueous Solutions*", Industrial and Engineering Chemistry, Vol. 43 No. 9, pp. 2117–2120, doi: 10.1021/ie50501a040.
- Sezgin, E., Levental, I., Mayor, S. and Eggeling, C. (2017), "*The mystery of membrane organization: composition, regulation and physiological relevance of lipid rafts*", Nature Reviews Molecular Cell Biology, Vol. 18 No. 6, pp. 361–374, doi: 10.1038/nrm.2017.16.The.
- Sharma, N., Gadhave, K., Kumar, P. and Giri, R. (2022), "*Transactivation domain of Adenovirus Early Region 1A (E1A): Investigating folding dynamics and aggregation*", Current Research in Structural Biology, Vol. 4, pp. 29–40, doi: 10.1016/j.crstbi.2022.01.001.
- Simons, K. and Sampaio, J.L. (2011), "*Membrane organization | Lipid rafts*", Cold Spring Harb Perspect Biol., Vol. 3 No. 10, p. a004697, doi: 10.1016/B978-0-12-819460-7.00583-1.
- Singer, S.J. and Nicolson, G.L. (1972), "*The fluid mosaic model of the structure of cell membranes*", Science, Vol. 175 No. 4023, pp. 720–731, doi: 10.1126/science.175.4023.720.
- Skrzypek, R., Iqbal, S. and Callaghan, R. (2018), "*Methods of reconstitution to investigate membrane protein function*", Methods, Vol. 147, pp. 126–141, doi: 10.1016/j.ymeth.2018.02.012.
- Snead, W.T., Hayden, C.C., Gadok, A.K., Zhao, C., Lafer, E.M., Rangamani, P. and Stachowiak, J.C. (2017), "*Membrane fission by protein crowding*", Proceedings of the

- National Academy of Sciences of the United States of America, Vol. 114 No. 16, pp. E3258–E3267, doi: 10.1073/pnas.1616199114.
- Sowers, A.E. and Hackenbrock, C.R. (1981), “*Rate of lateral diffusion of intramembrane particles: Measurement by electrophoretic displacement and rerandomization*”, Proceedings of the National Academy of Sciences of the United States of America, Vol. 78 No. 10, pp. 6246–6250, doi: 10.1073/pnas.78.10.6246.
- Stachowiak, J.C., Hayden, C.C. and Sasaki, D.Y. (2010), “*Steric confinement of proteins on lipid membranes can drive curvature and tubulation*”, Proceedings of the National Academy of Sciences of the United States of America, Vol. 107 No. 17, pp. 7781–7786, doi: 10.1073/pnas.0913306107.
- Stachowiak, J.C., Schmid, E.M., Ryan, C.J., Ann, H.S., Sasaki, D.Y., Sherman, M.B., Geissler, P.L., *et al.* (2012), “*Membrane bending by protein-protein crowding*”, Nature Cell Biology, Vol. 14 No. 9, pp. 944–949, doi: 10.1038/ncb2561.
- Stagg, L., Zhang, S.Q., Cheung, M.S. and Wittung-Stafshede, P. (2007), “*Molecular crowding enhances native structure and stability of  $\alpha/\beta$  protein flavodoxin*”, Proceedings of the National Academy of Sciences of the United States of America, Vol. 104 No. 48, pp. 18976–18981, doi: 10.1073/pnas.0705127104.
- Steinberg, R., Knüpffer, L., Origi, A., Asti, R. and Koch, H.G. (2018), “*Co-translational protein targeting in bacteria*”, FEMS Microbiology Letters, Vol. 365 No. 11, pp. 1–15, doi: 10.1093/femsle/fny095.
- Sun, X., Zhang, A., Baker, B., Sun, L., Howard, A., Buswell, J., Maurel, D., *et al.* (2011), “*Development of SNAP-tag fluorogenic probes for wash-free fluorescence imaging*”, ChemBioChem, Vol. 12 No. 14, pp. 2217–2226, doi: 10.1002/cbic.201100173.
- Svergun, D.I. (1992), “*Determination of the regularization parameter in indirect-transform methods using perceptual criteria*”, Journal of Applied Crystallography, Vol. 25, pp. 495–503, doi: 10.1107/S0021889892001663.
- Svergun, D.I., Petoukhov, M. V. and Koch, M.H.J. (2001), “*Determination of domain structure of proteins from x-ray solution scattering*”, Biophysical Journal, Vol. 80 No. 6, pp. 2946–2953, doi: 10.1016/S0006-3495(01)76260-1.
- Takatori, S.C., Son, S., Lee, D.S.W. and Fletcher, D.A. (2023), “*Engineered molecular sensors for quantifying cell surface crowding*”, Proceedings of the National Academy of Sciences, Vol. 120, doi: 10.1073/pnas.
- Tronchere, H. and Boal, F. (2017), “*Liposome Flotation Assays for Phosphoinositide-protein Interaction*”, Bio-Protocol, Vol. 7 No. 5, pp. 3–8, doi: 10.21769/bioprotoc.2169.

- Uversky, V.N., M. Cooper, E., Bower, K.S., Li, J. and Fink, A.L. (2002), "*Accelerated  $\alpha$ -synuclein fibrillation in crowded milieu*", FEBS Letters, Vol. 515 No. 1–3, pp. 99–103, doi: 10.1016/S0014-5793(02)02446-8.
- de Vrije, T., de Swartt, R.L., Dowhan, W., Tommassen, J. and de Kruijff, B. (1988), "*Phosphatidylglycerol is involved in protein translocation across Escherichia coli inner membranes*", Letters to Nature, Vol. 332 No. July, pp. 173–175.
- Wang, L., Biswas, K.H., Yoon, B.K., Kawakami, L.M., Park, S., Groves, J.T., Li, L., *et al.* (2018), "*Membrane Reconstitution of Monoamine Oxidase Enzymes on Supported Lipid Bilayers*", Langmuir, Vol. 34 No. 36, pp. 10764–10773, doi: 10.1021/acs.langmuir.8b01348.
- Wang, L.G. and Tonggu, L.G. (2015), "*Membrane protein reconstitution for functional and structural studies*", Science China Life Sciences, Vol. 58 No. 1, pp. 66–74, doi: 10.1007/s11427-014-4769-0.
- Wang, Y., Li, C. and Pielak, G.J. (2010), "*Effects of proteins on protein diffusion*", Journal of the American Chemical Society, Vol. 132 No. 27, pp. 9392–9397, doi: 10.1021/ja102296k.
- Wang, Y., Sarkar, M., Smith, A.E., Krois, A.S. and Pielak, G.J. (2012), "*Macromolecular crowding and protein stability*", Journal of the American Chemical Society, Vol. 134 No. 40, pp. 16614–16618, doi: 10.1021/ja305300m.
- Wu, J., Zhao, C., Lin, W., Hu, R., Wang, Q., Chen, H., Li, L., *et al.* (2014), "*Binding characteristics between polyethylene glycol (PEG) and proteins in aqueous solution*", Journal of Materials Chemistry B, Vol. 2 No. 20, pp. 2983–2992, doi: 10.1039/c4tb00253a.
- Wu, S.C. and Wong, S.L. (2005), "*Engineering soluble monomeric streptavidin with reversible biotin binding capability*", Journal of Biological Chemistry, Vol. 280 No. 24, pp. 23225–23231, doi: 10.1074/jbc.M501733200.
- Wu, Z.C., De Keyzer, J., Kedrov, A. and Driessen, A.J.M. (2012), "*Competitive binding of the SecA ATPase and ribosomes to the SecYEG translocon*", Journal of Biological Chemistry, Vol. 287 No. 11, pp. 7885–7895, doi: 10.1074/jbc.M111.297911.
- Ye, C., Chai, Q., Zhong, M. and Wei, Y. (2013), "*Effect of crowding by Ficolls on OmpA and OmpT refolding and membrane insertion*", Protein Science, Vol. 22 No. 2, pp. 239–245, doi: 10.1002/pro.2205.
- Zakeri, B., Fierer, J.O., Celik, E., Chittock, E.C., Schwarz-Linek, U., Moy, V.T. and Howarth, M. (2012), "*Peptide tag forming a rapid covalent bond to a protein, through engineering a bacterial adhesin*", Proceedings of the National Academy of Sciences of the United States

- of America, Vol. 109 No. 12, doi: 10.1073/pnas.1115485109.
- Zhu, J., Zheng, J., Liu, C. and Zhang, S. (2016), "*Ionic complexing induced fabrication of highly permeable and selective polyacrylic acid complexed poly (arylene ether sulfone) nanofiltration membranes for water purification*", *Journal of Membrane Science*, Vol. 520 No. October, pp. 130–138, doi: 10.1016/j.memsci.2016.07.059.
- Zimmerberg, J. and Kozlov, M.M. (2006), "*How proteins produce cellular membrane curvature*", *Nature Reviews Molecular Cell Biology*, Vol. 7 No. 1, pp. 9–19, doi: 10.1038/nrm1784.
- Zimmerman, S.B. and Harrison, B. (1987), "*Macromolecular crowding increases binding of DNA polymerase to DNA: An adaptive effect*", *Proceedings of the National Academy of Sciences of the United States of America*, Vol. 84(7), pp. 1871–1875, doi: 10.1073/pnas.84.7.1871.
- Zimmerman, S.B. and Pfeiffer, B.H. (1983), "*Macromolecular crowding allows blunt-end ligation by DNA ligases from rat liver or Escherichia coli*", *Proceedings of the National Academy of Sciences of the United States of America*, Vol. 80 No. 19 I, pp. 5852–5856, doi: 10.1073/pnas.80.19.5852.
- Zimmerman, S.B. and Trach, S.O. (1991), "*Estimation of macromolecule concentrations and excluded volume effects for the cytoplasm of Escherichia coli*", *Journal of Molecular Biology*, Vol. 222 No. 3, pp. 599–620, doi: 10.1016/0022-2836(91)90499-V.

## 6 Appendix

### I. Curriculum vitae

#### Maryna Löwe, Dipl.-Ing.

Geboren am 24. Feb 1992 in Kiew, Ukraine

Spitzangerweg 55, 50859 Köln

+49 152 0275 33 86

[loewe.maryna@gmail.com](mailto:loewe.maryna@gmail.com)



#### Education

---

March 2018 – December 2022 **PhD candidate**

Heinrich Heine University Dusseldorf

Synthetic Membrane Systems (WG Prof. Alexej Kedrov)

Dissertation: „*Effects of macromolecular crowding on protein targeting and translocation via SecYEG*“

March 2015 – September 2017 **Master's programm in biotechnology**

University of Natural Resources and Life Sciences, Vienna

Specialization: Medical biotechnology

Master thesis: „*Characterization of protein-ligand interactions by biophysical methods*“

Overall assessment: passed with distinction

October 2011 – March 2015 **Bachelor's degree in food- and biotechnology**

University of Natural Resources and Life Sciences, Vienna

Bachelor thesis: „*Development of a sample preparation method for qualitative analysis of cell culture supernatants via LC-MS/MS*“

Overall assessment: passed with distinction

## Appendix – I. Curriculum vitae

---

- March 2009 - June 2011    VWU - pre-study course of the Vienna universities  
University course for supplementary examinations
- September 2001 – June 2009    Gymnasium No.167 with extended German lessons Kiev,  
Ukraine
- September 1998 – June 2001    Elementary School No.201, Kyiv, Ukraine

## Internships and Work Experience

---

- Since June 2023    **Sales Consultant Service Projects**  
Cube Biotech GmbH
- March 2018 – December 2022    **Research associate/PhD candidate**  
Heinrich Heine University Dusseldorf  
Synthetic membrane systems (WG Prof. Alexej Kedrov)
- Protein biochemistry and analytics
  - Biophysics of biological membranes and membrane proteins
  - Fluorescence spectroscopy
  - Quartz Crystal Microbalance (QCM)
  - Surface Plasmon Resonance (SPR)
  - Isothermal Titration Calorimetry (ITC)
- February 2016    **Internship**  
Boehringer-Ingelheim, Vienna  
Cancer Cell Signaling Department  
Oncology Division NTC Discovery  
1 week in NanoTemper Technologies GmbH, Munich  
Training: Surface Acoustic Wave (SAW)
- March 2016– November 2016    **Diploma student**  
Boehringer-Ingelheim, Vienna  
Cancer Cell Signaling Department  
Oncology Division NTC Discovery
- Surface Acoustic Wave (SAW)
  - Surface Plasmon Resonance (SPR)
  - HPLC coupled with mass spectrometry

- SDS-PAGE und 2D-gelelectrophoresis
- Nano Differential Scanning Fluorimetry (nDSF)
- Microscale Thermophoresis (MST)

June 2014 – August 2014 **FEM Tech Internship**

ACIB GmbH

Department of Analytical Chemistry, BOKU

- Metabolomic analysis via LC-MS/MS
- Method development for quantitative analysis via LC-MS/MS

---

## Further Education and Trainings

---

November 2021 Training „Gentechnische Arbeiten in Gentechnischen Anlagen“ nach § 28 Abs. 5 Gentechnik-Sicherheitsverordnung, 12.08.2019

iGRAD\* / AdvoGenConsult (AGCT)

August 2021 Nutritionist education

Academy of Sport and Health

September 2020 Workshop „Analytisch denken und überzeugend Argumentieren“

iGRAD\* / ProArgument GbR

November 2019 Workshop „Introduction to Project Management and Working in Teams“, iGRAD\*

March 2019 Workshop „Leadership Skills“, iGRAD\*

February 2013 English Course at the Upper-Intermediate Level International House New York, New York, USA

April 2009 German language diploma

Conference of Ministers of Culture – Second Stage, Level C1

## Skills

---

**Computer skills** Sicherer Umgang mit dem PC und Mac

MS Office (sehr gut)

Mascot, Pymol, GPMW

Adobe Photoshop

**Languages** German – fluent

Englisch – fluent

Ukrainian and Russian – native speaker

**Hobbies** Scientific Illustrations, Food Fermentation, Soap crafting, Art, Photography, History

**Driver license** B class

Maryna Löwe

Cologne, 15.01.24



\*iGRAD – Interdisciplinary Graduate and Research Academy Dusseldorf

## II. List of publications

Löwe M, Hänsch S, Hachani E, Schmitt L, Weidtkamp-Peters S, Kedrov A. Probing macromolecular crowding at the lipid membrane interface with genetically encoded sensors. *Protein Science*. 2023;32(11):e4797, doi:10.1002/pro.4797

(Teil der Dissertation, die Eigenanteile sind auf der Seite 53 aufgeschlüsselt)

Bonda, L., Müller, J., Fischer, L., Löwe, M., Kedrov A., Schmidt, S., Hartmann, L. (2023). “Facile Synthesis of Catechol-Containing Polyacrylamide Copolymers: Synergistic Effects of Amine, Amide and Catechol Residues in Mussel-Inspired Adhesives”, *Polymers*, 15(18):3663, doi:10.3390/polym15183663

(Die Publikation ist in den Umfang dieser Dissertation nicht einbezogen)

Kamel, M., Löwe, M., Schott-Verdugo, S., Gohlke, H. and Kedrov, A. (2022), “Unsaturated fatty acids augment protein transport via the SecA:SecYEG translocon”, *FEBS Journal*, Vol. 289 No. 1, pp. 140–162, doi: 10.1111/febs.16140

(Die Publikation ist in den Umfang dieser Dissertsiion nicht einbezogen)

Löwe, M., Kalacheva, M., Boersma, A.J. and Kedrov, A. (2020), “The more the merrier: effects of macromolecular crowding on the structure and dynamics of biological membranes”, *FEBS Journal*, Vol. 287 No. 23, pp. 5039–5067, doi: 10.1111/febs.15429.

(Teil der Dissertation, die Eigenanteile sind auf der Seite 23 aufgeschlüsselt)

Löwe, M., Papadopoulos, A., Kamel, M. et al. Membranproteinfaltung — Kernwissen aus (nicht zu) vereinfachten Systemen. *Biospektrum* 25, 385–387 (2019), doi: 10.1007/s12268-019-1066-2

(Die Publikation ist in den Umfang dieser Dissertation nicht einbezogen)

### III. Supervised Student Projects

Anastasiia Romenska (2022) Bachelor thesis

Title: “Development of anchoring strategies for genetically-encoded sensors for measurement of macromolecular crowding at the lipid membrane interfaces”

Sven Cygan (2021) Bachelor thesis

Title: “Biophysical analysis of outer membrane protein insertion *in vitro*”.

Marie-Louise Müller (2021) Bachelor thesis

Title: “Developing quartz crystal microbalance as a tool for measuring protein-lipid interactions”

Carla Dannemann (2020) Bachelor thesis

Title: “Recombinant expression and isolation of Pel secretion complex of *Pseudomonas aeruginosa*”

Guillermo Manzano Fabre (2020) Bachelor thesis

Title: “Development of the asymmetric FRET-based sensor for macromolecular crowding at the interfaces”

Samet Kurt (2019) Bachelor thesis

Title: “Characterization of FRET-based sensors of interfacial macromolecular crowding”

Anuja Bernadet Joseph (2019) Bachelor thesis

Title: “Studying effects of the membrane complexity on protein translocation”

Nina Bornemann (2019) BachelorPLUS internship

Topic: Molecular crowding and early FRET-sensor desing and characterisation

Sören Rob (2019) Internship

Topic: Molecular crowding and early FRET-sensor desing and characterisation

## IV. Acknowledgements

As I reflect on my doctoral journey and the numerous persons, who supported me and made an invaluable contribution along the way, I would like to take a moment to extend my gratitude to them:

First of all, I'm deeply thankful to my supervisor Prof. Dr. Alexej Kedrov, who had the most significant impact on my academic, intellectual and personal development. Your guidance and insightful feedback have profoundly enhanced the quality of my research. You challenged me to think critically and find creative solutions, created an atmosphere of openness and motivated the entire research group. I cannot express how grateful I am for the opportunity to work under your guidance, where I have learned more than I ever could have imagine. As I move forward in my carrier, I want to extend my heartfelt wishes for ongoing success in your research, the mentorship of talented and motivated students and researchers and for you to making new discoveries that further expand the frontiers of human knowledge.

Next, I would like to extend my sincere appreciation to my second supervisor Prof. Dr. Laura Hartmann for her invaluable support and her contributions throughout my doctoral journey. I'm truly grateful for your support, providing insightful ideas and inputs that enriched my work.

From the outset of our doctoral work we worked closely with the research groups of Prof. Dr. Lutz Schmitt and Prof. Dr. Sander Smits. I want to thank you and the whole team from the Institute of Biochemistry I for exciting discussions held during our progress reports and for creating an inspiring academic environment. Your inputs and critical feedback have significantly shaped the course of my research.

Next, I want to extend my deepest gratitude to my group members, my little lab family, especially to Dr. Michael Kamel, Max Busch, Dr. Tim Kroll and Dr. Athanasios Papadopoulos. Our countless discussions and debates, exchange of new ideas served as a fuel that continuously propelled us forward new exiting experiments and discoveries. I will sincerely miss each one of you and want to wish all of you the very best in your future endeavors. May your paths be successful and may you continue to flourish both personally and academically.

My special thanks go to persons who contributed their expertise to conduct experiments without which I would not have achieved the progress I have made: Dr. Jens Reiners from Center for Structural Studies (CSS) for conduction SAXS experiments, Dr. Jakub Kubiak and Dr. Ralf Kühnemuth from the Institute of Physical Chemistry for their help with fluorescence-related measurements, Dr. Sebastian Hänsch for the SR-SIM measurements, Dr. Olivia Spitz and Eymen Hachiani for helping me to conduct SEC-MALS measurements, Florestan Bilsing

for teaching me how to make GUVs, Dr. Marcel Lagedroste for the first insights on how to handle chromatography systems.

My warmest gratitude goes out to my family, especially my husband Marcus Löwe for your endless support and understanding during this demanding period of our life as well as my parents Oleksiy Zyunkin and Victoria Zyunkina for your belief in me that constantly boosted my motivation.

I want to thank from the bottom of my heart to my grandpa Prof. Dr. Anatoliy Zyunkin. Your unraveling trust in me was the driving force behind the start of my PhD. It saddens me deeply that you are not with us to witness this moment.

Additionally, I would like to extend my gratitude to the Heinrich-Heine-University and Institute of Biochemistry I for provided facilities and resources making the current work possible.

## **V. Declaration**

Ich versichere an Eides Statt, dass die Dissertation von mir selbständig und ohne unzulässige fremde Hilfe unter Beachtung der „Grundsätze zur Sicherung guter wissenschaftlicher Praxis an der Heinrich-Heine-Universität Düsseldorf“ erstellt worden ist. Diese Dissertation ist keiner anderen Fakultät vorgelegt worden, es hat keinen erfolglosen oder erfolgreichen Promotionsversuch gegeben.